Anorganische Chemie

Homoleptic complexes of group 9 and 10 transition metals with phosphine-functionalized N-heterocyclic carbene ligands

Von der Fakultät für Naturwissenschaften
Department Chemie
Der Universität Paderborn

zur Erlangung des akademischen Grades eines
Doktors der Naturwissenschaften
Dr. rer. nat.
genehmigte Dissertation

von
Aziza A. Ahmida
aus Benghazi (Libyen)

Paderborn 2009

Date of submission: 23.11.2009
Date of examination: 18.12.2009

1. Referee: Prof. Dr. Gerald Henkel
2. Referee: PD. Dr. Hans Egold

The present work has been carried out during january 2005 and oktober 2009 at the university of Paderborn, Faculty of Science, Department of Chemistry under supervision of Prof. Dr G. Henkel.

Dedicated to

Spirit of my parents

My brothers and sisters

Abstract

This dissertation describes the synthesis of phosphane functionalized imidazolium salts and their use in the preparation of chelating mixed phoshane carbene ligands. The novel ligands were used for the synthesis of homoleptic complexes of Rh(I), Ir(I), Ni(II) and Pd(II). The reactivity of the Rh(I) and Ir(I) complexes with respect to small molecules has been investigated and the catalytic activity of the Pd(II) complexes for *Suzuki* coupling has been explored as well.

Starting from ethylvinylimidazolium iodide and $HPPh_2$ the imidazolium ligand precursors **E5** and **E6** were synthesized in high yield. Their conversion to the aspired mixed phoshane carbene ligand **E7** has been accomplished in situ by deprotonation with $K[N(SiMe_3)_2]$. The degree of conversion was almost quantitative as the reaction of the resulting solutions with CS_2 giving the thiocarboxylate **E8** proved.

In situ generated **E7** reacts with 0.5 equivalents $[Rh(\mu\text{-}Cl)(COD)]_2$ to give the novel homoleptic Rh(I) complexes *cis*-**E10**, *trans*-**E12,** *cis*-**E11**, *trans*-**E13** in high yields. All new complexes have been structurally characterized by single crystal X-ray crystallography. NMR spectroscopic stuidies of the dynamic behaviour of the complexes in solution have proved interconversion of *cis*- and *trans*-isomer at elevated temperatures. A mechanism for this reaction has been proposed.

The oxidative addition of small molecules like O_2, S_8, CH_3I, I_2 to *cis*-Rh(I) complexes **E10** or **E11**, respectively, afforded novel Rh(III) complexes **E14**, **E15**, **E16**, **E17**, **E19**. All new complexes have been characterized by standard spectroscopic methods and single crystal X-ray analysis. The complicated solution dynamics of the *cis*-peroxo-Rh(III) complex **E14** was explored in detail by ^{31}P NMR-spectroscopy. The synthesis of novel *cis*-Ir(I) complex **E20** has been achieved by reaction of **E7** with $[Ir(\mu\text{-}Cl)(COD)]_2$. It reacts with H_2, O_2, S_8, CO, CH_3I, I_2 giving the novel Ir(III) complexes, **E21**, **E22**, **E23**, **E24**, **E25, E26**. Their structures are described in detail. The synthesis of novel homoleptic *trans*-Ni(II) and Pd(II) complexes**, E27**, **E28** and their structural spectroscopic properties is described as well. The interconversion between *cis* and *trans* isomers of Pd(II) complex **E28** at high temperature was again proved by ^{31}P NMR spectroscopy. The catalytic activity of *trans*-Pd(II) complex **E28** with respect to *Suzuki* coupling was surveyed.

Acknowledgements

First of all thanks to Allah who enabled me to complete this work. I would like to express my deepest gratitude to my supervisor Prof. Dr. Gerald Henkel for giving me the opportunity of joining his group and giving me his valuable guidance and continuous encouragement through out this work.

From the depths of my heart I would like to express my thanks to PD Dr. Hans Egold for fruitful discussions throughout this work and continous encouragement. He constantally supported this work with both general advice and detailed comments and proof-reading.

I am grateful to Dr. Ulrich Flörke for his efforts of recording X-ray data and refining the X-ray structures described in this thesis.

Furthermore, I am gratful to Mr. Jörg Schröder for his useful advice on special working methods for experiments under inert gas atmosphere.

My gratitude goes to Mrs Karin Stolte for the countless hours of recording 2D NMR spectra and to Mrs Maria Busse and Mrs Christiane Gloger for carrying out the elemental analyses.

My special thanks goes to my ever helpful colleague Mehmet Özer who always gave me assistance with any computer related issues.

Also I would like to express my appreciation to Dr Ishtiaq Ahmed for proof-reading.

Thanks to all members of the working group of Prof. Dr. Gerald Henkel. Especially to my colleague Muhammad Ayaz for the nice working atmosphere in the lab.

Thank you for all friends who have been there for me during my stay in Germany – especially Intisar Elsharaa and Zuhl Gürbüz.

I gratefully acknowledge the financial support of Libyian Ministry of Higher Education and German Academic Exchange Service (DAAD).

Finally, a big thank to my family for their invaluable support during these five years.

Contents

List of Figures

List of Tables

Abbreviations

Ac	acetate
acac	acetyl acetonate
OAc	acetyl acetate
CD_3CN	acetonitrile-d_3
Ad	adamantyl
Å	angstrom(10^{-10}m)
Bu	butyl
Cat	catalyst
C_6D_6	benzene-d_6
δ	chemical shift
COD	1,5-cyclooctadiene
CV	cyclovoltametry
d	doublet
dd	double doublet
dba	dibenzylidenaceton
DMSO	dimethylsulfoxide
Et	ethyl
Et_2O	diethyl ether
PPh_2	diphenylphosphane
ν	frequency
hept	heptet
Hz	hertz
hr	hour
Im	imidazol-2-ylidene
iPr	isopropyl
IR	infrared
J	scalar coupling constant (NMR)
m	multiplet

Mes	mesityl
NHC	N-heterocyclic carbene
NHE	normal hydrogen electrode
NMR	nuclear magnetic resonance
ppm	parts per milion
Ph	Phenyl
q	quartet
s	singlet (NMR), strong (IR)
RT	room temperature
t	triplet
^{t}Bu	tertiary-butyl
THF	tetrahydrofuran
temp	temperature
Me_3Si	trimethylsilyl
sept	septet

1 Introduction

1.1 N-Heterocyclic carbenes (NHC)

Since the pioneering work of *Curtius*,[1a] *Staudinger*,[1b] and even earlier efforts[1c] carbenes have played an important role as transient intermediates over the last five decades.[2] The application of carbenes into organic chemistry and organometallic chemistry was introduced by *Doering* in the 1950s[3] and by *Fischer* 1964[4] respectively. Since then research on carbenes has rapidly expanded, but almost no attempts were made to stabilize carbenes until the 1980s when *Tomioka* started to study persistent triplet diaryl carbenes.[5] The first isolated singlet carbenes were reported in 1988 by *Bertrand*[6] **1** and in 1991 by *Arduengo*[7] **2**. The phosphino carbene **1** can be distilled at 80-85 °C ^{0} /10^{-2} Torr and the N-heterocyclic carbene (NHC) **2** is a crystalline solid that melts above 240 °C (Figure 1.1).

1 **2**

Figure 1.1: The first isolated singlett carbenes.

Although the use of N-heterocyclic carbenes as ligands for transition metal complexes was described almost 36 years ago by *Öfele* and *Wanzlick* who prepared compounds **3** and **4**.[8,9]

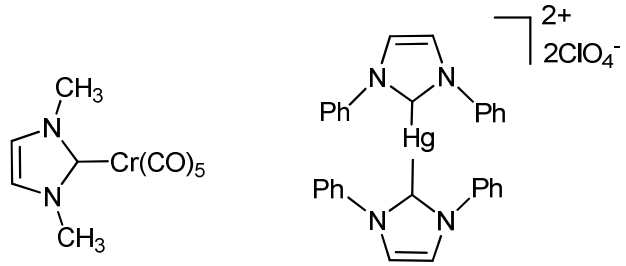

3 **4**

Figure 1.2: Transition metal complexes synthesised by *Öfele* and *Wanzlik*

In 1968 *Wanzlick* et al proposed that there is an unfavourable equilibrium between carbenes with their corresponding dimers [eq.1]. His suggestion came from molecular weight measurements.[10]

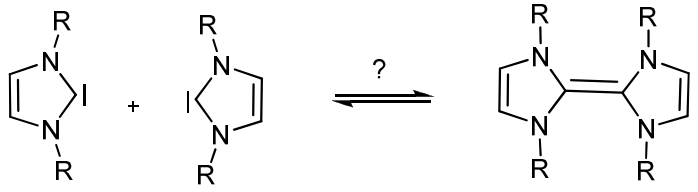

(eq. 1)

Lemal[11,12] proved *Wanzlick's* hypothesis of a carbene dimer equilibrium between the tetraaminoethylene **5** and the corresponding free carbene **6** (eq. 2) by NMR spectroscopy.

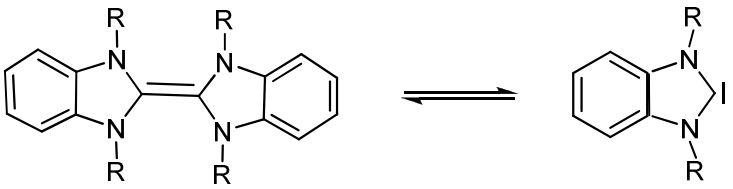

5 **6**

(eq. 2)

The particular stability of NHCs made them very popular and during the last years further analogues were synthesized (Figure 1.3). In 1995 *Arduengo* proved[13] by preparation of NHC **7** that aromaticity is not needed to stabilize a free singlet carbene. In 1996 *Alder* even isolated an example of the acyclic NHC **8**.[14]

This research area is continually expanding which can be seen from the isolation of novel four–membered carbene[15] **9** by *Grubbs* and the alkyl carbene[16] **10** by *Bertrand*. These types of NHCs are more electron rich, but also lack any aromatic character.

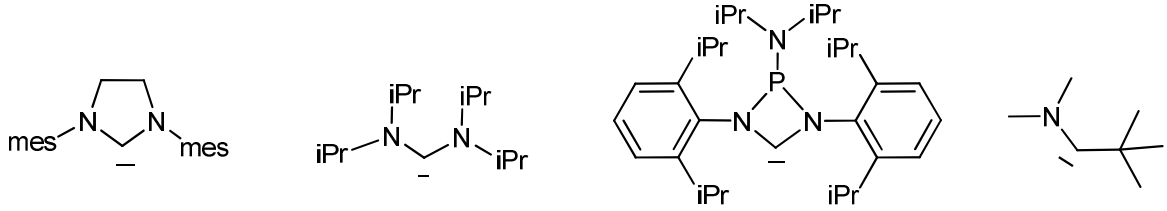

7 **8** **9** **10**

Figure 1.3: Stable NHCs and their derivatives

1.2 Hybridisation and structures

1.2.1 Singlet vs. triplet carbenes

Carbenes are neutral divalent carbon species linked to two adjacent groups by covalent bonds. They possess two non-bonding electrons and six valence electrons. The non-bonding electrons can be either spin paired (singlet state) or have parallel spins in different orbitals (triplet state).Figure 1.4 shows the possible arrangements of these two electrons.[17]

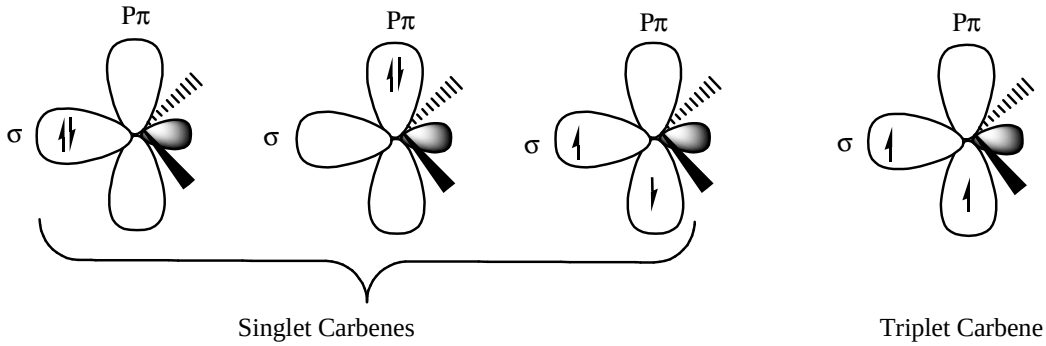

Figure 1.4: Electronic configuration of carbenes.[17]

1.2.2 Electronic properties of different types of singlet carbenes

Electronic effects generally control the spin multiplicity of a carbene although steric effects can also play a role in the stabilization and spin multiplicity. The difference in energy between the σ and p(π) orbitals can be used to predict the spin multiplicity of the carbene. The type of substituents bonded to the carbene atom can influence the energy of orbitals by their electron withdrawing or donating nature.The geometry of the carbenes substituted with inductive electron donating residues leads to non linear structures (but closer to 180º than 120º) favoring triplet states. This originates from the +I effect of the σ-electron donating substituents which induce a small σ-p(π) gap (HOMO/LUMO) between the non bonding σ orbital and anti bonding p(π) orbital. In this case the energy gap is smaller than the spin pairing energy and therefore these carbenes favors the triplet state (Figure 1.5).[17]

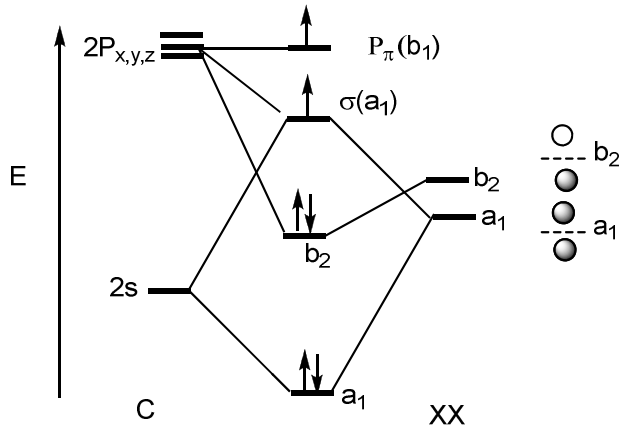

Figure 1.5: Molecular orbital diagram of a triplet carbene.[17]

σ-electron-withdrawing substituents favor the singlet state. Indeed σ-electron-withdrawing substituents inductively stablize the σ nonbonding orbital by increasing its s character and leave the p(π)orbital unchanged. The σ-p(π) gap is increased and the singlet state is favored. The free electrons are paired in the non bonding σ-orbital (Figure 1.6).[17]

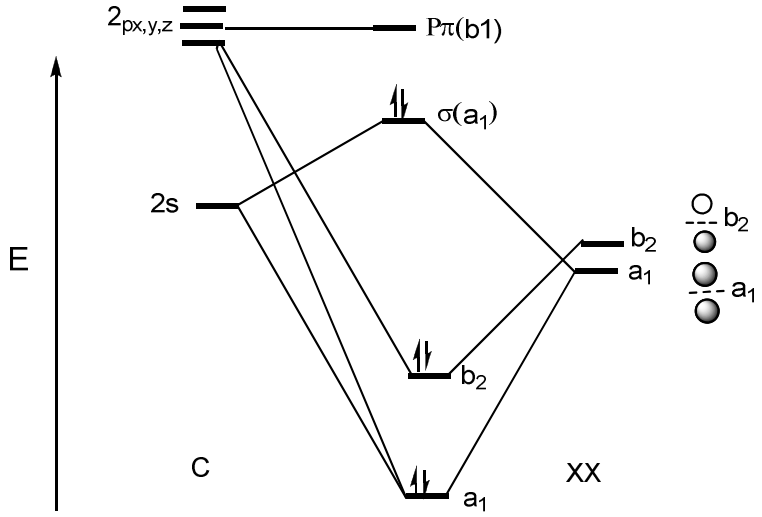

Figure 1.6: Molecular orbital diagram for a singlet carbene.[17]

1.2.3 Mesomeric effects

Substituents interacting with the carbene center can be classified into two types, namely X (for π-electron-donating groups such as (-F, -Cl, -Br, -I, -NR_2, -PR_2, -OR, -SR, -SR_3) and Z (for π-electron with withdrawing groups such as (-COR, -CN, -CF_3, -BR_2, -PR_3^+). Therefore according

to the substituents singlet carbenes can be classified into highly bent (X,X) carbenes and linear or quasi linear (Z,Z/X,Z) carbenes.

1.2.4 Carbenes containing two π-acceptor substituents

Most of the (Z,Z) carbenes are predicted to be linear singlet carbenes.[18,19] These carbenes are best described by the superposition of two zwitterionic structures featuring a positive charge at the carbene atom, an example of this type are diborylcarbenes **11**.[20]

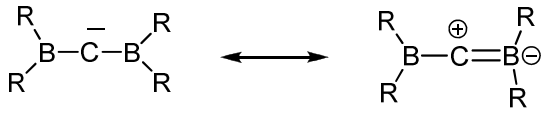

11 **12**

For this type of compound, the symmetric combination of the substituents vacant orbitals interacts with the p_y-orbital of the carbon atom, which is perpendicular to the valance plane (Figure 1.7). This interaction does not affect the p_x-orbital. Therefore the (p_x,p_y)-degeneracy is broken leading to a singlet state for this type of compounds.[17] Note that this pattern of substituents results in a polarized two electron three-center π-system. Hence the C-Z bonds have some multiple bond character.

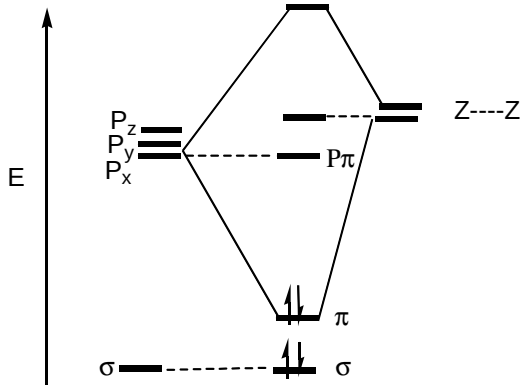

Figure 1.7: Molecular orbital diagram of a (Z,Z)-carbene.[17]

1.2.5 Carbenes with two π donor substituents

(X,X)-carbenes are predicted to be bent singlet carbenes.[18,19] The energy of the vacant p(π) orbital on the carbene carbon atom is increased by interaction with the symmetric combination of

the substituents lone pairs. Thus the σ-p(π) gap is increased and the singlet state is favored (Figure 1.8). Donation of the X-substituent lone pairs result in a polarized four electron three center bonding system.The C-X bonds acquire some multiple bond character. This type of carbenes can be described by the superposition of two zwitterionic structures with a negative charge at the carbene center

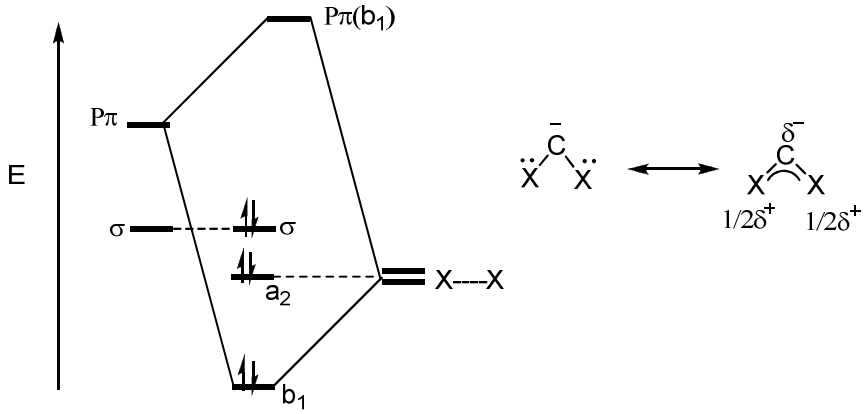

Figure 1.8: Molecular orbital diagram of (X,X) carbene.[17]

Representative examples for these carbenes are the transient dimethoxycarbene,[21] dihalocarbenes[22] and NHC–carbenes **13** in which the carbene electron deficiency is reduced by the donation of the two nitrogen lone pairs while the carbene lone pair is stabilized by the inductive effect of two electronegative nitrogen atoms.

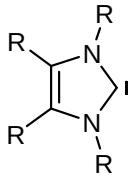

13

As described above NHC-carbenes do not undergo electrophilic reactions like insertion or cycloadditions. Furthermore, they can be handled in typical donor solvents including THF, liquid ammonia or acetonitrile.[23]

Wanzlick reported that delocalization of 6π electrons in unsaturated NHC five membered rings is responsible for the stability of these carbenes.[24] *Öfele* and *Hermann* on the other hand, showed that the addition of OsO_4 to the C-C double bond in the ring that little aromatic character exists[25]

(eq. 3). This observation is supported by quantum mechanical calculations of the charge distribution confirming these properties.[26,27]

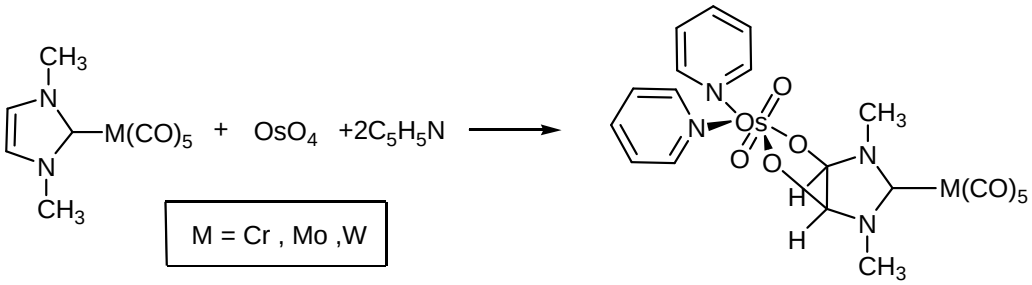

(eq. 3)

1.2.6 Carbenes with π-donor and π-acceptor substituents

(X,Z)-carbenes exist in the singlet state and are best described by the superposition of two zwitterionic structures with a negative charge at the carbene center or as an allene type system. A good example of this type of carbenes are phosphinosilylcarbenes.[28]

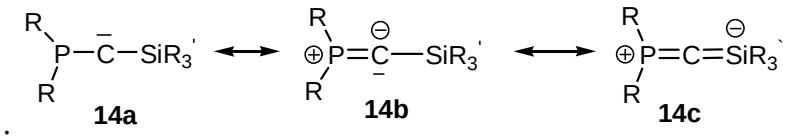

This carbene combines electron donating and accepting interactions (Figure 1.9). The P-substituent lone pair interacts with the empty p_y-orbital of the carbon atom while the Si-substituent vacant orbital interacts with the filled p_x-orbital of carbon. These substituent effects are both stabilizing and favor the singlet state. The vacant p_y-orbital is destabilized while the filled p_x-orbital is stabilized.

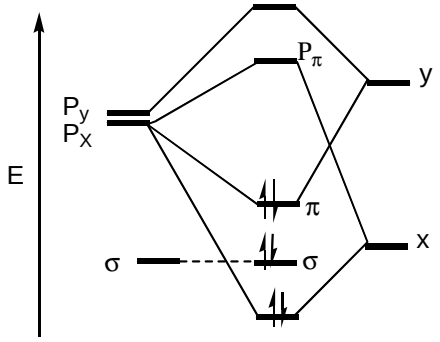

Figure 1.9: Molecular orbital diagram of a (X,Y)-carbene.[17]

1.3 Synthesis of free carbenes

In the early 1960s, *Wanzlick* tried to prepare 1,3-diphenylimdazolidin-2-ylidene **16** from **15** by thermal elimination of chloroform **(**eq. 4**).**[29] The formation of the electron-rich olefin is generally seen in the saturated imdazolium based systems but not in the unsaturated imidazolium systems. The formation of the olefin (dimer) may be indicative that the saturated carbenes are less stable than the unsaturated carbenes. The increased stability of the unsaturated carbenes is likely due to the stabilization of the p(π) orbitals by the aromatic π system.[7]

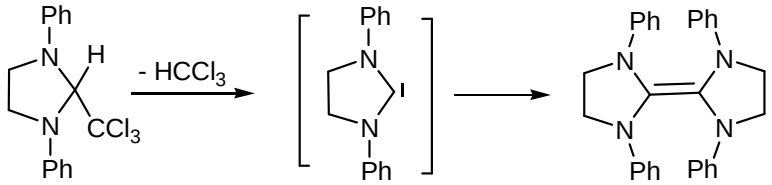

15 **16** **17**

(eq. 4)

At that time, only the dimeric electron rich olefine **17** was isolated and cross coupling experiments did not support an equilibrium between **17** and two carbene units of **16**.[30] In 1970 *Wanzlick* and coworkers demonstrated that the imidazolium salt **18** could be deprotonated by potassium tert-butoxide to afford the corresponding imidazole-2-ylidenes **19** which were not isolated, (eq. 5)[31] but allowed to react with phenylisothiocyanate to give the betaine **20**. The analogous reaction of **21** with mercury chloride results in the formation of the mercury carbene complex **23** (eq. 6).[32]

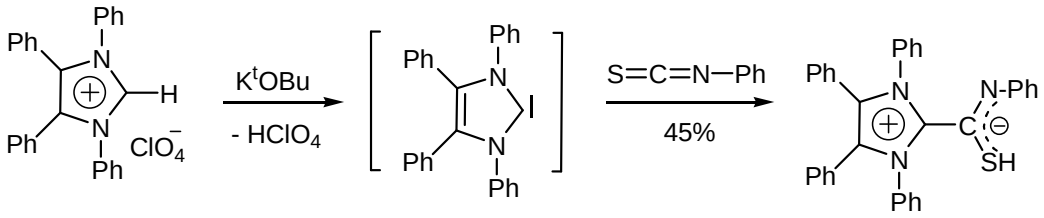

18 **19** **20**

(eq. 5)

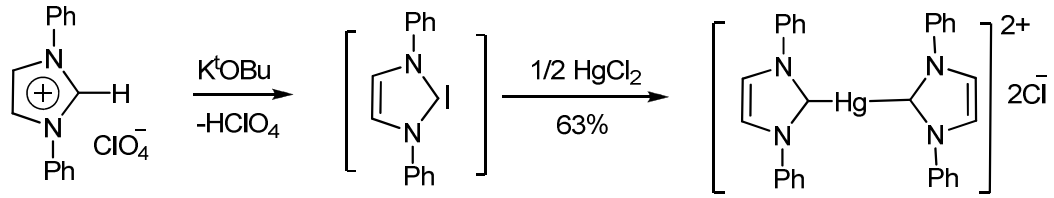

21 **22** **23**

(eq. 6)

However, in none of these examples the free carbene has been observed or isolated, respectively. The first isolated crystalline carbene was obtained by *Arduengo* et al. in 1990 (eq. 7)[7] Compounds **25** was synthesized by deprotonation of 1,3-di-adamantylimidazolium chloride **24** with sodium or potassium hydride, respectively, in dimethylsulfoxide. The colorless crystals of **25** are airstable and melt at 240-241°C. The free NHC has been characterized by a variety of spectroscopic methods.

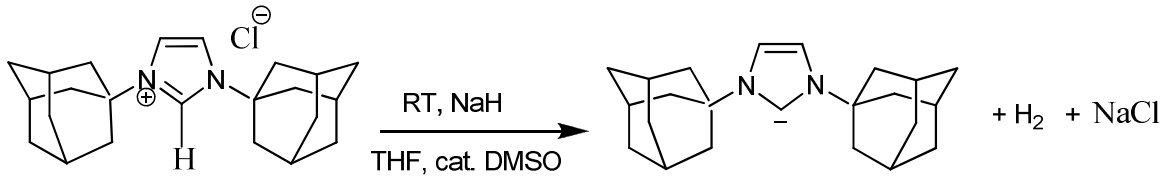

24 **25**

(eq. 7)

Hermann and coworkers [33] showed that the deprotonation of imidazolium salts like **26** with NaH occurs much faster in liquid ammonia. Carbenes with functional groups like e.g. alkoxy groups, amino groups or phosphanido groups (**27d-f)** as well as chiral carbenes like **27g** and bis-imidazol -2-ylidenes like **27h** have been prepared following this procedure (eq. 8).

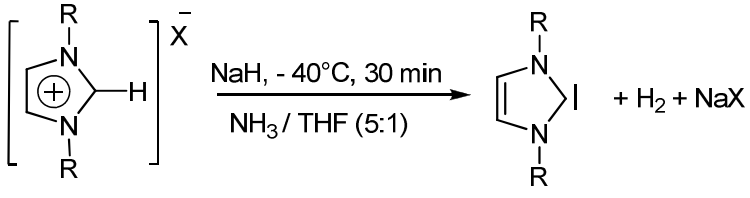

26 **27d- F**

R= CH_3, O-C_6H_{11}

(eq. 8)

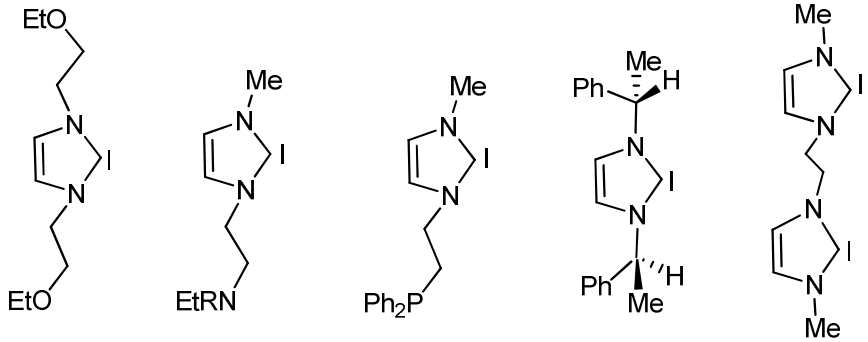

27d **27e** **27f** **27g** **27h**

R= H, Et

In 1993 *Kuhn* and co-workers developed a new and versatile approach to alkyl substituted NHCs.[34] In the first step they reacted the N,N-dialkylthioureas **29a-c** with 3-hydroxyl-2-butanone **28** to yield imidazole-2(3H)-thiones **30a-c** in high yield. The latter were reduced with potassium in boiling THF yielding the carbenes **31a-c** (eq. 9).

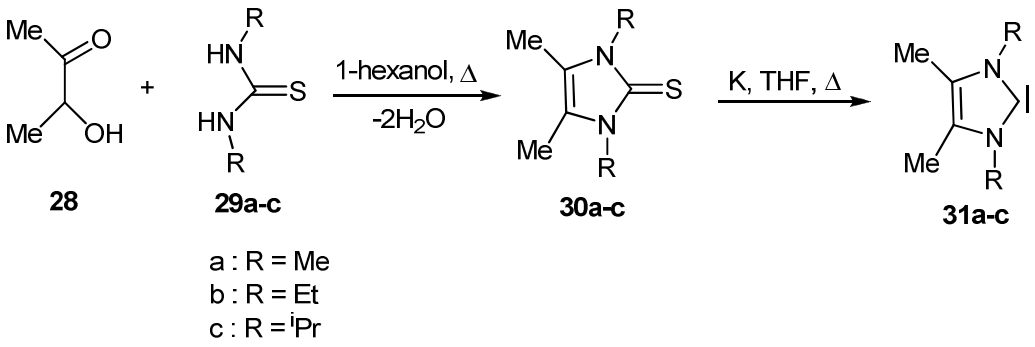

28 **29a-c** **30a-c** **31a-c**

a : R = Me
b : R = Et
c : R = ^{i}Pr

(eq. 9)

In the same year *Arduengo* isolated and characterized the saturated carbene **33** by deprotonation of the imidazolium salt **32** with potassium hydride in THF at room temperature (eq. 10).[13]

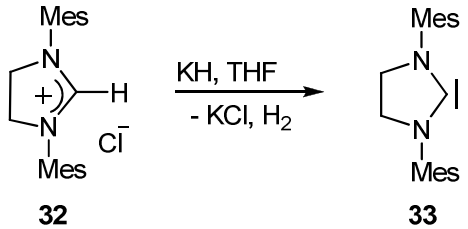

32 **33**

(eq. 10)

In 1995 *Enders* et al. developed another synthetic method for the preparation of NHCs. 1,2,4-triazol-5-ylidene **35** was obtained from the corresponding 5-methoxy-1,3,4-triphenyl-4,4-dihydro

-1,2,4-triazole **34** by thermal elimination of methanol at 80° C under reduced pressure (0.1 mbar) (eq. 11**)**.[35] Compound **35** became the first carbene to be commercially available.

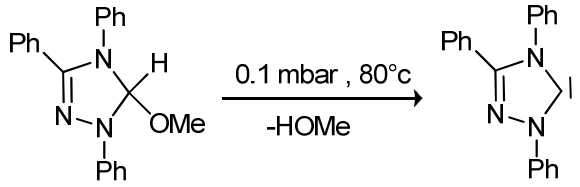

34 **35**

(eq. 11)

Following the above described synthetic routes many different types of stable amino-carbenes like imdazolidin-2-ylidenes **36,**[36] tetrahydropyrimid-2-ylidene **37,**[37]. Imidazol-2-ylidenenes **38,**[7,33,38-41], 1,2,4-triazol-5-ylidenes **39**[36], 1,3-thiazol-2-ylidenes **40**,[42] as well as acyclic diamino-**41**,[14,43] aminooxy **42**,[44] and aminothiocarbenes **43**[46] have been isolated (Figure.1.10). In all of these compounds, the carbene center bears two π-donor substituents, of which at least one is an amino group. The superior π-donor ability and therefore the superior stabilizing effect of amino groups has been evidenced experimentally.

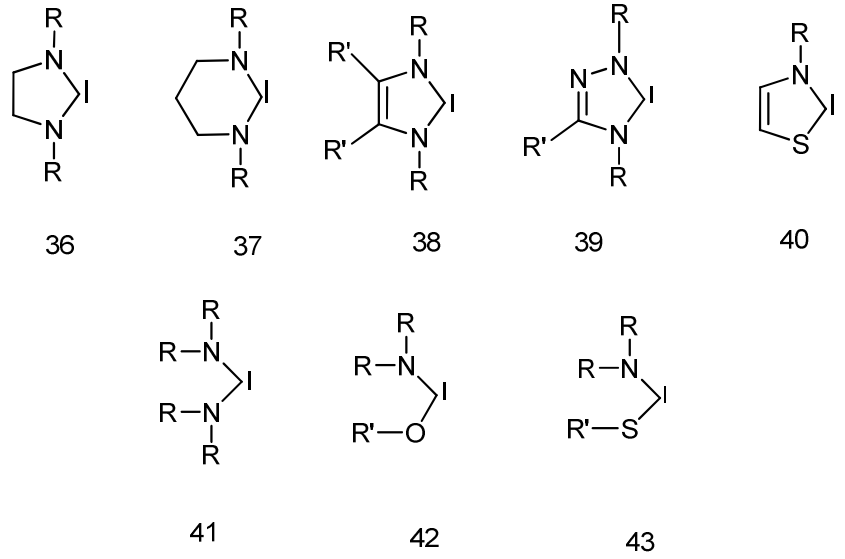

Figure 1.10: N-heterocyclic carbene complexes.[17]

1.4 NHC-Carbene complexes

1.4.1 Classification of *Fischer* and *Schrock*-Carbene Complexes

Carbene complexes have been divided into two types according to the nature of the formal metal-carbon double bond.[45] The molecular orbital diagrams in (Figure 1.11)[46] depict the bonding of *Fischer* (I)-and *Schrock* (II)-carbenes. In *Fischer* type carbene complexes a singlet carbene ligand binds to the metal. Therefore *Fischer* carbenes like **45**[4] (Figure 1.12) are linked to the metal with a σ-bond and have an empty p-orbital which is capable to accept electron density from the metal. Hence the carbene atom is an electrophile. At least one organic substituent of the carbene atom is able to act as a good π-donor. Consequently the empty p-orbital of the carbene atom is stabilized by significant π-contribution from both the substituents and the metal. However, good π-back-donation from the metal to the empty p-orbital of the carbene is critical. In order to be a good π-donor the transition metal in *Fischer* carbene complexes like **45** (Figure 1.12) must belong to the late transition metals and it should be preferably in a low oxidation state.

In *Schrock* type carbene complexes[47] a triplet carbene ligand binds to the metal. *Schrock* carbene ligands have nucleophlic character and tend to bind well with early transition metals in high oxidation states. Better π-donation from the filled p-orbital of the carbene to the d_{π}-orbital of the metal is achieved if the d-orbitals are empty thereby reducing electron repulsion in the overlapping orbitals. Good organic substituents for *Schrock* carbenes no π-donor functions, such as alkyl groups. Due to the presence of two π-donor substituents at the carbene center the N-heterocyclic carbene complexes are similar to *Fischer*-type compounds, however imidazoline-2-ylidenes bind to transition metals through σ-donation, π-backbonding being negligible. N-heterocyclic carbene complexes (III) are also depicted in Figure 1.11. The stability of an NHC is largly due to the π-donation from the p-orbitals of the adjacent nitrogen atoms to the empty p-orbital of the carbene. Due to that the electron density around the carbene atom increases and the σ-donating ability of the carbene ligands tends to increase the electron density at the metal center as shown in (Figure 1.11).[48]

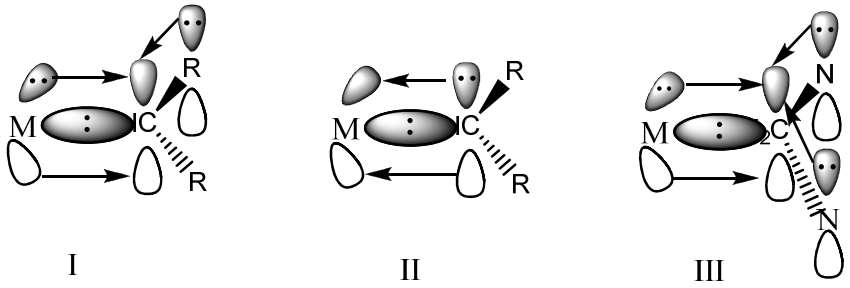

Figure 1.11: Orbital diagrams of a *Fischer*-(I), *Schrock*-(II), and N-heterocyclic carbene complexes (III) fragment [46]

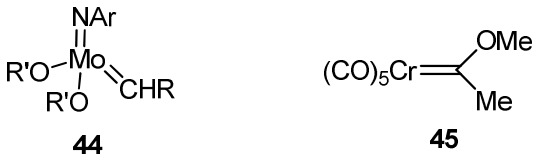

44 **45**

Figure 1.12: *Schrock* (**44**) and *Fischer* (**45**) carbene complexes

1.4.2 Comparsion between NHC-ligands and phosphine ligands

NHCs act as nucleophilic two electron donor ligands that can substitute classical $2e^-$donor ligands such as amide, ethers and phosphines in coordination chemistry.[25,33,49-56] Experimental studies in 1993 have demonstrated that NHC show bonding properties similar to those of trialkyl phosphines and alkyl phosphinites.[57] *Nolan* et al. concluded from structural and thermodynamical studies that generally NHC ligands are far better donor ligands than phosphines and phosphinites.[58] Several advantages are gained in using NHC rather than phosphine analogues. These include high M-L bond strengths compared to phosphine ligands.[58,59-63] This property appears to foster higher ligand stability even under oxidizing reaction conditions (eq. 12).

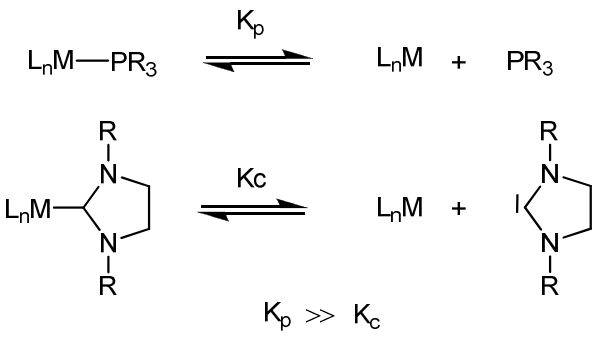

(eq. 12)

Measurements of the carbonyl stretching frequencies of $Ni(CO)_3L$ have revealed that NHC carbonyl complexes have lower C-O stretching frequencies than their phosphine counterparts.[59,63-65] These data which have been confirmed by other studies suggest that NHCs are stronger σ-donors than even the most basic tertiary phosphines.[36] Due to this strong σ-donor character NHCs also stabilize metals in high oxidation states and their high M-L bond dissociation energy renders them less susceptible to oxidative decomposition

.

1.5 Synthesis of imidazolium salts as educts for the preparation of free NHC ligands and NHC complexes

There are three different routes to synthesize unsaturated imidazolium salts. The first route (eq 13) involves a reaction between potassium imidazol **46** and a primary halide to give the substituted imidazol **47**, followed by a second addition of a primary halide to yield the imidazolium salts **48**.[66-68]

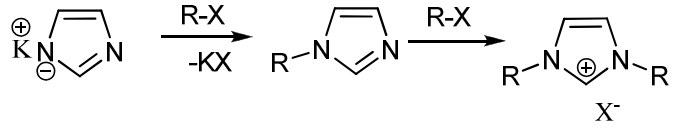

46 **47** **48**

(eq. 13)

The second route (eq.14) involves a reaction between the trimethylsilyl-substituted imidazole **49** and two equivalents of a primary alkylchloride. The trimethylsilyl group is replaced, forming the volatile trimethylsilylchloride and the alkyl substituted imidazolium salt **50**.[69]

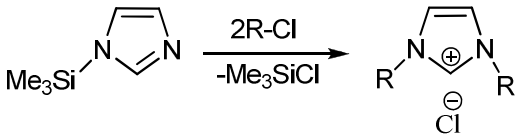

49 **50**

(eq. 14)

In order to introduce a bulky substituent group at the nitrogen atoms of the ring, a reaction between two molecules of primary amines, glyoxal and formaldehyde in the presence of hydrochloric acid is carried out. The straightforward reaction and is depicted in (eq 15).[6,54,70]

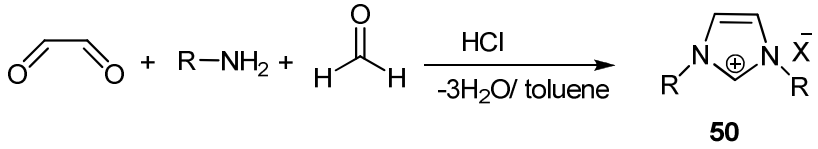

(eq.15)

A combination of the previous two methods allows the synthesis of bulky imidazolium salts by firstly preparing a substituted imidazole through the formaldehyde/glyoxal route in the presence of ammonium salt and a subsequently alkylation using a primary alkylhalide giving unsymmetrically N-substituted derivatives (eq.16).[71]

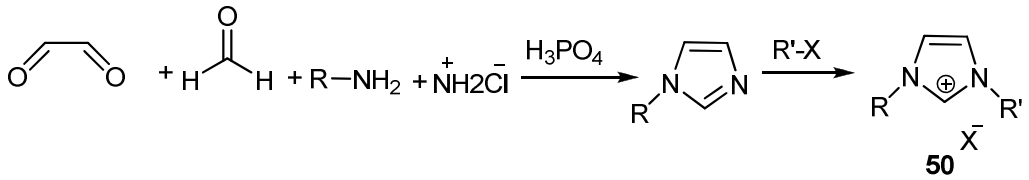

(eq 16)

By use of this route a potentially bidentate imidazoilum salt were synthesized through the reaction of two equivalents of the alkylimidazol **51** with methylene iodide to yield the bis imidazolium iodides **52** (eq. 17).

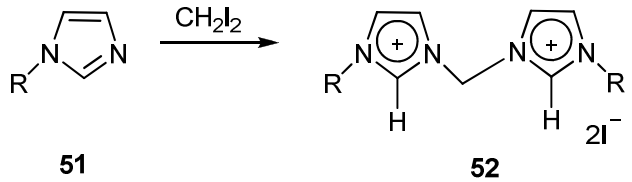

(eq. 17)

N-arylimidazoles are synthesized by reaction of aryl halide **53** and imidazole **54** in the presence of the catalyst $(CuOTf)_2.PhH$ and the base Cs_2CO_3 to yield an arylsubstituted imidazole **55** followed by alkylation (eq. 18).[73]

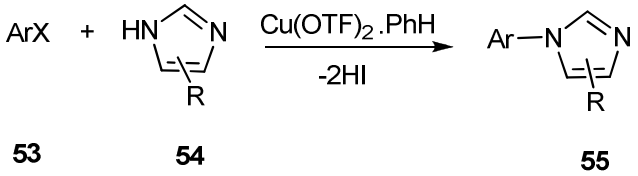

(eq. 18)

A reaction between a secondary diamine **56** and triethylorthoformate **57** in the presence of

1 equivalent of ammoniumtetrafluoroborate at 120°C leads ring closure to give imidazolium salts like **58** (eq.19).[73,74]

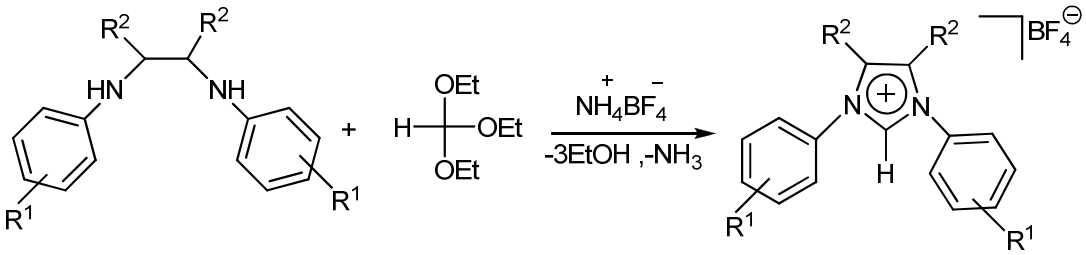

56 **57** **58**

(eq. 19)

1.6 Synthetic routes to N-heterocyclic carbene complexes

In the literature many methods have been described to prepare NHC-metal complexes. They vary with the metal center of interest. NHCs can be introduced as imidazolium salts, as free carbenes or via transmetallation routes. The most important synthetic approaches are given below.

1.6.1 Substitution reactions with free NHCs

Generation of a free NHC succeeds by deprotonation of an imidazolium salt precursor **59** with a strong base such as hydride,[8,75] alkoxide,[53] Na / liquid NH_3[33b] (eq. 20).

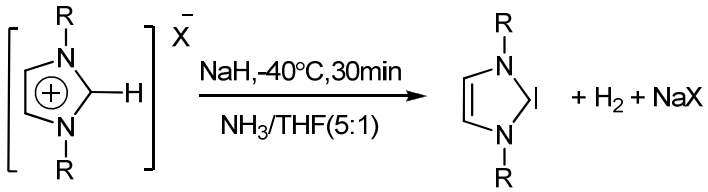

59 **60**

(eq.20)

The resulting imidazol-2-ylidenes **60** can be reacted with many metal metal complexes replacing another two-electron donor ligand (e.g. CO, CH_3CN, phosphane, thioether etc) giving a substitution product (eq. 21).[50,76,77]

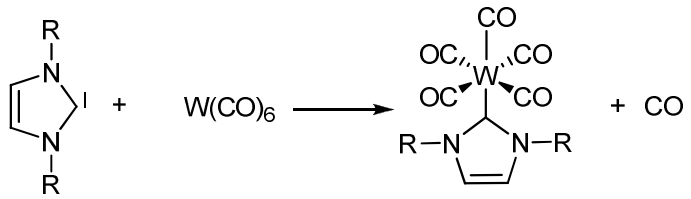

61

(eq.21)

Substitution of two phosphane ligands by two NHC ligands in *Grubbs'*catalyst.The resulting product is catalytically inactive as the NHC ligands does not dissociate at all (eq. 22).[78]

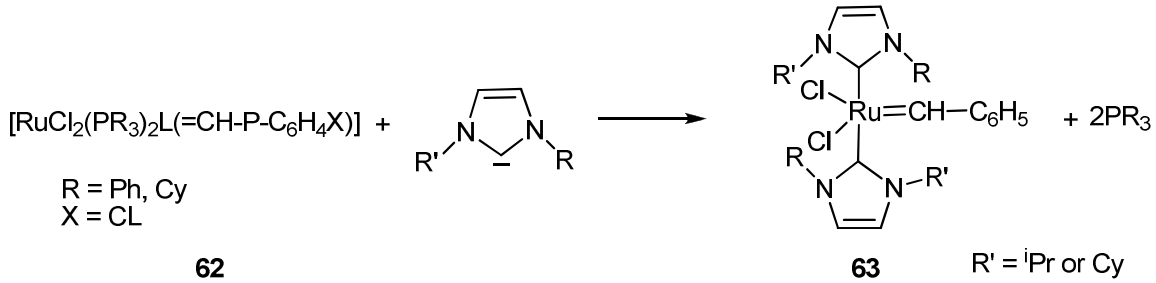

62 **63**

(eq.22)

Deprotonation of 2,6-bis(arylimidazolium)pyridine **64** with $KN(SiMe_3)_2$ gave the pincer carbene ligand **65** which was reacted with $RuCl_2(PPh_3)_3$ to give the ruthenium pincer complex **66** which shows catalytic activity with respect to transfer hydrogenation of carbonyl compounds (eq. 23)[79]

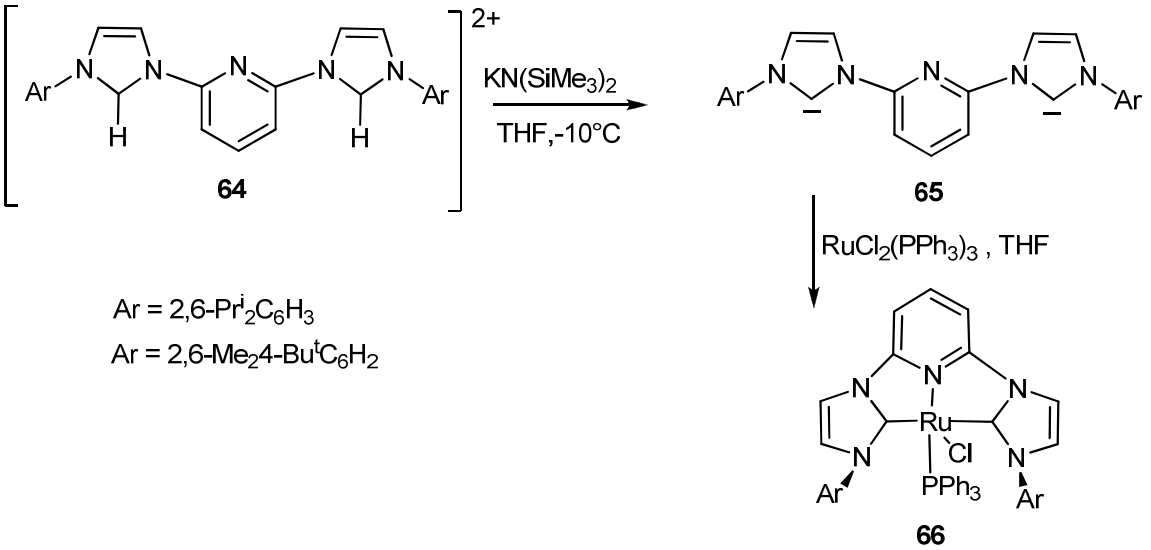

64 **65** **66**

(eq. 23)

1.6.2 Reaction of imidazolium salts with metal complexes comprising basic ligands

The NHC ligand can be generated by deprotonation of an imidazolium salt with a basic ligand coordinated to a transition metal. In many of these cases the free base (e.g. alkoxide, acetate, acetylacetonate etc) would not be able to deprotonate the imidazolium salt. Hence, the metal to which it is coordinated to catalyses the deprotonation and traps the the liberated NHC by coordination.

In a typical reaction *Herrmann* et al. synthesized a rhodium NHC-complex by reacting $[Rh(COD)(\mu\text{-}OEt)]_2$ with an imidazolium salt giving the novel complex **67** (eq. 24).[80]

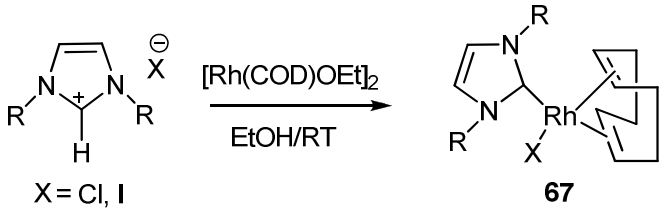

(eq. 24)

Light and coworkers prepared an iron (II) pincer-NHC-complex **69** by direct metallation of $[Fe(N(SiMe_3)_2]_2$, which is an active catalyst for polymerization, C-C bond formation or oxidation reaction (eq.25).[81]

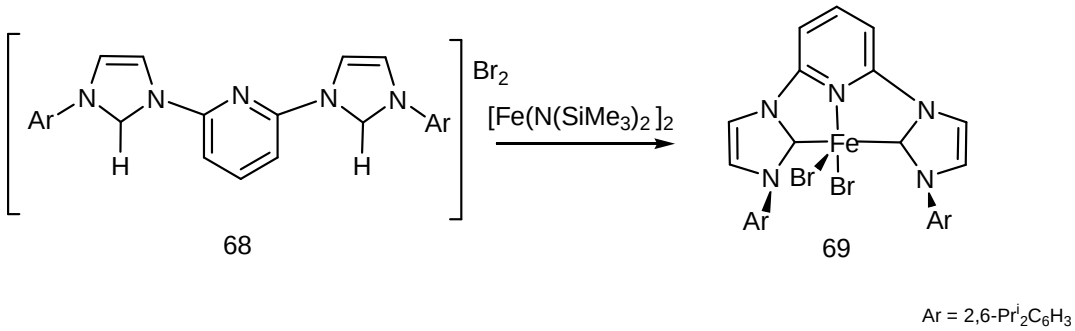

(eq. 25)

1.6.3 Reaction of transition metal complexes with electron rich olefines

This method was introduced by *Lappert*. The reaction of electron-rich olefines like tetraalkyl aminoethylenes with organometallic complexes (eq. 26) gives NHC complexes by insertion of the transition metal into the carbon-carbon double bond. In this way mono-, bis-, tris-, and even tetrakis carbene complexes of various metal have been prepared.[82,83] These examples are shown in Figure 1.13

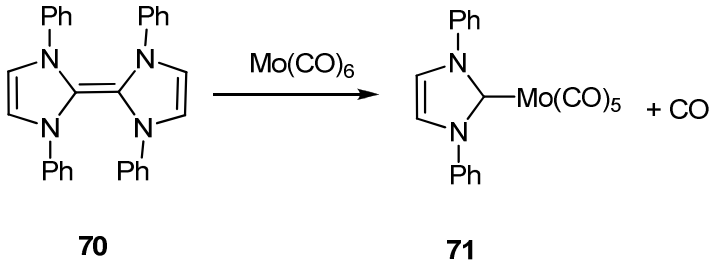

70 **71**

(eq. 26)

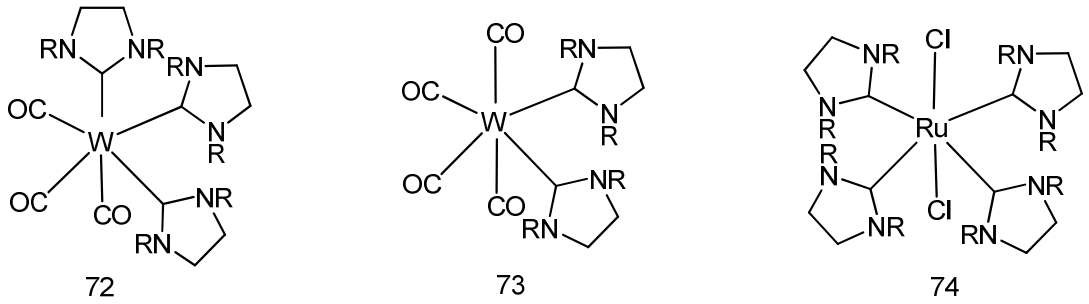

72 73 74

Figure 1.13: bis, tris, tetreakis carbene complexes.

1.6.4 Unusual methods

In a completely new approach a NHC complex was prepared by the deoxygenation of M $(CO)_6$ (M = Cr, Mo, w) with aminophosphine **75** to form the corresponding isocyanide complex **76**, which subsequently underwent intramolecular cyclization to give **77**. The N-H moiety of carbene complex **77** is converted into the alkylated species **78** by treatment of **77**with an excess of sodium hydride followed by an alkylating agent to give the NHC-complex aimed for.[84] This procedure is quite similar to that reported by *Angelici* and co-workers.[85]

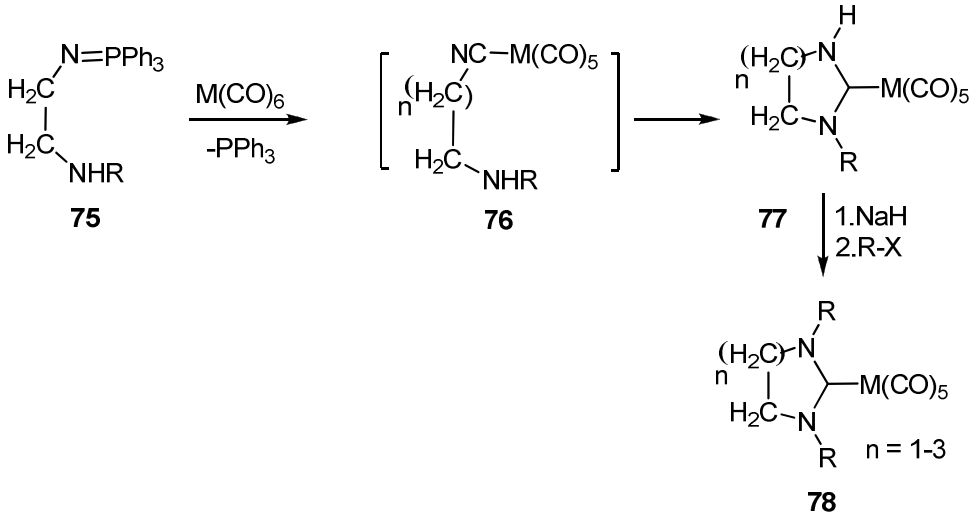

75 **76** **77** **78**

(eq. 27)

1.6.5 Transmetallation reactions

Another synthetic method for the preparation of NHC-complexes is transmetalation of transition metal carbene complexes. A typical example of transmetalation from tungsten to palladium is shown below[86](eq. 28).

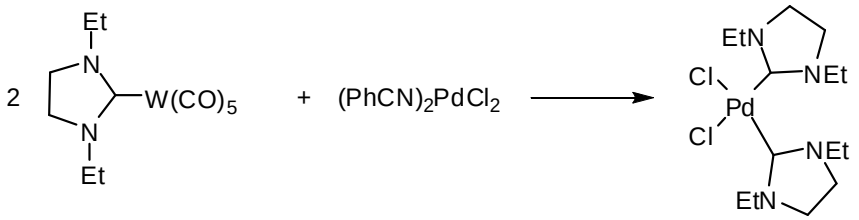

79 **80**

(eq. 28)

Recently, a novel method for preparing NHC metal complexes via silver complexes has been developed by *Lin and Wang*.[87] Silver NHC-complexes are readily prepared upon mixing the corresponding imidazolium salts with Ag_2O in methylene chloride at room temperature as shown in (eq. 29)

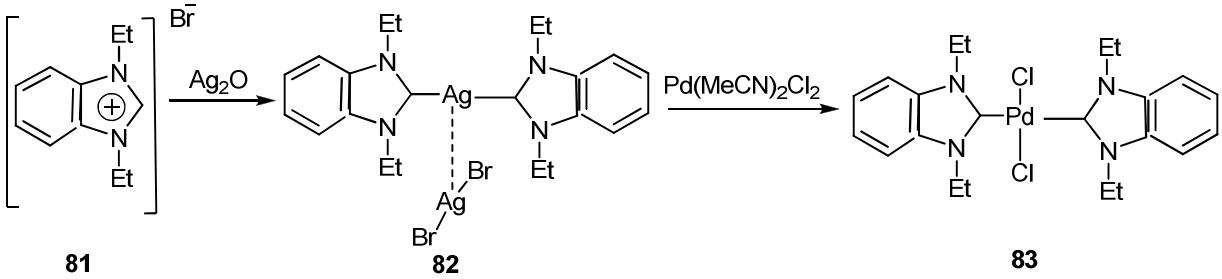

81 **82** **83**

(eq. 29)

Hermann and co-workers[88] synthesized rhodium and iridium complexes of new chiral N-heterocyclic carbene ligands by transmetalation of corresponding silver(I) complexes (eq. 30).

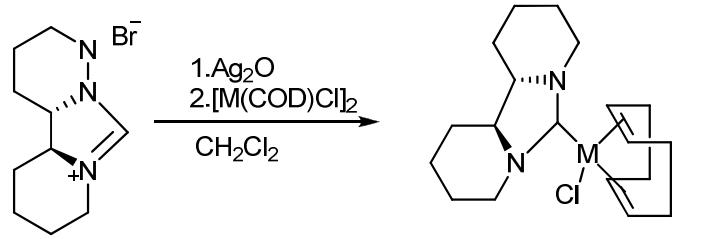

84 **85** M = Rh, Ir

(eq. 30)

Also homoleptic metal carbene complexes **87** were synthesized by co-condensation of metal vapors (group 10) with imidazol-2-ylidene **86** (eq. 31) This synthetic route is straightforward but limited by the experimental conditions.[89]

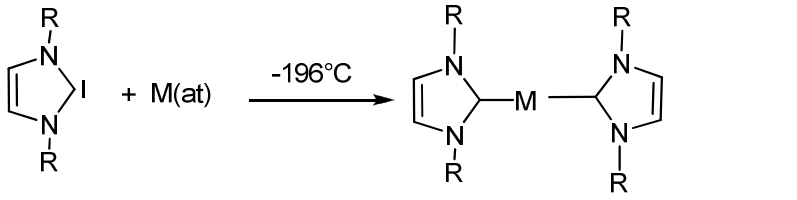

86 **87** M = Ni, Pd, Pt

(eq.31)

Oxidative addition of an imidazolium cation by activation of the C2-X (X = Me, I, H) bond has been achieved with low valent precursors such as $Pt(PPh_3)_4$ giving NHC-complexes.[90,91]. Furthermore *Fürstner* has shown that oxidative addition of *Vilsmaier* salts **88** is a facile and convenient method for the preparation of NHC complexes of Pd **89** (eq. 32).[92]

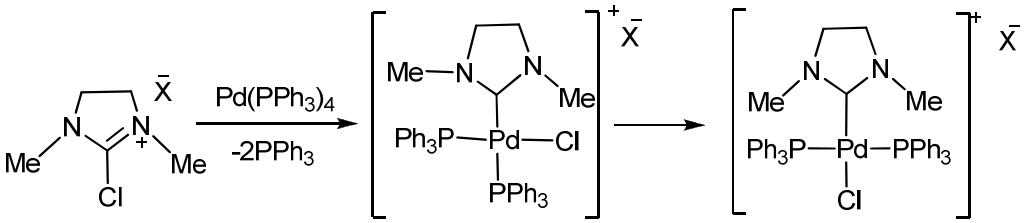

88 *cis*-**89** *trans*-**89**

(eq. 32)

Imidazolium salts react in some cases with strong nucleophiles like $KOBu^t$ by formation of a neutral adduct in which the nucleophile is bonded to the C2 position. These adducts can eliminate alcohol to unmask the carbene, which is then coordinated to the metal center[73] as illustrated in (eq. 33).

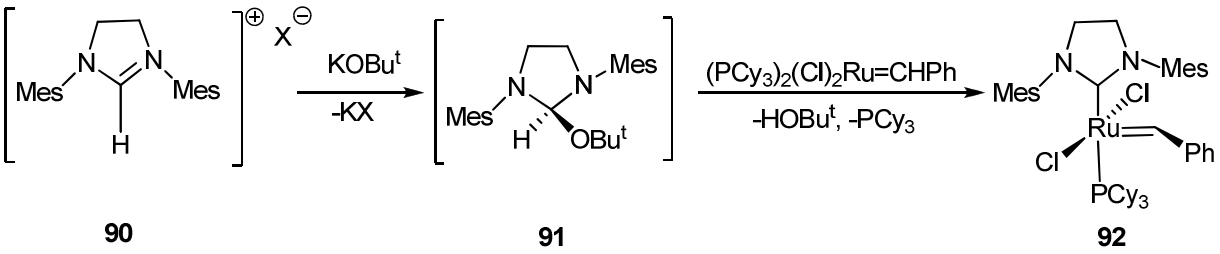

90 **91** **92**

(eq. 33)

1.7 N-heterocyclic carbenes in catalysis

Recentaly, N-heterocyclic carbenes have become a very important class of ligands in organometallic chemistry and catalysis.[93] Their strong σ-donating ability, strong metal-carbon bond and poor π-accepting ability leads to the formation of many stable metal complexes which are good catalysts in numerous organic transformations.[94] The catalytic activity of various rhodium carbene complexes has been investigated by *Nile* in 1977.[95] In 1981 *Lappert* introduced imidazoline-2-ylidene instead of phosphane ligands complexes in catalytically active complexes of rhodium and ruthenium. The first the use of an NHC-ligated complex **93** in the *Mizoroki-Heck* reaction was reported by *Hermann* in 1995 (eq. 34).[96]

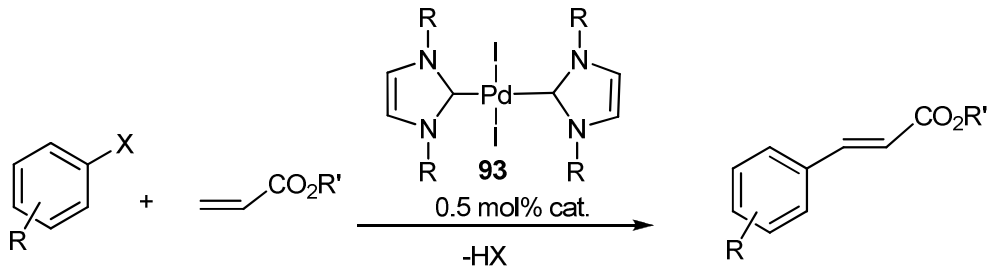

(eq. 34)

Catalysts containing N-heterocyclic carbenes have been employed in a wide variety of reactions[97c-j] including polymerization (e. g. copolymerization of ethylene and CO),[97b] hydrogenation,[23,96a,97] hydrosilylation,[97k-q] hydroboration,[97r] hydroformylation,[97r-u] allylic-

substitution,[97u] methylation, ruthenium catalyzed olefine metathesis, 2,4-transfer hydrogenation reactions and cross coupling reactions to form C-C or C-N bonds.[77b,82,83 98]

1.7.1 Hydrosilylation

Hermann and co-workers synthesized the chiral rhodium carbene complex **94** which was applied as a catalyst in the asymmetric hydrosilylation of acetophenone according to (eq. 35).[99] Compared to standard hydrosilylation catalysts (e.g. H_2PtCl_6 / Ethanol, *Karstedt*'s catalyst) the complex is active without an induction period and even at low temperatures.

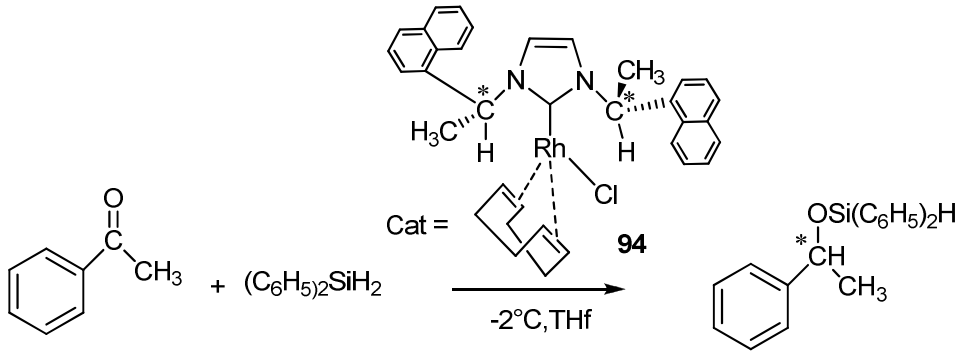

(eq. 35)

1.7.2 Hydrogenation

The rhodium(I) complex **95** containing a pyrazoyl-N-heterocyclic carbene ligand is an efficient catalyst for hydrogenation of styrene (eq. 36).[100]

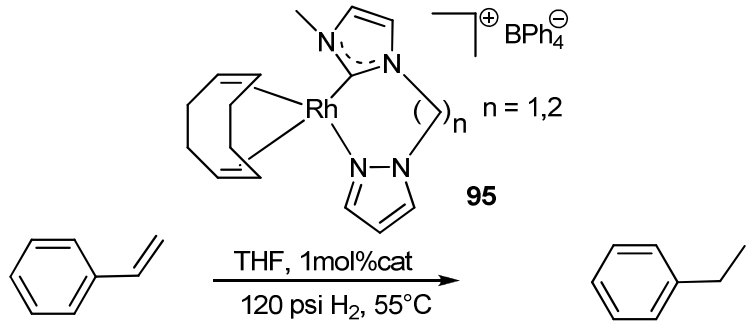

(eq. 36)

1.8 Cross-coupling in homogeneous catalysis

Cross-coupling reactions represent an extremely versatile tool in organic synthesis.[101] Indeed C-C, C-N bond formations are the key steps in a wide range of preparative organic reactions. From the synthesis of natural products[102] to supramolecular chemistry and material science, various frequently used cross-copuling reactions are mediated by palladium catalysts (Figure 1.14).[103]

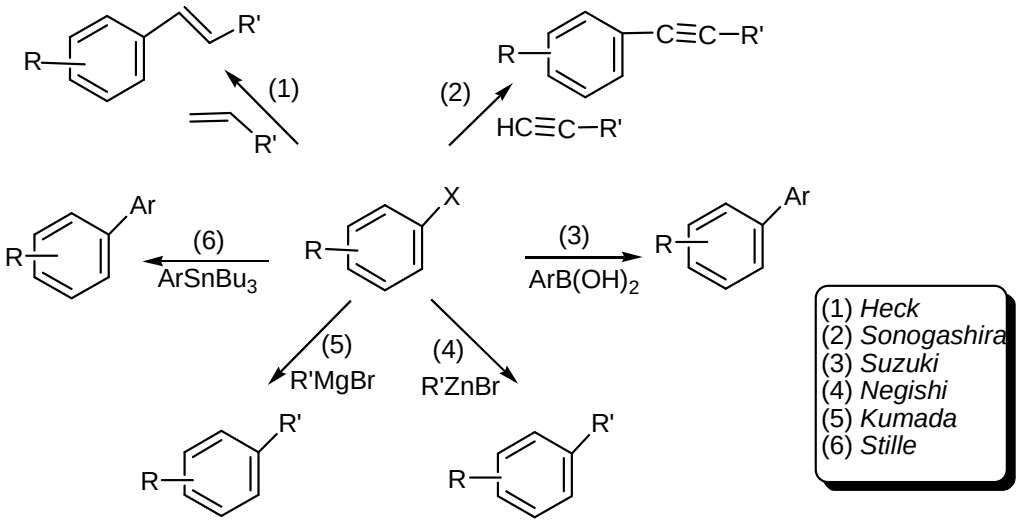

Figure 1.14: Principle of palladium catalyzed cross-coupling reactions (X = I, Br, Otf, Cl, F).[103]

For several years aryl bromides and iodides were preferably used as substrates in such reactions. The far more readily available and industrially important aryl chlorides are transformed very sluggishly by standard palladium catalysts. The problem with aryl chlorides is the strength of the C-Cl bond, which impedes the oxidative addition to 14 e^- Pd (0)-phosphine complexes.

The mechanism of palladium cross-coupling reactions is shown in Figure 1.15. A zero valent palladium species, stabilized by electrondonating and/or bulky ligands, undergoes oxidative addition with an aryl halide to afford a Pd(II)(Ar)(X) complex. Ar-M then effects transmetallation with this species removing the halide as MX to afford a Pd(Ar)(Ar') intermediate, which undergoes a reductive elimination to couple the two aryl moieties and regenerate the palladium (0)species.

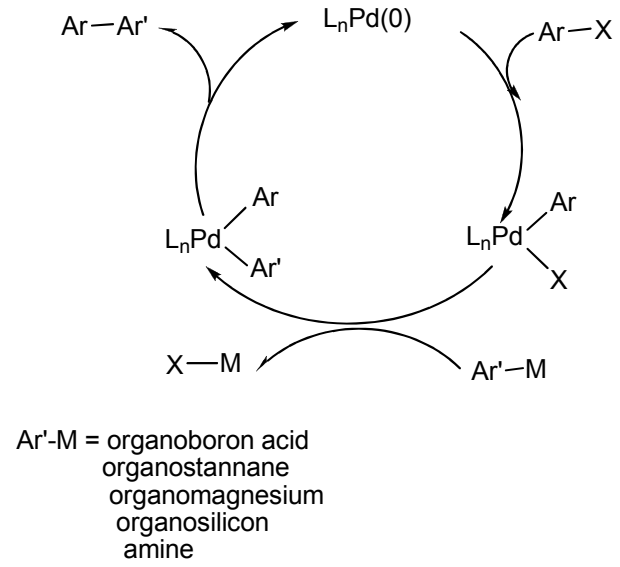

Figure 1.15: Simplified catalytic cycle for palladium mediated cross-coupling reactions**.**

1.8.1 *Sonogashira* coupling.

This coupling reaction proceeds with terminal alkynes and aryl halides or vinyl halides. As an example the palladium(0) species **96** which is also active in *Heck* and *Suzuki* C-C coupling, is employed in a *Sonogashira* type coupling to make the bromo-enyen **97**, a common building block for natural products (eq. 37).[104]

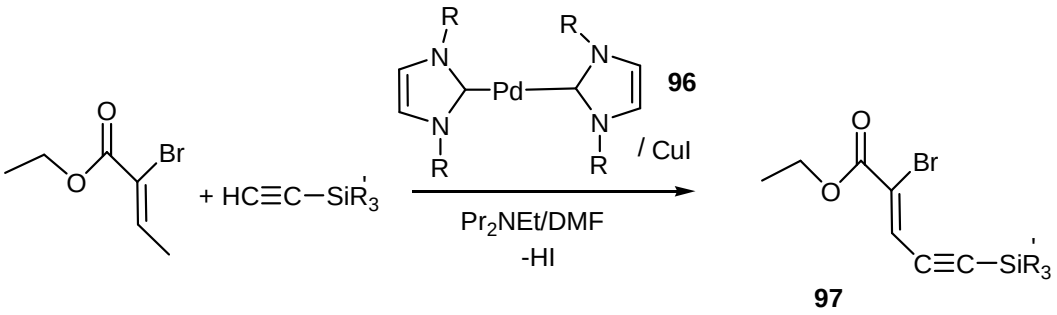

(eq. 37)

Copper free conditions were reported for the *Sonogashira* coupling of aryl bromides with alkenylsilanes Pd $(OAc)_2$.[105]

1.8.2 *Kumada* coupling (*Grignard* cross-coupling)

The coupling of aryl *Grignard* reagents with aryl halides, triflates or ethers which is catalysed by nickel[106] or palladium,[107] is one of the earliest methods of the catalytic synthesis of unsymmetrical biaryls. The coupling of aryl chlorides as sketched in (eq. 38) is afforded by a NHC-catalyst of nickel. The latter is generated *in situ* from $Ni(acac)_2$ and imidazolium salts. Catalysts like **98** or **99** effect the C-C coupling even at room temperature (3 mol% Ni).

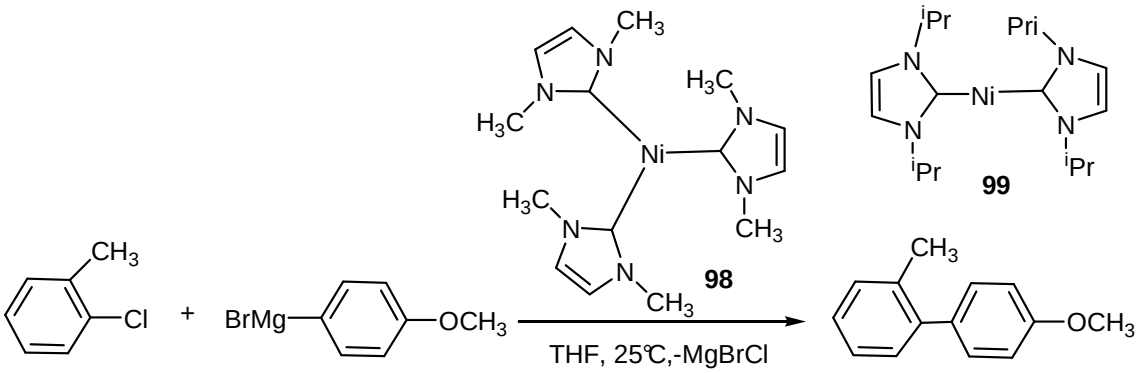

(eq. 38)

1.8.3 *Stille* coupling

For the palladium catalyzed cross-coupling of organostannanes and aryl halides or sulfonates (eq. 39) traditionally triaryl or trialkyl-phosphine ligands have been used.

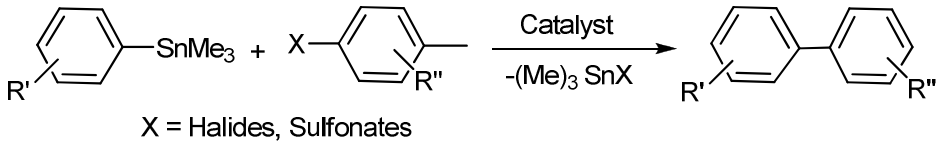

(eq. 39)

Mixed NHC complexes of palladium like **100** are the most active catalysts in *Stille* reactions. They are even able to couple 4-bromoacetophenone and phenyltributylstannane in toluene without any promoting additives.[108]

Nolan and co workers have shown that the Pd $(OAc)_2$/imidazolium chloride system mediates the catalytic cross coupling of aryl halides with organostannanes[109] The imidazolium salt **101** in combination with $Pd(OAc)_2$ and TBAF(tetrabutyammonium fluoride) was found to be most effective for the cross coupling of aryl bromides and electron deficient aryl chlorides with aryl and vinyl stannanes.

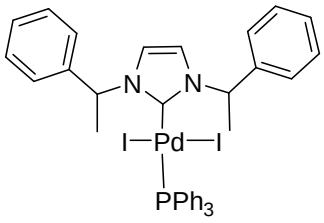

100

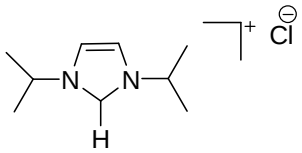

101

1.8.4 *Heck* coupling

Hermann and co-workers[110] reported NHC coordinated metal complexes for the first time in *Heck* coupling for aryl chlorides and aryl bromides with n-butyl acrylate (eq. 40). The catalysts used for these transformations contain the monodentate and bidentate NHC ligands **102**, **103** as shown in Figure 1.16. The work also demonstrated that the active catalyst can be generated *in situ* using $Pd(dba)_2$ and the imidazolium salt 1,3-dimethylhydroimidazole-2-ylidene. Turnover numbers as high as 250,000 have been observed for these *Heck* reactions with the NHC containing catalysts.[110] Palladium catalysts used in *Heck* reactions have also been applied in other cross coupling reactions.

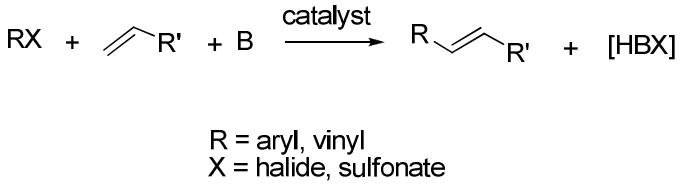

(eq. 40)

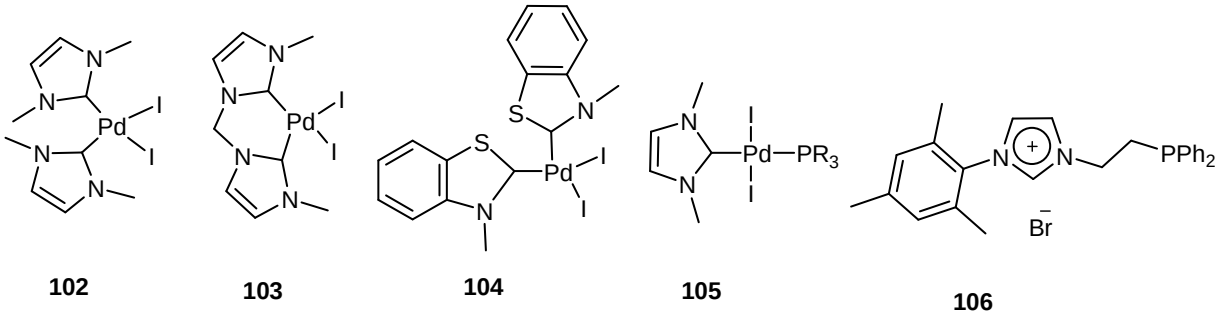

102 **103** **104** **105** **106**

Figure 1.16: some example of Pd(II) complexes which used in *Heck* reaction.

1.8.5 *Suzuki* coupling

The coupling of organoboron derivatives with aryl, vinyl or alkyl halides or sulfonates (eq. 41) has emerged as one of the most important carbon-carbon bond forming methods in the synthesis of pharmaceutical agents, organic materials and natural products.[111] The air and moisture stability of aryl boronic acids make this reagent particularly attractive when compared to *Stille* (aryl stannanes) and *Kumada* (aryl *Grignard)* reagents. Traditionally monodentate phosphine ligands have been used for the palladium catalyzed.*Suzuki* coupling of aryl chlorides is accomploished with sterically crowded, electron rich phosphines.[102,112] Recently NHCs have been used as ligands for a varity of transition metal–catalysed cross-coupling reactions including the *Suzuki* reaction.[83]

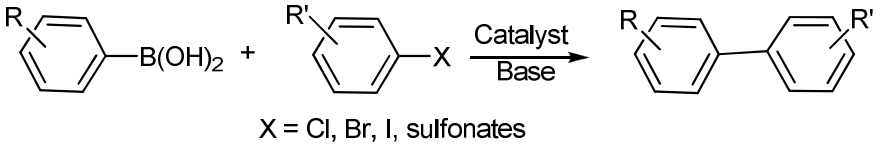

(eq. 41)

Caddick, *Cloke* and co-workers have shown that the use of a palladium/imidazolium salt system like pd(dba)$_2$/N,N-di-(2,6-diisopropylphenyl) imidazolium chloride(^{i}pr•HCl) **107** in the presence of KOMe at 40°C and tetra-n-butylammonium bromide as a co-catalyst acts as highly efficient catalyst in *Suzuk*i reactions.[113] The synthesis and catalytical application of air and moisture stable (NHC)Pd(η^3-C_3H_5)Cl **108** was reported by *Nolan* and co-workers. This catalyst has proven to be highly active for *Suzuki* cross coupling of activated and unactivated aryl chlorides and bromides, but a high reaction temperature was required to achieve acceptable yield.[114] *Lebe*l et al. found that N,N-di-(2,4,6-trimethylphenyl)-imidazolyidene (Imes, **109**) also works as an effective supporting ligand in *Suzuki* cross coupling reactions, but again high reaction temperatures were required.[115]

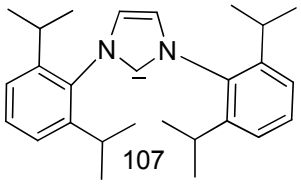

107

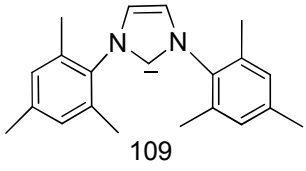

109

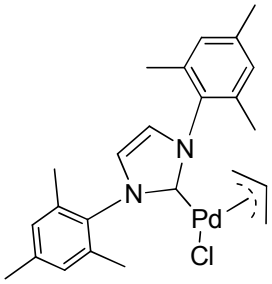

108

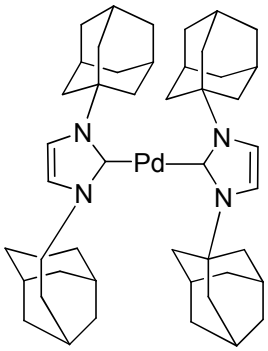

110

The use of the bis-NHC Pd(0) catalyst **109** by *Hermann* et al. was shown to be very efficient for the room temperature cross coupling of both electron-rich and electron-poor aryl chlorides with phenyl boronic acid. The extremely efficient reactions are generally completed in 20 minutes to a few hours with high yields. The combination of $Pd(OAc)_2$ or $Pd(dba)_2$ with imidazolium salts as ligand precursors allows for *in situ* generation of the active catalyst for *Suzuki* cross couplings of aryl chlorides with aryl boronic acids.[98d]

The Palladium/imidazolium salt system like Pd(0)/Ipr·HCl **96** or Pd(II) Imes·HCl **111** were found to be efficient in mediating the *Suzuki* cross coupling of aryl chlorides and aryl triflates[116] with various arylboronic acids. In this case electron rich and electron poor aryl chlorides as well as sterically hindered substrates are converted in high yield under moderate reaction conditions.

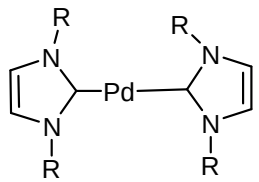

96

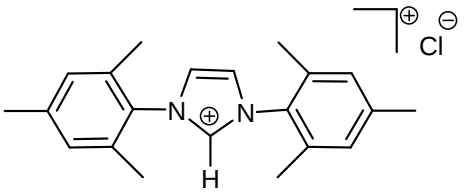

111

Glorius and co-workers[117] reported a *Suzuki* reaction for hindered and unhindered activated and deactivated aryl chlorides with aryl boronic acids at room temperature. They used compound **112**

which is a carbene ligand derived from a bisoxazolin system and $Pd(OAc)_2$. The mixture acts a highly efficient catalyst. The activity of this system was attributed to the steric flexibility of the carbene ligand. For the first time di- and tri-ortho-substituted biaryl compounds were formed under the reaction conditions and high turnover numbers were obtained *Nolan* and co-workers have combined the use of highly electron donating and sterically demanding NHC ligands with a palladacycle framework in compound **113**. This catalyst displays the ability to cross couple sterically hindered unactivated aryl chlorides with sterically demanding boronic acids at room temperature in very short periods of time to lead to di- and tri ortho-substituted biaryls in high yields.[118]

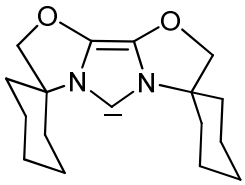

112

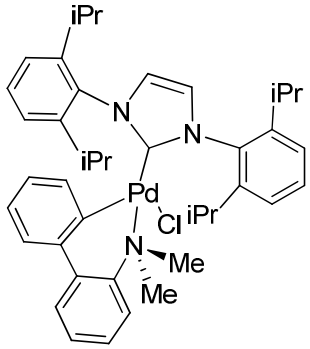

113

The classical mechanism of Pd catalyzed cross coupling reactions (Figure 1.15) involves three discrete steps: oxidative addition, transmetallation and finally reductive elimination. Recently a reinvestigation of these type of reactions has shown that the mechanism is more complicated. Initially a precatalyst like $PdCl_2(PPh_3)_2$ is reduced (either by nucleophiles or by independent reduction) to the catalytically active Pd(0) species to afford the tricoordinated anionic complex $[Pd(PPh_3)_2Cl]^-$ Then oxidative addition of ArX (Ar = aryl) to this intermediate gives a pentacoordinated σ-aryl palladium(II) complex $[PhPdXCl(PPh_3)_2]^-$. Subsequently the chloride ligand is substituted by solvent giving the neutral complex $[PhPdX(Solv)(PPh_3)_2]$. Nucleophilic attack of ArM (M = counter cation associated with the nucleophile used) on the pentacoordinated neutral complex to yields an anionic penta coordintated complex $ArPdX(Nu)(PPh_3)_2^-$, in which Ar and Nu ligands are adjacent and so in a favourable position for fast reductive elimination under formation of the catalytically active complex $Pd^0(PPh_3)_2X^-$, which intiates the next catalytic cycle (Figure 1.16 (main cycle)).

As catalytically reactions proceed halide anions and cations are progressively released due to ArX and Mnu conversion The released ions are free and shall be considered as in (eq. 42), as follow

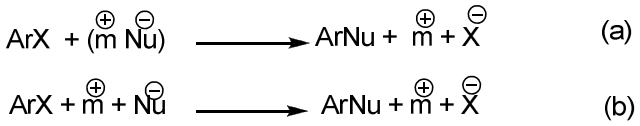

(eq. 42)

Due to this possibility, the nature of the metal cation m plays a crucial role in the overall mechanism by controlling possible comptitation between the main cycle in Figure 1.17 and classical mechanism. When halide ions are free like in (eq. 42) or free halide ions added.$Pd^0L_2X^-$ and $ArPdX(X)L_2^-$ are formed, the main cycle is expected to dominate .how ever the, the situation is not so simple because the classical mechanism and main mechanism interconnected at the level of intermediate $ArPdX(solv)L_2$ The nature of free-ion of nucleophile is also crucial in the selection of mechanisms.when the nucleophile is a free anions, the metal cation has no influence at all except therefore the classical mechanism and new mechanism are finely tuned by the ion-pairing equlibria involving halide anions and metal cations are released while the reaction proceeds.[120]

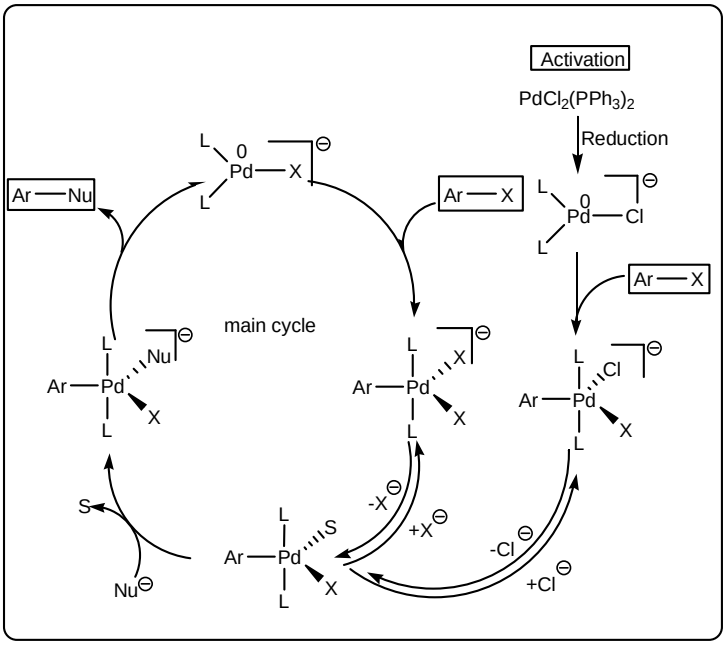

Figure 1.17: New mechanism for palladium catalysed cross-coupling reactions.[120]

2. Aim of work

After the isolation of the first stable carbene by *Arduengo*[7], N-heterocyclic carbenes have become an important class of ligands in organometallic chemistry and homogeneous catalysis These ligands are often compared to tertiary phosphanes in their bonding to transition metals. In general nucleophilic N-heterocyclic carbenes as mimics for phosphanes have attracted a considerable amount of attention. These ligands are strong σ-donors with negligible π-acceptor ability. Phosphanes and N-heterocyclic carbenes and can be combined in bidentate ligands giving chelating ligands with extremely strong bonding properties. These ligands don't dissociate from the metal center, consequently only stoichiometric amounts of these ligands are needed in order to stabilize metal centers even in very low oxidation states. However, research into the organometallic chemistry of mixed bidentate phosphane-NHC donor ligands has been surprisingly limited and the application of metal complexes with mixed phosphane-NHC donor ligands in homogeneous catalysis has not been widely explored. There are examples of palladium catalysed *Heck*,[120] *Suzuki*[121] cross coupling, rections using Pd, Ir[122], Rh[122] and Ru complexes with mixed phosphine-NHC ligands.

According to the introduction NHC-complexes have a great variety and uses. The aim of this work is focused on the following questions:

1. Synthesis of homoleptic metal complexes of Rh(I), Ir(I), and Pd(II) with mixed phosphane N-heterocyclic carbene ligands starting from the imidazolium salts $[EtImCH_2CH_2PPh_2][X]$ (X = I, PF_6) and the metal precursors $[M_2(\mu\text{-}Cl)_2(COD)_2]$ (M = Rh, Ir), and $[Pd(COD)Cl_2]$.

2. Investigation of the reactivity of the Rh(I) and Ir(I)-complexes towards small molecules like O_2, H_2, S_8, CH_3I, I_2, CO. Spectroscopic characterization of the resulting complexes.

3. Survey on the catalytic acivitiy of the Pd(II) complex with respect to *Suzuki*-coupling. Comparison of the catalytic acitivy with standard catalysts.

4. Synthesis of a first example of a homoleptic Nickel complex with mixed phosphane N-heterocyclic carbene ligands.

The main focus of this work lies on the synthesis and characterization of $M(\eta^2\text{-}L)_2$-complexes (M =Rh, Ir, Pd; L = mixed phosphane N-heterocyclic carbene ligand) as described in the list above. All complexes obtained within this work should be characterized by X-ray crystallographic methods and ^{1}H, ^{13}C and ^{31}P-NMR spectroscopy. In addition some of the complexes will be characterized by IR-spectroscopy and cyclovoltammetry.

3. Results and Discussion

3.1 Synthesis of ligand

3.1.1 Ligand precursors 3-[2-(diphenylphosphino)ethyl]-1-ethylimidazolium-hexa fluorophosphate (E6)

In 1996 *Herrmann* and co-workers [33b] first synthesized the ligand precursor **E6** which has the potential to coordinate to a metal center as a mixed bidentate phosphine-NHC ligand. In our group the ligand precursors **E6** was synthesized following on another way in a three steps reaction sequence (Figure 3.1), the first step being alkylation of 1-vinyl imidazole **E1** with an excess of ethyl iodide **E2** under reflux in methylene chloride to give 1-ethyl-3-vinylimidazolium iodide **E3** in good yield after recrystallization from methanol. The second step involves reaction of **E3** with potassium diphenylphosphide which was generated in situ from $KOBu^t$ and diphenylphosphine **E4** in THF under nitrogen atmosphere at ambient temperature. The reaction proceeds via a nucleophilic attack of one of the lone pairs of the phosphorus atom at the vinyl group forming a carbanion which is subsequently protonated by t-butanol affording the ligand precursor **E5** in good yield. Counter ion exchange with hexafluorophosphate is achieved in degassed water. After working up the imidazolium salt **E6** was isolated. Alternatively we have also obtained **E5** by refluxing the reaction mixture for 24h followed by addition of diethyl ether to precipitate **E5**.

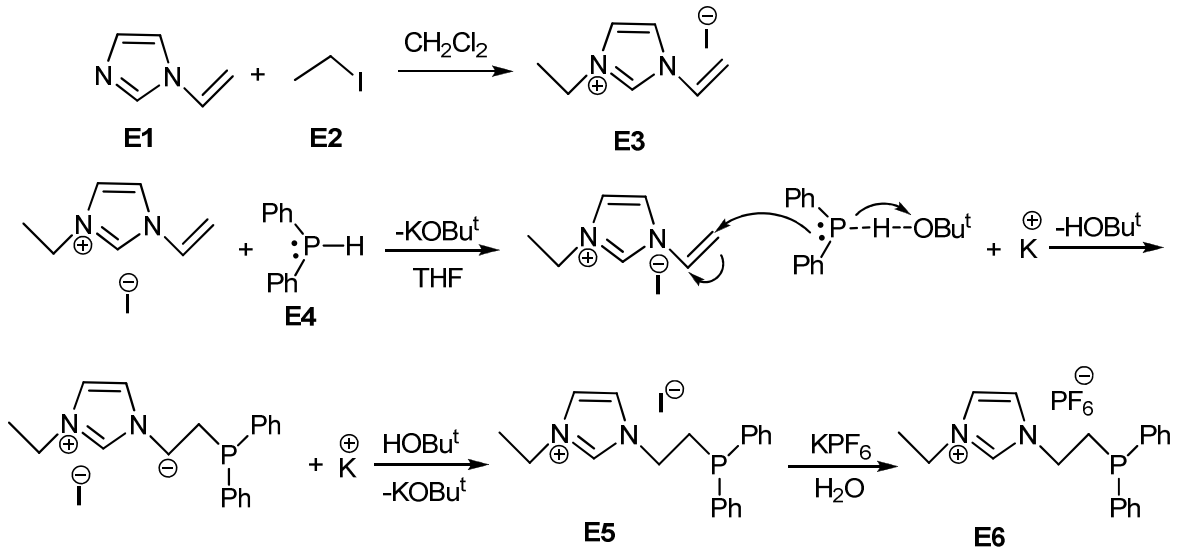

Figure 3.1: Synthesis of 3-[2-(diphenylphosphino)ethyl]-1-ethylimidazolium-hexafluorophosphate.

3.1.2 Properties of the imidazolium salts

The resulting imidazolium salts **E5** and **E6** are white to yellow powders. They are extremely hygroscopic and react with air to form the phosphine oxides. **E5** shows a low solubility in THF while **E6** is very good soluble in that solvent.

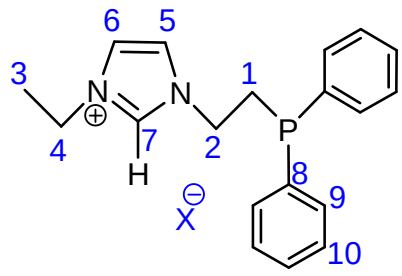

E5, X= I
E6, X= PF_6

The data of the ^{1}H-NMR spectrum recorded in CD_3CN of the imidazolium salts **E5** and **E6** are shown in Table 3.1. As both data sets are similar only the data of **E6** are discussed in detail. **E6** exhibits resonances due to the aromatic protons of the imidazolium ring H^7, H^5 and H^6 at 8.51 (s), 7.39 (t) and 7.31 (m) ppm, respectively. The observed chemical shifts are in good agreement with similar imidazolium salts.[123] The strong deshielding of H^7 is the direct consequence of the positive charge of the imidazolium ring. The protons of the ethylene bridge show resonances at 2.72 (t) for H^1 and 4.32 (td) for H^2, respectively. The lines of the resonance of H^1 are slightly broadened most likely due to coupling with phosphorous. However, this coupling is too weak to determine the exact coupling constant $^2J_{PH}$. The chemical shifts of the ethylene and ethyl protons are in the expected range showing no further specific features.

The ^{13}C resonances of the imidazolium carbon atoms C^7, C^5 and C^6 appear at 134.9, 122.6, 122.1, respectively. The deshielding of C^7 is typical for imidazolium salts and confirms the cationic nature of ring[93a]. The resonances of the carbon atoms of the ethylene bridge are found at 27.9 ppm for C^1 and 47.3 ppm for C^2. The low field chemical shift of C^2 is a result of the high electronegativity of the neighboring nitrogen atom. Both resonances are doublet due to coupling with phosphorous. Interestingly the $^1J_{PC}$ coupling constant (15 Hz) is smaller than the $^2J_{PC}$ coupling constant (25 Hz). This observation is in accordance with the observed HP-coupling constants discussed above. The ^{31}P{1H} NMR spectrum of **E6** exhibits a resonance due to the tertiary phosphours atom at -21.6 ppm as expected for alkyl diaryl phosphines[124] and signal for PF_6^- at -144 ppm which is splited into a heptet with $^1J_{PF}$ = 710 Hz.

Table 3.1: ^{1}H-NMR-spectra of **E5** and **E6** in CD_3CN

	E5		**E6**	
	δ H [ppm]	$^{n}J_{HH}$ [Hz]	δ H [ppm]	$^{n}J_{HH}$ [Hz]
H1	2.78 (t)	$^{3}J_{HH}$ = 8.0	2.72 (t)	$^{3}J_{HH}$ = 7.7
H2	4.35 (td)	$^{3}J_{PH}$ = 9.2, $^{3}J_{HH}$ = 7.8	4.32 (td)	$^{3}J_{PH}$ = 9.5, $^{3}J_{HH}$ = 7.7
H3	1.45 (t)	$^{3}J_{HH}$ = 7.3	1.44 (t)	$^{3}J_{HH}$ = 7.1
H4	4.16 (q)	$^{3}J_{HH}$ = 7.3	4.11 (q)	$^{3}J_{HH}$ = 7.67
H5	7.46 (m)	$^{3}J_{HH}$ = 1.8	7.39 (t)	$^{3}J_{HH}$ = 1.7
H6	7.30 (t)	$^{3}J_{HH}$ = 1.8	7.31 (t)	$^{3}J_{HH}$ = 1.9
H7	8.92 (s)		8.51 (s)	
H9	7.51 (m)		7.47 (m)	
H10	7.49 (m)		7.41 (m)	
H11	7.49 (m)		7.40 (m)	

Table 3.2: ^{13}C-NMR-spectra of **E5** and **E6** in CD_3CN.

	E5		**E6**	
	δ C [ppm]	$^{n}J_{PC}$ [Hz]	δ C [ppm]	$^{n}J_{PC}$ [Hz]
C1	28.0 (d)	$^{1}J_{PC} = 16$	27.9 (d)	$^{1}J_{PC} = 15$
C2	47.4 (d)	$^{2}J_{PC} = 27$	47.3 (d)	$^{2}J_{PC} = 25$
C3	14.5 (s)		14.5 (s)	
C4	44.9 (s)		44.9 (s)	
C5	121.9 (s)		122.6 (s)	
C6	122.4 (s)		122.1 (s)	
C7	135.8 (s)		134.9 (s)	
C8	136.93 (d)	$^{1}J_{PC} = 12$	136.8 (d)	$^{1}J_{PC} = 12$
C9	132.7 (d)	$^{2}J_{PC} = 20$	132.6 (d)	$^{2}J_{PC} = 20$
C10	128.8 (d)	$^{3}J_{PC} = 7.0$	128.8 (d)	$^{3}J_{PC} = 7.5$
C11	129.24 (s)		129.3 (s)	

3.1.2.1 X-ray crystallographic analysis of 3-[2-(diphenylphosphino)ethyl]-1-ethylimidazolium -hexafluorophoshate **(E6**)

Colorless crystals of **E6** were grown by layering of hexane onto a THF solution of **E6**. **E6** crystallized monoclinic in the space group P2(1)/n with four molecules per unit cell. Selected bond lengths and angles are listed in Table 3.3. The molecular structure containing the atom numbering schemes is shown in Figure 3.2. Crystallographic data are presented in the Table 7.1.

E6 contains an imidazole ring which is substituted at both nitrogen atoms. N(1) is bonding to an ethyl group and N(2) is linked to an ethylene group which is bonded to the diphenyl phosphide moiety. The bond lengths within the imidazole ring N(1)-C(1)[1.320(4) Å] and N(2)-C(1)[1.322(4) Å] are identical. The bond lengths of N(1)-C(2) and N(2)-C(3) of 1.378(4) Å and 1.376(4) Å, respectively, are similar to the values reported in the literature.[125]

The bond angles in the imidazole ring N(1)-C(1)-N(2) [109.1(3)°], C(3)-C(2)-N(1) [107.3(3)°], C(2)-C(3)-N(2) [106.9(3)°], C(1)-N(1)-C(2) [108.2(3)°] and C(1)-N(2)-C(3) [108.5(3)°] are similar to those reported in the literature.[40a,126,127]

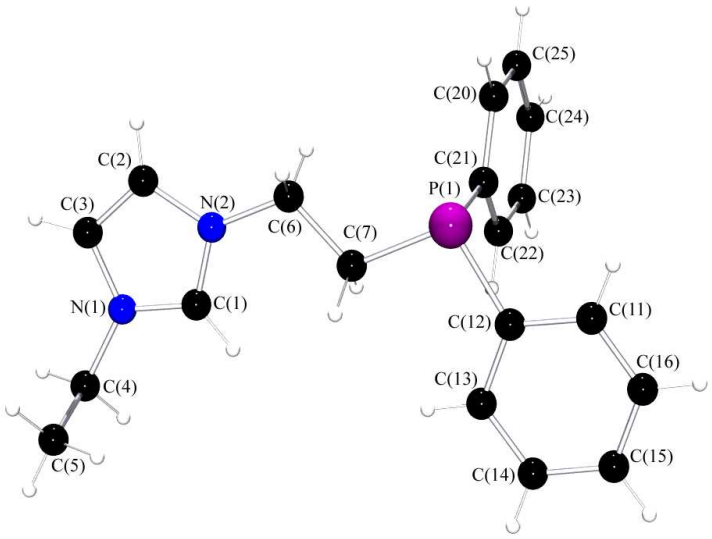

Figure 3.2: Structure of the 3-[2-(diphenylphosphino)ethyl]-1-ethylimidazolium cation in crystals of **E6**.

Table 3.3: Selected Bond lengths [Å] and Bond Angles [°] for **E6**

Bond lengths			
N(1)-C(1)	1.320(4)	N(2)-C(4)	1.474(4)
N(2)-C(1)	1.322(4)	C(2)-C(3)	1.343(5)
N(1)-C(2)	1.378(4)	P(1)-C(11)	1.831(4)
N(2)-C(3)	1.376(4)	P(1)-C(21)	1.836(3)
N(1)-C(6)	1.471(4)	P(1)-C(7)	1.841(4)
Bond angles			
N(1)-C(1)-N(2)	109.1(3)	C(3)-C(2)-N(1)	107.3(3)
C(1)-N(1)-C(2)	108.2(3)	C(2)-C(3)-N(2)	106.9(3)
C(1)-N(2)-C(3)	108.5(3)	N(1)-C(6)-C(7)	111.9(3)
C(11)-P(1)-C(21)	99.41(5)		
C(21)-P(1)-C(7)	99.90(16)		

3.1.3 In situ synthesis of free carbene

3-[2-(diphenylphosphino)ethyl]-1-ethylimidazol-2-ylidene (E7)

The free NHC-phosphane mixed ligand 3-[2-(diphenylphoshino)ethyl]-1-imidazole-2-ylidene **E7** was synthesized by deprotonation of the corresponding imidazolium salts **E5** or **E6**, respectively, in THF using the strong non nucleophilic base $KN(SiMe_3)_2$.

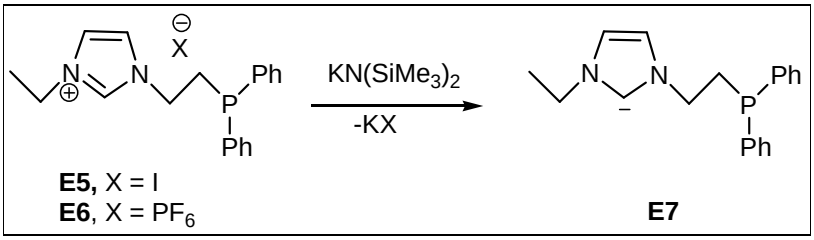

Figure 3.3: Synthesis of 3-[2-(diphenylphosphino)ethyl]-1-ethylimidazole-2-ylidene.

The free NHC-phosphane hybrid ligand is extremely sensitive to oxygen, water and other electrophiles and shows indication of decomposition on attemps to remove the solvent completely. Therefore no attempt has been made to isolate it from solution. Instead we proved its *in situ* formation through the reaction with CS_2 which gives the dithiocarboxylate compound **E8** in high yield.

3.1.3.1 Identification of imidazol-2-ylidendithiocarboxylat (E8)

On addition of one equivalent of CS_2 to a solution of **E7** in THF the color changes to deep red indicating the formation of the zwitterionic dithiocarboxylate **E8** which precipitates from the solvent in high yield. The reaction is a simple nucleophilic attack of the carbene at the electrophilic carbon of CS_2. Recrystallization from $CHCl_3$ / Et_2O gives single crystals which are suitable for X-ray diffraction analysis.

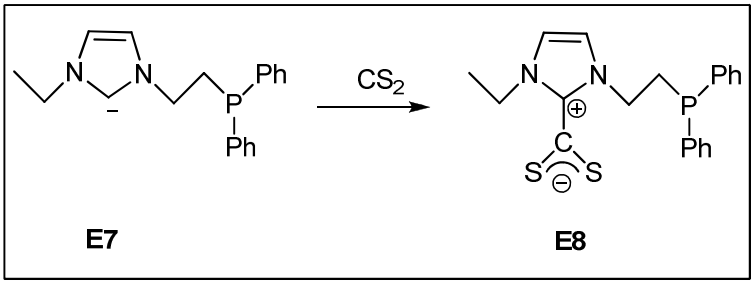

Figure 3.4: Transformation of **E7** to dithiocarboxylate **E8**.

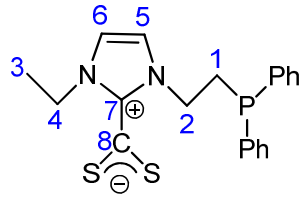

The absence of a resonance above 8 ppm in the proton NMR-spectrum of **E8** in $CDCl_3$ proves the deprotonation of the starting material and indicates coordination to CS_2. The aromatic protons are observed at 6.85-7.4 ppm and the protons of the ethylene bridge show a resonances at 2.67 (t) for H^1 and 4.1 (q) for H^2, respectively. The lines of the resonance of H^1 are slightly broadened most likely due to coupling with phosphorous atom. The signal of methyl group is observed at 1.44 (t). The ^{13}C resonance of the imidazolium carbon atom C^7 (quaternary carbon) is shifted by 15 ppm to low field (149.5 ppm) compared to the corresponding carbon atom of the imidazolium salt due to binding to CS_2. The carbon atom of the CS_2 group exhibits a low field signal at 224.7 ppm. The strong deshielding of this carbon must be attributed to its bonding to a positively charged aromatic ring and to the electronegative sulfur atoms. The remaining aromatic carbons of the imidazolium ring are observed at 117.3 ppm and 118.5 ppm for C^5 and C^6, respectively. Compared to the corresponding carbon atoms in the imidazolium salt **E6** they are shifted to high field by approximately 4 ppm. The carbon atoms of phenyl rings exhibit signals in the same range as in the imidazolium salts.

3.1.3.2 X-ray crystallographic analysis of 3-[2-(diphenylphosphino)ethyl]-1-ethylimidazol-2-dithiocarboxylate (E8)

Red crystals of **E8** suitable for X-ray crystallography were obtained by diffusion of diethyl ether into a $CHCl_3$ solution of **E8**. **E8** crystallized monoclinic in the space group C2/c with eight molecules per unit cell. Selected bond lengths and angles are listed in Table 3.4. Molecular structure containing the atom numberings is shown in Figure 3.5. Crystallographic data are presented in the Table 7.2. In **E8** the molecule contains of imidazole ring which substituted in the three positions the N(1) binding with ethyl group and N(2) with ethylene group which bonded with diphenyl phosphide and C1 bonded with CS_2 group.

The X-ray structure of **E8** (Figure 3.5) confirms the addition of the free carbene to CS_2. The C2 atom lies in the plane of the five remembered ring while S1 and S2 lie out of plane and the dihedral angle formed by the two planes containing the CS_2 position and the imidazol ring is 72.6°. The bond angles in the imidazol ring, viz, C(6)-C(5)-(N1) and C(5)-C(6)-N(2) are

107.14(15) and 107.32(13) and C(1)-N(1)-C(5) and C(1)-N(2)-C(6) are 109.17(15) and 109.10(14), respectively. The N(1)-C(1)-N(2) angle is 107.26(14). All of these bond angles are similar to values reported in the literature.[40a,126,127]]

The bond lengths within the imidazol ring C(1)-N(1)[1.346 (2) Å] and C(1)-N(2) [1.343(2) Å] are identical. The bond lengths of N(1)-C(5) and N(2)-C(6) of 1.384(2) Å and 1.385(2) Å, respectively, are very similar to those found both in the pentamethylimidazolium cation[128] and in 2-telluro-1,3-diisopropyl-4,5-dimethylimidazoline[129] confirming that the π-electrons are completely delocalized over the five-membered aromatic ring. The bond length C(6)-C(5) amounts to 1.344 (3)Å which is indicates a double bond.

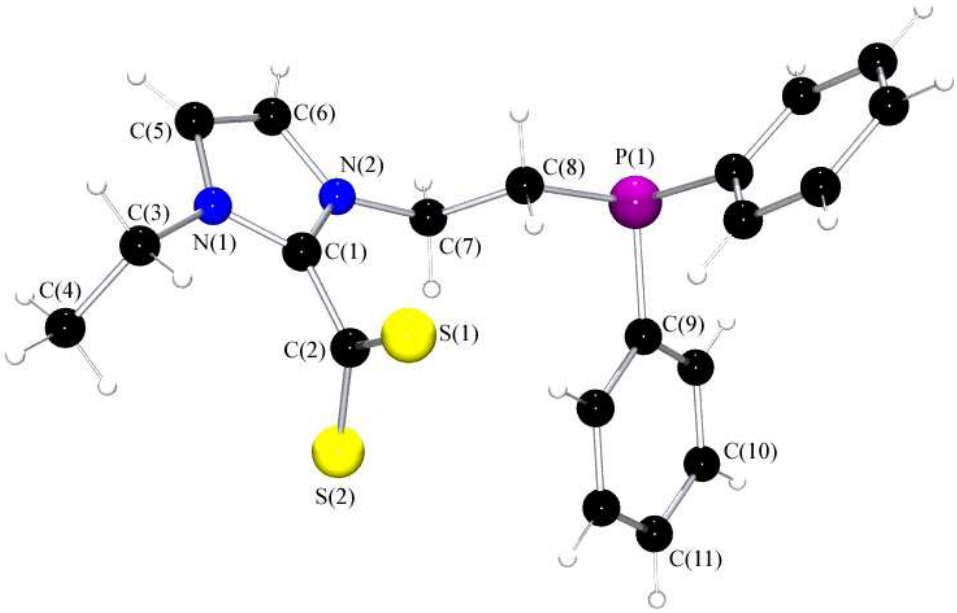

Figure 3.5: Structure of 3-[2-(diphenylphosphino)ethyl]-1-ethylimidazol-2-dithiocarboxylate **E8** in the crystal.

The bond angle of S(1)-C(2)-S(2) is 129.40(10)° and the bond lengths of S(1)-C(1) and S(2)-C(2) are 1.6717(17) and 1.6740(16), respectively, indicating delocalization of π-electrons over the S_2C moiety. This leads to a shortening of the C(1)-C(2) single bond by 0.05 Å to 1.491(2) Å But this is considerably longer than that observed in the 1,1-dithiolateanion $2C_4H_8N_2O.1/3K_2S_2$

(1.375(13) Å) where in the CS_2 group is oriented coplanar to the five membered substituted imidazol ring.[130]

It is helpful to compare the structure of the imidazol-dithiolate **E8** with the higher symmetrical imidazol CS_2 adduct, bis-1,3-isopropyl-bis-4,5-methylimidazoldithiocarboxylate **E9**. This was crystallised by diffusion of diethyl ether into an acetonitrile solution. The crystals belong to the monoclinic space group C2/c containing four molecules per unit cell.

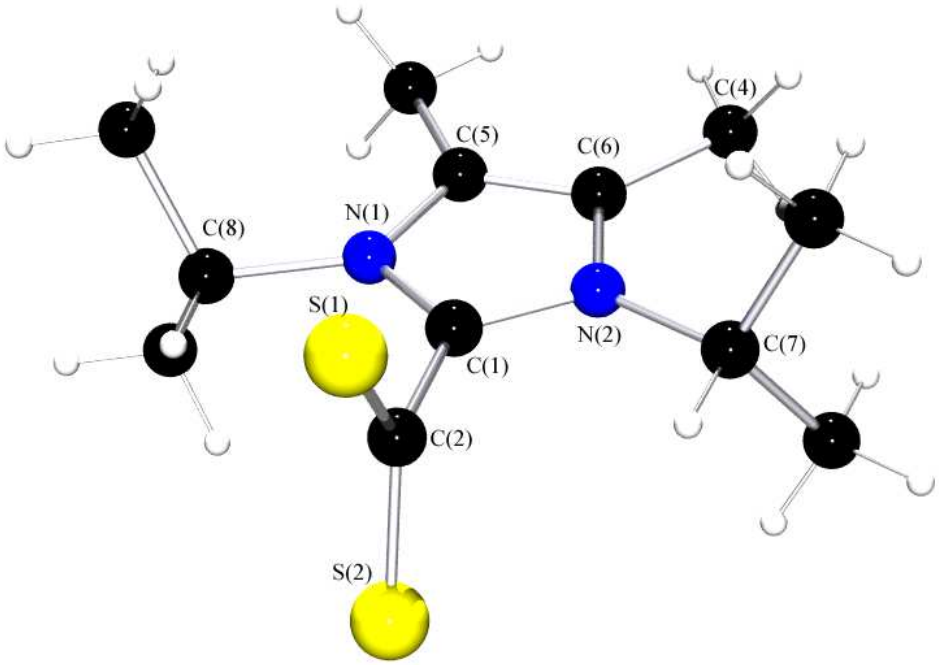

Figure 3.6: Structure of 1,3-di-isopropyl-bis-4,5-methylimidazolium-dithio-carboxylate **E9** in the crystal.

In **E9** the molecules contains aromatic imidazol rings which are substituted in five positions the aromatic carbons of imidazol ring C(5) and C(6) bonding with methyl group while N(1) and N(2) substituted with isopropyl group and C1 of imidazol ring substituted with CS_2 group.
The imidazol ring in **E9** is planar as in **E8** but there is significant difference with respect to the dihedral angles of the planes containing the CS_2 groups and the imidazol rings. In the compound **E9**, the plane of the CS_2 group is perpendicular (dihedral angle, 89.14°) to the plane of the five membered imidazol ring while in **E8** the dihedral angle is 72.6°. The deviation from

perpendicular orientation in **E8** seems to be due to a crystallographic packing effect. The bond lengths and angles for both **E8** and **E9** are given in Table 3.4.

Table 3.4:.Selected Bond lengths [Å] and Bond Angles [°] for **E8** and **E9**

Bond Lengths					
E8		E9	E8		E9
C(1)-N(1)	1.346(2)	1.3365(16)	C(5)-C(6)	1.344 (3)	1.349 (3)
C(1)-N(2)	1.343(2)	1.3365(16)	C(1)-C(2)	1.491(2)	1.485(3)
N(1)-C(5)	1.384(2)	1.3970(17)	S(1)-C(2)	1.6717(17)	1.6621(9)
N(2)-C(6)	1.385(2)	1.3970(17)	S(2)-C(2)	1.6740(16)	1.6621(9)
P(1)-C(8)	1.8564(17)		P(1)-C(10)	1.8383(16)	
P(1)-C(9)	1.8380(16)				
Bond Angles					
E8		E9	E8		E9
N(1)-C(5)-C(6)	107.14(15)	107.10(8)	C(1)-N(2)-C(6)	109.10(14)	108.59(12)
N(2)-C(6)-C(5)	107.32(15)	107.10(8)	N(1)-C(1)-N(2)	107.26(14)	108.61(17)
C(1)-N(2)-C(5)	109.10(14)	108.59(12)	S(1)-C(2)-S(2)	129.40(10)	129.47(12)
C(8)-P(1)-C(9)	96.88(7)		C(8)-P(1)-C(10)	103.52(7)	

3.1.3.3 Electrochemistry of 3-[2-(diphenylphosphino)ethyl]-1-ethyl-imidazolium-hexa-fluorophosphate (E6)

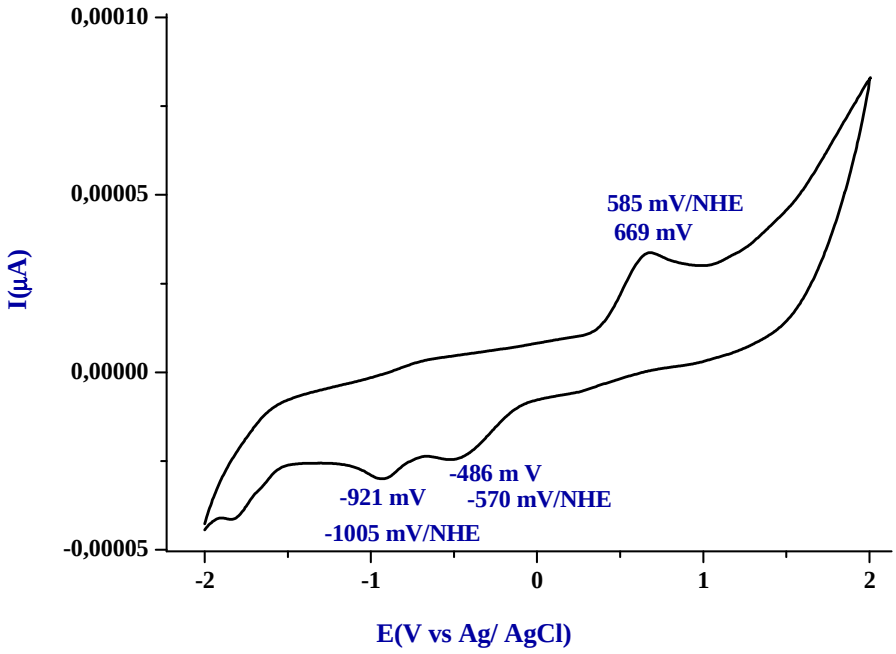

Figure 3.7: Cyclovoltammogram of **E6** in THF.

The cyclovoltammogram of imidazolium salt E6 (0.1mol/L $[NBu_4][PF_6]$ was obtained at a scan rate of 200 mV/s in THF. The imidazolium salt shows irreversible oxidation wave at 586 mV/NHE and two reduction waves at -570 mV/NHE and -1005 mV/NHE.

3.2 Rhodium complexes

3.2.1 Syntheses and characterization of cationic *cis*-and *trans*-rhodium(I) complexes with E7

The syntheses of the cationic *cis* and *trans* Rh(I) complexes $[Rh(EtImCH_2CH_2PPh_2)_2][X]$ (**E10** (X = Cl), **E11** (X = PF_6)) $[Rh(EtImCH_2CHPPh_2)_2]X$ (**E12** (X = Cl), **E13**(X = PF_6)) with the bidentate phosphine-NHC ligand **E5**, **E6** were carried out as outlined in Figure(3.8). The carbene ligands were obtained by the reaction of imidazolium salt **E5**, **E6** with the base $KN(SiMe_3)_2$ in THF solution at room temperature under an inert gas atmosphere. Subsequentaly addition of the metal precursor $[Rh(\mu\text{-}Cl)(COD)]_2$ afforded the novel *cis* and *trans* square planar Rh(I) complexes.

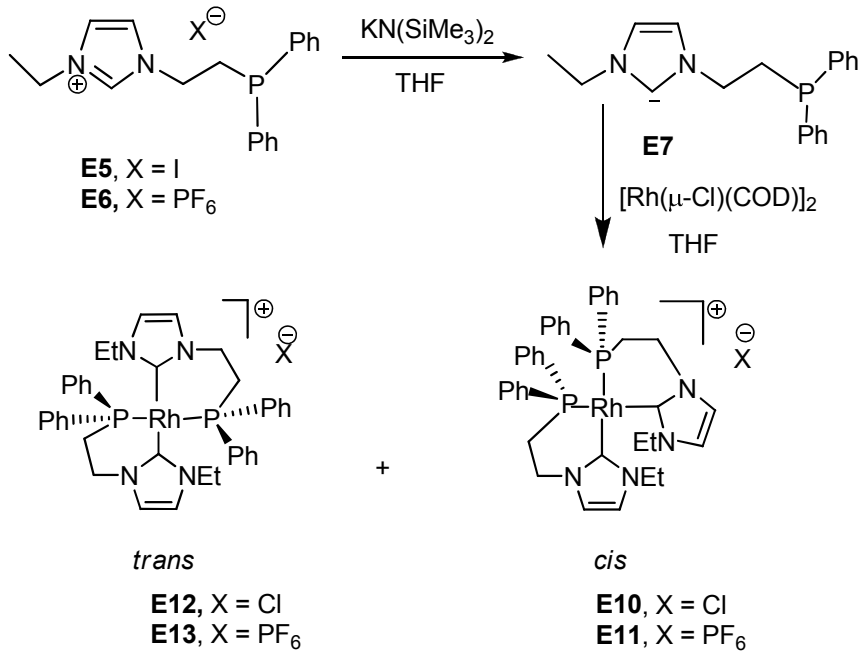

Figure 3.8: Synthesis of *cis*- and *trans*-Rh(I) complexes.

E12 was obtained only in case of imidazolium iodide salts as soluble product in THF solution while the *cis*-isomer **E10** which is also generated in this reaction as an orange yellow precipitate. On starting with **E6** the same reaction leads selectively to the *cis* complex **E11** in high yield. In the solid state the latter is a compound of yellow green color which in contrast to **E10** is easily soluble in THF. **E13** was synthesized from **E12** via counter ion exchange by adding $NaPF_6$ in methyene chloride solution.

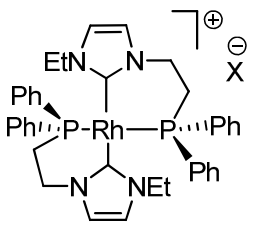

trans

E12, X = Cl
E13, X = PF_6

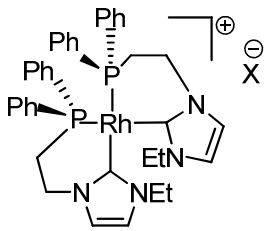

cis

E10, X = Cl
E11, X = PF_6

The new mononuclear bidentate phosphine-NHC Rh(I) complexes were characterized by ^{1}H, ^{13}C, ^{31}P-NMR spectroscopy and single crystal X-ray structure analyses.

Compared to the imidazolium salt **E6** the ^{1}H-NMR spectra of all complexes **E10**, **E11**, **E12**, **E13** show important differences with respect to the chemical shift and the multiplicities of the resonances of the ethylene protons. As expected protons attached to C^2 cannot be observed due to deprotonation and subsequent cordination to rhodium. The bidentate coordination of the ligands can be infered from the presence of four diasterotopic proton resonances for the ethylene bridge in the range of 2.50-2.56 and 3.73-3.80 ppm. The chemical shift of the resonance of the carbene carbon C^2 were observed at low field in the ^{13}C {^{1}H}-NMR spectra. The *cis* complex shows a ddd at 183.0 ppm ($^{1}J_{RhC}$ = 47 Hz, $^{2}J_{PC,\ trans}$ = 103 Hz, $^{2}J_{PC,\ cis}$ = 30 Hz) while for the *trans* complex a doublet of triplett is found at 185.1 ppm ($^{1}J_{RhC}$ = 39 Hz, $^{2}J_{PC}$ = 17 Hz). These chemical shifts and coupling constants compare well with values reported in the literature for the C^2 resonance of other rhodium NHC complexes.[49,59,131-135] The appearance of the $^{1}J_{(Rh\text{-}C2)}$ coupling constant confirms the bonding of the carbene atom to the metal center in solutiuon. The number of aromatic resonances proves that the phenyl rings of the PPh_2 residue are not equivalent in all complexes.

The ^{31}P NMR resonances of the phosphorous atoms in the metal complexes **E10**, **E11**, **E12** and **E13** were observed at 32.2 ppm for both *cis* complexes (d, $^{1}J_{RhP}$ = 128 Hz) and at 25.9 ppm for both *trans* complexes (d, $^{1}J_{RhP}$ = 152 Hz). The resonances of the phosphorous atoms are shifted to lower field compared to the values observed for the free ligands **E5** (-21.4 ppm) and **E6** (-22.1 ppm), respectively. This observation confirmes the coordination of phosphorous to the metal center.

3.2.2 Single crystal X-ray structure analyses of *cis*-[Rh(EtImCH$_2$CH$_2$PPh$_2$)$_2$][X] (X=Cl (E10), PF$_6$ (E11))

Single crystals of **E10** and **E11** suitable for X-ray diffraction analysis were obtained by slow diffusion of diethyl ether into a concentrated acetonitrile solution of **E10** and from concentrated THF solution of **E11**, respectively.

Selected bond lengths and angles of both compounds are listed in Table 3.5. Molecular structure containing the atomic numbering schemes are shown in Figure 3.9, Table 3.5 for **E10** and Figure 3.10, Table 3.5 for **E11**, respectively., Crystallographic data are listed in the Table 7.3. The *cis* complexes **E10** and **E11** crystallized in the triclinic space group P-1.The latter incorporated one molecule of THF in the crystal lattice.The crystals contain two molecules per asymmetric unit. As both complexes show only minor differences with respect to their structure only the structure of complex **E10** will be dicussed in detail.

In the complex **E10** the Rh center is coordinated by two bidentate NHC-phosphane-ligands in a square planar arrangement. The metal center forms with each ligand a six membered ring exhibiting a distorted boat conformation. Both rings can be mapped onto each other by a 180° rotation about the axis dividing the angles P(11)-Rh(1)-P(12) and C(101)-Rh(1)-C(120). Hence the molecule is chiral as it belongs to the point group C_2. The sums of angles at the Rh atoms equals 360.1(2)° and 359.8(2)°, respectively, in accordance with the square planar geometry of the complex. However, the angles C(120)-Rh(1)-P(12) of 81.19(15)° and P(11)-Rh(1)-P(12) of 98.74(6)° deviate strongly form the expected 90° angle in square planar complexes. This observation can be traced back to the fact that the phenyl rings in these *cis*-isomers are quite close to each other leading to sterical strain. The latter is reduced by a slight distortion from the ideal square planar arrangement of the ligand atom. The repulsion of the two PPh$_2$ residues is also strongly indicated by the angle C(101)-Rh(1)-P(12) which deviates by 8.34(12)° from the expected 180° angle. Consequently this deviation can also be found in the angle C(120)-Rh(1)-P(12). In **E10**, the Rh(1) atom is located only 0.036 Å above the coordination plane defined by C (101), C(122), P(11) and P(12). The bite angles C(101)-Rh(1)-P(11) of 89.45(15°) and and C(101)-Rh(1)-C(120) of 91.5(2), respectively, are close to the ideal angle of 90° expected for square planar complexes. The dihedral angles of P(11)-Rh(1)-P(12) to C(101)-Rh(1)-C(120) and C (101)-Rh(1)-P(11) to C(120)-Rh(1)-P(12) amount to 9.29° and 10.31°, respectively. Again this slight distorsion must be attributed the sterical interaction of the PPh$_2$ residues. The bond lengths

of Rh(1)-C(101), Rh(1)-C(120), Rh(1)-P(11) and Rh(1)-P(12) are 2.033(6) Å, 2.034(5) Å, 2.2686(15) Å and 2.2781(16) Å, respectively, are similar to the those of other Rh-NHC complex with monodentate ligands reported in the literature.[131,133,136]

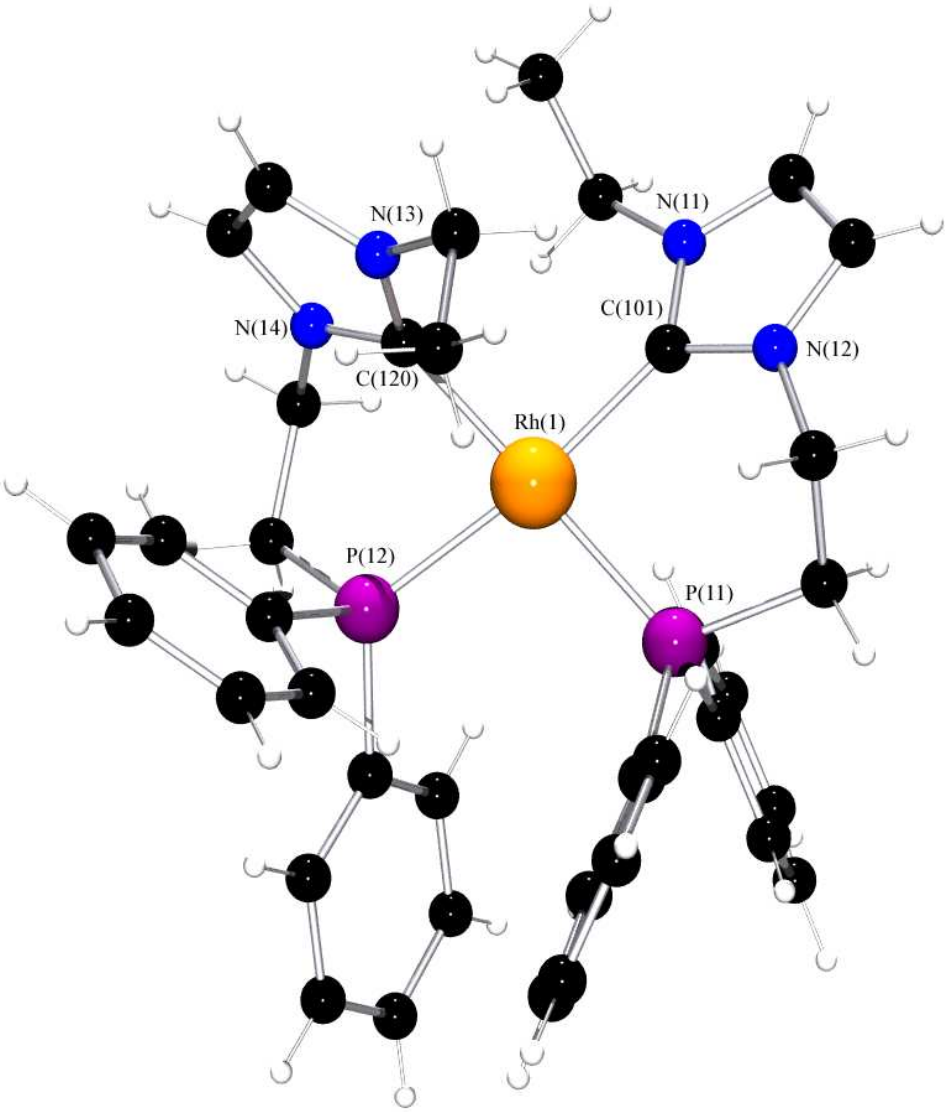

Figure 3.9: Structure of *cis*-$[Rh(EtImCH_2CH_2PPh_2)_2]^+$ in crystals of **E10**

Table 3.5: Selected bond lengths [Å] and bond angles [°] of *cis*-[Rh(EtIm$CH_2CH_2PPh_2)_2$]Cl (**E10**) and *cis*-[Rh(EtIm$CH_2CH_2PPh_2)_2$][PF_6] (**E11**)

E10		**E11**	
Bond Lengths			
Rh(1)-C(101)	2.033(6)	Rh(1)-C(135)	2.044(4)
Rh(1)-C(120)	2.034(5)	Rh(1)-C(165)	2.057(4)
Rh(1)-P(11)	2.2686(15)	Rh(1)-P(11)	2.2565(11)
Rh(1)-P(12)	2.2781(16)	Rh(1)-P(12)	2.2739(11)
Bond Angles			
C(101)-Rh(1)-P(11)	89.45(15)	C(135)-Rh(1)-P(11)	88.75(12)
C(120)-Rh(1)-P(12)	81.19(15)	C(165)-Rh(1)-P(12)	80.54(11)
P(11)-Rh(1)-P(12)	98.74(6)	P(11)-Rh(1)-P(12)	99.27(4)
C(101)-Rh(1)-C(120)	91.5(2)	C(135)-Rh(1)-C(165)	91.24(16)
C(120)-Rh(1)-P(11)	170.66(15)	C(165)-Rh(1)-P(11)	174.23(12)
C(101)-Rh(1)-P(12)	170.46(15)	C(135)-Rh(1)-P(12)	171.66(12)

For **E11** the unit cell contains two independent molecules. In both of these molecules the rhodium atoms show a slightly distorted square planar coordination sphere. The rhodium atoms are 0.072 Å and 0.003 Å, respectively, located above the coordination plane. Apart from that there are no significant differences with respect to bond angles and bond distances compared to the structure of **E10**. Obviously the counterion does not interfere with structural arrangement of the complexes.

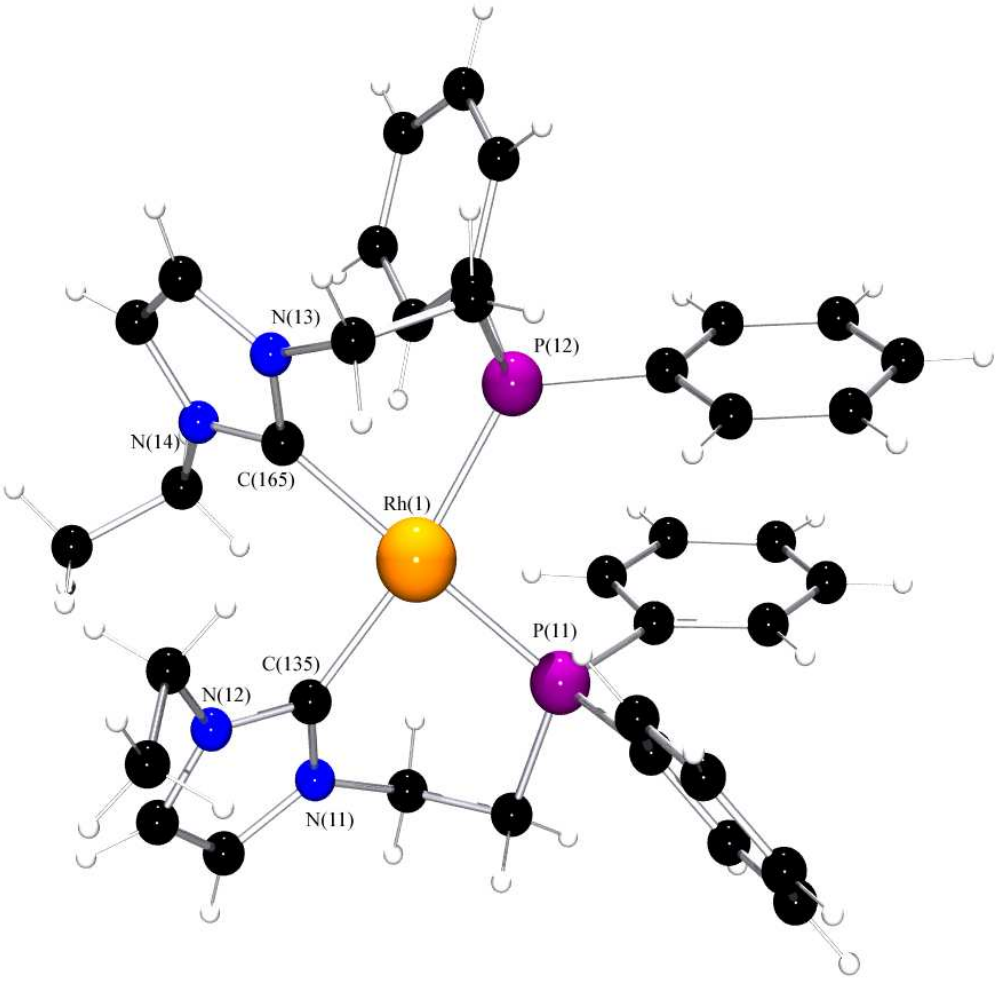

Figure 3.10: Structure of *cis*-$[Rh(EtImCH_2CH_2PPh_2)_2]^+$ in crystals of **E11**.

3.2.3 Single crystal X-ray structure analyses of *trans*-$[Rh(EtImCH_2CH_2PPh_2)_2][X]$ (X = Cl (E12), PF_6 (E13))

Single crystals of **E12** and **E13** suitable for X-ray diffraction analysis were obtained by slow evaporation of a concentrated solution of **E12** in THF and by layering of concentrated dichloromethane of **E13** solution with diethyl ether, respectively. Selected bond lengths and angles of both compounds are listed in Table 3.6. Crystallographic data are presented in Table 7.4. Molecular structure containing atom numbering schemes are shown in Figure 3.11 for **E12** and 3.12 for **E13**, respectively. **E12** crystallized in the monoclinic space group Cc while **E13** crystallized in the monoclinic in space group C2/c.

Crystals of the *trans* complex **E12** contain 4 molecules in the unit cell. And crystals of **E13** contains four molecules per unit cell in which two molecules of complex and two molecules of diethyl ether incorporated in the unit cell In both complexes the arrangement around rhodium is distorted square planar. The rhodium centers are coordinated by two bidentate ligands **E7.** The ligating phosphorous atoms occupy *trans* coordination sites. The same holds for the ligating carbon atoms. The sums of angles at the Rh atoms equals 359.35(6)° for **E12** and 358.56(6)° for **E13**. In **E12** the rhodium atom is located only 0.133 Å from the coordination plane. In **E13** the rhodium atom is located 0.208 Å above the coordination plane defined by C(1), C(1A), P(1) and P(1A). In **E12** and **E13** the six membered rings defined by Rh(1), P(1), C(7), C(6), N(2), C(1) and Rh(1), C(1), N(2), C(6), C(7), C(16), P(1), respectively, have pseudo-boat conformation. Both complexes show C_2 symmetry. The C_2 axis is perpendicular to the coordination plane passing through the rhodium atom. The ligand bite angles in case of **E12** C(1)-Rh(1)-P(1) and C(1)-Rh(1)-P(1)#1 amount to 79.58(6)° and 100.09(6)°, respectively. They deviate by approximately 10° from the ideal 90° angle expected for this type of complex. Due to that the phenyl ring in the *trans* complex are quite close to each other leading to steric strain which cases distortion around the Rh (1) center The C(1)#-Rh(1)-C(1) of 176.47 close to linearity 180° and the P(1)#-Rh(1)-P(1) of 169.67(3) deviates from ideal angle 180° the rhodium carbene distance of Rh(1)-C(1)# of 2.029(2) and Rh(1)-P(1)# of 2.2619(6)and 2.2620(6) respectively in **E13**. The bite angle C(1)-Rh(1)-P(1) of 84.81(6) close to ideal angle 90°, the C(1)#-Rh(1)-P(1)# of 94.47(6) and C(1)#-Rh(1)-C(1) of 175.07(12) close to the linearity while P(1)#-Rh(1)-P(1) of 163.24(3) deviates from 180º. The Rhodium carbene and phosphour bond lengths of 2.031(2) Å and 2.2551(5) Å, respectively. Are similar to those of other Rh-NHC complexes.[124,137,138] The Rh-P bond length is longer than Rh-C bond by 0.2241(5) Å due to *trans* effect of phosphine ligand.

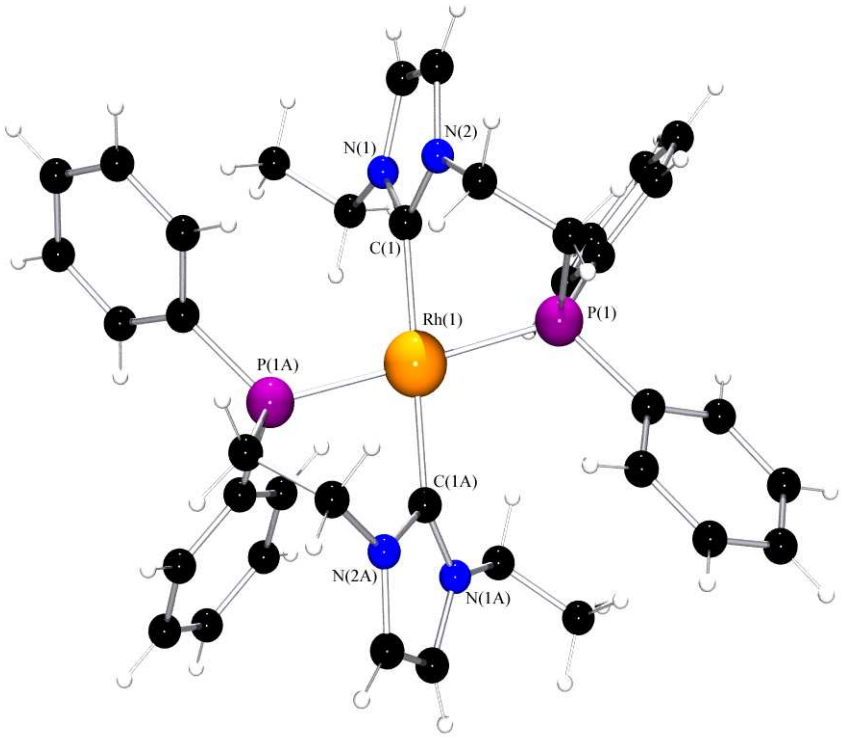

Figure 3.11: Structure of *trans*-[Rh(EtIm$CH_2CH_2PPh_2)_2$]$^+$ in crystals of **E12**.

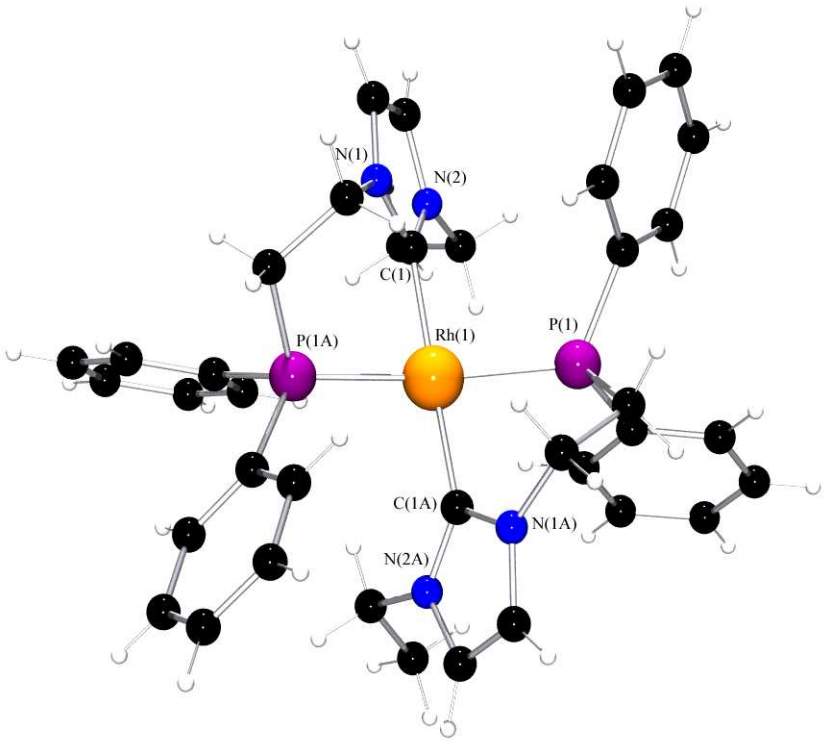

Figure 3.12: Structure of *trans*-[Rh(EtIm$CH_2CH_2PPh_2)_2$]$^+$ in crystals of **E13**.

Table 3.6: Selected bond lengths [Å] and bond angles [º] for *trans*-[Rh(EtImCH$_2$CH$_2$PPh$_2$)$_2$]Cl (**E12**) and *trans*-[Rh(EtImCH$_2$CH$_2$PPh$_2$)$_2$][PF$_6$] (**E13**)

E12		**E13**	
Bond Lengths			
Rh(1)-C(1)A	2.029(2)	Rh(1)-C(1)A	2.031(2)
Rh(1)-C(1)	2.029(2)	Rh(1)-C(1)	2.031(2)
Rh(1)-P(1)A	2.2619(6)	Rh(1)-P(1)A	2.2551(5)
Rh(1)-P(1)	2.2620(6)	Rh(1)-P(1)	2.2551(5)
Bond Angles			
C(1)-Rh(1)-P(1)	79.58(6)	C(1)-Rh(1)-P(1)	84.81(6)
C(1)A-Rh(1)-P(1)A	79.59(6).	C(1)A-Rh(1)-P(1)A	84.81(6)
C(1)-Rh(1)-P(1)A	100.09(6)	C(1)-Rh(1)-P(1)A	94.47(6)
C(1)A-Rh(1)-P(1)	100.09(6)	C(1)A-Rh(1)-P(1)	94.47(6)
P(1)A-Rh(1)-P(1)	169.67(3)	P(1)A-Rh(1)-P(1)	163.24(3)
C(1)A-Rh(1)-C(1)	176.47(12)	C(1)A-Rh(1)-C(1)	175.47(12)

.

3.3 Equilibrium between *cis* and *trans* isomers at higher temperatures

The interconversion of *cis*-complex and *trans* complex is studied by measuring ^{31}P-NMR of both complexes at different temperatures and for different times. Generally ^{31}P-NMR spectra of the *cis* isomers **E10** shows a signal at 32 ppm which splitting to a doublet ($^{1}J_{RhP}$ = 126 Hz), while the *trans* complex **E12** exhibits a doublet at 26 ppm ($^{1}J_{RhP}$ = 153 Hz) as shown in Figure.3.13.

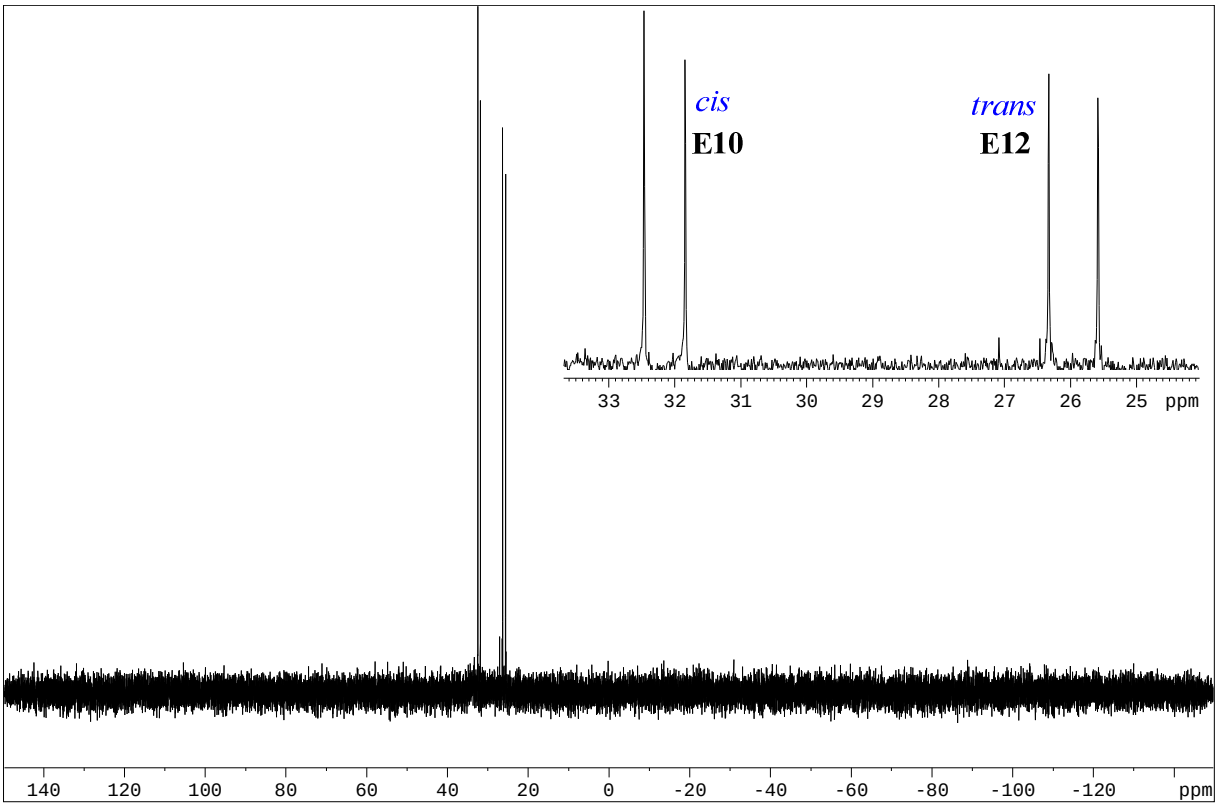

Figure 3.13: ^{31}P-NMR spectrum of a mixture of *cis* and *trans* isomers **E10** and **E12**.

The relative stability of both isomers was checked by temperature dependent ^{31}P-NMR spectroscopy. Initially the sample of the *cis* isomer dissolved in d^{6}-DMSO shows a signal at 32 ppm and small signal of the *trans* isomers at 26 ppm as a side product with a ratio of *cis* to *trans* of 10:1 Figure 3.14. The ratio has been determined by integration of the peaks as the phosphorous atoms in both complexes most likely have similar relaxation times due to the similar structure of the complexes. On heating for 2 h at 45°C the ratio of the isomers did not change. Increasing the temperature to 80°C and heating for 21 h leads to a new ratio of 2:1. Heating at 100°C for 70 h gives a spectrum with sharp peaks of both isomers in a ratio of *cis* to *trans* 1:2. Prolonged heating

at 120°C gave no change in ratio of both isomers indicating that an equilibrium due to interconservion of both isomers (Figure 3.16).

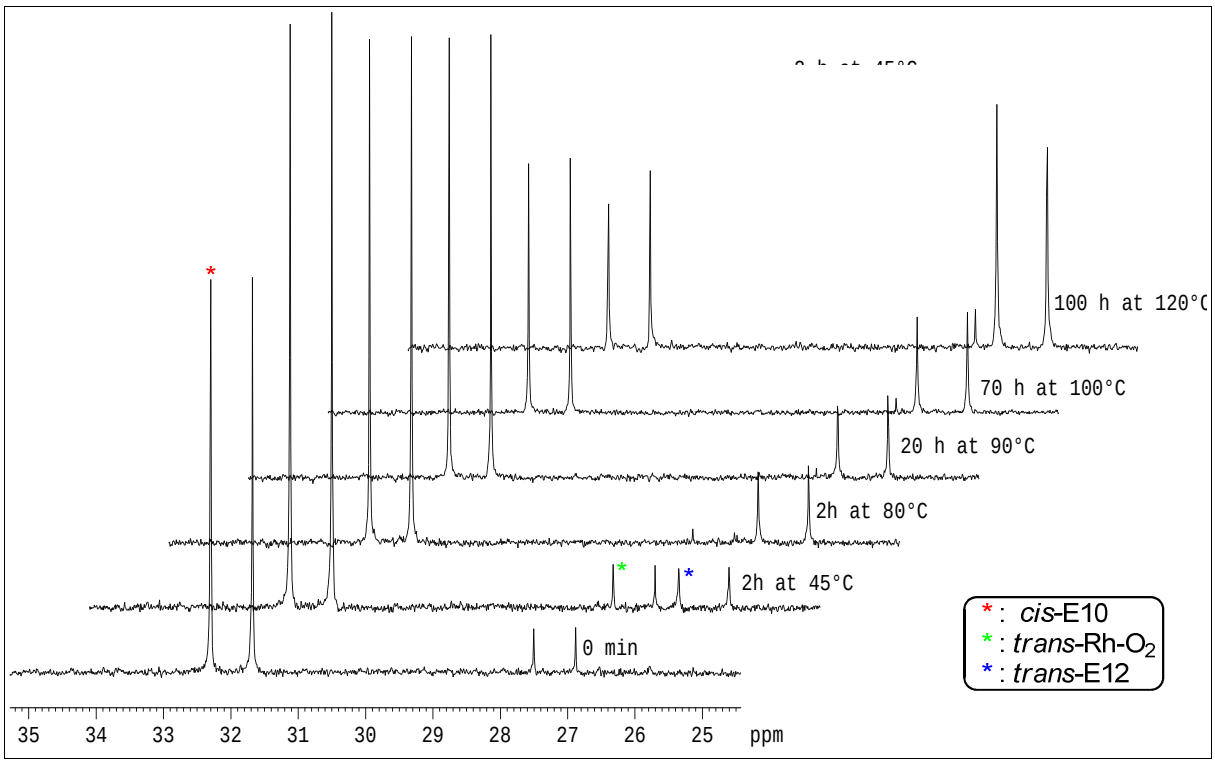

Figure 3.14: Temperature dependent ^{31}P NMR-spectrum of isomerization of *cis*-**E10** to *trans*-**E12**.

In order to prove the proposed interconversion the *trans* isomer was dissolved in CD_3CN and again temperature dependent ^{31}P-NMR spectra were recorded. The starting material contains both isomers in a ratio of 10:1 (*trans*: *cis*) at room temperature. On heating the *trans* isomer at 50°C for 2h there is no change in the ratio of both isomers. By increasing the temperature to 70°C and heating again for 8 h there the ratio changes to 5:2 (*trans* : *cis*). Finally on heating at 78°C for 18 h the ratio of *trans* to *cis* becomes 2:1. Heating for another 24 h does not change the observed ratio for both isomers confirming the above postulated equilibrium in solution as shown in Figure (3.15)

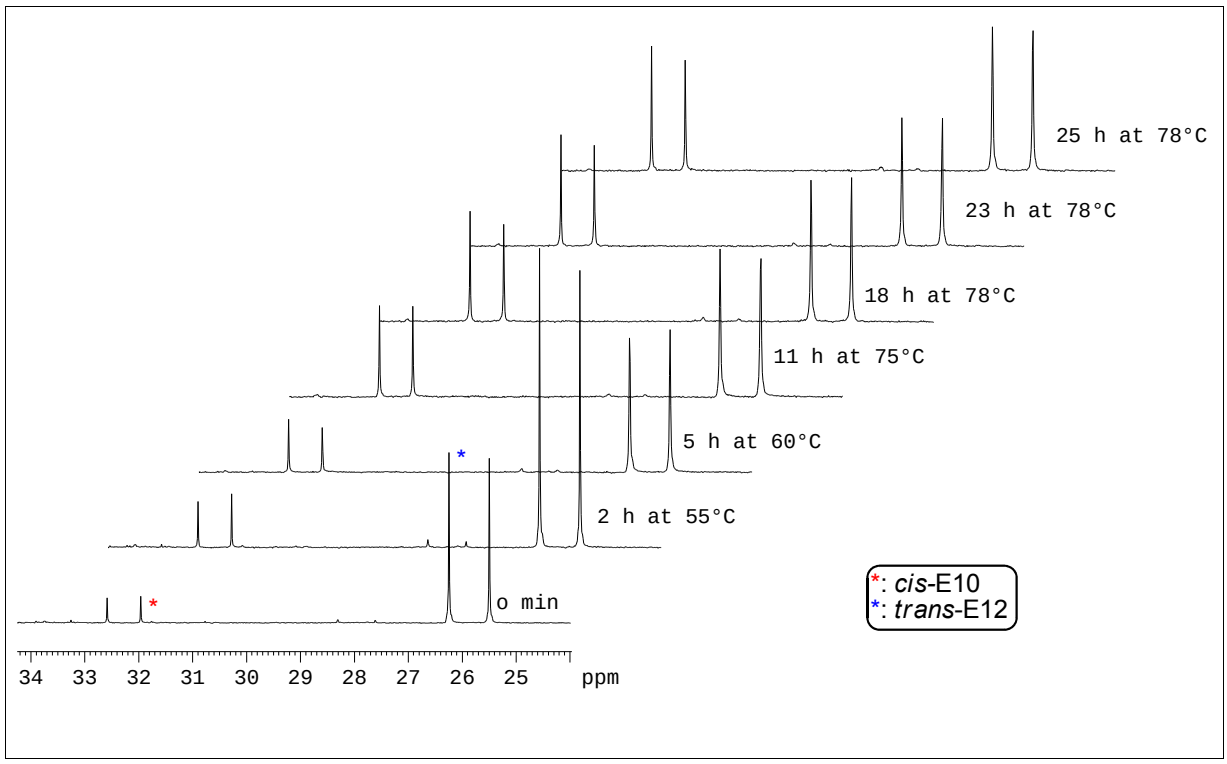

Figure 3.15: Temperature dependent ^{31}P-NMR spectra of thermal isomerization of *trans*-**E12** to *cis*-**E10**.

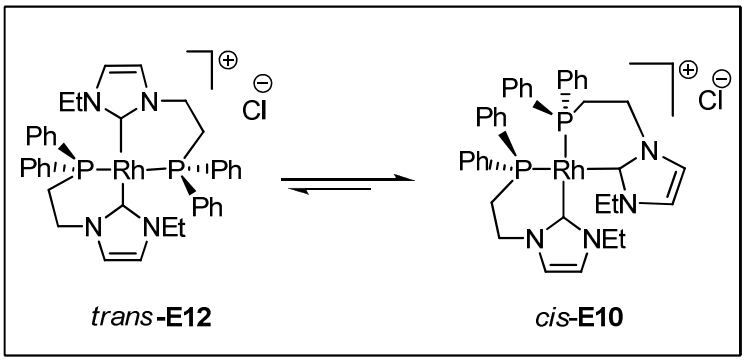

Figure 3.16: The equilibrium between *cis*-**E10** and *trans*-**E12** isomers of [Rh(EtIm$CH_2CH_2PPh_2)_2$]Cl**.**

The mechanism of interconversion of *trans*-**E12** and *cis*-**E10** can occur through two different mechanisms as depicted in Figure 3.17. In mechanism A the reaction is initiated by a dissociation of the phosphane moieties and subsequent pseudo rotation around rhodium atoms. Recoordination of the phosphorous atom forms the *cis* complex. In mechanism B reaction occurs through a tetrahedral transition state subsequent rearrangemen of the molecules. If the reaction proceeds via pathway A the intermediate complex I should give a ^{31}P-NMR resonances at about -20 ppm

(compare to $MePPh_2$, δ = -27. 1 ppm).[124] However, we did not observe any signal in the negative range of the ppm scale. This strongly points toward mechanism B, but we cannot completely rule out that the transformation via intermediate I (mechanism A) is so rapid that NMR-spectroscopy is not able to detect it.

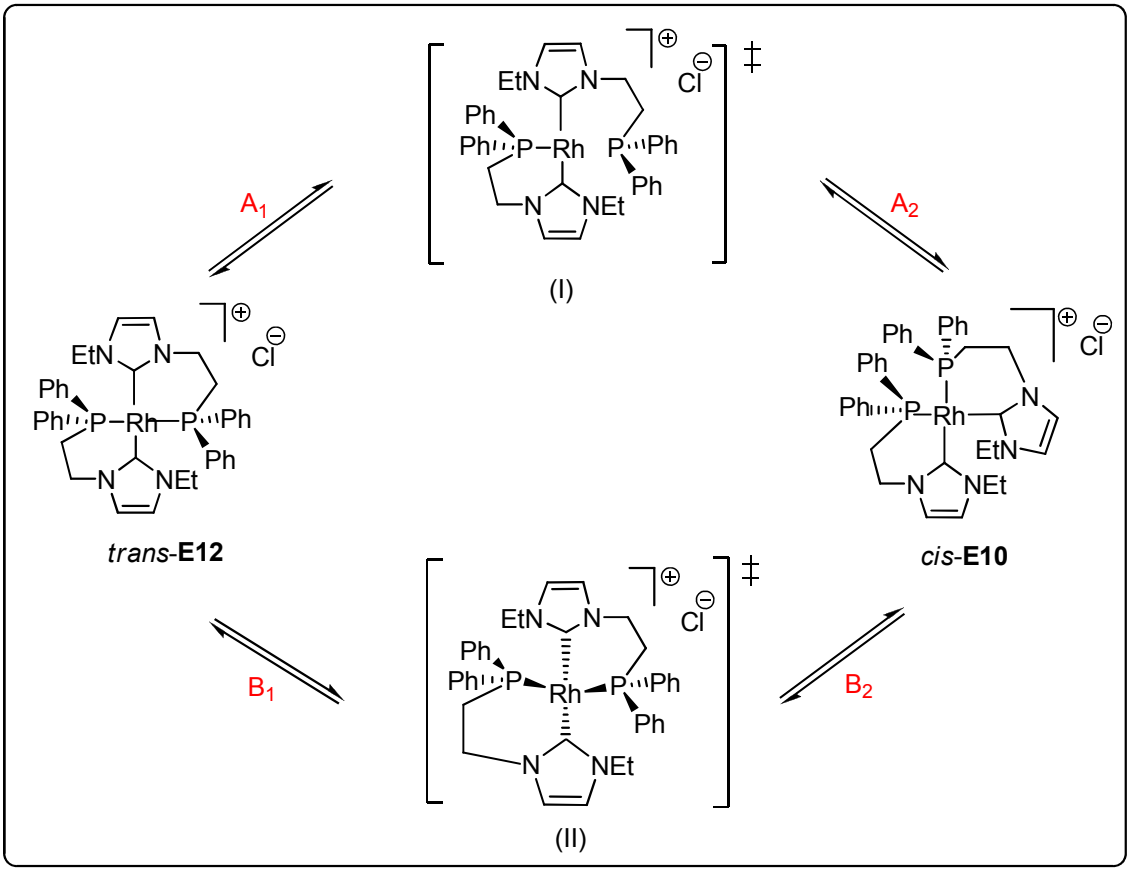

Figure 3.17: Postulated mechanisms for the interconversion of **E10** and **E12**.

3.4 Electrochemistry of *cis*-[Rh(EtImCH$_2$CH$_2$PPh$_2$)$_2$][PF$_6$] (E11)

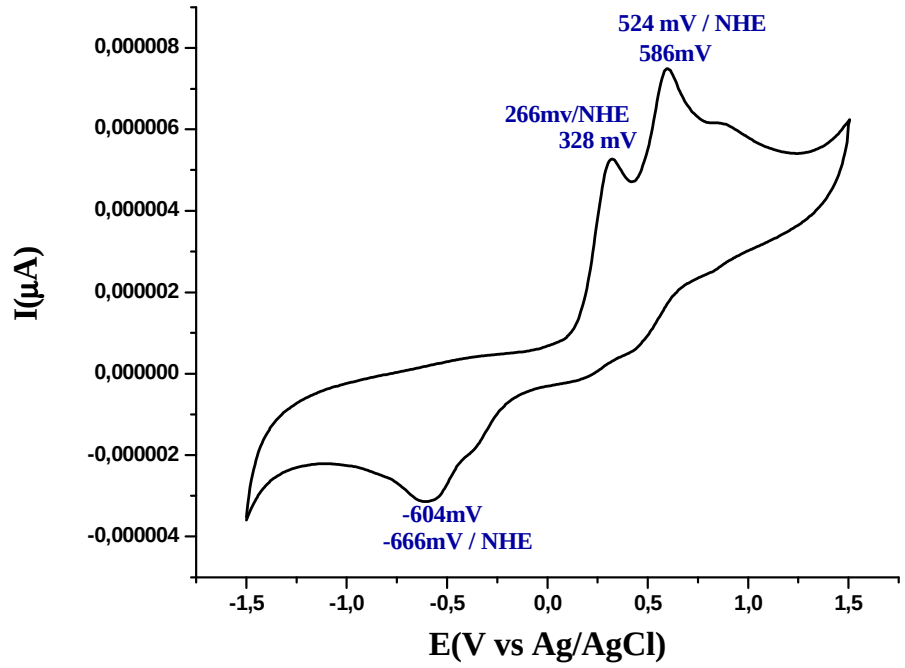

Figure 3.18: Cyclovoltammogram of **E11** in CH_3CN.

The cyclovoltammogramm of *cis*-rhodium(I) complex **E11** (0.1 mol/L [NBu$_4$][PF$_6$]) was obtained at a scan rate of 50 mV/s in acetonitrile. The *cis*-Rh(I) complex shows irreversible oxidation waves at 266 mV/NHE and 542 mV/NHE and a reduction wave at -666 mV/NHE.

3.4.1 Electrochemistry of *trans*-[Rh(EtImCH$_2$CH$_2$PPh$_2$)$_2$]Cl (E12)

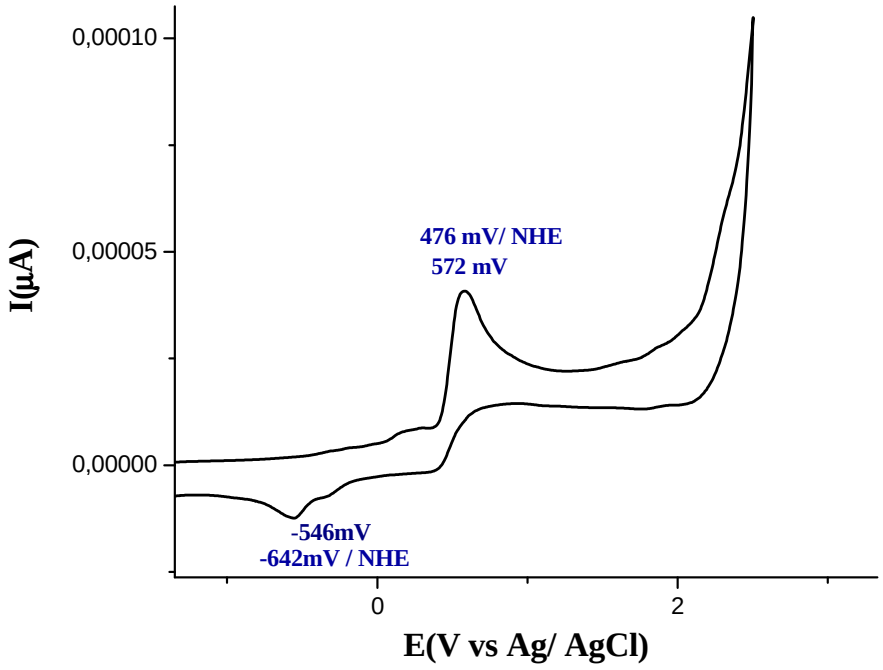

Figure 3.19: Cyclovoltammogram of **E12** in CH_3CN.

The cyclovoltammogram of **E11** (0.2 mol/L [NBu_4][PF_6]; 50 mV/s; Au/Pt/Ag-AgCl) shows quasi irreversible electron transfers (Figure 3.19) The oxidation wave at 476 mV/NHE and reduction wave at -642 mV/NHE.

3.5 Synthesis of peroxo complexes

3.5.1 Synthesis and dynamic behaviour of *cis*- and *trans*-[Rh(η^2-O_2)($EtImCH_2CH_2PPh_2$)$_2$]X (X = Cl (E14), PF_6 (E15))

The novel peroxo complexes **E14** and **E15** were synthesized by exposure of methylene chloride solutions of **E10** or **E11**, respectively, to air (Figure 3.20). The reactions are finished after a few minutes. The color changes in both cases from yellow orange to pale brown.

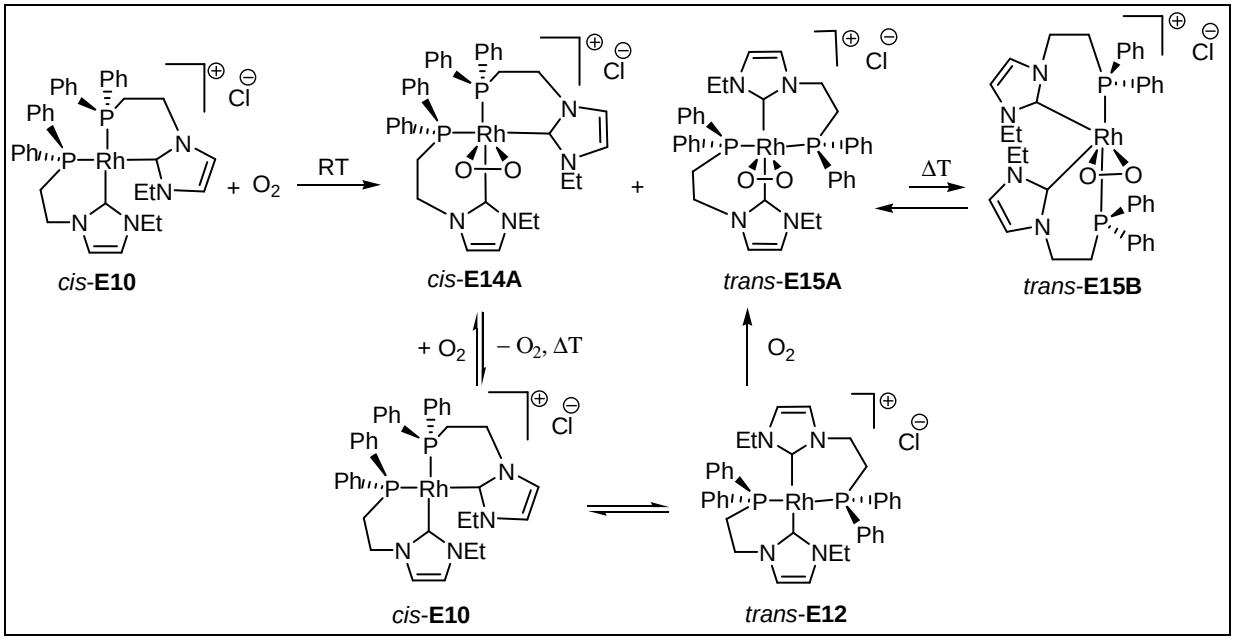

Figure 3.20: Formation of *cis*- and *trans*-peroxo complexes **E14**, **E15**.

The ^{31}P-NMR spectrum of **E14** at room temperature shows a broad dublett at 27.5 ppm (d, $^1J_{Rh\text{-}P}$ = 125 Hz) and an extremely broad peak at 8.5 ppm. In addition the signal of **E15** at 26.5 ppm (d, $^1J_{RhP}$ = 125 Hz) is observed. On heating to 343 K the peak at 27.5 ppm becomes a sharp dd ($^1J_{RhP}$ = 125 Hz, $^2J_{PP}$ = 20 Hz) and the peak at 8.5 ppm is transformed into a dublett ($^1J_{RhP}$ = 125 Hz) with much lower half band width than before. The observed transformation of the resonances must be attributed to a fluxional process. **E14** consists of two isomers (**E14A** and **E14B**) which are in a dynamic equilibrium with each other. At 343 K the interconversion is so rapid that only 2 resonances for the two phosphorous atoms can be observed. On lowering the temperature to 303 K the interconversion slows down and the peaks broaden due to coalescence of the resonances of **E14A** and **E14B**. This is confirmed by further temperature dependent ^{31}P-NMR spectra which

have been mesaured down to 233 K (Figure 3.21). In the low temperature range 4 sharp resonances at 30.9 (dd, $^{1}J_{RhP}$= 125 Hz, $^{2}J_{PP}$ = 20 Hz), 26.2 (dd, $^{1}J_{RhP}$ = 125 Hz, $^{2}J_{PP}$ = 20 Hz), 12.4 (dd, $^{1}J_{RhP}$ = 85 Hz, $^{2}J_{PP}$ = 20 Hz), -3.1 (dd, $^{1}J_{RhP}$ = 85 Hz, $^{2}J_{PP}$ = 20Hz) are detected which must be assigned to **E14A** and **E14B**. From the intensities of the signals it becomes immediately clear that the resonances at 30.9 ppm and 12.4 ppm belong to one of the isomers (**E14A**) and the resonances at 26.2 ppm and -3.1 ppm belong to the other isomer (**E14B**). The most notable feature of their ^{31}P-NMR data are the coupling constants. The recorded $^{2}J_{PP}$ value of 20 Hz is typical for a *cis* arrangement of the two phosphorous atoms in each isomer. The $^{1}J_{RhP}$ values of 125 Hz and 85 Hz allow the assignment of the phosphorous atoms with respect to the Rh–O_2 plane. The phosphorous atoms exhibiting a coupling constant of 125 Hz lie in the Rh–O_2 plane while those with 85 Hz are perpendicular orientated with respect to that plane. The assignment is based on the observed coupling constants in **E15** and other Rh-O_2 complexes containing phosphorous ligator atoms.[139] In **E15** both phosphorous lie in the Rh-O_2 plane and show a $^{1}J_{RhP}$ coupling constant of 125 Hz. Are similar to [Rh(O_2)(P-N)(PPh_3)Cl],[139] [Rh(O_2)(4-C_5F_4N)(CNtBu)(PEt_3)$_2$][140]] 85Hz From the coupling constants it is clear, that **E14A** and **E14B** have the same arrangement of the ligands around the rhodium center. Hence the structural difference between both isomers must be attributed to the conformation of the 6-membered rings which are part of both molecules. This evaluation of the recorded data is confirmed by the single crystal X-ray analyses of **E14A** and **E16** which shows the same ligand arrangement as **E14A**, but another conformation of the 6-membered rings. The latter conformation of the rings must be attributed to **E14B** too. A deeper discussion of these structural aspects can be found in section 3.6.1.1.

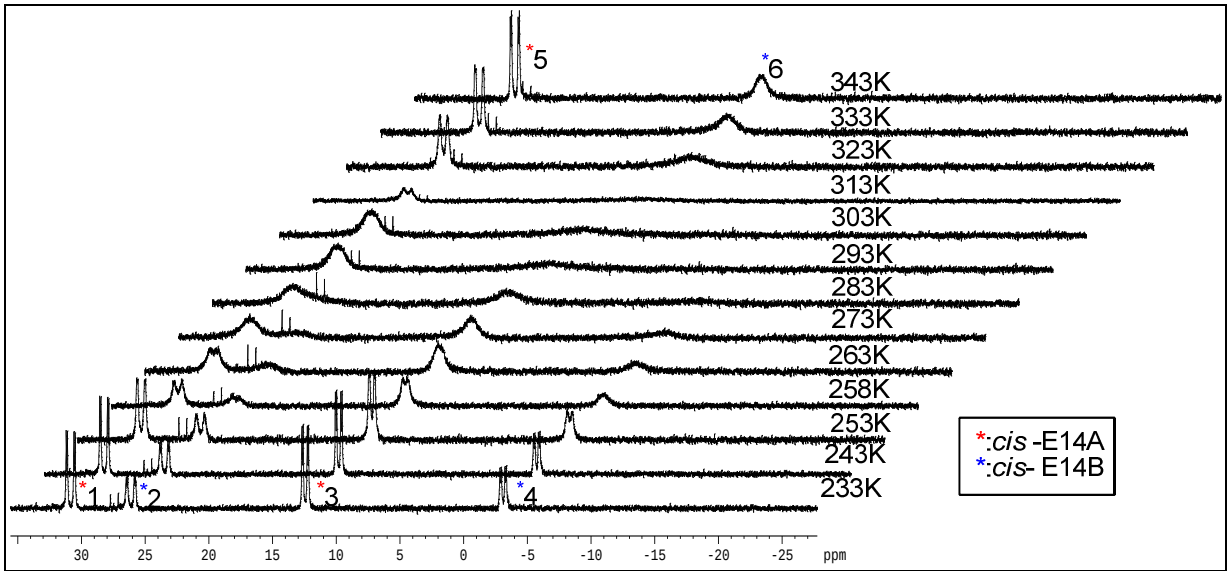

Figure 3.21: ^{31}P-NMR spectrum of peroxo adduct **E14** at different temperature.

In order to find out if the addition of O_2 to *cis*-**E10** is reversible a sample was heated during NMR measurements (Figure 3.22). The first spectrum recorded at 303 K shows the signals of **E14** and small amounts of *trans*-complex **E15B**. On heating to 343 K some remarkable changes are observed. Firstly, the signals of **E14** a sharpened due to the rapid interconversion of **E14A** and **E14B** (vide supra). Secondly, the intensity of the resonances of **E15A** has strongly increased and the resonances of *cis*-**E10** can be observed with low intensity. The latter observation is a clear indication that the addition of O_2 to *cis*-**E10** is reversible. At higher temperatures **E14** releases O_2 and starts to isomerize to give **E12** (vide supra) which subsequently reacts with O_2 to irreversibly form **E15A**. Prologned heating gives an additional minor resonance at 4 ppm which must be attributed to the isomerization product **E15B**, which shows a $^1J_{RhP}$-coupling constant of 88 Hz typical for phosphorous perpendicular to the Rh-O_2 plane. The above discussed reaction pathways can be proved in a single experiment. Therefore a sample of **E14** is heated in the presence of excess O_2. The accompanying NMR spectra show the gradual conversion of **E14** to **E15A** and finally the formation of **E15B**. Form the spectrum recorded after 21 hours of heating it can be concluded that **E15A** is thermodynamically more stable than **E15B**.

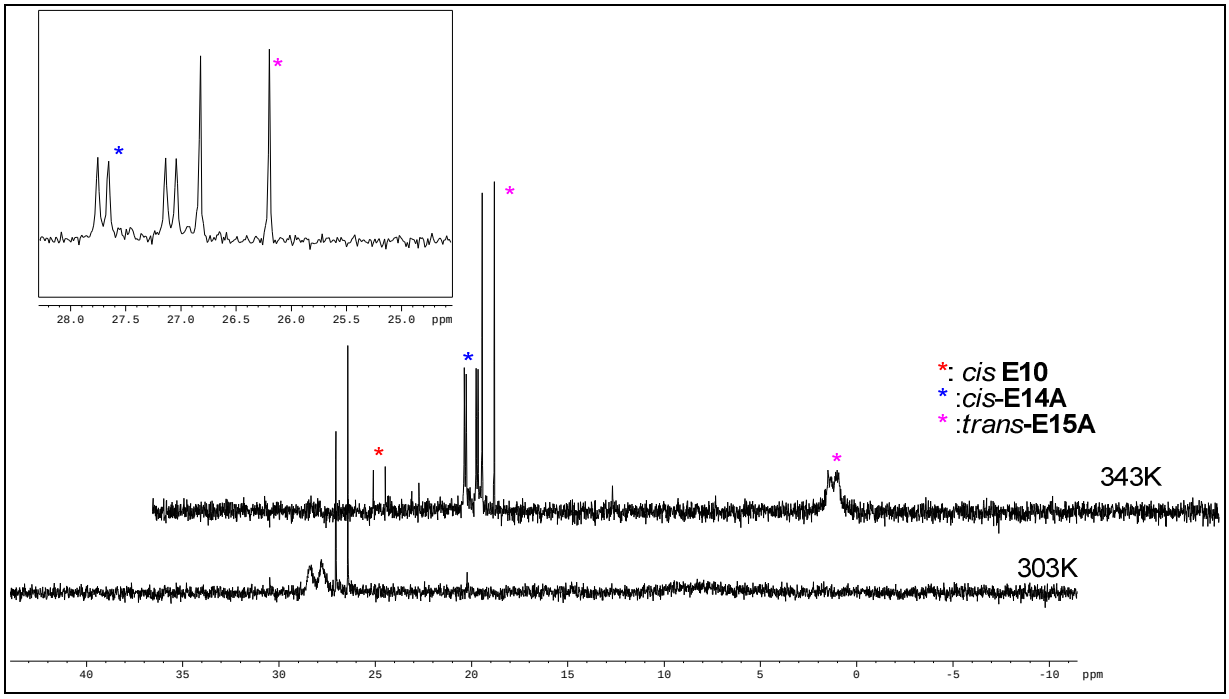

Figure 3.22: ^{31}P-NMR spectra of [Rh(η^2-O_2)($EtImCH_2CH_2PPh_2$)$_2$]Cl at 343K.

Notable feature of The ^{1}H-NMR spectra of **E15** inCD_3CN is the absence of a signal at 8.5 ppm which indicates the coordination of the carbene ligand to the Rh-atom. The protons **H^5** and **H^6** of the imidazolium ring have been detected at 6.97 ppm (d,$^3J_{HH}$ = 2 Hz) and 7.09 ppm (d, $^3J_{HH}$ = 2Hz), respectively. Compared to the protons of the imidazolium salts the latter resonances are shifted to high field. As a consequence of the coordination to Rh the protons of the ethylene bridge become diasterotopic and they are shifted to high field δ = 1.84 (m, NCH_2), 3.91 (dt, 1H ,$^2J_{HH}$ = 15 Hz, $^3J_{HH}$ = 7 Hz, PCH_2) and 3.03 (dq, 1H, $^2J_{HH}$ = 14 Hz, $^3J_{HH}$ = 7 Hz, PCH_2)]

The ^{13}C-NMR spectrum shows a high field shifted signal for the carbene atoms at 160.4 ppm (dt, $^1J_{RhP}$ = 125 Hz, $^2J_{PC}$ = 17 Hz) due to the formation of a rhodium (III) center. The carbon atoms of the imidazolium ring **C^5** and **C^6** are observed at δ 125.2(s) ppm and 121.7(s), respectively. ^{1}H and ^{13}C-NMR data for **E14** are given in the experimental section. The IR spectrum (KBr) of both **E14** and **E15** shows an absorption band at 845 cm^{-1} attributable to oxygen-oxygen stretching band which are typical for side-on coordinated peroxide.[141]

3.5.2 X-ray crystallographic analyses of *cis*-$[Rh(\eta^2\text{-}O_2)(EtImCH_2CH_2PPh_2)_2]^+$ (E14A)

Single crystals of *cis*-peroxo complex **E14A** suitable for X-ray diffraction were obtained by layering a concentrated methylene chloride solution of **E14** with diethyl ether. The peroxo complex **E14A** with counterion Cl^- crystallizes in space group P-1 with two molecules per unit cell incorporating two chloride anions and four methylene chloride solvent molecules. Crystallographic data are presented in the Table 7.5 and selected bond lengths and angles are listed in Table 3.7. Molecular structure containing the atom numbering scheme is shown in Figure 3.23a. The central rhodium atom is coordinated in a trigonal bipyramidal fashion by the carbene carbon donor atoms and phosphorous donor atoms of the two bidentate NHC ligands. The coordination is completed by the peroxo ligand. In **E14A** the carbene carbon atom C(35) and phosphorous atom P(2) occupy axial positions of the trigonal bipyramid while the carbene atom C(65), P(1) and the oxygen atoms of the peroxo ligand lie in the equatorial plane. The sum of the bond angles formed around the Rh atom in the equatorial plane is 360°.

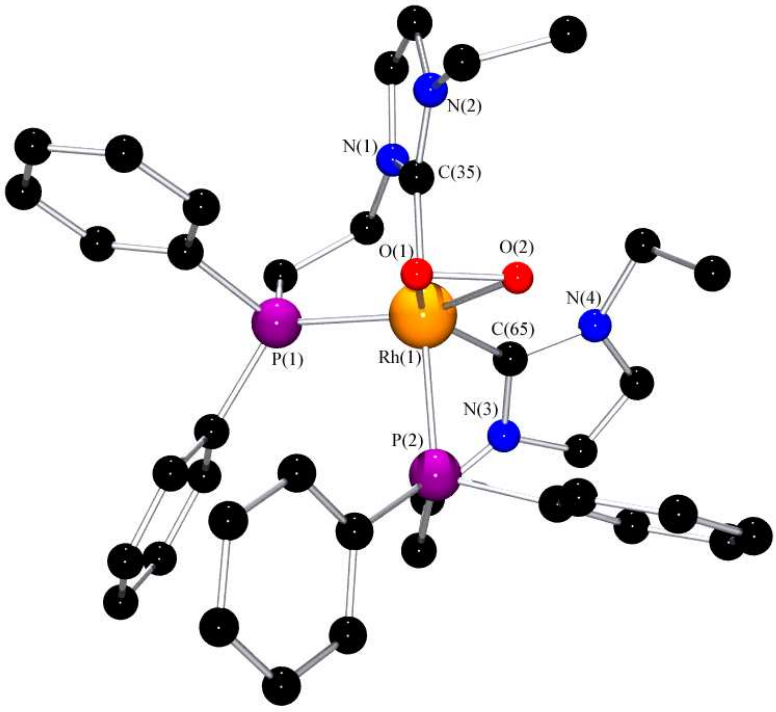

Figure 3.23a: Structure of the Δ-isomer of *cis*-$[Rh(\eta^2\text{-}O_2)(EtImCH_2CH_2PPh_2)_2]^+$ in crystals of **E14A,** with counterion **Cl^-,** (without hydrogen atoms).

Table 3.7: Selected bond lengths [Å] and angles [°] of peroxo complex **E14A**

Bond Lengths			
O(1)-O(2)	1.442(4)	Rh(1)-C(35)	2.090(4)
Rh(1)-O(2)	2.030(3)	Rh(1)-P(1)	2.3113(10)
Rh(1)-O(1)	2.062(3)	Rh(1)-P(2)	2.3156(10)
Rh(1)-C(65)	2.048(3)		
Bond Angles			
O(1)-Rh(1)-O(2)	41.25(11)	C(65)-Rh(1)-O(2)	102.87(13)
C(65)-Rh(1)-O(1)	143.41(13)	C(35)-Rh(1)-P(2)	176.23(10)
O(1)-Rh(1)-P(1)	112.47(8)	C(65)-Rh(1)-P(1)	103.91(10)
O(2)-Rh(1)-P(1)	153.02(8)		

The dioxygen molecule is coordinated to rhodium in a side on fashion. The O(1)-O(2) bond distance is 1.442(4) Å which is considerably longer than that of free dioxygen (1.21 Å) and comparable to that of H_2O_2 (1.49 Å). The bonding distance is typical for coordinated peroxides. [142]. The elongation of the O-O bond distance of the dioxygen unit is also observed in the rhodium dioxygen complexes such as $RhCl(O_2)(PPh_3)_3$, (1.413(9) Å) and $[RhCl(O_2)(PPh_3)_2]_2$ (1.44(1) Å). The difference in the Rh(1)-O(1) and Rh(1)-O(2) bond lengths is 0.032(3) Å while the O(1)-Rh(1)-O(2) angle is amounts to 41.25(11). The Rh-C bond lengths of 2.048 (3) and 2.090 (4) Å are close to those reported for comparable complexes.[142-144] The Rh-P bond lengths are 2.3156(10) Å and 2.3113(10) Å which are typical values for phosphorous coordinated to Rh(+III). The peroxide ligand is not symmetrically coordinated with respect to the axis C(35)/P(2). It is shifted towards the carbene atom C(65) and lifted from the equatorial plane by 0.179 Å. Consequently the bond angle P(1)-Rh(1)-O(2) is larger than O(1)-Rh(1)-C(65) by about 9.6°. The bond angle formed by the axial ligands, C(35)-Rh(1)-P(2) is 176.23(10)° and thus close to linearity.

In addition single crystals of *cis*–peroxo complex **E14A as** counter ion PF_6^- were obtained by layering a concentrated acetonitrile solution of **E14** with diethyl ether. In this case **E14A** crystallized in the space group $P2_12_12_1$ with four molecules per unit cell incorporating one acetonitrile molecule in the unit cell. Molecular structure containing the atomic numbering

scheme is shown in Figure 3.23b and Crystallographic data are presented in the Table 7.5. It must be noted that in this case a crystal containing only one enantiomer of **E14A** is obtained. Hence during crystallisation a spontaneous separation of the enantiomers takes place.

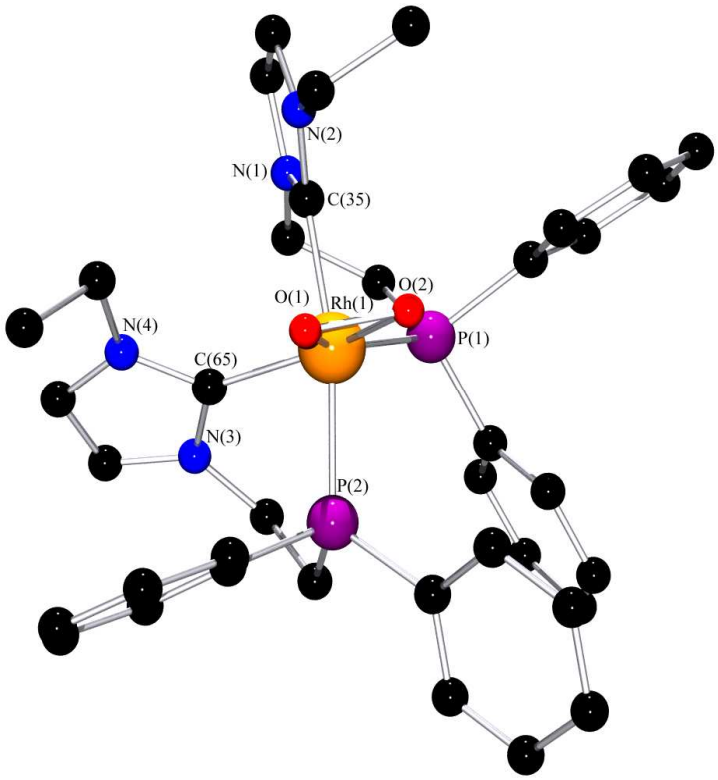

Figure 3.23b: Structure of the Λ-isomer of *cis*-$[Rh(\eta^2\text{-}O_2)(EtImCH_2CH_2PPh_2)_2]^+$ in enantiomerically pure crystal of **E14A** with counterion PF_6^-, (without hydrogen atoms).

3.5.3 Single crystal X-ray structure analysis of *trans*-$[Rh(\eta^2\text{-}O_2)(EtImCH_2CH_2PPh_2)_2][PF_6]$ (E15)

Red brown crystals of **E15** were grown by layering a concentrated methylene chloride solution with diethyl ether. **E15** crystallizes in orthorhombic space group, Pna2(1) with four molecules per unit cell in which two of the bidentate ligands are coordinated to the Rhodium(III) center. Two molecules of methylene chloride are also found in the unit cell. Crystallographic data are presented in theTable 7.6 and selected bond lengths and angles are listed in Table 3.8. Molecular structure containing the atom numbering schemes is shown in Figure 3.24.

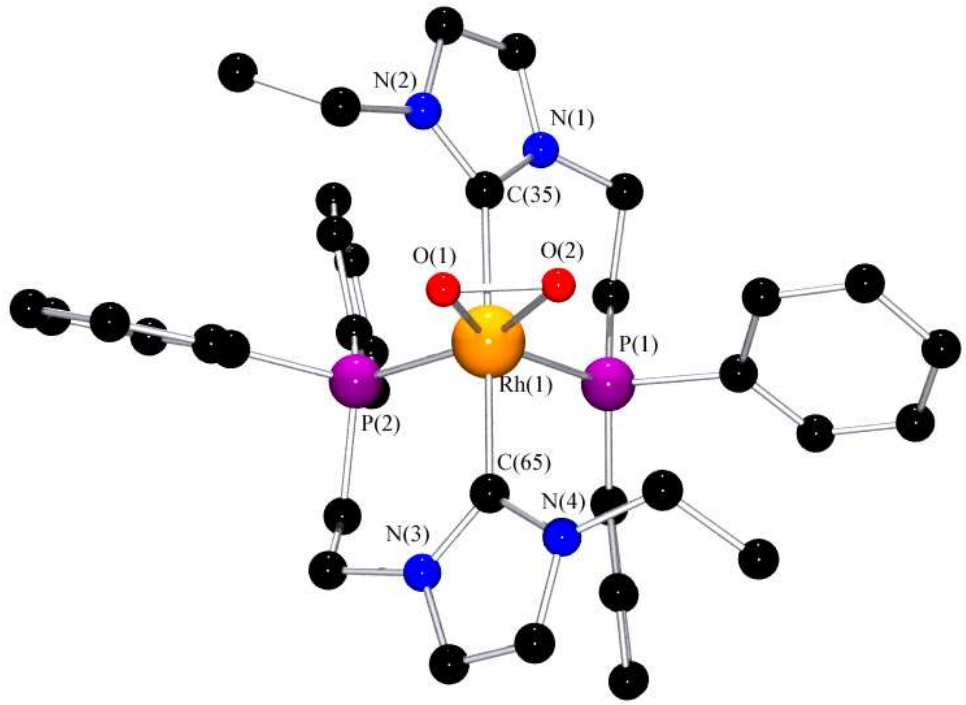

Figure 3.24: structure of *trans*-$[Rh(\eta^2\text{-}O_2)(EtImCH_2CH_2PPh_2)_2]^+$ in crystals of **E15**, (without hydrogen atoms).

The geometry around the rhodium center is trigonal bipyramidal. The phosphorous atoms and the peroxo ligand lie in the equatorial plane of the trigonal bipyramid. The sum of bond angles formed by these donors around the rhodium atom is 360°. In the *trans*- peroxo complex **E15**, the peroxo ligand is symmetrically coordinated with respect to the axis C(35)/C(65) and lies in the equatorial plane. Hence, the angles P(1)-Rh(1)-O(1) and P(2)-Rh(1)-O(2) viz., 151.4(3)° and 154.5(3) ° respectively, are almost identical. The two phosphourous donor atoms are also lying in the equatorial plane of the trigonal bipyramidal structure. The most significant difference between the structures of **E14** and **E15** is that the position of the peroxo ligand. In **E14** the the plane Rh(1)-O(1)-O(2) shows a significant torsion angle with respect to the equatorial plane of the complex and the O_2 unit is shifted towards one of the other equatorial ligands. However, in **E15** the peroxo ligand is symmetrically embeded in the equatorial plane of the molecule. Consequently in **E14**, the peroxo ligand exhibits almost identical bond distances Rh(1)-O(1) and

Rh(1)-O(2), 2.038(9) Å and 2.043(9) Å, respectively The bond lengths of Rh-C in **E14** are similar to those found in **E15** while the bond distances of Rh-P in **E14** are larger than the bond distances in **E15** by 0.037 Å.

Table 3.8: Selected bond lengths [Å] and angles [º] of peroxo complex **E15**

Bond lengths			
O(1)-O(2)	1.444(12)	Rh(1)-C(35)	2.104(12)
Rh(1)-O(2)	2.043(9)	Rh(1)-P(1)	2.280(3)
Rh(1)-O(1)	2.038(9)	Rh(1)-P(2)	2.272(3)
Rh(1)-C(65)	2.103(12)		
Bond angles			
O(1)-Rh(1)-O(2)	41.4(4)	O(1)-Rh(1)-P(1)	151.4(3)
C(65)-Rh(1)-C(35)	176.0(5)	O(2)-Rh(1)-P(2)	154.5(3)
O(1)-Rh(1)-P(2)	113.1(3)	P(2)-Rh(1)-P(1)	95.42(12)
O(2)-Rh(1)-P(1)	110.1. (3)		

3.6 Oxidative addition of small molecules viz, (S_8, CH_3I, I_2) to the *cis*-rhodium(I) complex E11

cis-Rhodium(I) complex **E11** undergoes oxidative addition recations with small molecules like elemental sulfur, methyl iodide and iodine under varying reaction conditions to give the novel rhodium(III) complexes **E16**, **E17** and **E18** as shown in Figure 3.25. The synthesis of complexes and their structures are discussed below.

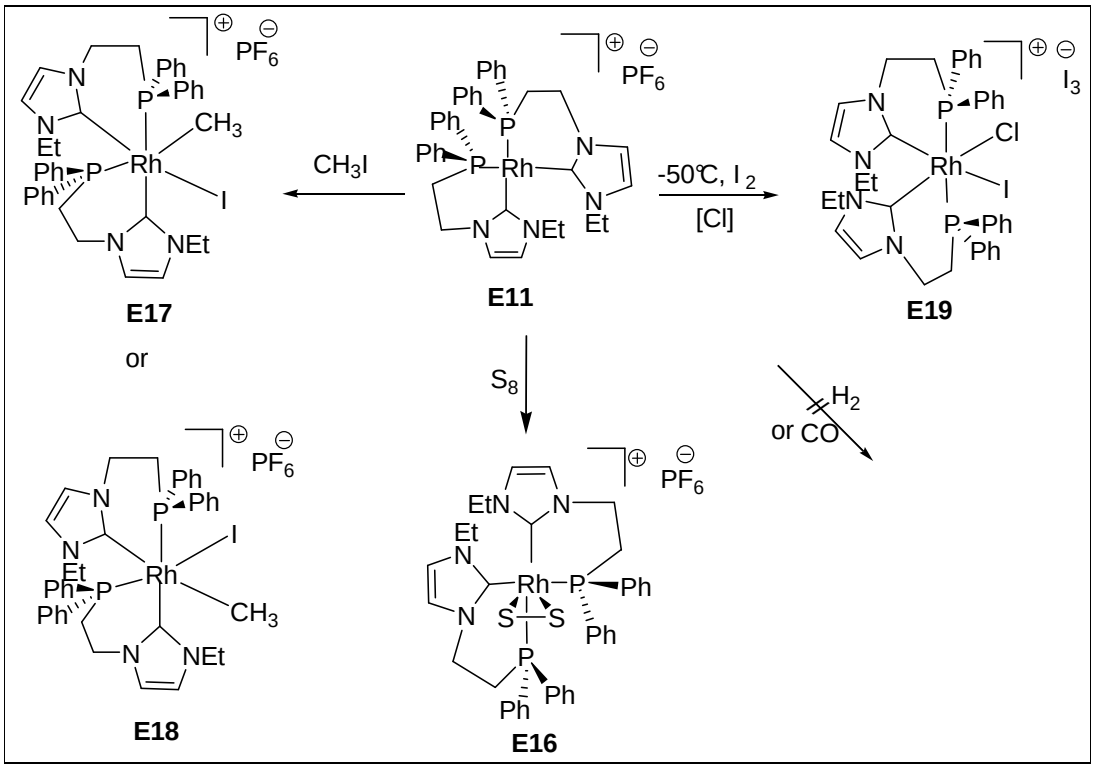

Figure 3.25: Synthesis of novel rhodium(III) complexes**.**

3.6.1 Synthesis and structure of *cis*-[Rh(η^2-S_2)(EtImCH$_2$CH$_2$PPh$_2$)$_2$][PF_6] (E16)

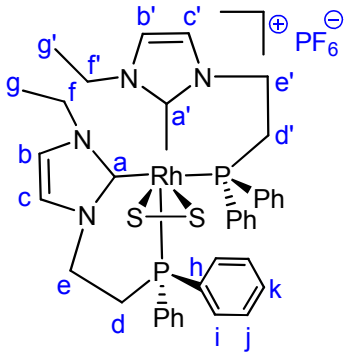

The synthesis of the *cis*-rhodium(III) complex [Rh(η^2-S_2)(EtIm $CH_2CH_2PPh_2)_2$][PF_6] **(E16)** was accomplished by oxidative addition of **E11** with elementary sulfur at room temperature in methylene chloride. In the course of the reaction the color of the solution changed from yellowish brown to green. The solvent was removed after one hour to give the product. Green crystals of the

novel *cis*-Rh(III) complex, **E16** were obtained in high yield (80 %) by layering a methylene chloride solution with diethyl ether.

The X-ray crystal structures were corroborated by NMR and IR-spectroscopy. X-ray crystallography, proves the formation of the novel *cis*-Rh(III) complex **E16** in which the rhodium is coordinated to two bidentate NHC-phosphine ligands and the disulfide molecule.

The ^{1}H-NMR spectrum of **E16** shows signals of diasterotopic protons around 2.59-3.35 ppm (m, 2H e,) and around 3.06-3.30 ppm (m, e', 2H) as well as around 4.50-5.01 ppm (m, d', 2H) and around 4.73-5.24 ppm (m, 2H ,d) which are shifted down field compared to the diasterotopic protons in the starting material **E11**. The protons of the imidazol ring were observed at 7.04 ppm (m, 1H, c), 7.15 ppm (m, 1H, b), 7.32 ppm (m, 1H, c') and 7.71 ppm (s', 1H, b), respectively.

Accordingly the ^{13}C-NMR spectrum shows four resonances which can be assigned to the carbon atoms of the imidazolium rings at δ = 119.7 (d, $^{3}J_{PC}$ = 5.0 Hz, c) and δ = 121.4 (s, c') and δ = 123.5 (d, ^{3}J = 6 Hz, b) and δ = 124.9 (s, b`), respectively. Two high field signals have been observed for carbene carbon atoms bound to the rhodium(III) center at 162.0 ppm (ddd, $^{1}J_{RhC}$ = 161, $^{2}J_{PC,\ cis}$ = 12.7, $^{1}J_{PC,\ trans}$ = 40 Hz, a) and 169.5 ppm (ddd, $^{1}J_{RhC}$ = 48 Hz, $^{2}J_{PC,\ cis}$ = 6 Hz, $^{2}J_{PC,\ trans}$ = 19 Hz, a'). Compared to *cis* **E11** in which the carbene atoms show a resonance at 183.0 ppm the resonances of **E16** are shifted to high field.

In the ^{31}P{^{1}H}-NMR spectrum of **E16** two signals are observed at δ = 3.7 (dd, $^{1}J_{RhP}$ = 128 Hz, $^{2}J_{PP}$ = 23 Hz) and δ = 18.5 (dd, $^{1}J_{RhP}$ = 76.4 Hz, $^{2}J_{PP}$ = 23 Hz) ppm. Compared to the starting matrial **E11** the phosphorous atoms of **E16** are more shielded. This observation compares well with the above described shielding of the carbene atoms. As discussed for the analogous Rh-O_2-complex **E14** the rhodium-phosporous coupling constants give a clear indication of the position of the phosphorous atoms within the complex (page 61). Hence, the signal at 3.7 ppm belongs to the phosphorous atom in the Rh-S_2 plane, whereas the other phosphorous resonance belongs to the remaining P-atom which is perpendicular to the Rh-S_2 plane. The IR spectra of **E16** exhibit a band at 557 cm^{-1} which can be assigned to the S-S-stretching vibration of η^2-S_2 ligand.[145]

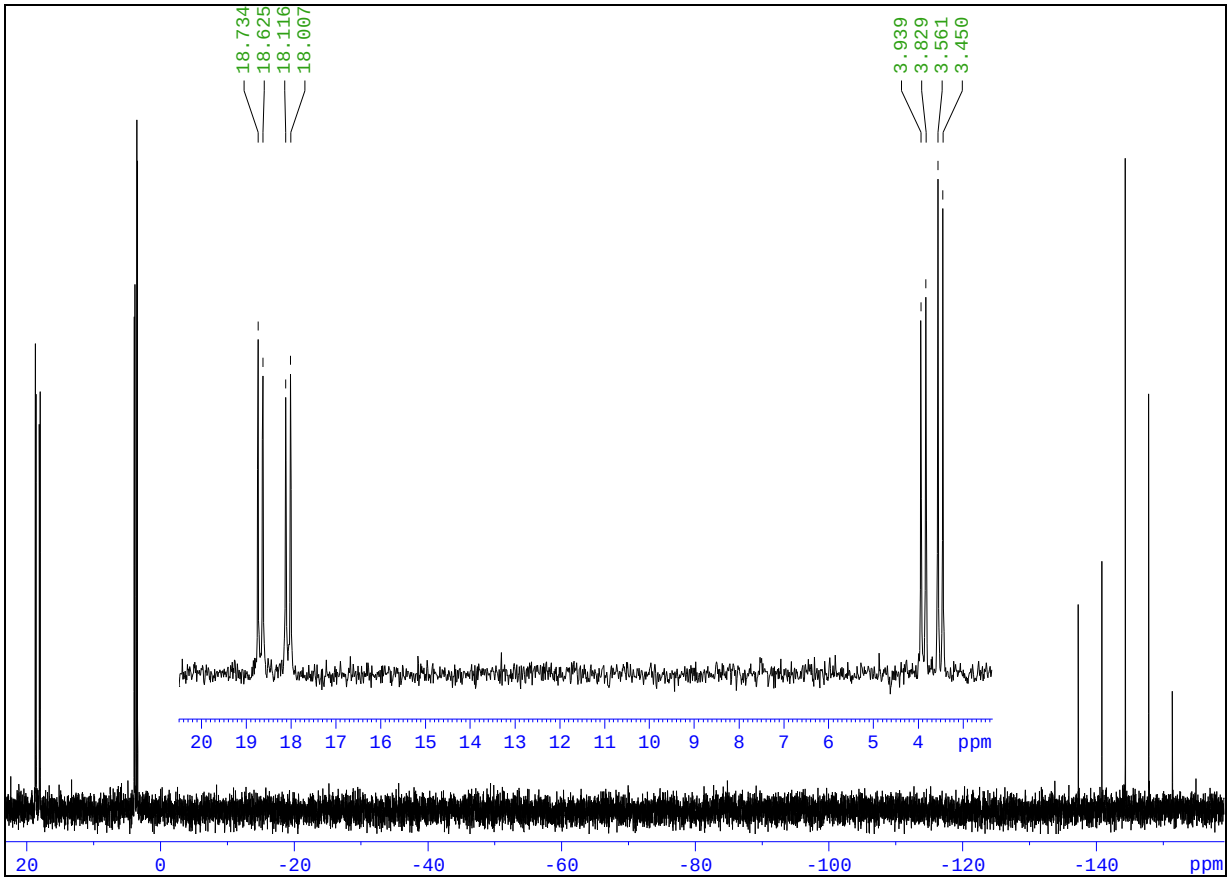

Figure 3.26: ^{31}P-NMR spectra of *cis*-[Rh(η^2-S_2)(EtIm$CH_2CH_2PPh_2$)$_2$][PF_6] (**E16**).

3.6.1.1 Single crystal X-ray structure analyses of *cis*-[Rh(η^2-S_2)(EtIm$CH_2CH_2PPh_2$)$_2$][PF_6] (E16)

Green crystals of **E16** suitable for X-ray crystallographic analysis were obtained by overlaying a concentrated methylene chloride solution of **E16** with diethyl ether. **E16** crystallizes in the monoclinic space group, P2(1)/c with four molecules per unit cell in which two of the bidentate ligands are coordinated in a *cis* arrangement with respect to the rhodium(III) center. Two molecules of methylene chloride are also found in the unit cell. Crystallographic data are presented in the Table 7.7 and selected bond lengths and angles are listed in Table 3.9. Molecular structure containing the atom numbering scheme is shown in Figure 3.27.

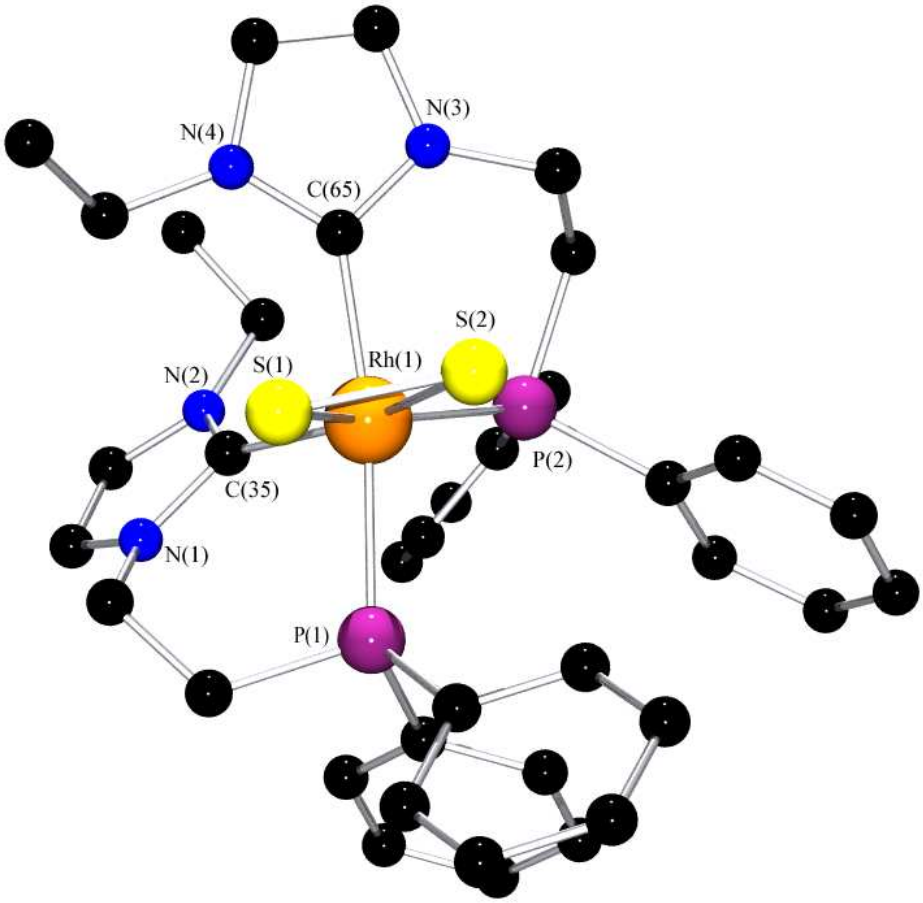

Figure 3.27: Structure of *cis*-[Rh(η^2-S_2)(EtIm$CH_2CH_2PPh_2$)$_2$]$^+$ in crystals of **E16**, (without hydrogen atoms).

The arrangement of the ligating atoms around the rhodium(III) atom is distorted trigonal-bipyramidal with two bidentate NHC-phosphane ligands and one disulfide ligand, which occupies one position in the equatorila plane, coordinated to Rh. The equatorial plane of the complex is formed by the carbene carbon atom C(35), phosphorous atom P(2) and the disulfide ligand. The axial positions are occupied the carbene carbon atom C(65) and the phosphorous atom P(1). The S_2-ligand is not symmetrically coordinated with respect to the axis C(65)-Rh(1)-P(1). The S(2) atom is slightly shifted from by 0.135 Å toward the P(2) atom. The sum of bond angles formed at rhodium atom in the equatorial plane by the equatorially lying donor atoms is

360º indicating planarity. The six membered rings in **E16** containing the rhodium center both exhibit a boat form conformation.

In **E16** the rhodium carbene bond lengths Rh(1)-C(65) and Rh(1)-C(35) are 2.058(4) Å and 2.061(5) Å, respectively, are similar to the bond lengths of rhodium carbene bond in the analogous Rh-O_2 complex **E14**. The S(1)-S(2) bond lengths of 2.0412(17) are similar to the Complex *cis* **E16** shows an analogous structure compared to to *cis*-peroxo complex **E14** but there are some significant differences. Firstly the bond distance of Rh(1)-P(1) and Rh(1)-P(2) differ from the value found in **E14** by 0.0824 and 0.0166 Å, respectively. As expected for the bigger sulfur atoms the bite angle S(1)-Rh(1)-S(2) is larger than the bite angle of O(1)-Rh(1)-O(2) by 9.18° and the equatorial bond angle of S(2)-Rh(1)-C(35) is smaller than the bond angle in **E14**, O(1)-Rh(1)-P(1) by 5.06°. The bond angle P(2)-Rh(1)-S(1) are similar to the bond angle in P(1)-Rh(1)-O(2) and The bond angle of S(2)-Rh(1)-P(2) is smaller than the bond angle P(1)-Rh(1)-O(1) by 9.86°. The angle C(65)-Rh(1)-P(1) in **E16** is smaller the respective angle C(35)-Rh(1)-P(2) by 6.83°. The former angle deviates from linearity by 10.6° most likely due to more steric strain in **E16** than in **E14** due to different conformations of the 6-membered rings containg the rhodium center. values found in literature.[146] for S-S single bonds.

Table 3.9: Selected bond lengths [Å] and angles [º] of *cis*-[Rh(η^2-S_2)(EtIm$CH_2CH_2PPh_2$)$_2$][PF_6] (**E16**)

Bond lengths			
S(1)-S(2)	2.0412(17)	Rh(1)-C(35)	2.061(5)
Rh(1)-S(2)	2.3985(13)	Rh(1)-P(1)	2.3937(12)
Rh(1)-S(1)	2.3931(13)	Rh(1)-P(2)	2.3322(13)
Rh(1)-C(65)	2.058(4)		
Bond angles			
S(1)-Rh(1)-S(2)	50.43(4)	P(2)–Rh(1)–S(1)	153.03(4)
C(65)–Rh(1)–C(35)	91.33(17)	C(65)–Rh(1)–P(1)	169.40(14)
P(2)–Rh(1)–S(2)	102.61(4)	C(35)–Rh(1)–S(2)	157.59(14)
S(1)–Rh(1)–C(35)	107.41(14)		

3.6.2 Synthesis of *cis*-[Rh(CH$_3$)(I)(EtImCH$_2$CH$_2$PPh$_2$)$_2$][PF$_6$] (E17, E18)

Cis-Rh(III) complexes **E17**, **E18** were synthesised as depicted in Figure(3.25) by oxidative addition of one equivalent of methyl iodide to one equivalent of *cis* rhodium(I) complex **E11** in THF solution at room temperature. The reaction mixture was monitored by ^{31}P NMR spectra which shows two signals at 13.39 ppm (dd, $^2J_{PP}$ = 25 Hz, $^1J_{RhP}$ = 88 Hz), -6.2 ppm (dd, $^2J_{PP}$ = 24 Hz, $^1J_{RhP}$ = 88 Hz). After removing the solvent under vacuum high yield 86 % of yellow product which characterised by ^{1}H, ^{13}C and ^{31}P NMR spectroscopy, attempts to get crystals failed.

3.6.3 Synthesis of *cis*-[Rh(Cl)(I)(EtImCH$_2$CH$_2$PPh$_2$)$_2$][I$_3$], (E19)

The synthesis of rhodium(III) complex **E19** was carried out by conducting an oxidative addition reaction in THF between *cis*-rhodium(I) complex [Rh(EtImCH$_2$CH$_2$PPh$_2$)$_2$][PF$_6$] **E11** and two equivalents of iodine at -50°C (Figure(3.25)). The color of the reaction mixture changed from yellow orange to dark brown yellow. The reaction was monitored by ^{31}P-NMR spectroscopy which confirms the formation of five isomers in the solution. All signals are simple doublets with similar chemical shifts and coupling constants between 85 and 90 Hz which are typicall for $^1J_{RhP}$ coupling, confirming that the phosphourous atoms are orthognal to coordination plane of the halides. In all isomers the phosphourous atoms are chemically equivalent and exhibit resonances at 4.04 ppm (d, $^1J_{RhP}$ = 90 Hz), 1.69 ppm (d, $^1J_{RhP}$ = 90 Hz), -1.11ppm (d, $^1J_{RhP}$ = 85 Hz), -2.78 ppm (d, $^1J_{RhP}$ = 87 Hz) and -3.38 ppm (d, $^1J_{RhP}$ = 85 Hz) with an integral ratio of 0.3:1:1:0.1:0.4. The formation of five isomers may be attributed to a radical reaction mechanism. After completion of the reaction the solvent was removed under vacuum to give a yellow brown crude product in 65% yield which gives yellow brown crystals suitable for X-ray crystallography upon recrystallization. The result of the single crystal X-ray analysis shows an unexpected iodine-chloride adduct most likely resulting from the exchange of iodine with chloride from small impurities of [Rh(COD)Cl]$_2$ in the starting material. In addition the counterion I_3^- is formed due to reaction of iodide with excess I_2. The NMR data strongly point towards 5 isostructural isomers with different halide substitution. Besides **E19** containing Cl^- and I^- coordinated to the rhodium center, isomers containing I_3^- and I^- or Cl^- and I_3^- etc. may have formed.

The ^{1}H-NMR spectra of the mixture of isomers show the appearance of two signals of diasterotopic protons at 2.69-3.65 ppm (m, CH$_2$-<u>CH$_2$</u>-P) and 2.81-3.49 (m, CH$_2$-<u>CH$_2$</u>-P) which are shifted to down field compared to **E10**, confirm the formation of a rhodium(III) center. The

resonances of the NCH_2-protons at 5.06 ppm and 6.22 ppm are shifted downfield compared to the starting complex. The protons of imidazol ring were observed at low field at 7.24 ppm and 7.8 ppm, 7.15 ppm and 7.21 ppm. In the ^{13}C-NMR spectrum the resonances of the carbene atoms coordinated to rhodium could not be detected most likely due to extremely long relaxation times of these atoms.

3.6.3.1 Single crystal X-ray structure analysis of *cis*-[Rh(Cl)(I)(EtImCH$_2$CH$_2$PPh$_2$)$_2$][I$_3$] (E19)

Yellow brown single crystals of **E19** suitable for X-ray crystallography are grown by layering a concentrated acetonitrile solution of **E19** with diisopropyl ether. It crystallizes in the monoclinic space group, P2(1)/c with four molecules per unit cell in which two of the bidentate ligands are coordinated to the rhodium(III) atom with the carbene atoms in *cis* position. The crystal also incorporated one acetonitrile molecule per unit cell. Full crystallographic data are presented in the Table 7.8 and the selected bond lengths and angles are listed in Table 3.10. Molecular structure containing the atom numbering scheme is shown in Figure 3.28. The structural arrangement around rhodium atoms is octahedral and the sum of angles around rhodium(III) center is 360°. The rhodium atom is located only 0.051 Å from the coordination plane spanned by the halides and the carbene atoms. Generally, the ligand bite angles C(31)-Rh(1)-P(2) and C(1)-Rh(1)-P(1) are close to the ideal angle of 90° expected in an octahedral enviroment. However, the large iodine atom leads to noticable distortions of the geometry of this complex. For example the angle P(1)-Rh(1)-P(2) which is expected to be 180° amounts only to 167.05(11)° as the phosphorous atoms are bend away from the free electron pairs of the iodine ligand. Due to the same reason the angle C(31)-Rh(1)-P(1) is widened from ideally 90° to 99.3(3)°. The bonding distances of Rh(1)-C(1) and Rh(1)-C(31) are of equal length and similar to those found in the literature.[131,133,136]

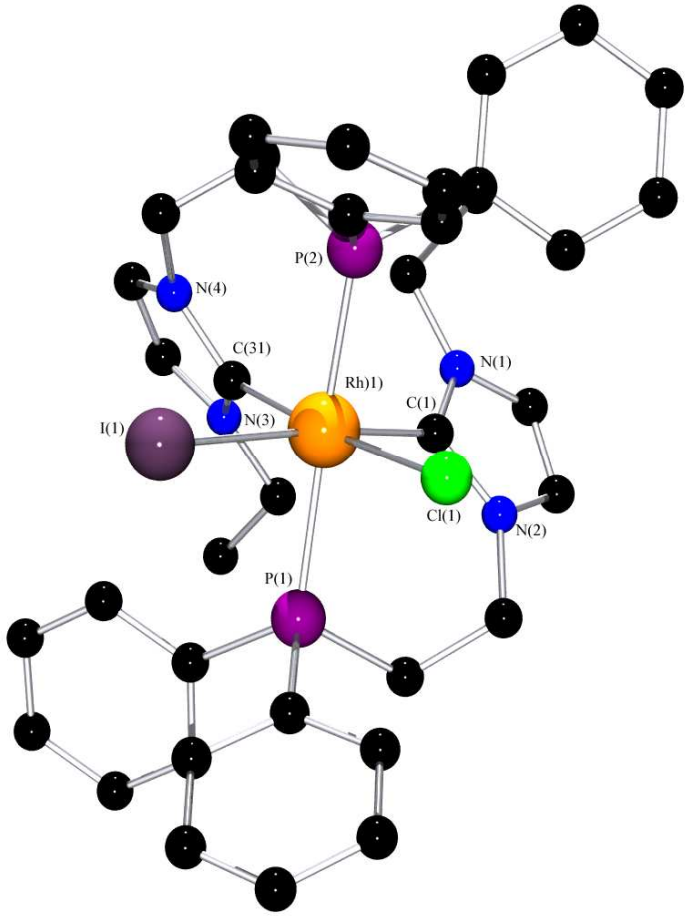

Figure 3.28: Structure of *cis*-[Rh(Cl)(I)(EtImCH$_2$CH$_2$PPh$_2$)$_2$]$^+$ in crystals of **E19**, (without hydrogen atoms).

Table 3.10: Selected bond lengths [Å] and angles [°] of **E19**

Bond lengths			
I(1)-Rh(1)	2.7531(12)	Rh(1)-P(2)	2.353(3)
Rh(1)-Cl(1)	2.442(3)	Rh(1)-C(1)	2.038(11)
Rh(1)-P(1)	2.378(3)	Rh(1)-C(31)	2.054(10)
Bond angles			
C(31)-Rh(1)-P(2)	91.6 (3)	P(1)-Rh(1)-Cl(1)	85.26(10)
C(1)-Rh(1)-P(1)	91.9(3)	C(1)-Rh(1)-I(1)	175.2(3)
P(2)-Rh(1)-Cl(1)	83.85(10)	P(2)-Rh(1)-P(1)	167.05(11)
C(31)-Rh(1)-P(1)	99.3(3)	Cl(1)-Rh(1)-C(1)	91.5(3)

3.7. Iridium complexes

3.7.1 Synthesis of *cis*-[Ir(EtImCH$_2$CH$_2$PPh$_2$)][PF$_6$] (E20)

The novel *cis*-iridium(I) complex **E20** was synthesized according to Figure 3.29. The first step of the sequence involves the deprotonation of two equivalents of imidazolium salt **E6** in THF solution with one equivalent of potassium dimethylsilylamide at room temperature under inert gas atmosphere to afford 1-ethyl-3-ethyldiphenylimidazole-2-ylidene **E7**. The formation of the latter was indicated via its reaction with carbondisulfide. Then one equivalent of the metal precursor [(Ir(μ-Cl)(COD)]$_2$ was added to the carbene solution. The colorless solution turned immediately to orange red. Subsequently the reaction mixture was stirred for 1 hour. The formation of novel *cis* cationic iridium(I) complex **E20** was confrimed by measuring a ^{31}P-NMR spectrum which exhibits a signal of the phosphorous atoms at 16.8 ppm which is similar to other phosphorous resonances in iridium(I) complexes reported in the literature.[135]

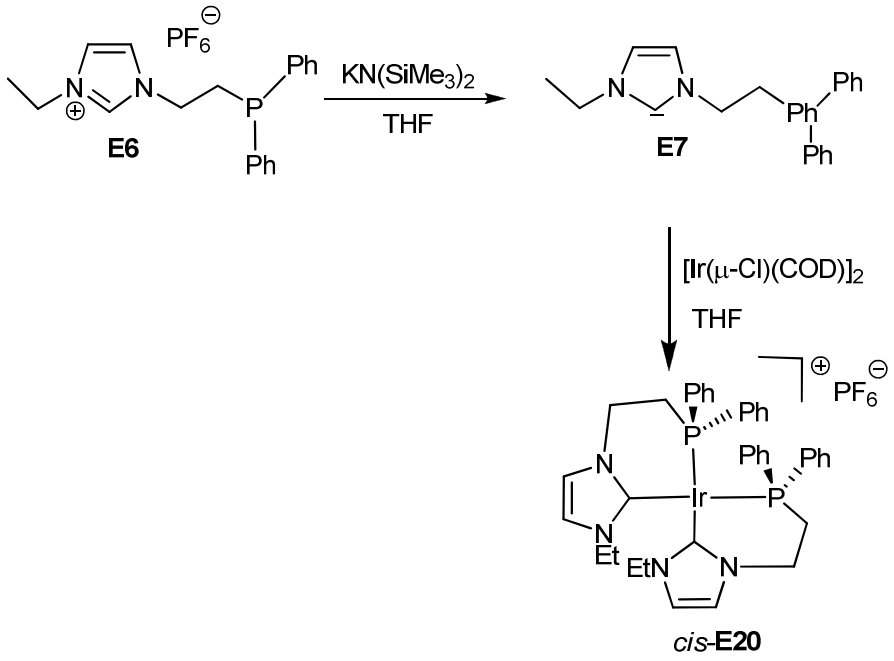

Figure 3.29: Synthesis of *cis*-[Ir(EtImCH$_2$CH$_2$PPh$_2$)$_2$][PF$_6$] (**E20**).

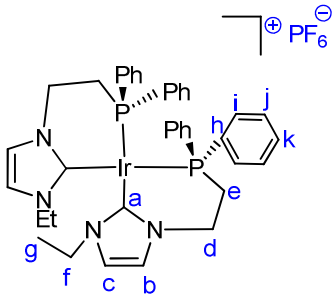

cis-E20

The novel Iridium(I) complex is soluble in THF solution. After removing of the solvent under vacuum an orange red crude product was crystallized by layering a concentrated methylene chloride solution with diethyl ether to give orange red crystals of **E20** in high yield. The structure of **E20** was characterized by NMR spectroscopic methods and single crystal X-ray analysis.

The ^{1}H-NMR spectrum of **E20** shows the absence of the signal at 8.49 ppm proving the deprotonation of the imidazolium salt **E6** and indicating the coordination of the bidentate NHC-phosphane ligand to iridium(I). The signals of the diastereotopic protons of the CH_2-units were observed around 2.12-2.59 ppm (m, 4H, e) and 4.36-4.91(m, 4H, d). Compared to the imidazolium salts **E6** these resonances are downfield shifted. In contrast the signals of the protons of the imidazol ring are shifted to higher field with δ = 6.94 (d, 2H, $^{3}J_{HH}$ = 1.3 Hz, b) and δ = 7.07 (d, 2H, $^{3}J_{HH}$ = 2.1 Hz, c), respectively. This shift is easy to understand as the deprotonation of the imidazolium rings leads to a strong decrease of their aromaticity. The signals of aromatic protons of phenyl ring were observed at 6.82-7.80 ppm.

The resonances in the ^{13}C-NMR spectrum of **E20** shows the signal of carbenic carbon atom (a) at at 174.4 ppm which appears as a double doublett ($^{2}J_{PC\ (cis)}$ = 20 Hz, $^{2}J_{PC\ (trans)}$ = 97 Hz) confirming the stereochemistry of the whole complex. The double doublett arises from phosphorous carbon coupling. It can only be explained by phosphorous atoms located in *cis*- and *trans*-position with respect to the carbene atoms. The values of the coupling constants are similar to other iridium-NHC metal complexes reported in the literature.[131,135,136,147,148]

The ^{31}P-NMR spectrum of the iridium complex shows a signal at 16.9 ppm (s) which similar to other value reported in the literature.[135] This observation confirms the coordination of iridium atom to the bidentate ligands. The signal of [PF_6] appears at high field at -144.0 ppm (hep, $^{1}J_{PF}$ = 711 Hz).

3.7.1.1 Single crystal X-ray structure analyses of *cis*-[Ir(EtImCH$_2$CH$_2$PPh$_2$)$_2$][PF$_6$] (E20)

Orange red single crystals of **E20** suitable for single crystal X-ray crystallography are obtained by layering diethyl ether onto concentrated methylene chloride solution. **E20** crystallizes in the

monoclinic space group, P2(1)/n with four molecules per unit cell in which two of the bidentate ligands are coordinated in a *cis* fashion to the iridium(I) center. The structural arrangement around iridium atoms is square planar and the iridium atom lies in the plane of the ligating atoms (deviation 0.003 Å) and the sum of angles around the iridium center is 360° as expected for square planar complexes. Crystallographic data are presented in the Table 7.9 and selected bond lengths and angles are listed in Table 3.11. Molecular structure containing the atom numbering is shown in Figure 3.30.

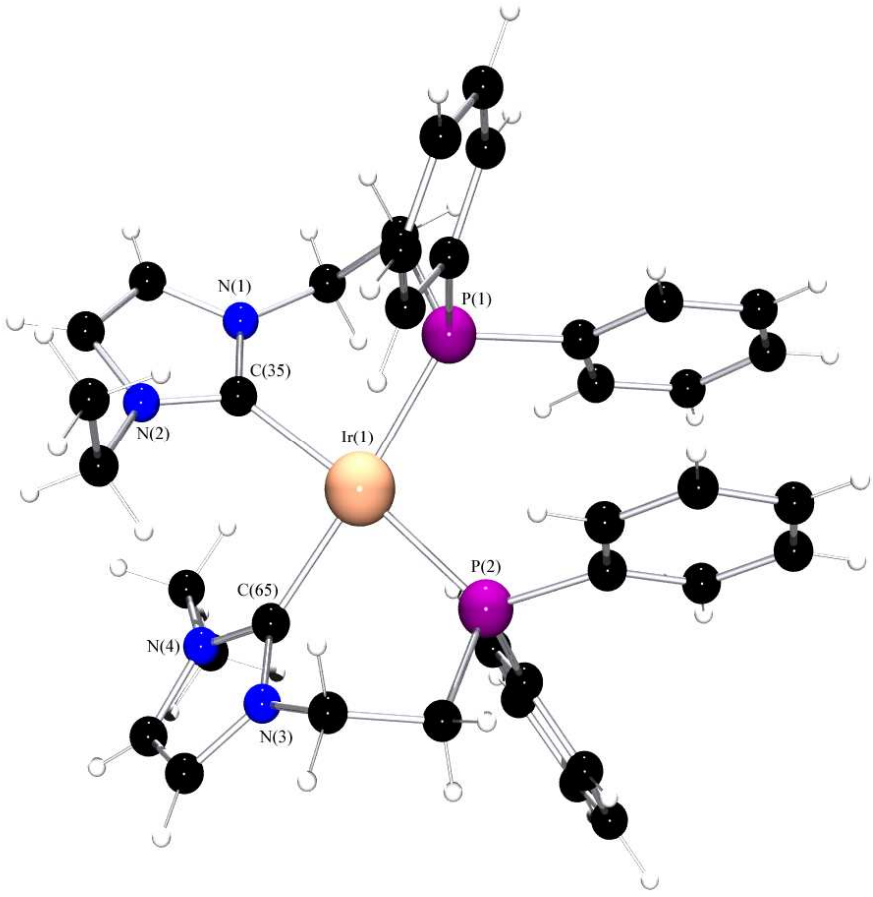

Figure 3.30: Structure of *cis*-$[Ir(EtImCH_2CH_2PPh_2)_2]^+$ in crystals of **E20**.

In **E20** the phosphorous atoms lie on one side of the square and carbene atoms are on the other side. In **E20** both six membered rings form boat conformations. Similar pseudo-boat conformations have also been observed in the reported X-ray structures of other Ir-NHC complexes.[149,150] Generally, in **E20** the bite angle P(1)-Ir(1)-C(35) deviates from the ideal 90° angle by 5.6° and for P(2)-Ir(1)-C(65) by 3.5°. The deviation is most likely due to steric effects

imposed by the interaction of phenyl rings. Due to that the arrangement around the iridium atom is gives as ligthly distorted square. The angle P(2)-Ir(1)-C(35) of 176.2(3)° is close to the linearity while the angle P(1)-Ir(1)-C(65) which amounts to 174.1(4)° is a little bit more distorted. The bond distances of Ir(1)-C(65) and Ir(1)-C(35) are 2.054(12) and 2.059(12), they are similar to other iridium-NHC metal complexes which are found in the literature.[59,97f,97h,151] The bond distance of Ir(1)-P(2) and Ir(1)-P(1) are 2.267(3) and 2.265(3), respectively, are within the range reported in the literature for similar complexes.[152-154]

Table 3.11: Selected bond lengths [Å] and angles [°] of *cis*-Ir(I) complex **E20**

Bond lengths			
Ir(1)-C(65)	2.054(12)	Ir(1)-P(1)	2.265(3)
Ir(1)-C(35)	2.059(12)	Ir(1)-P(2)	2.267(3)
Bond angles			
C(65)-Ir(1)-C(35)	89.8(5)	C(35)-Ir(1)-P(2)	176.2(3)
C(65)-Ir(1)-P(2)	86.5(4)	C(65)-Ir(1)-P(1)	174.1(4)
C(35)-Ir(1)-P(1)	84.4(3)	P(1)-Ir(1)-P(2)	99.37(12)

The comparison between *cis*-Ir(I) complex **E20** and the Rh(I) complex **E11** shows the close similarity of both complexes. There are only minor differences with respect to the observed angles within both molecules. Most of the bonding distances are equal according to the standard deviations determined (Table 3.12).

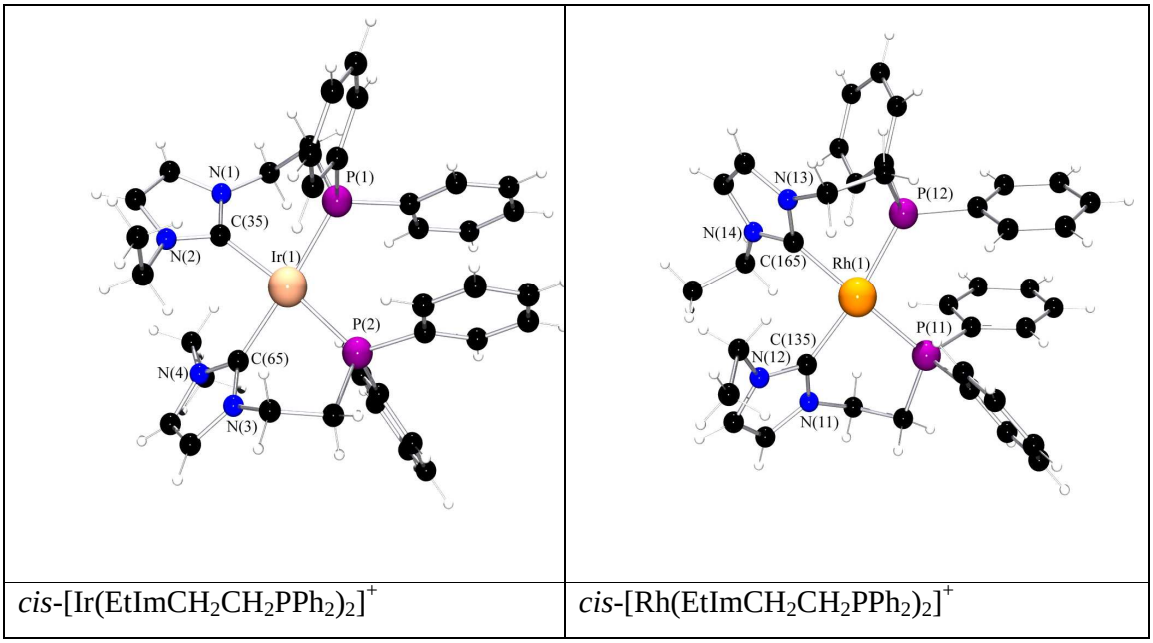

cis-[Ir(EtImCH$_2$CH$_2$PPh$_2$)$_2$]$^+$	*cis*-[Rh(EtImCH$_2$CH$_2$PPh$_2$)$_2$]$^+$

Figure 3.31: Structure representation of *cis*-[Ir(EtImCH$_2$CH$_2$PPh$_2$)$_2$]$^+$ and *cis*-[Rh(EtImCH$_2$CH$_2$PPh$_2$)$_2$]$^+$ in crystals of **E20** and **E11**.

Table 3.12: Selected bond lengths [Å] and angles [°] for **E20** and **E11**

Bond length			
E11		**E20**	
Rh(1)-C(135)	2.044(4)	Ir(1)-C(65)	2.054(12)
Rh(1)-C(165)	2.057(4)	Ir(1)-C(35)	2.059(12)
Rh(1)-P(11)	2.2565(11)	Ir(1)-P(2)	2.267(3)
Rh(1)-P(12)	2.2739(11)	Ir(1)-P(1)	2.265(3)
Bond angles			
E11		**E20**	
C(135)-Rh(1)-C(165)	91.24(16)	C(65)-Ir(1)-C(35)	89.8(5)
C(135)-Rh(1)-P(11)	88.75(12)	C(65)-Ir(1)-P(2)	86.5(4)
C(165)-Rh(1)-P(12)	80.54(11)	C(35)-Ir(1)-P(1)	84.4(3)
C(135)-Rh(1)-P(12)	171.66(12)	C(65)-Ir(1)-P(1)	174.1(4)
C(165)-Rh(1)-P(11)	174.23(12)	C(35)-Ir(1)-P(2)	176.2(3).

3.8 Reaction of small molecules viz, (H_2, O_2, S_8, CO, CH_3I, I_2) with *cis*-Iridium(I) complex E20.

The *Cis*-Iridium(I) complex **E20** undergoes reactions with small molecules like hydrogen, oxygen, elemental sulfur, methyl iodide and iodine in different solvents to afford the novel Ir(III) complexes **E21, E22, E23, E24, E25** and **E26** as outlined in Figure 3.32. The synthesis of all complexes and their structures are discussed in details below.

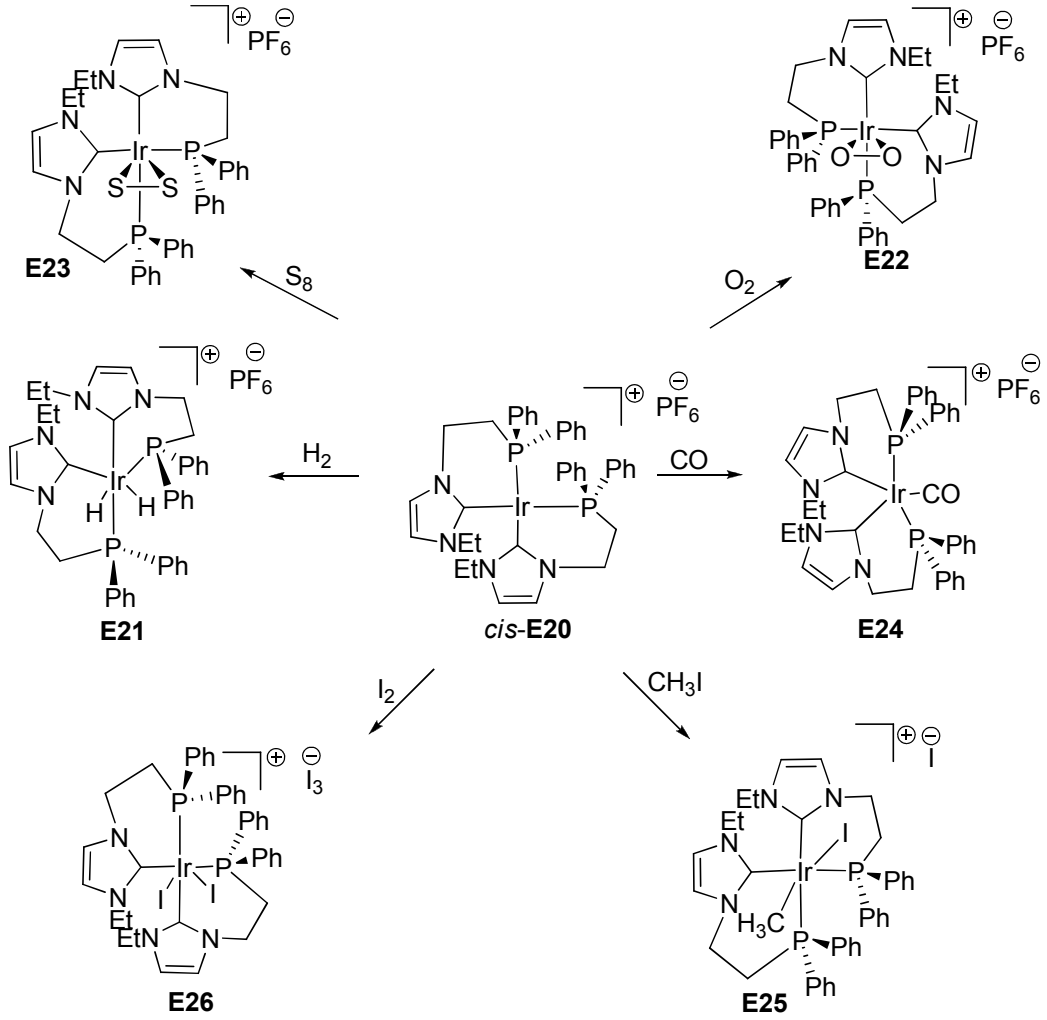

Figure 3.32: Reactions of small molecules with **E20**.

3.8.1. Synthesis and characterization of *cis*-$[Ir(H)_2(EtImCH_2CH_2PPh_2)_2]^+$(E21)

Exposure of *cis*-$[Ir(EtImCH_2CH_2PPh_2)_2]^+$ **E20** to H_2 (1bar) in methylene chloride solution afforded the novel hydride complex *cis*-$[Ir(H_2)(EtImCH_2CH_2PPh_2)_2]^+$ **E21**. The reaction was

completely finished within one hour. After the removal of the solvent under vacuum the yellow product was isolated in high yield (70 %) and recrystallised by layering diethyl ether onto a concentrated methylene chloride solution. The ^{1}H, ^{13}C and ^{31}P NMR spectra are in agreement with solid state structure of **E21** (Figure 3.33).

The most significant features in the ^{1}H-NMR spectrum of **E21** are the hydride signals at δ = -9.79 (td, $^{2}J_{PH\ cis}$ = 32 Hz, $^{2}J_{HH}$ = 4 Hz) and -7.71 (ddd, $^{2}J_{PH\ trans}$ = 129 Hz, $^{2}J_{HH}$ = 4 Hz, $^{2}J_{PH\ cis}$ = 18 Hz) corresponding to a terminal hydride ligands bonded to the iridium center. The small $^{2}J_{HH}$ coupling constant proves the *cis* arrangement of the hydride ligands. Their coupling patterns indicates that one of them (δ = -9.79) is in *trans* position to one phosphorous atoms while the other (δ = 7.71) is in *cis* position to both phosphorous atoms.[155-157]

Coordination of the carbene ligands is confirmed by their ^{13}C-NMR resonances which are shifted to high field δ = 160.2 (m) compared to the signals of **E20** in which they appeared at 170 ppm. The ^{31}P-NMR spectrum exhibits two signal due to the presence of inequivalent phosphorous atoms at -0.86 (d, $^{2}J_{PP}$ = 15 Hz) and -2.17 (d, $^{2}J_{PP}$ = 15 Hz). The IR spectrum shows a sharp Ir-H stretching mode at 2013 and 2050 cm^{-1} which are in good agreement with other iridium hydride complexes reported in the literature.[158]

3.8.1.1 Single crystal X-ray structure analysis of *cis*-$[Ir(H)_2(EtImCH_2CH_2PPh_2)_2][PF_6]$ (E21)

Single crystals of **E21** were obtained by over layering diethyl ether onto a concentrated methylene chloride solution. **E21** crystallized in the monoclinic space group P2(1)/c with four molecules in the unit cell. Figure 3.33 shows the Molecular structure of **E21,** the relevant bond lengths and angles are presented in Table 3.13, Crystallographic data are presented in the Table 7.10. In **E21** the iridium atom is coordinated with two hydride ligands in *cis* orientation and two bidentate NHC-phosphane ligands. Both the phosphorous atoms and the carbene carbon atoms adopt a *cis* coordination. Hence, the complex is in an all *cis*-configuration reflecting the stereochemistry of the starting complex **E20**. The iridium atom exhibits a distorted octahedral geometry. The carbene carbon atoms and the iridium center build an angle of 93.22(17)°. The bond angle H(1)-Ir(1)-H(2) is 96.1(29)°deviates slightly from ideal angle due to strong interaction of hydride ligand with one of the hydrogen atoms of the phenyl ring. The angles C(35)-Ir(1)-P(2) and P(1)-Ir(1)-P(2) deviate by 11° from ideal 90° angle due to the interaction of

the phenyl rings. The angle C(65)-Ir(1)-P(1) deviates by 16° from linearity due to the steric strain imposed by the phenyl rings. The angle C(65)-Ir(1)-H(2) is also diminished to 83.92° due to interaction between the phenyl rings and the hydride ligand. The iridium carbene carbon bond distances of 2.043(4) and 2.099(4) Å for Ir(1)-C(65) and Ir(1)-C(35), respectively, lie in the range of previously reported Ir-C bond lengths.[100] The Ir-P distance amount to 2.2876(13) and 2.3174(12) Å. They are similar to other Ir-P bonds observed in Ir(III) phosphine complexes.[159] The iridium hydrogen bond distances are 1.68(3) and 1.70(3) Å.

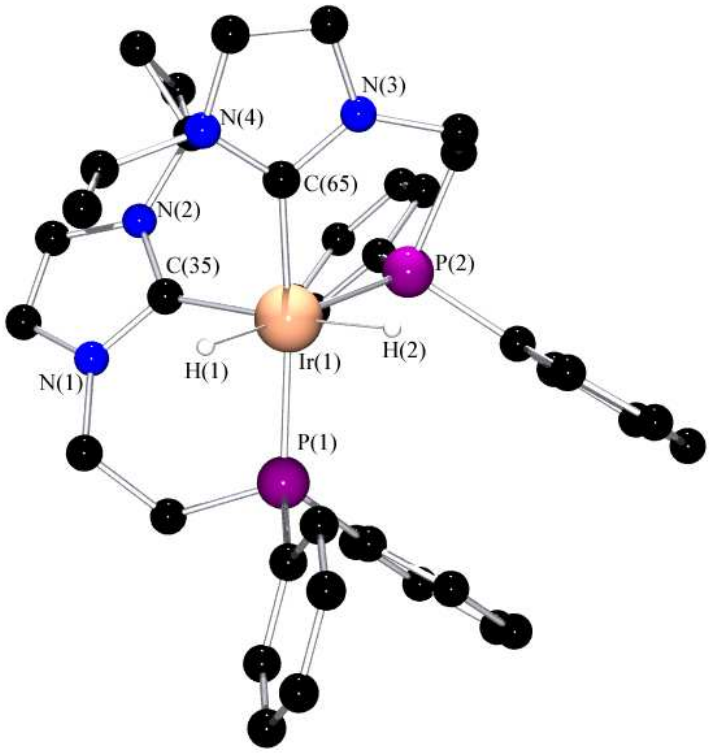

Figure 3.33: Structure of *cis*-$[Ir(H)_2(EtImCH_2CH_2PPh_2)_2]^+$ in crystals of **E21**, (without hydrogen atoms).

Table 3.13: Selected bond lengths [Å] and angles [°] of *cis*-$[Ir(H)_2(EtImCH_2CH_2PPh_2)_2]^+$ (**E21**)

Bond Lengths			
Ir(1)-C(65)	2.043(4)	Ir(1)-P(2)	2.3174(12)
Ir(1)-C(35)	2.099(4)	Ir(1)-H(1)	1.68(3)
Ir(1)-P(1)	2.2876(13)	Ir(1)-H(2)	1.70(3)
Bond Angles			
C(65)-Ir(1)-C(35)	93.22(17)	C(35)-Ir(1)-P(2)	101.53(13)
C(35)-Ir(1)-P(1)	92.00(13)	P(1)-Ir(1)-P(2)	101.95(4)
C(65)-Ir(1)-P(1)	163.80(13)	C(35)-Ir(1)-H(2)	176.11
P(2)-Ir(1)-H(1)	173.01	C(65)-Ir(1)-H(2)	83.92

3.8.2 Synthesis and characterization of *cis*-$[Ir(\eta^2\text{-}O_2)(EtImCH_2CH_2PPh_2)_2][PF_6]$ (E22)

Exposure of complex **E20** to air at room temperature in THF gives the complex *cis*-$[Ir(\eta^2\text{-}O_2)(EtImCH_2CH_2PPh_2)_2][PF_6]$ within 5 minutes. The formation of the peroxo complex is immediately indicated by the change of the color of the solution from orange red to pale yellow. ^{31}P-NMR spectra prove complete conversion of the starting material. The formation of the iridium peroxo complex is irreversible which has been proved by measuring the ^{31}P-NMR spectra at different temperatures (230K-345K) in CD_3CN solution. Over the whole temperature range only the signals of **E22** were observed, hence dissociation of oxygen can be excluded.

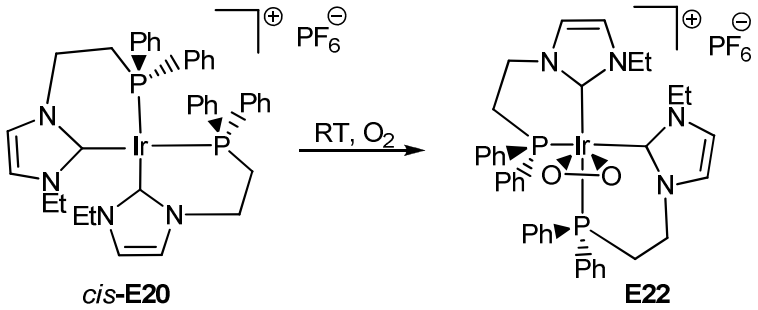

cis-**E20** **E22**

Peroxo complex **E22** are characterised by ^{1}H, ^{13}C, ^{31}P-NMR spectra, IR-spectroscopy and single crystal X-ray analysis. The significant features in ^{1}H-NMR spectrum is a significant downfield shift of the protons of the imidazol rings compared to **E20**. Their resonances are observed at 7.14 (d, 1H, $^3J_{HH}$ = 2 Hz) and 7.59 (d, 1H, $^3J_{HH}$ = 2 Hz). In the ^{13}C-NMR spectrum the resonances of

the carbene atoms were strongly shifted to lower frequencies due to the formation of an iridium(III) center. The signals are observed at 143.6 ppm (m) and 147.2 (m). The ^{31}P-NMR spectrum shows two signals in close proximity at about -12.5 ppm (d, $^{2}J_{PP}$ = 15 Hz) (compare figure 4). The coupling constanr proves *cis*-orientation of the phosphorous atoms and indicates that the stereochemistry of the starting complex **E20** in preserved in this type of oxidative addition. The IR spectrum shows a sharp peak which can be assigned to ν(O-O) band at 854 cm^{-1}. Its position is comparable e.g. with the band of $[(\eta^2\text{-}O_2)IrCl(CO)(PPh_3)_2]$[160] which is located at 858 cm^{-1}.

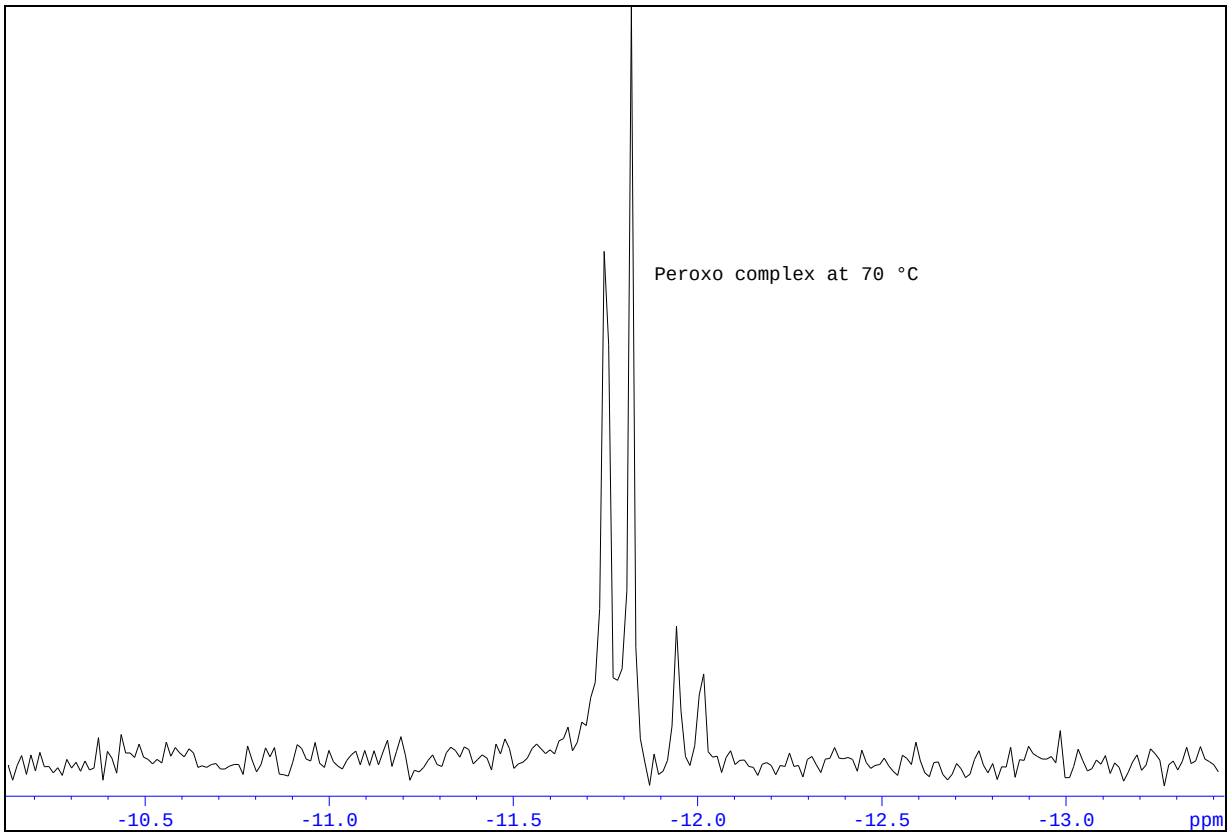

Figure 3.34: ^{31}P-NMR spectra of *cis*-$[Ir(\eta^2\text{-}O_2)(EtImCH_2CH_2PPh_2)_2][PF_6]$ (**E22**) at 70°C.

3.8.2.1 Single crystal X-ray structure analysis of *cis*-[Ir(η^2-O_2)(EtImCH$_2$CH$_2$PPh$_2$)$_2$][PF$_6$] (E22).

Yellow crystals of the novel *cis*-peroxo complex **E22** suitable for X-ray diffraction were obtained by layering a concentrated THF solution of **E22** with di-isopropyl ether. The *cis*-peroxo complex **E22** crystallizes in the orthorhombic space group $P2_12_12_1$ with four molecules per unit cell incorporating four THF molecules in the unit cell. Crystallographic data are presented in the Table 7.11. Selected bond lengths and angles are listed in Table 3.14. Molecular structure containing the atom numbering scheme is displayed in Figure 3.35. The geometry around the iridium center is trigonal bipyramidal. The coordination polyhedron is formed by the peroxo ligand, carbene carbon atom C(35) and the phosphorous atom P(2) lying in equatorial plane and the axial donors C(65) of the carbene moiety and P(1) of the phosphane moiety. The arrangement of all ligands gives a chiral complex as can be seen from Figure 3.32. As no chiral reagents were used to prepare this complex a racemic product is expected. However, the space group of the investigated crystal proves that it consists of one enantiomer only. Hence, in the course of the crystallization a sponateous separation of the racemat took place giving crystals which are made of only one of the two enantiomers. Unfortunaltely these two types of crystals could not be separated by manual picking as no apparent differencies in their shape and color were observable on inspection under the microscope. The sum of bond angles formed by the equatorially placed donors, C(35), P(2) and the peroxo ligand around iridium is 359.8°. In **E22,** the peroxo ligand is not symmetrically bonded with respect to the axis C(25)-Ir(1)-P(2). It is shifted towards the phosphine donor atom P(1). The angles formed by the peroxo ligand are 149.08(11)° for P(2)-Ir(1)-O(1) and 154.18(18) for C(35)-Ir(1)-O(2). Furthermore, the peroxo ligand is shifted from equatorial plane by 0.023 Å and 0.011 Å for O(2) and O(1), respectively. The bond angle formed by the axial ligands C(65)-Ir(1)-P(1) deviates from linearity by -11° due to the steric hindrance imposed by the phenyl rings of the phosphane residues. The angles formed by the peroxo ligand with the central iridium atoms e.g. O(2)-Ir(1)-O(1) with 42.24(14)° and the distance between O(1)-O(2) with 1.482 (5) Å are typical for peroxo complexes of iridium[161] Consequently the iridium center is in the formaloxidation state +3.

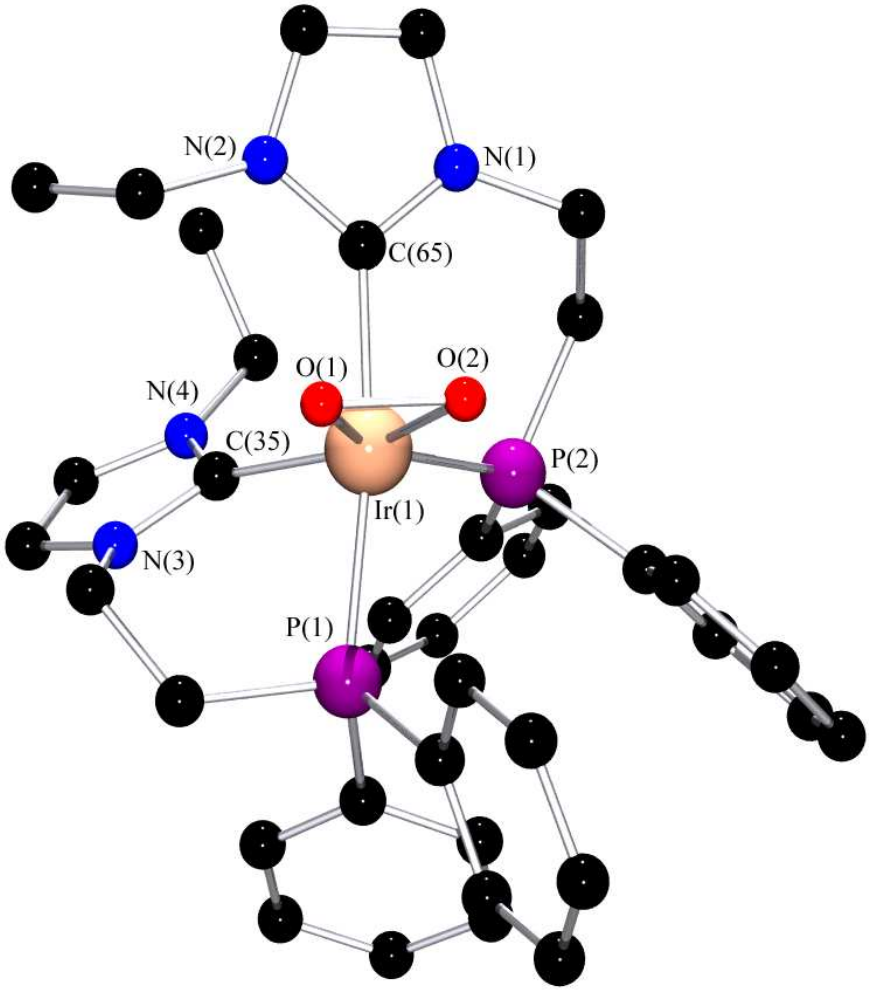

Figure 3.35: Structure of *cis*-[Ir(η^2-O_2)(EtIm$CH_2CH_2PPh_2$)$_2$]$^+$ in crystals of **E22**, (without hydrogen atoms).

The Ir-O bond lengths are almost equivalent with 2.045(3) and 2.069(4) Å. They are in the typical range observed for known Ir(η^2-O_2) complexes.[162] The Ir(1)-P(2) and Ir(1)-P(1) distances are 2.2857(15) Å and 2.3863 (16) Å and are similar to those observed in other reported iridium(III) complexes.[162]

Table 3.14: Selected bond lengths [Å] and angles [°] of *cis*-Ir(III) complex **E22.**

Bond lengths			
O(1)-O(2)	1.482(5)	Ir(1)-C(35)	2.034(5)
Ir(1)-O(2)	2.045(3)	Ir(1)-P(1)	2.3863(16)
Ir(1)-O(1)	2.069(4)	Ir(1)-P(2)	2.2857(15)
Ir(1)-C(65)	2.055(5)		
Bond angles			
O(2)-Ir(1)-O(1)	42.24(14)	C(35)-Ir(1)-O(1)	112.08(19)
C(65)-Ir(1)-P(1)	168.98.(15)	O(2)-Ir(1)-P(2)	106.48(11)
C(35)-Ir(1)-O(2)	154.19(18)	P(2)-Ir(1)-P(1)	98.54(5)
O(1)-Ir(1)-P(2)	149.08 (11)	C(35)-Ir(1)-P(2)	98.77(16)

3.8.3 Synthesis and characterization of *cis*-[Ir(η^2-S_2)(EtImCH$_2$CH$_2$PPh$_2$)$_2$][PF$_6$] (E23).

The novel iridium(III) disulfide complex *cis*-[Ir(η^2-S_2)(EtImCH$_2$CH$_2$PPh$_2$)$_2$]$^+$ **E23** was synthesised by the reaction of one equivalent of the *cis*-iridium(I) complex **E20** with 0.25 equivalents of elemental sulfur S_8 in THF (Figure 3.32). The color of the reaction mixture changed from orange red to yellow orange and a suspension was formed. It was stirred over night and was monitored by ^{31}P-NMR spectra which confirmed the formation of *cis* **E23.** The solvent was evaporated under vacuum and the resulting yellow orange residue was redissolved in a mixture of acetonitrile /THF. Overlaying with diethyl ether yielded yellow single crystals of **E23** suitable for single crystal X-ray structure analysis.

The structure of the *cis*-iridium (III) complex **E23** was corroborated by one and two dimensional NMR-spectroscopy and IR spectroscopy. The significant features of the ^{1}H-NMR spectrum of **E23** are the downfield resonances of the aromatic protons of the imidazol ring (δ (ppm), 7.27 (d, 2H, $^3J_{HH}$ = 2 Hz, b); **7.15 (**s, 1H**,** b'); 7.03 (s, 1H, c') and 7.65 (d, 1H, $^3J_{HH}$ = 2 Hz, c). Compared to the starting material **E20** the resonances are shifted to higher frequencies on coordination of sulfur. The ^{13}C spectrum shows the resonance of the carbene carbon atoms at 145 ppm (dd, $^2J_{PC}$ = 132 Hz, $^2J_{PC}$ = 9 Hz, a) and 149.7 ppm (d, $^2J_{PC}$ = 12 Hz, a'). The large coupling constant of the first signal shows that the corresponding carbon atom is located opposite to a phosphorous atom while the small coupling constants of the second resonance proves that two phosphorous atoms

are in *cis*-position to the corresponding carbon atom. Compared to **E20** the resonances are shifted to high field due to the formation of an iridium(III) complex. The ^{31}P NMR spectrum of **E23** shows two phosphorous signals at -12.7 ppm (d, $^{2}J_{PP}$ = 18 Hz) and -30.7 ppm (d, $^{2}J_{PP}$ =15 Hz)) consistent with the *cis* orientation of ^{31}P nuclei. The IR (KBr disc) spectrum of **E23** shows a band at 557 cm^{-1} tentatively assigned as ν(S-S) which is also observed in other reported iridium (III) complexes with side on coordination of the S_2-ligand.[163]

3.8.3.1 Single crystal X-ray structure analysis of *cis*-[Ir(η^2-S$_2$)(EtImCH$_2$CH$_2$PPh$_2$)$_2$][PF$_6$] E23

Yellow crystals of iridium(III)-disulfide complex **E23** suitable for X-ray crystallography were obtained by layering diethyl ether onto a mixture of an acetonitrile/THF solution of **E23**. **E23** crystallizes in the monoclinic space group P2(1)/c with four molecules in the unit cell. The crystallographic data are presented in the Table 7.12 and the selected bond lengths and angles are given in Table 3.15. Moleculer structure of **E23** is depicted in Figure (3.36)

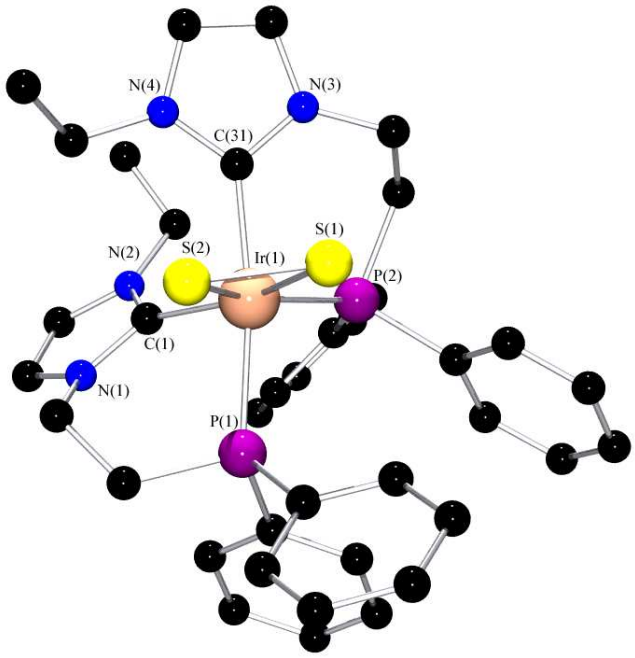

Figure 3.36: Structure of *cis*-[Ir(η^2-S$_2$)(EtImCH$_2$CH$_2$PPh$_2$)$_2$]$^+$ in crystals of **E23**, (without hydrogen atoms).

The geometry around iridium(III) center is trigonal bipyramidal. The carbene and the phosphorous donors are coordinated in *cis* position to iridium(III) and the disulfide ligand is coordinated in a side on fashion. The sum of angles around iridium(III) in the equatorial plane amounts to 359.7°. The disulfide ligand is slightly shifted from the equatorial plane by 0.037 and 0.030 Å for S(1) and S(2), respectively. The bond angle C(31)-Ir(1)-P(1) formed by the axial ligands is 169.02(11)° and the bending of the axial ligands is due to the steric hindrance imposed by the phenyl rings of the phosphane residues. The angles formed by the sulfide ligand S(1)-Ir(1)-S(2) is 50.45(3)° and the S(1)-S(2) bond length amounts to 2.0581(14) Å is equal to the bond length in S_8(2.06Å). The bond distances between the iridium atom and carbenic carbon atoms Ir(1)-C(1) and Ir(1)-C(31) are 2.052(4) Å and 2.063(4) Å, respectively. The bond lengths Ir(1)-S(1) and Ir(1)-S(2) are equal with 2.4140(10) and 2.4156(11). The structure of the iridium (III) sulfide complex **E23** is analogous to the iridium(III) peroxo complex with marginal differences in the bond parameters of both of the complexes. The Ir(1)-P(2) distance in **E23** is shorter than that in **E22** by 0.07 Å and the equatorial angles C(35)-Ir(1)-O(1) in **E22** is bigger than that in **E23** (C(1)-Ir(1)-S(1)) by 5°.

Table 3.15: Selected bond lengths [Å] and angles [°] for the *cis*-iridium(III) complex **E23**.

Bond lengths			
S(1)-S(2)	2.0581(14)	Ir(1)-C(31)	2.063(4)
Ir(1)-S(2)	2.4156(11)	Ir(1)-P(2)	2.3071(10)
Ir(1)-S(1)	2.4140(10)	Ir(1)-P(1)	2.3787(10)
Ir(1)-C(1)	2.052(4)		
Bond angles			
S(1)-Ir(1)-S(2)	50.45(3)	C(1)-Ir(1)-S(2)	107.17(11)
C(31)-Ir(1)-P(1)	169.02.(11)	P(2)-Ir(1)-S(1)	103.81(3)
C(1)-Ir(1)-S(1)	157.37(11)	P(2)-Ir(1)-S(2)	154.26(4)
C(1)-Ir(1)-P(2)	98.53(11)	P(2)-Ir(1)-P(1)	100.21(3)

3.8.4 Synthesis of five coordinate Iridium(I) $[Ir(CO)(EtImCH_2CH_2PPh_2)_2][PF_6]$ (E24)

The novel five coordinate iridium(I) carbonyl complex **E24** was synthesized by bubbling carbon monoxide gas through a solution of the *cis* iridium(I) complex **E20** in THF at room temperature for 30 minutes (Figure 3.32). The reaction was confirmed by a change of color from red orange to light yellow. The reaction also was monitored by measuring ^{31}P-NMR spectra and IR spectra. After removal of the solvent a yellow product was obtained in high yield (95%). The latter was characterized by NMR- and IR spectroscopy. Attempts to get crystals of **E24** failed

The most significant feature of the ^{13}C-NMR spectrum are two peaks of quaternary carbon atoms at 191.2 (t, $^2J_{PC}$ = 4.0 Hz) and 143.8 (t, $^2J_{PC}$ = 13.0 Hz) ppm which can be assigned to CO and to the carbene carbon atoms, respectively. The ^{13}C shift of the metal-bound carbene carbon is significantly shifted to higher field in comparison to other iridium(I)-bound carbene carbon atoms (170–185 ppm) reported in the literature.[97g,131,136,164,165] Octahedral iridium(III) complexes of NHC normally have metal-bound carbene ^{13}C chemical shifts in the range of 127-145 ppm.[149,151,166-168] The unexspected high field shift of the carbene carbon atoms in **E24** is most likely because of the unusual trigonal-bipyramidal geometry of the iridium(I) complex. The ^{31}P-NMR signal observed at δ = -12.0 (s) ppm confirms the chemical equivalence of the phosphorous atoms, which are shifted to high field compared to phosphorous resonance of the starting material observed at 16.9 ppm for **E20**.

The IR spectrum in THF solution of **E24** shows a single CO absorption band at 1900 cm^{-1} which similar to other iridium carbonyl complexes.[169]

3.8.5 Synthesis of the iridium(III)complex, *trans*-$[Ir((CH_3)(I)(EtImCH_2CH_2PPh_2)_2)]I$ (E25)

The cationic iridium(III) complex *trans*-**E25** was synthesized by reaction of one equivalent of **E20** with excess of methyl iodide in THF solution at room temperature. The color of the reaction mixture immediately changed from orange yellow to yellow brown. The progress of the reaction was monitored by measuring ^{31}P-NMR spectra which show two signals at high field at δ = -25.1 ppm (d, $^2J_{PC}$ = 20 Hz) and δ = -41.2 ppm (d, $^2J_{PC}$ = 20 Hz) (structure **E25A**). The reaction was stirred overnight followed by measuring another ^{31}P-NMR spectrum which showed the same

signals as before. Both spectra confirm the formation of two isomers **E25A** and **E25B** with *cis* and *trans* orientation of the coordinated methyl group und the iodine atom, respectively. The intregration of the phosphorous atoms in the ^{31}P-NMR spectrum gives a ratio of *trans*/*cis* of approximately 1:4.

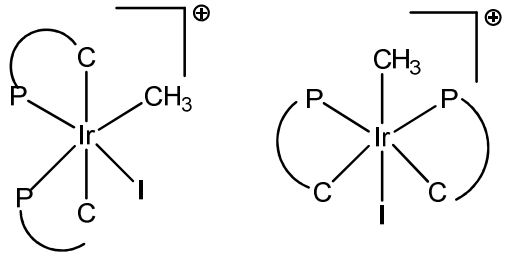

E25A **E25B**

Subsequently the solvent was evaporated giving a crude yellow brown product. From the crude product **E25B** was separated by fractional crystallization from aconcentrated THF solution. The colorless single crystal of **E25B** was obtained which was suitable for x-ray crystallography. The structure of the molecule is in a good agreement with ^{1}H-, ^{13}C- and ^{31}P-NMR spectroscopic data. The ^{1}H-NMR-spectrum of **E25B** shows the signal of methyl protons at δ = 0.15 ppm (s). The strong shielding of the protons must be attributed to their close proximity to the electron rich metal center. The resonances of the protons of imidazol rings were observed in the range of δ = 7.36-7.92 ppm which is a slight downfield shift compared to imidazol protons of **E20**. The most important feature of the ^{13}C-NMR spectrum is the resonance of the methyl group at δ = 0.4 ppm which unexpectedly appears only as a singlett. Obviously the $^{2}J_{CP}$ coupling constant is in this case to small to be resolved by the NMR-spectrometer. Two signals were observed for the unequivalent carbene carbon atoms at δ = 146.6 (dd, $^{2}J_{PC,\ cis}$ = 13 Hz, $^{2}J_{PC,\ trans}$ = 115 Hz) and 147.6 (dd, $^{2}J_{PC}$ = 13 Hz, $^{2}J_{PC,\ trans}$ = 115 Hz). These values are in the range of similar iridium(III) complexes reported in the literature.[59,149,168] The ^{31}P NMR-spectrum shows two signals at -25.6 (d, $^{2}J_{PC}$ = 20 Hz) and -42.4 ppm (d, $^{2}J_{PP}$ = 20 Hz) for phosphourous donors of the bi-dentate NHC-ligands as a dominant product. The coupling constant proves their mutual *cis*-coordination.

3.8.5.1 Single crystal X-ray structure analysis of *trans*-[Ir((CH$_3$)(I)(EtImCH$_2$CH$_2$PPh$_2$)$_2$)]I (E25)

Single crystals of **E25** suitable for X-ray crystallography were grown by layering hexane onto concentrated THF solution of complex. **E25** crystallized in monoclinic space group P2(1)/c with four molecules in the unit cell and iodide counter ions and THF molecules in the unit cell. Crystallographic data are presented in the Table 7.13 and the selected bond lengths and angles are given in Table 3.16. Molecular structure of **E25** is depicted in Figure 3.37. The geometry around iridium(III) ion is distorted octahedral with the sum of angles around iridium(III) being 360.52° and the iridium atom is displaced from the plane by 0.022 Å. The bidentate NHC phosphane ligands are coordinated in *cis* arrangement around iridium(III) center in which C(1), C(31), P(1) and P(2) lie in the plane of molecule whereas the CH_3 and iodide lignads are *trans* to each other and lie in the axial position. The significant features in this molecules the bite angle C(31)-Ir(1)-P(2) deviates by 9° from ideal angle and the equatorial angle C(31)-Ir(1)-P (1) and C(1)-Ir(1)-P(2) deviates by 7° and 11° from linearity and the axial angle C(60)-Ir(1)-I(1) slightly deviates from linearity by 5°and the angle P(2)-Ir(1)-P(1) deviates from ideal angle by +10° may due to the close contact of phenyl ring The bond length of Ir(1)-C(31) and Ir(1)-C(1) are 2.077(7) and 2.096(7) Å respectively the bond distance of Ir(1)-P(1) is longer than Ir(1)-P(2) by 0.0292 Å and the bond length of Ir(1)-I(1) and Ir(1)-C(60) are 2.8005(7) and 2.128(7) respectively. Similar to the value found in [{Ir(CO)I$_2$(μ-I)Me}$_2$]$^{2-}$.[170]

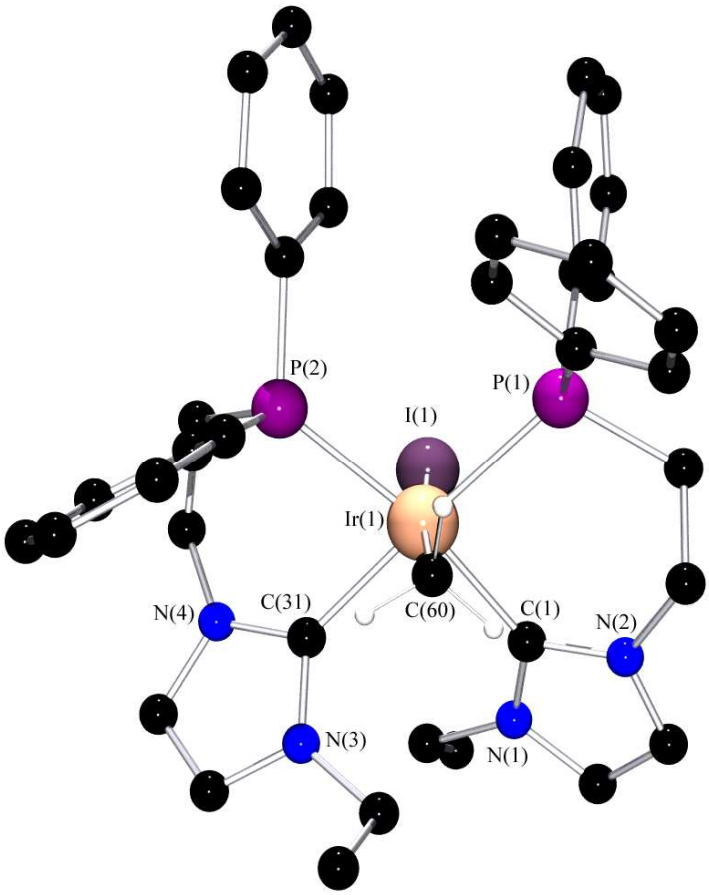

Figure 3.37: Structure of *trans*-[Ir((CH$_3$)(I)(EtImCH$_2$CH$_2$PPh$_2$)$_2$)]$^+$ in crystals of **E25**, (without hydrogen atoms).

Table 3.16: Selected bond lengths [Å] and angles [°] for the *trans*-iridium(III) complex **E25**.

Bond lengths			
I(1)-Ir(1)	2.8005(7)	Ir(1)-C(60)	2.128(7)
Ir(1)-C(31)	2.077(7)	Ir(1)-P(2)	2.3501(18)
Ir(1)-C(1)	2.096(7)	Ir(1)-P(1)	2.3793(18)
Bond angles			
C(31)-Ir(1)-C(1)	88.6(3)	C(31)-Ir(1)-P(1)	172.9(2)
C(31)-Ir(1)-P(2)	81.2(2)	C(60)-Ir(1)-I(1)	174.87(19)
C(1)-Ir(1)-P(1)	91.2(2)	P(2)-Ir(1)-P(1)	99.58(6)
C(1)-Ir(1)-P(2)	168.7(2)	C(60)-Ir(1)-P(1)/P(2)	86.7(2)/92.0(2)

3.8.6 Synthesis and characterization of *cis*-$[Ir(I)_2(EtImCH_2CH_2PPh_2)_2][I_3]$ (E26)

The synthesis of novel iridium(III) complex **E26** was carried by conducting an oxidative addition reaction in THF between *cis*-iridium(I) complex **E20** and iodine at -50Cº, the color of the reaction mixture changed from red orange to yellow, reaction was monitored by ^{31}P-NMR spectra which confirm The formation of two isomers (**A** and **B**) in a ratio 1:3. In isomers A the inequivalent phosphorous atom in *cis* position which shows the signal at -25.2 (d, $^2J_{PP}$ = 20 Hz) phosphorus *cis* to iodine), (-54.7 (d, $^2J_{PP}$ = 20 Hz), (phosphorus *trans* to iodine) and in isomer **B** shows the signal at -43.80 (s) in which the phosphorous atoms in *trans* position. The solvent removed under vacuum to give high yield 65 % of yellow crude product which gives yellow crystals suitable for X-ray crystallography which confirmed the formation of isomer B crude product was characterised by NMR-spectroscopic method.

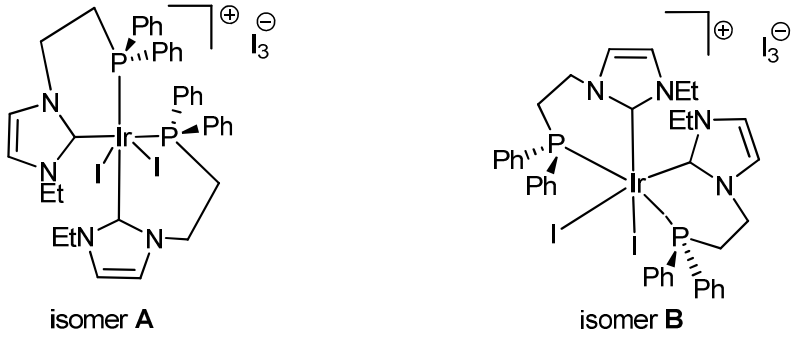

Figure 3.38: Chemical structure of the isomers in **E26.**

The significant features in the ^{1}H-NMR spectrum of **E26** shows four signals of aromatic protons of imidazol ring at downfield δ = 7.49 (d, 2H, $^3J_{HH}$ = 2.2 Hz, b); **7.**38 **(**s, 1H**,** b'); 7.03 (s, 1H, c') and 7.65 (d, 1H, $^3J_{HH}$ = 2.2 Hz, c)) compared to the *cis* complex **E20** which showe the resonances of aromatic protons of imidazol ring at high field. In the ^{13}C-NMR spectrum the peak of the iridium-carbene bound resonance could not be detected and four signals were observed for carbon atoms of imidazol ring.

^{31}P spectra of crude product shows the presence of two signals consistent of presence of in equivalent two phosphorous atoms in *cis* position at -25.2 (d, $^2J_{PP}$ = 20 Hz) and -54.7 (d, $^2J_{PP}$ = 20 Hz). In addtion another signal at -43.8 (s) which consistent in the presence of two equivalent phosphorous atoms which are in agreement with X-ray crystallography which confirm the formation of isomer **B**.

3.8.6.1 Single crystal X-ray structure analysis of *cis*-$[Ir(I)_2(EtImCH_2CH_2PPh_2)_2][I_3]$ (E26)

Single crystals of **E26** were grown by over layering diisopropyl ether into acetonitrile solution E26 crystallized in monoclinic space group P2(1)/c with four molecules in the unit cell and their counter ion and a cetonitrile. Due to the poor quality of the crystals, good set of data could not be collected Structure representation of **E26** is depicted in Figure 3.39. The geometry around iridium(III) ion is distorted octahedral.

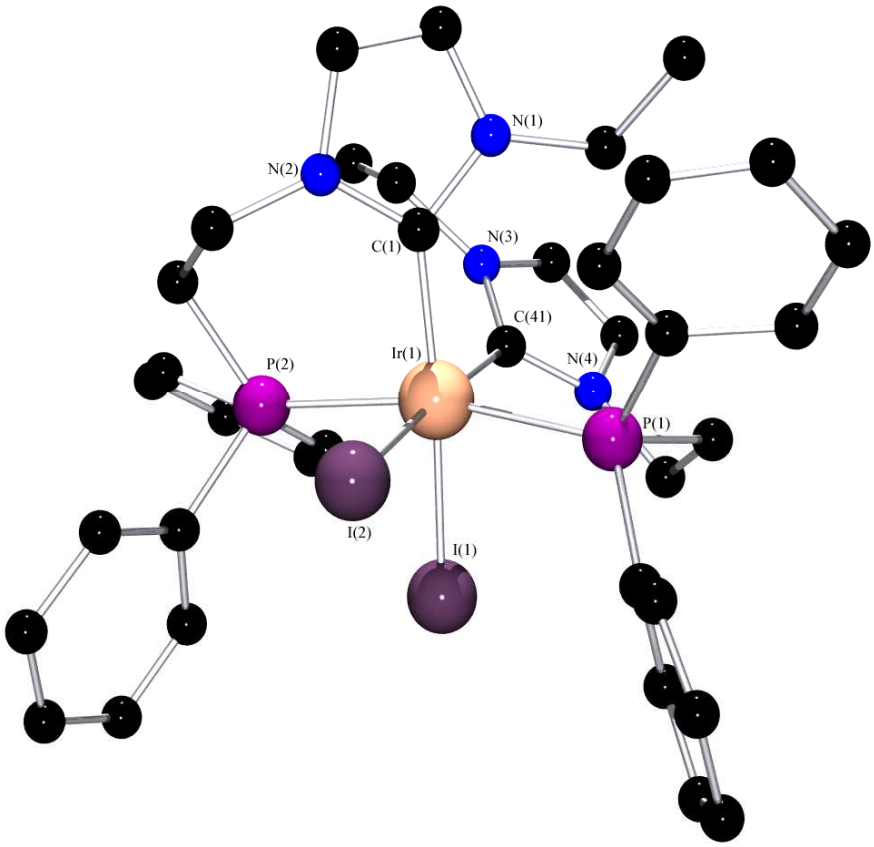

Figure 3.39: Structure of the *cis*-$[Ir(I)_2(EtImCH_2CH_2PPh_2)_2]^+$ in crystals of **E26**, (without hydrogen atoms).

3.8.7 Electrochemistry of *cis*-[Ir(EtImCH$_2$CH$_2$PPh$_2$)$_2$][PF$_6$] (E20)

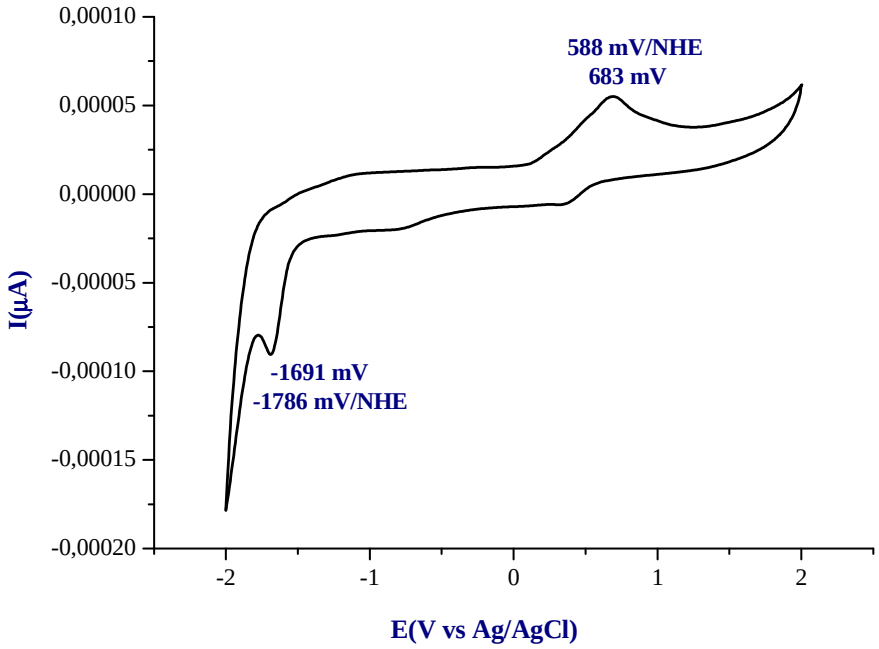

Figure 3.40: Cyclovoltammogram of **E20** in THF

The cyclovoltammogramm of *cis*-Ir(I) complex **E20** (0.1mol/L [NBu$_4$][PF$_6$] was obtained at scan rate 100 mV/s in THF. The Iridium(I) complex shows irreversible redox process at 588 mV/NHE and reduction waves at -1786 mV/NHE.

3.9 Nickel complex

3.9.1 Synthesis and spectroscopic characterization of *trans*-[Ni(EtImCH$_2$CH$_2$PPh$_2$)$_2$][I]$_2$ (E27)

The synthesis of *trans* nickel(II) complex **E27** is illustrated in Figure 3.41. **E27** was synthesised by reaction of one equivalent [Ni$_7$S(S^{t}Bu)$_8$][BzEt$_3$N] with 2 equivalent of carbenes **E7** at room temperature in THF solution the reaction color changed immediately to brown black reaction was completely finished in 30 min. reaction was monitored by measure ^{31}P-NMR spectra which shows the signal of phosphorous atom as singlets δ = 21.0 ppm which confirm the presence of two equivalent phosphorous atoms, which shifted to down field contrast to the signal of imidazolium salts which appears at -21 ppm, after work up brown black residue was crystallised by slow evaporated from concentrated acetonitrille solution of **E27** to gives single yellow crystals suitable of X-ray crystallography **E27** was characterised by ^{1}H, ^{13}C and ^{31}P-NMR spectroscopy. attempts to get this complex from NiCl$_2$ was failed.

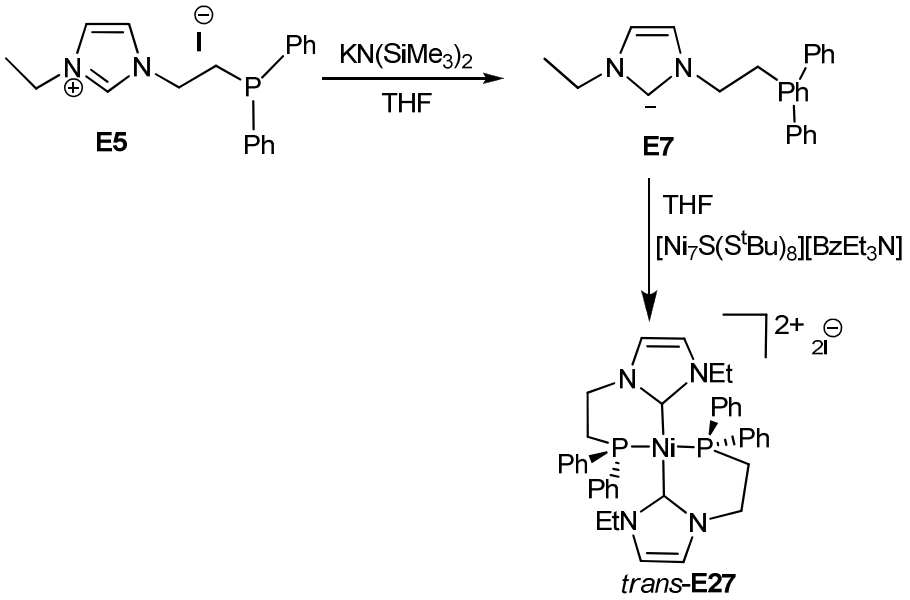

Figure 3.41: Synthesis of *trans*-[Ni(EtImCH$_2$CH$_2$PPh$_2$)$_2$][I]$_2$ (**E27**).

The significant feature in the ^{1}H-NMR spectra of **E27** the apsence of the signat at 8.5 ppm which assign to the coordinatig of the bidentate ligand with nickel (II), the resonance of the sigmal ofdisterotopic protonsof ethylene linkage was observed at δ = 4.0-6.1 ppm, in ^{13}C-NMR spectra

the carbenic carbon atom of **E27** was observed as a triplet at δ = 174 ppm, which is in the normal range of other nickel(II) complexes reported in the literature.[171-173]

3.9.1.1 Single crystal X-ray structure analysis of *trans*-$[Ni(EtImCH_2CH_2PPh_2)_2][I]_2$ (E27)

Yellow single crystals from **E27** were grown from slow evaporated of concentrated solution of **E27**. *trans*-Nickel(II) complex was crystallized in monoclinic space group P2(1)/n with four molecules in the unit cell and their counter ion and two molecules of acetonitrile. Figure 3.42 depicated the Molecular structure of **E27** and selected bond lengths and angles are given in Table 3.17. Crystallographic data are presented in the Table 7.14. The Nickel(II) center is coordinated by two bidentate NHC-phosphane ligands in a distorted square-planar environments with a sum of four bond angles at Ni(1) of 358.68°. The two carbene-phosphane moieties are coordinated *trans* to the two ethylene linkages situated on one side of coordination plane. Generally the C-Ni-C angle is closer to linearity than the P-Ni-P angle, C(1)-Ni(1)-C(8) bond angle in **E27** is 175.02(10), whereas the P(1)-Ni(1)-P(2) deviates by 16° from the ideal 180°. The bit angle C(8)-Ni(1)-P(2) and C(1)-Ni(1)-P(1) deviates by 7° and 6° from the ideal 90°. The Ni-C and Ni-P bond distance are within the normal range for Ni-NHC complexes reported in the literature.[172-176]

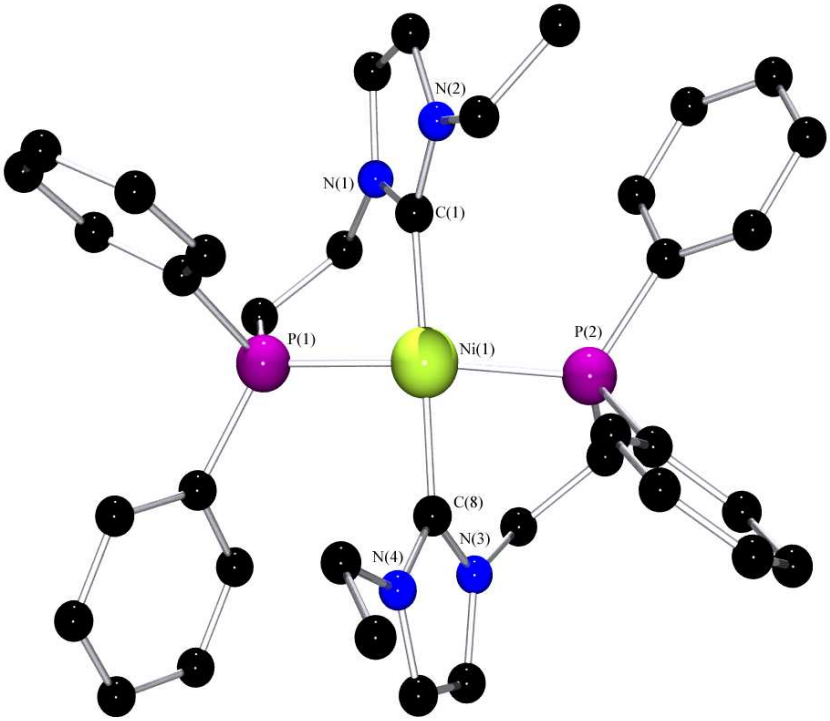

Figure 3.42: Structure *of trans*-$[Ni(EtImCH_2CH_2PPh_2)_2]^{++}$ in crystals of **E27**, (without hydrogen atoms).

Table 3.17: Selected bond lengths [Å] and angles [°] for *trans*-Nickel(II) complex **E27**.

Bond lengths			
Ni(1)-C(1)	1.904(2)	Ni(1)-P(2)	2.1909(7)
Ni(1)-C(8)	1.906(2)	Ni(1)-P(1)	2.1925(7)
Bond angles			
C(1)-Ni(1)-C(8)	175.02(10)	C(8)-Ni(1)-P(1)	93.94(7)
P(2)-Ni(1)-P(1)	164.02(3)	C(1)-Ni(1)-P(1)	84.07(7)
C(1)-Ni(1)-P(2)	97.75(7)	C(8)-Ni(1)-P(2)	82.92(7)

3.10 Palladium complex

3.10.1 Synthesis and spectroscopic characterization of

Cis-and *trans*-$[Pd(EtImCH_2CH_2PPh_2)_2][PF_6]_2$ (E28)

trans- and *cis*-Pd(II) complex was synthesised by treatment two equivalent of imidazolium salts with one equivalent of $KN(SiMe_3)_2$ in THF solution at room temperature, after deprotonation of imidazolium salts one equivalent of $[Pd(COD)CL_2]$ was added to carbene solution **E7**, as depicted in Figure (3.43).

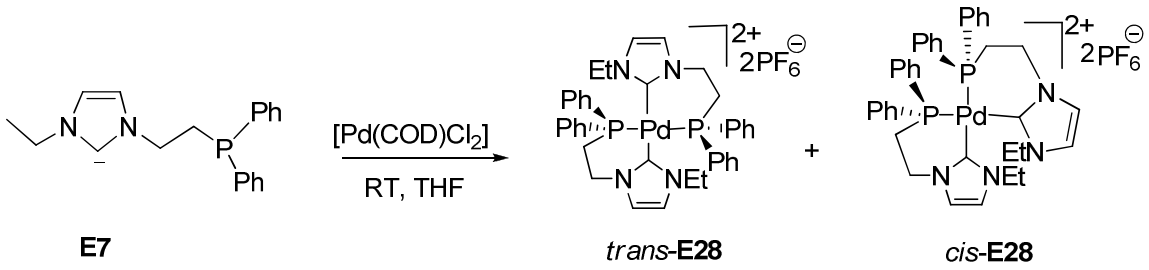

Figure 3.43: Synthesis of *cis*- and *trans*-$[Pd(EtImCH_2CH_2PPh_2)_2][PF_6]_2$ (**E28**).

The color of the reaction mixture changed to orange red which stirred for 1 hour to give high yield (70 %) of orange red isomers product which gives single yellow crystals suitable for X-ray crystallography of *trans* isomers. The product was characterized by ^{1}H, ^{13}C and ^{31}P-NMR spectroscopy, and it is potential as a catalyst in *Suzuki* coupling reaction has been investigated.

The significant features in the ^{1}H-NMR spectrum of *trans* **E28** include the absence of a resonance at 8.5 ppm which is diagnostic for the loss of the carbonium protons confirm the coordination of palladium(II) to carbene. Also the bidentate coordination of ligand around the palladium ion can be detected from the presence of of four diasterotopic proton signal for the ethylene linkage in the range of δ = 2.37-5.01 ppm. Addtionally two signals was observed for aromatic protons of imidazol ring which shifted slightly up field δ = 7.15 and 7.34 ppm contrast to imidazolium salts. In the ^{13}C-NMR spectrum, the resonance of the carbene-Pd carbon appears as triplt δ = 165.4 ppm ($^{2}J_{PC}$ = 12 Hz). ^{31}P-NMR spectrum of crude product shows two signal δ = 17.7 (s) for *cis* isomer and 17.9 (s) for *trans* isomer with a ratio 2:1 which confirm the formation of two isomers, X-ray crystallography show the formation of *trans*-isomer.

.

3.10.1.1 Single crystal X-ray structure analysis of *trans*-$[Pd(EtImCH_2CH_2PPh_2)_2]^{2+}$ (E28)

X-ray-quality crystals of *trans*-**E28** were grown by layering diethyl ethere onto acetonitrile solution. *trans*-palladium(II) complex was crystallized in triclinic space group P-1 with two molecules in the unit cell and their counter ion and one molecules of acetonitrile incorporated in the unit cell. Figure 3.44 depicted the Molecular structure of **E28** and selected bond lengths and angles are given in Table 3.18. Crystallographic data are presented in the Table 7.15. The geometry around the palladium(II) center is distorted square planar with a sum of four bond angles at Pd(1) of 358.41°. The palladium centers are coordinated by two bidentate ligands **E7**. The ligating phosphorous atoms occupy *trans* coordination sites. The same holds for the ligating carbene atoms. The palladium(II) ion lie away from the coordination plane by 0.168 Å. The formation of the six membered chelate ring of NHC-phosphane ligand distortes the coordination geometry of the palladium only slightly with C(1)-Pd(1)-P(1) and C(31)-Pd(1)-P(2) bite angles being reduced to 84.1(4) and 83.5(4) respectively, thid deviation from 90° ideal angle resulted from the strain associated with the six membered ring. Generally The C-Pd-C angle is closer to linearity than the P-Pd-P angle, C(1)-Pd(1)-C(31) bond angle in **E28** is 173.8(5), whereas the P(1)-Pd(1)-P(2) deviates by 16° from the ideal 180°. The Pd-C bond length at 2.030(13) Å and 2.032(12) Å fall within the normal range, the same trend was also observed in Pd-NHC complexes.[114,177] The Pd-P bond distance are comparable to those in analogous complexes containing Pd-NHC phosphane ligands.[120,178]

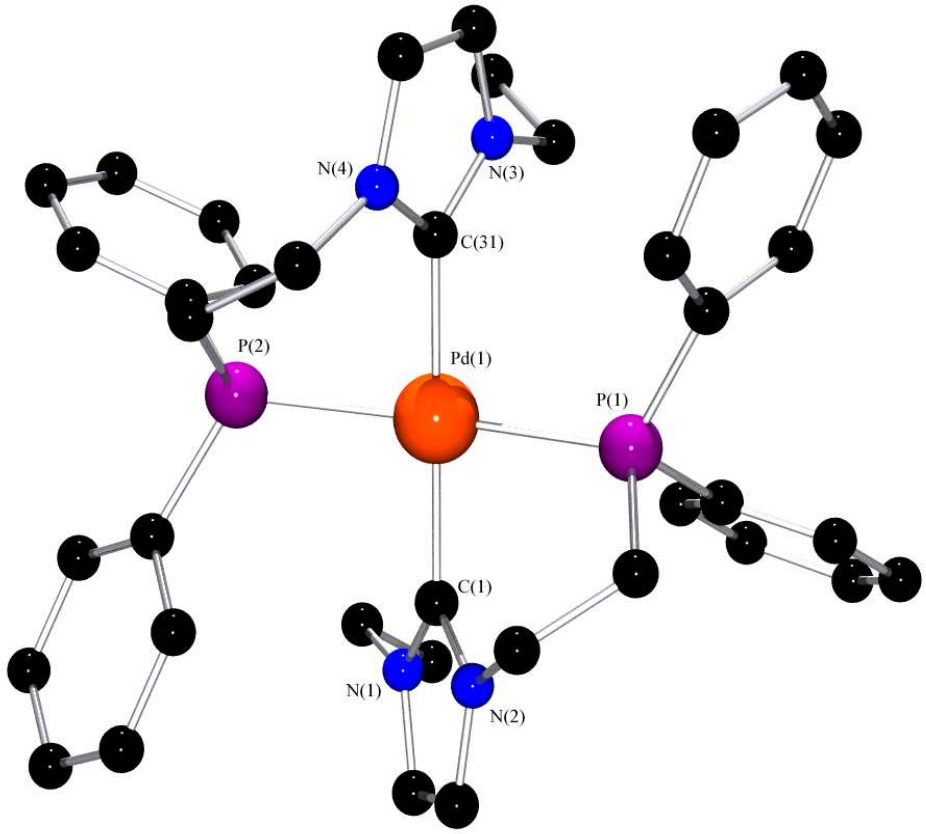

Figure 3.44: Structure of *trans*-$[Pd(EtImCH_2CH_2PPh_2)_2]^{2+}$ in crystals of **E28**, (without hydrogen atoms).

Table 3.18: Selected bond lengths [Å] and angles [°] for *trans*-palladium(II) complex **E28.**

Bond lengths			
Pd(1)-C(1)	2.030(13)	Pd(1)-P(1)	2.308(3)
Pd(1)-C(31)	2.032(12)	Pd(1)-P(2)	2.310(3)
Bond angles			
C(1)-Pd(1)-C(31)	173.8(5)	C(1)-Pd(1)-P(1)	84.1(4)
P(1)-Pd(1)-P(2)	164.46(13)	C(31)-Pd(1)-P(1)	94.2(4))
C(31)-Pd(1)-P(2)	83.5(4)	C(1)-Pd(1)-P(2)	96.5(4)

3.10.2 Equilibrium between *cis*- and *trans*-isomers of E28 at higher temperatures.

Generally, palladium(+II) and rhodium(+I) are isoelectronic and therfore they have similar properties of their complexes are to be expected. Due to that we anticipated the interconversion of *cis*-**E28** and *trans*-**E28** in close analogy to the isoelectronic *cis*-*trans* rhodium(I) complexes. The interconversion of *cis* isomer to *trans* isomer is studied by measuring ^{31}P-NMR spectra of **E28** at different temperatures. The crude product of **E28** shows the signal of the *cis*-isomer at 17.7 ppm (s) and small signal at 18.0 (s) ppm for *trans* complex with a ratio of 10:1 (*cis*:*trans*). The relative stability of isomers was checked by temperature dependent ^{31}P-NMR spectroscopy as shown in Figure 3.45.

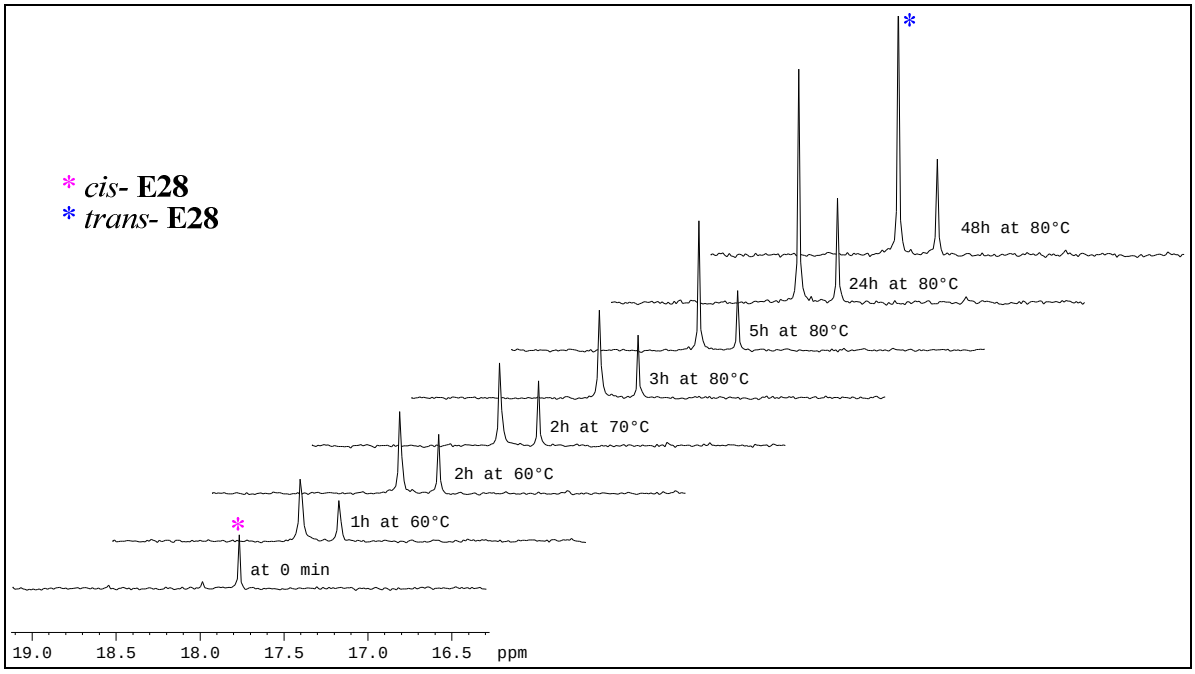

Figure 3.45: Temperature dependent ^{31}P NMR-spectra of isomerization of *cis*- to *trans*- of **E28**

Initially a sample of the *cis* isomer dissolved in d^3-CD_3CN shows a signal at 17.7 ppm and small signal of the *trans*-**E28** at 18 ppm as side product with a ratio of *cis* to *trans* of 10:1. The ratio has been determined by integration of the peaks as the phosphorous atoms in both complexes have similar relaxation times, due to the similar structures of the complexes. On heating at 60°C for one hour the ratio of isomers changed to 4:2 *cis* to *trans*. By increasing the temperature to 70°C and heating for another two hours the ratio changed to 1:2 *cis* to *trans*. Prolonged heating for 24 hours gave no change in a ratio of *cis* to *trans* and appearance of a signal of a new side product at

19 ppm. Further heating at 80°C gave no change in the ratio of both isomers indicating that an equilibrium due to interconservion of both isomers (Figure 3.46) has been reached.

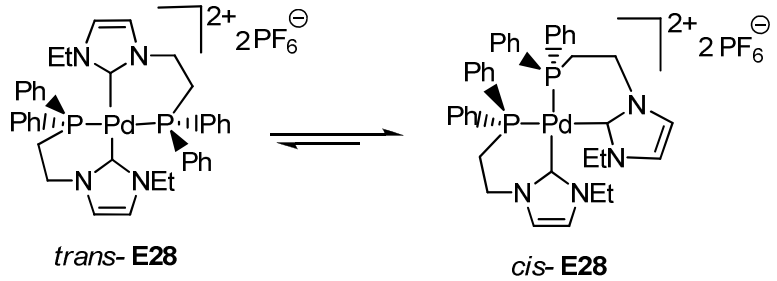

Figure 3.46: The equilibrium between *cis*-**E28** and *trans*-**E28** isomers of $[Pd(EtImCH_2CH_2PPh_2)_2][PF_6]_2$.

3.10.3 Electrochemistry of *trans*-$[Pd(EtImCH_2CH_2PPh_2)_2]^{2+}$ (E28)

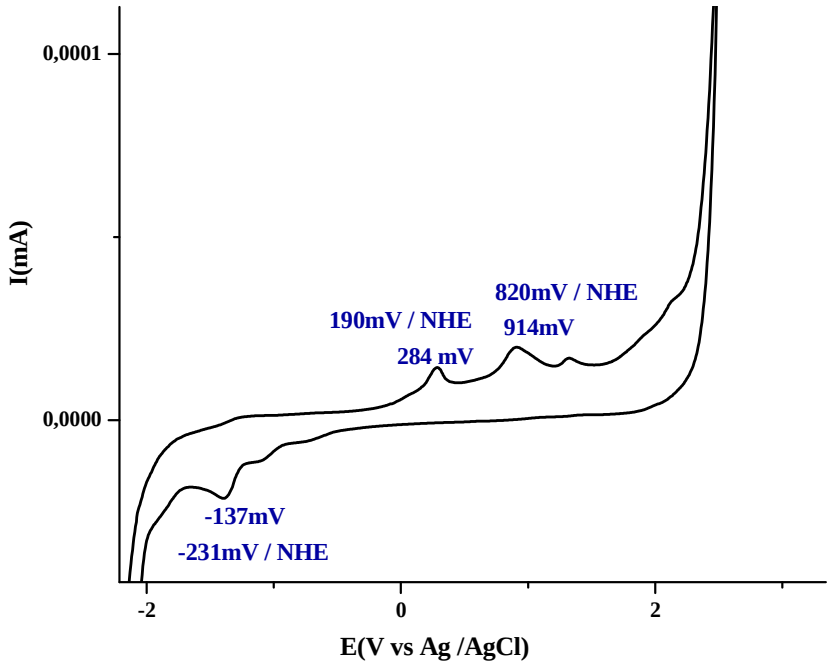

Figure 3.47: Cyclovoltammogram of **E28** in CH_3CN.

The cyclovoltamogram of **E28** (0.1 mo/L $[NBu_4][PF_6]$ was obtained at a scan rate of 200 mV/s in acetonitrile solution. The compound shows several irreversible oxidation waves at 190 mV/NHE, 820 mV/NHE and 1246 mV/NHE) and reduction peak at -231 mV /NHE.

3.10.4 *Suzuki*-coupling with E28

It is known that palladium complexes with mixed phosphane NHC ligands have been used in the *Heck* coupling of aryl bromides and acrylates[120,122], as well as in the copolymerization of ethylene and CO.[97b] We examined if the palladium complex, *trans*-**E28** is a suitable catalyst for the closely related *Suzuki* coupling. The catalytic efficency of *trans*-**E28** in this type of coupling reaction between aryl halides and phenyl boronic acids is summarized in Table 3.19.

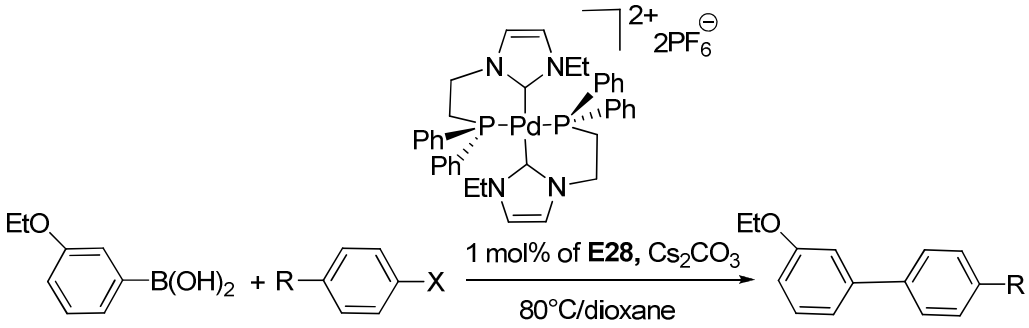

(eq. 44)

Table 3.19: *Suzuki* coupling of aryl halides and 3-ethoxyphenyl boronic acid for *trans*-**E28**.

Entry	X	R	Time(h)	Temperature(°C)	Yield %
1	Br	4-Me	8	80	21
2	Br	4-Me	16	80	42
3	Br	4-Me	24	80	57
4	Br	4-Me	63	80	50
5	Br	4-Me	48	65	8
6*	Br	4-Me	48	80	98
7	Br	4-OMe	24	80	14
8	Br	4-COMe	24	80	34
9	Cl	4-Me	24	80	5

Reaction conditions: 1mmol of aryl halide, 1.5 mmol of phenylboronic acid, 2.0 mmol of Cs_2CO_3, 1 mol% of Pd catalyst, 3 mL of 1,4-dioxane; isolated yield. * 24h at 80°C, cool down to room temperature, addition of another mol% of Pd catalyst, heating for another 24h

The efficency of cationic *trans* NHC-Pd complex **E28** (1 mol%) as catalyst was examined with the base Cs_2CO_3 in dioxane in the reaction of 3-ethoxy phenyl boronic acid with substituted aryl halide contains electron donating and withdrawing groups under argon atmosphere. It is clear that reaction times of approximately 24 h are needed for the production of unsymmetrical biaryl products at 80°C in good yield. In general, **E28** shows good activities for aryl bromide, the activity with respect to aryl chlorides is very poor. Low conversion of substrates to product was obtained at 65°C, increasing the temperature to 80°C resulted in a significant improvement in the overall conversion of the substrates to the products. Excellent yield of coupling product (Table 3.18, entry 6, 98% yield) was achieved when the reaction was carried out for 24 h at 80°C and subsequent additon of another mol % of catalyst and heating again for 24 h. The conversion of substrates to products was firstly determined by integration of ^{1}H-NMR spectra, secondly by separation of the pure product by plate chromatography In conclusion the catalytic activity of **E28** reaches its optimum in dioxane at 80°C and 24 h of reaction time.

4. Experimental Section

4.1 Material and Methods

4.1.1 General Consideration

All manipulation were performed under pure dinitrogen atmosphere (99, 99.6%) dried with P_4O_{10} granulate using Schlenk techniques or in a nitrogen-filled glovebox and with absolute solvents. Solvents were dried and distilled under an atmosphere of nitrogen or argon using standard procedures[179] and also kept under nitrogen. Tetrahydrofuran (THF), diethyl ether and *n*-hexane, were distilled from sodium-benzophenoneketyl. Acetonitrile and dichloromethane were distilled from calcium hydride.

Chemicals were purchased from different companys and used as received: 1-vinyl-imidazol (Acros), KPF_6 (Merck), diphenylphosphine (Aldrich), 1,5-cyclooctadiene (Riedel-deHaen), Ethyliodide (Fluka), K^tOBu (Merck), $KN(SiMe_3)_2$ (Aldrich), CS_2 (Aldrich), rhodium chloride hydrate (Degussa), iridium chloride hydrate (Alfa Aesar, Degussa), palladium chloride (Degussa), cesium carbonate (Sigma-Aldrich), 4-bromotoluene (Sigma-Aldrich), 3-ethoxyphenylboronic acid (Sigma-Aldrich), chlorotoluene (Sigma-Aldrich), 4-bromoanisol (Sigma-Aldrich), 2-bromo-1,3-dimethylbenzene (Sigma-Aldrich), Iodine (Fluka), elemental sulphur (Sigma-Aldrich), methyl iodide (Sigma-Aldrich), 4-bromoacetophenone (Sigma-Aldrich). The bulk compressed gases carbon monoxide, and hydrogen were obtained from Air Liquide Deutschland GmbH. The following compounds $[Ir(\mu\text{-}Cl)(COD)]_2$[180], $[Rh((\mu\text{-}Cl)(COD)]_2$[181], $[Pd(COD)Cl_2]$[182] and $[Ni_7S(S^tBu)_8][BzEt_3N]$[183] were prepared as reported in the literature.

4.1.2 Physical measurements

The ^1H, ^{13}C and ^{31}P NMR spectra were recorded on Bruker Avance 500 (^1H: 500.13 MHz, ^{13}C: 125.76 MHz, ^{31}P: 202.46 MHz).The chemical shift are quoted in ppm. ^1H NMR and ^{13}C chemical shifts were referenced to the residual proton signals of the deuterated solvent. ^{31}P NMR was referenced externally using H_3PO_4 (85% in H_2O). Coupling constants (*J*) are given in Hz. The assignment of the proton and carbon resonances was assured by measurement of DEPT, COSY, HMQC and HMBC spectra.

IR spectroscopy: The infrared spectra were recorded on the FTIR spectrometer Nicolet P510.

Crystal Structure Analyses Crystal data for all measured compounds are presented in the appendix. X-ray diffraction data were collected with a Bruker-AXS SMART APEX CCD diffractometer using MoK_α radiation (λ = 0.71073 Å).

Elemental analyses: The elemental analyses were performed with a Perkin-Elmer-2400 analysator and a vario Micro Cube of the company *elementar*.

Cyclic voltammetry: Cyclic voltammetric measurements were performed with the electro chemical device Metrohm 757 VA equipped with a potential Model Versastat by EG&G in combination with the PC-program electrochemical analysis software 3.0 Model 250 by EG&G. The electrochemical cell was operated under argon, with glassy C/Ag/AgCl or Au/Pt/saturated Ag/AgCl serving as working, counter and refrence electrodes, respectively. CV curves were obtained at scan rates of 100 mV/s working at 25 °C in MeCN/0.1mol l^{-1} $[Bu_4N][PF_6]$. As most of the complexes are exteremely air sensitive all experimental were performed in a glove box. The dissolved complexes were transferred into the CV cell with a steel capillary under argon pressure.

4.2 Synthesis of NHC-Phoshane ligands.

4.2.1 Synthesis of 3-ethyl-1-vinylimidazolium-3-iodide (E3)

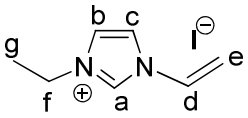

1-vinylimidazol (20 g, 212.5 mmol) was dissolved in 50 mL CH_2Cl_2 and ethyliodide (49.8 g, 319.3 mmol) dissolved in 20 mL CH_2Cl_2 was added. The reaction mixture was stirred under reflux for 18 h. Subsequently the solvent was removed under vacuum to give a crude white residue which crystallized from methanol to yield a white crystaline precipitate **E3** (45.18 g, 0.173 mmol, 81.7 %).

^{1}H-NMR (500 MHz, CD_3CN): δ = 1.47 (t, 3H, $^3J_{HH}$ = 7.9 Hz, g), 4.31 (q, 2H, f ,$^3J_{HH}$ = 7.5 Hz), 5.7 (dd, 1H, $^2J_{HH}$ = 2.9 Hz, e'), 5.98 (dd, 1H, $^2J_{HH}$ = 2.8 Hz, e), 7.35 (q , 2H , d, $^3J_{HH}$ = 9.0 Hz) , 7.78 (s, 1H, c), 8.01 (s, 1H, b), 9.73 (s, 1H, a).

^{13}C-NMR (125 MHz, CD_3CN): δ = 14.7 (s, CH_3, g), 45.5 (s, CH_2, f), 109.4 (s, CH_2, e), 119.7 (s, CH, b), 122.9 (s, CH, c), 128.9 (s, CH, d), 135.5 (s, CH, a).

E.A.: Anal. Found: C, 33.56; H, 4.32; N, 11.15, $C_7H_{11}N_2I$ requires C, 33.60; H, 4.40; N, 11.20 %

4.3 Synthesis of 3-[2-(diphenylphosphino)ethyl]-1-ethylimidazoliumiodide (E5)

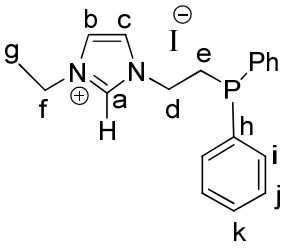

A solution of diphenylphosphane (1.99 g, 10.8 mmol), KO^{t}Bu (0.11 g, 0.98 mmol) in 20 mL of THF was stirred at room temperature under inert gas atmosphere for 5 min. The color of the reaction mixture changed to orange yellow. 3-ethyl-1-vinylimidazoliumiodide (2.72 g, 10.8 mmol) **(E3)** was added. The reaction mixture was stirred at room temperature for four days giving a colorless precipitate which was washed with diethyl ether and dried under vacuum to give a high yield of product **E5** (3.62 g, 8.30 mmol, 79 %).

^{1}H-NMR (500 MHz, CD_3CN): δ = 1.5 (t, 3H, $^3J_{HH}$ = 7.3 Hz, g), 2.78 (t, 2H, e, $^3J_{HH}$ = 8 Hz), 4.16 (q, 2H, $^3J_{HH}$ = 7.4 Hz, f), 4.35 (td, 2H, $^3J_{PH}$ = 9.2 Hz, $^3J_{HH}$ = 7.8 Hz, d), 7.46 (m, 1H, c, $^3J_{HH}$ = 1.8 Hz), 7.30 (t, 1H, b, $^3J_{HH}$ = 1.8 Hz), 8.92 (s, 1H, a), 7.49-7.55 (m, 10H, k, i , j).

^{13}C-NMR (125 MHz, CD_3CN): δ = 14.6 (s, CH_3, g), 28.1 (d, CH_2, $^1J_{PC}$ = 15 Hz, e), 44.9(s , CH_2, f), 47.5 (d, CH_2, $^2J_{PC}$ = 25 Hz, d), 121.9 (s, CH, b or c), 122.5 (s, CH, b or c), 128.7 (d, CH, j, $^3J_{PC}$ = 7 Hz), 129.2 (s, CH, i), 132.7 (d, CH, k ,$^3J_{PC}$ = 20 Hz), 135.8 (s, CH, a), 136.9 (d, C_q, h, $^1J_{PC}$ = 12 Hz).

^{31} P-NMR (202 MHz, CD_3CN): δ = -21.4 (s).

E.A: Anal. Found: C, 52.25; H, 4.68; N, 6.36, $C_{19}H_{22}N_2PI$ requires C, 52.31; H, 5.04; N, 6.42 %

4.4 Synthesis of 3-[2-(diphenylphosphino)ethyl]-1-ethylimidazolium-hexa-fluorophosphate (E6)

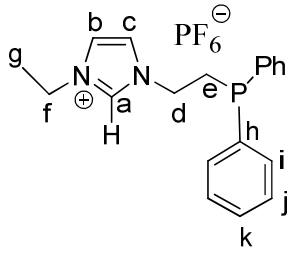

A solution of $NaPF_6$ (1.26 g, 7.5 mmol) was added to a suspension of imidazolium iodide salt **E5** (3.29 g, 7.5 mmol) in degassed water (10 mL) The reaction mixture was stirred overnight, the solid material was filtered off and washed with degassed water and diethyl ether. Finally it was dried under vacuum for 24 h to yield the colorless

product **E6** (2.6 g, 5.73 mmol, 75.8 %).

^{1} H-NMR (500 MHz, CD_3CN): δ = 1.44 (t, 3H, $^{3}J_{HH}$ = 7.3 Hz, g), 2.72 (t, 2H, $^{3}J_{HH}$ = 7.7 Hz, $^{2}J_{PH}$ = 9.5 Hz, e), 4.11 (q, 2H, f, $^{3}J_{HH}$ = 7.6 Hz), 4.32 (td, 2H, $^{3}J_{PH}$ = 9.5 Hz, $^{3}J_{HH}$ = 7.7 Hz, d), 7.39 (t, 1H, $^{3}J_{HH}$ = 1.7 Hz, c), 7.31 (t, 1H, $^{3}J_{HH}$ = 1.9 Hz, b) 7.40-7.47 (m, 10H, k, i , j), 8.51 (s, 1H, a).

^{13}C-NMR (125 MHz, CD_3CN): δ = 14.65 (s, CH_3, g), 27.9 (d, CH_2, $^{1}J_{PC}$ = 15 Hz, e), 44.9 (s, CH_2, f), 47.3 (d, CH_2, $^{2}J_{PC}$ = 25 Hz, d), 122.6 (s, CH, c), 122.1 (s, CH, b), 128.7 (d, CH, $^{3}J_{PC}$ = 7 Hz, j), 129.2 (s, CH, k), 132.7 (d, CH, $^{2}J_{PC}$ = 20 Hz, i), 135.8 (s, CH, a), 136.9 (d, C_q, $^{1}J_{PC}$ = 12 Hz, h).

^{31} P-NMR (202 MHz, CD_3CN): δ = -21.4 (s), -144.0 (hept, $^{1}J_{PF}$ = 710 Hz).

4.5 Synthesis of 3-[2-(diphenylphosphino)ethyl]-1-ethylimidazol-2-dithio-carboxylate (E8)

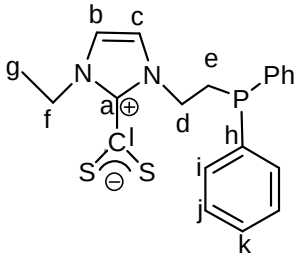

To a solution of 3-[2-(diphenylphosphino)ethyl]-1-ethylimidazolium iodide **E5** (200 mg, 0.46 mmol) in THF 20 mL was added $KN(SiMe_3)_2$ (100 mg, 0.46 mmol + 10 % excess). The reaction mixture was stirred at room temperature for 90 min. After filtration CS_2 (35 mg, 0.03 ml, 0.460 mmol) was added and the color changed immeditely to red. The reaction mixture was stirred for 18 h. Then the solvent was removed under vacuum to give a red crude product which was washed with diethyl ether. Red crystalls were obtainede by layering diethyl ether onto a concentrated chloroform solution of **E8** (104 mg, 270 mmol, 58.8 %).

^{1}H-NMR (500 MHz, $CDCl_3$): δ = 1.44 (t, 3H, $^{3}J_{HH}$ = 7.3 Hz, g), 2.67 (t, 2H, $^{3}J_{HH}$ = 7.8 Hz, e), 4.13 (q, 2H, $^{3}J_{HH}$ = 7.3 Hz, f), 4.22 (q, 2H, $^{3}J_{HH}$ = 7.8 Hz, d), 6.86-7.40 (m, 12H, b, c, Ph).

^{13}C- NMR (125 MHz, $CDCL_3$): δ = 15.14 (s, CH_3, g), 29.0 (d, CH_2, $^{3}J_{PC}$ = 16 Hz, e), 43.4 (s, CH_2, f), 46.1 (d, CH_2, $^{3}J_{PC}$ = 25 Hz, d), 117.3 (s, CH, b or c), 118.5 (s, CH, b or c), 128.8 (d, CH, $^{3}J_{PC}$ = 7 Hz, j), 129.3 (s, CH, k), 132.7 (d, CH, $^{3}J_{PC}$ = 19 Hz, i), 136.3 (d, C_q, $^{3}J_{PC}$ = 11 Hz, h), 149.4 (s, $C_{Carbene}$, a), 224.6 (s, CS_2, l).

^{31}P-NMR (200 MHz, $CDCl_3$): δ = -21.1 (s).

4.6 Synthesis of metal complexes

4.6.1 Synthesis of *cis*-[Rh(EtImCH$_2$CH$_2$PPh$_2$)$_2$]Cl (E10)

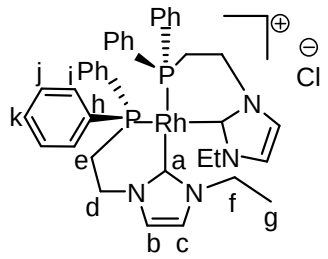

E10

$KN(SiMe_3)_2$ (100 mg, 0.46 mmol) was added to a solution of $[EtImCH_2CH_2PPh_2]I$ (200 mg, 0.46 mmol) in THF (20 mL). The suspension was stirred at room temperature for 60 min. After filtration and removel of KI, $[Rh_2(\mu\text{-}Cl)_2(COD)_2]$ (57 mg, 0.230 mmol) was added to the filtrate. The color of the resulting suspension changed from pale yellow to orange. The mixture was allowed to stirr for another 15 min to give **E10**, $[Rh(EtImCH_2CH_2PPh_2)_2]Cl$ which was isolated by filtration and subsequently dried in vacuo. It was obtained as a pale yellow solid product, which forms yellow single crystals by diffusion of diethyl ether into an acetonitrile solution of **E10** (100 mg, 0.132 mmol, 58.8 %).

^{1}H-NMR (500 MHz, CD_3CN): δ = 1.38 (t, 6H, $^3J_{HH}$ = 7.1 Hz, g), 2.50-2.56 (m, 4H, e), 3.73-3.80 (m, 4H, f), 3.96-4.04 (m, 4H, d), 4.42-4.54 (m, 2H, b or c), 4.89-4.98 (m, 2H, b or c), 6.85-7.75 (m, 20H, Ph).

^{13}C-NMR (125 MHz, CD_3CN): δ = 14.9 (s, CH_3, g), 25.3 (s, CH_2, e), 45.1 (s, CH_2, f), 49.3 (s, CH_2, d), 119.4 (s, CH, b or c), 121.0 (s, CH, b or c), 127.5-127.6 (m, CH, j or k), 127.7-127.9 (m, CH, j or k), 129.9-130.3 (m, CH, i), 135.5-135.7 (m, C_q, h), 183.0 (ddd, $C_{Carbene}$, a, $^1J_{RhC}$ = 47 Hz, $^2J_{PC,\,trans}$ = 103 Hz, $^2J_{PC,\,cis}$ = 30 Hz).

^{31}P-NMR (202 MHz, CD_3CN): δ = 32.0 (d, $^1J_{RhP}$ = 128 Hz).

E.A: Anal. Found: C, 60.38; H, 5.28; N, 7.36, $C_{38}H_{42}N_4P_2RhCl$ requires C, 60.44; H, 5.6; N, 7.42%.

4.7 Synthesis of *cis*-[Rh(EtImCH$_2$CH$_2$PPh$_2$)$_2$][PF$_6$] (E11)

To a solution of 3-[2-diphenylphosphino)ethyl]-1-ethyl-imidazoliumhexafluorophosphate (195 mg, 0.46 mmol) in 10 mL THF was added KN(SiMe$_3$)$_2$ (100 mg, 0.46 mmol) and the mixture was stirred at room temperature under inert atmosphere for 30 min. [Rh$_2$(μ-Cl)$_2$(COD)$_2$] (57 mg, 0.115 mmol) was then added to the reaction mixture. The color changed from pale yellow to yellow orange. After the removal of the solvent the residue was crystallised from a concentrated THF solution to give yellow crystals of **E11** (0.18 g, 0.208 mmol, 92 %).

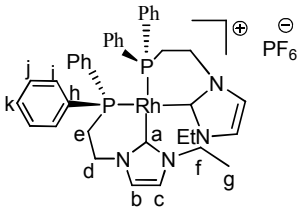

E11

^{1}H-NMR (500 MHz, CD_3CN): δ = 1.38 (t, 6H, $^{3}J_{HH}$ = 7.3 Hz, g), 2.50-2.56 (m, 4H, e), 3.73-3.79 (m, 4H, f), 3.96-4.03 (m, 4H, d), 4.43-4.54 (m, 2H, b or c), 4.89-4.97 (m, 2H, b or c), 6.84-7.78 (m, 20H, C_6H_5).

^{13}C-NMR (125 MHz, CD_3CN): δ = 15.5 (s, CH_3, g), 25 (s, CH_2, e), 45.5 (s, CH_2, f), 49.0 (s, CH_2, d), 118.7 (s, CH, b or c), 120.8 (s, CH, b or c), 127.9-128.1 (m, CH, j or k), 128.4-128.5 (m, CH, j or k), 130.1 (t, CH, $^{3}J_{PC}$ = 6, i), 134.2 (t, C_q, $^{3}J_{PC}$ = 8 Hz, h), 185.2 (ddd, $C_{Carbene}$, $^{1}J_{RhC}$ = 6 Hz, $^{2}J_{PC}$ = 17 Hz, a).

^{31}P-NMR (202 MHz, CD_3CN): δ = 32.0 (d, $^{1}J_{RhP}$ = 128 Hz), -144.0 (hept, $^{1}J_{PF}$ = 710 Hz).

E.A.: Anal. Found: C, 53.23; H, 5.23; N, 6.05, $C_{42}H_{50}F_6N_4OP_3Rh$ requires C, 53.85; H, 5.38; N, 5.98 %

4.8 Synthesis of *trans*-[Rh(EtImCH$_2$CH$_2$PPh$_2$)$_2$]Cl (E12)

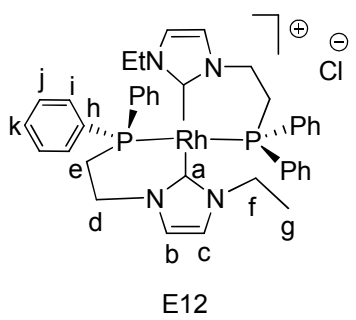

E12

$KN(SiMe_3)_2$ (111 mg, 0.460 mmol) was added to a solution of [EtImCH$_2$CH$_2$PPh$_2$]I (200 mg, 0.460 mmol) in 15 mL of THF. The suspension was stirred at room temperature for 30 min. After filtration a solution of $[Rh_2(\mu\text{-}Cl)_2(COD)_2]$ (57 mg, 0.115 mmol) in 5 mL THF was added dropwise to the filtrate. The color changed to orange and some precipitate formed giving **E9** while the *trans* isomer **E12** remained dissolved in the mother liquor. The reactiom mixture was allowed to stirr for another 30 min. **E10** was separated by filtration and the filtrate was taken to dryness yielding a brown crude product which was recrystallized from a concentrated THF solution to give **E12** (42 mg, 0.058 mmol, 12.6 %).

^{1}H-NMR (500 MHz, CD_3CN): δ = 1.16 (t, 6H, $^3J_{HH}$ = 8 Hz, g), 2.21-2.54 (m, 4H, e), 3.63-4.09 (m, 4H, f), 4.22-4.44 (m, 4H, d), 6.57 (d, 2H, $^3J_{HH}$ = 1.9 Hz, c), 6.82 (d, 2H, b, $^3J_{HH}$ = 2 Hz), 7.08-7.66(m , 20H, Ph).

^{13}C-NMR (125 MHz, CD CN): δ = 15.5 (s, CH_3, g), 45.5 (s, CH_2, f), 30.8 (d, CH_2, $^1J_{PC}$ = 15 Hz, e), 48.7 (s, CH_2, d), 118.7 (s, CH, c), 120.8 (s, CH, b), 128.0-128.6 (m, CH, j or k), 130.1-130.2 (m, CH, j or k), 134.2 (t, CH, i), 138.7 (t, C_q, $^1J_{PC}$ = 19 Hz, $^2J_{PC}$ = 40 Hz, h), 185.1 (dt, $C_{Carbene}$, $^1J_{RhC}$ = 40 Hz, $^2J_{PC,trans}$ = 103 Hz, $^2J_{PC,cis}$ = 30 Hz, a).

^{31}P-NMR (202 MHz, CD_3CN): δ = 26.0 (d, $^1J_{RhP}$ = 152 Hz).

4.9 Synthesis of *trans*-[Rh(EtImCH$_2$CH$_2$PPh$_2$)$_2$][PF$_6$] (E13)

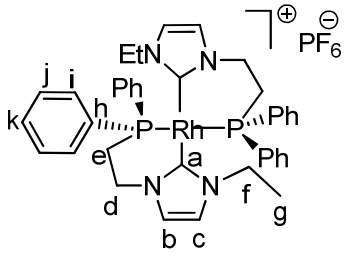

E13

trans-**E13** was prepared starting from **E12**. 250 mg (0.331 mmol) of **E12** were disolved in CH_2Cl_2, and KPF_6 (60 mg, 0.331 mmol) was added. The reaction mixture was stirred for 2 hours. After filtration and removal of the solvent **E13** was obtained in good yield (42 mg, 0.058 mmol, 12.6 %). It was recrystallised by layering diethyl ether onto a methylene chloride solution.

^{1}H-NMR (500 MHz, CD_3CN): δ = 1.16 (t, 6H, $^{3}J_{HH}$ = 8 Hz, g), 2.21-2.54 (m , 4H, e), 3.63-4.09 (m, 4H, f), 4.22-4.44 (m, 4H, d), 6.57 (d, 2H, $^{3}J_{HH}$ = 2 Hz, c), 6.82 (d, 2H, b, $^{3}J_{HH}$ = 2 Hz), 7.08-7.66 (m, 20H, Ph).

^{13}C-NMR (125 MHz, CD_3CN): δ = 15.5 (s, CH_3, g), 45.5 (s, CH_2, f), 30.8 (d, CH_2, $^{1}J_{PC}$ = 15 Hz, e), 48.7 (s, CH_2, d), 118.7 (s, CH, c), 120.8 (s, CH, b), 128.0-128.6 (m, CH, j or k), 130.1-130.2 (m, CH, j or k), 134.2 (t, CH, i), 138.7 (t, C_q, $^{1}J_{PC}$ = 19 Hz, $^{2}J_{PC}$ = 40 Hz, h), 185.1 (dt, $C_{Carbene}$, $^{1}J_{RhC}$ = 40 Hz, $^{2}J_{PC}$ = 17 Hz, a).

^{31}P-NMR (202 MHz, CD_3CN): δ = 25.9 (d , $^{1}J_{RhP}$ = 152 Hz), -144.0 (hept, $^{1}J_{RhF}$ = 710 Hz).

E.A: Anal. Found: C, 54.42; H, 6.09; N, 5.45, $C_{46}H_{62}F_6N_4O_2P_3Rh$ requires C, 54.50; H, 6.12; N, 5.53 %

4.10 Synthesis of *cis*-[Rh(η^2-O_2)(EtImCH$_2$CH$_2$PPh$_2$)$_2$][X] (X = Cl or PF_6), (E14)

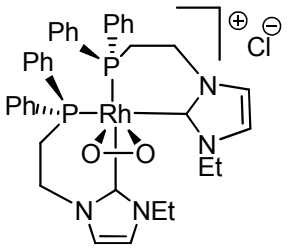

cis-O_2,**E14**

A solution of *cis*-[Rh(EtImCH$_2$CH$_2$PPh$_2$)$_2$][X] **E10 or E11** (50 mg, 0.066 mmol) in CH_2Cl_2 (10 mL) at room temperature was exposed to air for 5 min. The color changed from orange to pale yellow. After evaporation of the solvent [Rh(η^2-O_2)(EtImCH$_2$CH$_2$PPh$_2$)$_2$][X] **E14** was obtained as pale yellow solid which gave yellow brown crystals contaning both enantiomers, by layering a concentrated methylene chloride solution with diethyl ether. Alternativelly layering a concentrated acetonitrile solution with diethyl ether gave a mixture of enantiomerically pure crystals (48 mg, 0.064 mmol, 97.0 %), Δ/Λ = 1/1.

^{31}P-NMR (202 MHz, $CDCl_3$, **233 K**): δ = -3.4 (dd, $^{1}J_{RhP}$ = 85 Hz, $^{2}J_{PP}$ = 20 Hz), 12.4 (dd, $^{1}J_{RhP}$ = 85 Hz, $^{2}J_{PP}$ = 20 Hz), 26.2 (dd, $^{1}J_{RhP}$ = 125 Hz, $^{2}J_{PP}$ = 20 Hz), 30.9 (dd, $^{1}J_{RhP}$ = 125 Hz, $^{2}J_{PP}$ = 20 Hz).

^{31}P-NMR (202 MHz, $CDCl_3$, **343 K**): δ = 8.5 (d, $^{1}J_{RhP}$ = 125 Hz), 27.5 (dd, $^{1}J_{RhP}$ = 126 Hz, $^{2}J_{PP}$ = 20 Hz).

IR (KBr disc): ν[cm^{-1}] 3410, 3053, 2365, 1739, 1651, 1435, 1248, 1167, 1119, 1100, 845(ν_{OO}) , 808, 746, 697, 534, 504.

4.11 Synthesis of *trans*-[Rh(η^2-O_2)(EtImCH$_2$CH$_2$PPh$_2$)$_2$][PF_6] (E15)

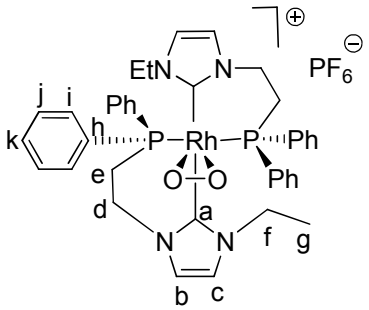

trans-**E15**

A yellow orange solution of **E11** (190 mg, 0.219 mmol) in 10 mL of acetonitile was stirred exposed to O_2 for 10 min at room temperature. The solvent was removed under vacuum to give a pale brown crude product which gave brown crystals by layering a concentrated methylene chloride solution of **E15** with diethyl ether (170 mg, 0.199 mmol, 86.3 %).

^{1}H-NMR (500 MHz, CD_3CN): δ = 1.0 (t, 3H, $^3J_{HH}$ = 7 Hz, g), 1.84 (m, 2H, e), 3.91 (dt, 1H, $^2J_{HH}$ = 15 Hz, $^3J_{HH}$ = 4 Hz, d), 3.03 (dq, 1H, $^2J_{HH}$ = 14 Hz, $^3J_{HH}$ = 7 Hz, f), 4.7 (dq, 1H, $^2J_{HH}$ = 14 Hz, $^3J_{HH}$ = 7 Hz, f), 6.97 (d, 1H, $^3J_{HH}$ = 2 Hz, b), 7.09 (d, 1H, $^3J_{HH}$ = 2 Hz , c), 7.48-7.59 (m, 16H, i , j), 7.63 (t, 2H, $^3J_{HH}$ = 8 Hz ,K), 7.71 (t, 2H, $^3J_{HH}$ = 9.8 Hz, k).

^{13}C-NMR (125 MHz, CD_3CN): δ = 15.7 (s, CH_3, g), 22.7 (d, $^1J_{PC}$ = 26 Hz, e), 44.9 (s, CH_2 , d), 45.3 (s, CH_2, f), 121.7 (s, CH, c), 125.2 (s, CH, b), 129.1, 131.5, 134.4 (d, CH, $^2J_{PC}$ = 13 Hz, i, j, k), 134.46 (d, C_q, $^1J_{PC}$ = 13 Hz, h), 160.4 (dt, $C_{Carbene}$, $^1J_{RhC}$ = 34 Hz, $^2J_{PC}$ = 17 Hz, a)

IR (KBr disc): ν[cm^{-1}] 3410, 3053, 2365, 1739, 1651, 1435, 1248, 1167, 1119, 1100, 850(ν_{OO}), 808, 746, 697, 534, 504.

E.A: Anal. Found: C, 47.53; H, 4.50; N, 5.62, $C_{39}H_{44}Cl_2F_6N_4O_2P_3Rh$ requires C, 47.72; H, 4.52; N, 5.71 %

4.12 Synthesis of *cis*-[Rh(η^2-S_2)($EtImCH_2CH_2PPh_2$)$_2$][PF_6] (E16)

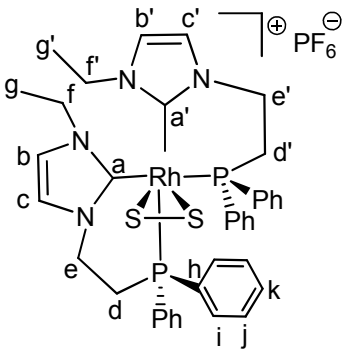

To a solution of *cis*-[Rh($EtImCH_2CH_2PPh_2$)$_2$][PF_6] (180 mg, 0.208 mmol) in 10 mL of dichloromethane 13 mg sulfur (0.416mmol) was added at room temperature. The color changed from orange yellow to green. Then the reaction mixture was stirred overnight. Finally the solvent was evaporated under vacuum and green crystals were obtained by layering diethylether onto a methylene chloride solution of **E16** (180 mg, 0.203 mmol, 92%).

^{1}H-NMR (500 MHz, CD_3CN): δ = 0.6 (t, 3 H, $^3J_{HH}$ = 15 Hz, g'), 1.2 (t, 3H, $^3J_{HH}$ = 13 Hz, g), 2.22-2.60 (m, 2H, f'), 2.84-3.67 (m, 2H, f), 2.59-3.35 (m, 2H, e), 3.06-3.30 (m, 2H, e'), 4.50-5.01 (m, 2H, d'), 4.73-5.24 (m, 2H, d), 6.5-7.46 (m, 20H, Ph), 7.04 (m, 1H, c), 7.15 (m, 1 H, b), 7.32 (m, 1H, c'), 7.71 (s, 1H, b').

^{13}C-NMR (125 MHz, CD_3CN): δ = 12.7 (s, CH_3, g), 14.7 (s, CH_3, g'), 28.4 (d, CH_2, $^2J_{PC}$ = 38 Hz, e'), 30.2 (d, CH_2, $^1J_{PC}$ = 31 Hz, e), 44.4 (s, CH_2, f), 46.5 (s, CH_2, f'), 49.6 (s, CH_2, d), 49.9 (s, CH_2, d'), 119.7 (d, CH, $^4J_{PC}$ = 5 Hz, c), 121.4 (s, CH, c'), 123.5 (d , CH, $^4J_{PC}$ = 6 Hz, b), 124.9 (s , CH, b'), 125.5-126.8 (d, CH, $^3J_{PC}$ = 5 Hz, k), 128.4-130.4 (m, CH, j or k), 131.7-133.2 (q, CH, $^3J_{PC}$ = 10 Hz, i), 140.2 (dd, C_q, $^1J_{PC}$ = 3 Hz, $^2J_{RhC}$ = 30 Hz, h), 142.95 (dd, C_q, $^1J_{PC}$ = 3 Hz, $^2J_{RhC}$ = 42 Hz, h'), 162.0 (ddd, $C_{Carbene}$, $^1J_{RhC}$ = 161 Hz, $^2J_{PC,\ cis}$ = 13 Hz, $^2J_{PC,\ trans}$ = 40 Hz, a), 169.5 (ddd, $C_{Carbene}$, $^1J_{RhC}$ = 48 Hz, $^2J_{PC,\ cis}$ = 6 Hz, $^2J_{PC,\ trans}$ = 19 Hz, a').

^{31} P-NMR (202 MHz, CD_3CN): δ = 4.2 (dd, $^1J_{RhP}$ = 128 Hz, $^2J_{PP}$ = 22 Hz), 19.5 (dd, $^1J_{RhP}$ = 77 Hz, $^2J_{PP}$ = 22 Hz), -144.0 (hept, $^1J_{PF}$ = 710 Hz).

IR (KBr disc): ν[cm^{-1}], 3456, 3187, 2950, 2836, 1651, 1434, 1331, 1263, 1020, 873, 744, 690, 557(ν_{SS}), 519.

E.A.: Anal. Found: C, 43.67; H, 4.16; N, 5.21, S, 5.79, $C_{40}H_{46}Cl_4F_6N_4P_3RhS_2$ requires C, 43.69; H, 4.18; N, 5.09, S, 5.82 %

4.13 Synthesis of *cis*-[Rh(CH$_3$)(I)(EtImCH$_2$CH$_2$PPh$_2$)$_2$][PF$_6$] (E17)

To a solution of *cis*-[Rh(EtImCH$_2$CH$_2$PPh$_2$)$_2$][PF$_6$] (180 mg, 0.208 mmol) in 10 mL of THF methyl iodide in excess (29.51 mg, 0.208 mmol, 1.5 mL) was added dropwise over 10 min. The reaction mixture was stirred at room temperature for 2 hours during this period of time the color changed to pale yellow. The solvent was removed under vacuum to give crude yellow product **E17** (130 mg, 0.134 mmol, 61.6%).

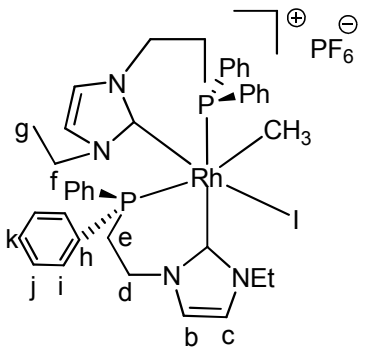

E17

^{1}H-NMR (500 MHz, CD$_3$CN): δ = 1.21 (t, 3H, g), 1.04 (t, 3H, g), 2.51-2.39 (m, 2H, d), 3.78 (s, 2H, CH$_3$), 4.13-4.56 (m, 2H, e), 6.19 (s, 1H, b or c), 7.37 (s, 1H, b or c), 7.59 (s, 1H, b or c), 7.92-7.12 (m, 20H, Ph).

^{13}C-NMR (125 MHz, CD$_3$CN): δ = 14.9 (s, CH$_3$, g), 15.5 (s, CH$_3$, g), 25.3 (s, CH$_2$, e), 27.8 (d, CH$_2$, e), 46.7 (s, CH$_2$, f), 48.7 (s, CH$_2$, d), 49.2 (s, CH$_2$, d), 125.1 (s, CH, b or c), 119.9 (s, b or c), 122.8 (s, CH, b or c), 127.0-135.2 (m, CH, Ph).

^{31}P-NMR (202 MHz, CD$_3$CN): δ = 13.4 (dd, $^{2}J_{PP}$ = 25 Hz, $^{1}J_{RhP}$ = 88 Hz), 6.2 (dd, $^{2}J_{PP}$ = 24 Hz, $^{1}J_{RhP}$ = 88 Hz).

4.14 Synthesis of *cis*-[Rh(Cl)(I)(EtImCH$_2$CH$_2$PPh$_2$)$_2$][I$_3$] (E19)

A solution of *cis*-[Rh(EtImCH$_2$CH$_2$PPh$_2$)$_2$][PF$_6$] (170 mg, 0.197 mmol) in 10 mL of THF was cooled to -50°C. Then iodine (100 mg, 0.394 mmol) in 5 mL of THFwas added through a needle steel capillary under argon atmosphere. The reaction mixture was stirred for 1 hour at -50°C and then allowed to warm to room temperature and eventually stirred over night. Removal of the solvent afforded a yellow brown crude product which was recrystallised by layering di-isopropyl ether into a concentrated acetonitrile solution of **E19** (140 mg, 0.122 mmol, 61 %).

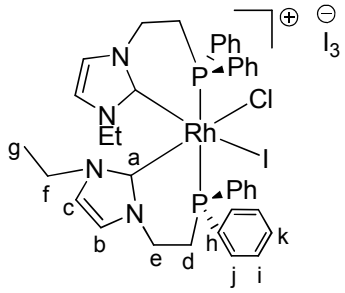

E19

^{1}H-NMR (500 MHz, CD_3CN): δ = 0.18 (t, 3H, $^{3}J_{HH}$ = 7 Hz, g), 1.10 (t, 3H, $^{3}J_{HH}$ = 7 Hz, g'), 2.22-2.60 (m, 2H, f'), 2.84-3.67 (m, 2H, f), 2.69-3.65 (m, 2H, d), 2.81-3.49 (m, 2H, d), 5.06-3.19 (m, 2H, e), 6.22-3.19 (m, 2H, e), 7.04 (m, 1H, c), 7.15 (m, 1H, b), 7.32 (m, 1H,c'), 7.71 (s, 1H, b').

^{13}C-NMR (125 MHz, CD_3CN): δ = 12.3 (s, CH_3, g), 15.5 (s, CH_3, g), 25.4 (d, CH_2, $^{1}J_{PC}$ = 26 Hz, d), 27.1 (d, CH_2, $^{1}J_{PC}$ = 26 Hz, d'), 44.4 (s, CH_2, f), 46.6 (s, CH_2, f'), 49.0 (s, CH_2, e), 50.0 (s, CH_2, e'), 120.8 (d, CH, b or c), 121.0 (s, CH, b or c), 126.6 (s, CH, b or c), 126.8 (d, CH, b or c), 127.1 (s, CH, i, j or k), 129.5 (s, CH, i, j or k), 135.4 (s, CH, i, j, k), 136.5 (dd, C_q, $^{2}J_{PC}$ = 5 Hz, $^{1}J_{RhC}$ = 50 Hz, h), 136.8 (dd, C_q, $^{2}J_{PC}$ = 5 Hz, $^{1}J_{RhC}$ = 50 Hz, h).

^{31} P-NMR (202 MHz, CD_3CN): δ = 4.0 (d, $^{1}J_{RhP}$ = 90 Hz), 1.7 (d, $^{1}J_{RhP}$ = 90Hz), -1.1 (d, $^{1}J_{Rh-P}$ = 85 Hz), -2.8 (d, $^{1}J_{RhP}$ = 87 Hz), -3.4 (d, $^{1}J_{RhP}$ = 85 Hz).

4.15 Synthesis of *cis*-[Ir(EtImCH$_2$CH$_2$PPh$_2$)][PF$_6$] (E20)

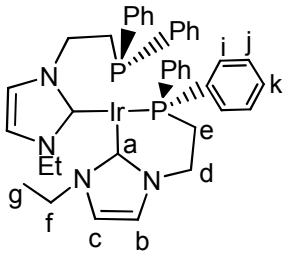

cis-**E20**

To a solution of 3-[2-(diphenylphosphino)ethyl]-1-ethylimidazolium-hexafluorophosphate **(**195 mg, 0.46 mmol) in 10 mL of THF was added $KN(SiMe_3)_2$ (100 mg, 0.46 mmol) and the mixture was stirred at room temperature under inert atmosphere for 30 min. $[Ir(COD)Cl]_2$ (77 mg, 0.115 mmol) was then added. The color changed to orange red. After the removel of the solvent under reduced pressure an orange residue was obtained which yielded red orange crystals by layering diethyl ether into methylene chloride solution **E20** (0.13 g, 61.9%).

^{1}H-NMR (500 MHz, CD_3CN): δ = 1.05 (t , 6H, $^{3}J_{HH}$ = 7 Hz, g), 2.12-2.59 (m, 4H, e), 3.76-3.9 (m, 4H, f), 4.36-4.90 (m, 4H, d), 6.94 (d, 2H, b, $^{3}J_{HH}$ = 2 Hz), 7.06 (d, 2H, c, $^{3}J_{HH}$ = 2 Hz), 6.82-7.80 (m, 20H, Ph).

^{13}C-NMR (125 MHz, CD_3CN): δ = 14.5 (t, CH_3, g), 31.0-31.3 (m, CH_2, e), 44.8 (s, CH_2, f), 49.8 (s, CH_2, d), 119.3 (s, CH, b), 120.1 (s, CH, c), 127.5-128.5 (m, CH, j or k), 130.1-130.7 (m, CH, j or k), 132.8-135.7 (m, CH, i), 138 .5 (d, C_q, $^{1}J_{PC}$ = 50 Hz, h), 138.8 (d , C_q, $^{1}J_{PC}$ = 48 Hz, h), 174.4 (dd, $C_{Carbene}$, a, $^{2}J_{PC,\ cis}$ = 20 Hz; $^{2}J_{PC,\ trans}$ = 98 Hz).

^{31}P-NMR (202 MHz, CD_3CN): δ = 16.5 (s), -144.4 (hept, $^1J_{PF}$ = 711 Hz).

4.16 Synthesis of *cis*-[Ir(H)$_2$(EtImCH$_2$CH$_2$PPh$_2$)$_2$][PF$_6$] (E21)

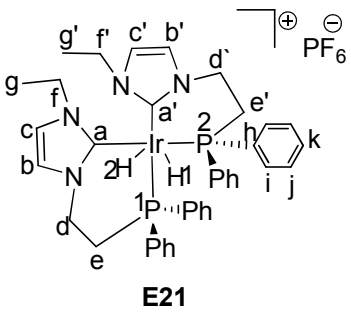

E21

Into a solution *cis*-[Ir(EtImCH$_2$CH$_2$PPh$_2$)$_2$][PF$_6$] (**E20),** (130 mg, 0.136 mmol) in 10 mL of CH_2Cl_2 H_2 gas was bubbled for 30 min. The color changed immediately from orange red to pale yellow. The solution was removed under vacuum to give a yellow crude product, which gave yellow crystals by layering diethylether onto methylene chloride solution of **E21** (100 mg, 0.117 mmol, 83 %).

^{1}H-NMR (500 MHz, CD_2Cl_2): δ = -13.16 (td, 1H (2), $^1J_{H1H2}$ = 4 Hz), - 11.5 (ddd, 1H (1), $^2J_{P1H1}$ = 129 Hz, $^2J_{P2H1}$ = 18 Hz, $^2J_{P2H2}$ = 16 Hz, $^1J_{H1H2}$ = 4 Hz), 0.47 (t, 3H, $^3J_{HH}$ = 7.59, g'), 1.28 (t, 3H, $^3J_{HH}$ = 7.34 Hz, g), 2.49-2.69 (m, 2H, f'), 2.68-2.95 (m, 2H, e'), 3.22-3.58 (m, 2H, f), 4.14-4.40 (m, 2H, d'), 4.40-4.47 (m, 2H, e), 6.86 (d, 1H, $^3J_{HH}$ = 2 Hz, b), 7.05 (s, 1H, b'), 7.16 (s, 1H, c), 7.29 (d ,1H, c'), 6.60-7.49 (m, 20 H, Ph).

^{13}C-NMR (125 MHz, CD_2CL_2): δ = 13.1 (s, CH_3, g'), 15.0 (s, CH_3, g), 26.0 (s, CH_2, d), 29.0 (s, CH_2, d'), 46.0 (d, CH_2, f), 49.5 (s, CH_2, d'), 49.9 (s, CH_2, e), 117.8 (s, CH, b'), 118.5 (d, CH, b), 122.2 (d, CH, c'), 122.9 (s, CH, c), 133.8, 127.7, 130.4, 130.9 (m, CH, i, j, k), 152.9 (s, C_q, $^1J_{PC}$ = 8 Hz, h), 153.6 (s, C_q, $^1J_{PC}$ = 8 Hz, h'), 160.2 (m, $C_{Carbene}$, a or a').

^{31}P-NMR (202 MHz, CD_2Cl_2): δ = -0.86 (d, $^2J_{PP}$ = 15 Hz), -2.17 (d, $^2J_{PP}$ = 15 Hz), -144.0 ($^1J_{PF}$ = 710 Hz).

IR (KBr disc): ν[cm^{-1}], 2050(ν_{HH})**,** 2013(ν_{HH}), 1460, 1453, 1419, 1405, 1434, 1097, 877, 755, 741, 700, 557, 534, 517, 488.

E.A.: Anal. Found: C, 49.97; H, 5.72; N, 5.21, $C_{46}H_{64}F_6IrN_4O_2P_3$ requires C, 49.90; H, 5.79; N, 5.07 %

4.17 Synthesis of *cis*-[Ir(η^2-O_2)(EtImCH$_2$CH$_2$PPh$_2$)$_2$][PF$_6$] (E22)

A solution of *cis*-[Ir(EtImCH$_2$CH$_2$PPh$_2$)$_2$][PF$_6$] (130 mg, 0.136 mmol) in 10 mL of CH_2Cl_2 exposed to air for 10 min. The color of the reaction mixture changed immeditaly from orange red to pale yellow. The solvent was evaporated to afford a yellow residue which was dried under vacuum. Crystals were grown from a concentrated THF solution or by layering diethyl ether onto a methylene chloride solution **E22** (110 mg, 0.11 mmol, 84.6%).

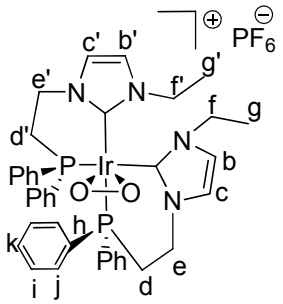

E22

^{1}H-NMR (500 MHz, CD_3CN): δ = 0.55 (t, 3H, $^3J_{HH}$ = 7 Hz, g), 1.32 (t, 3H, $^3J_{HH}$ = 8Hz , g'), 2.36-2.73 (m, 2H, d), 2.98 (m, 2H, d'), 3.95 (m, 2H, f), 4.19 (m, 2H, f'), 4.73 (m, 2H, e'), 3.89-4.54 (m, 2H, e), 6.98 (s, 1H, c'), 7.11 (s, 1H, b'), 7.14 (d, 1H, $^3J_{HH}$ = 2 Hz, b), 7.59 (d, 1H, $^3J_{HH}$ = 2 Hz, c), 6.95-7.36 (m, 20H, Ph).

^{13}C-NMR (125 MHz, CD_3CN): δ = 13.2 (s, CH_3, g), 15.7 (s, CH_3, g'), 25.5 (s, CH_2, d), 27.5 (s, CH_2, d'), 43.1 (s, CH_2, f'), 45.7 (s, CH_2, f), 47.4 (s, CH_2, e'), 49.1 (s, CH_2, e), 120.2 (s, CH, c), 122.8 (d, $^3J_{HH}$ = 4 Hz, c'), 124.3 (s, CH, b), 127.6 (d, CH, b'), 130.6, 133.0, 132.7 (m, CH, Ph), 139.9 (d, C_q, $^1J_{PC}$ = 50 Hz, h), 143.7 (m, $C_{Carbene}$, a), 147.2 (m, $C_{Carbene}$, a').
^{31}P-NMR (125 MHz, CD_3CN, 323K): δ = -11.6 (d, $^2J_{PP}$ = 15 Hz), -11.5 (d, $^2J_{PP}$ = 13 Hz), -144.0 (hept, $^1J_{PF}$ = 713 Hz).

IR (KBr disc): ν[cm^{-1}], 3500, 3054, 2475, 1435, 1419, 1409, 1260, 1098, 1059, 1028, 858((ν_{OO}), 748, 696, 558, 531, 506.

4.18 Synthesis of *cis*-[Ir(η^2-S_2)(EtImCH$_2$CH$_2$PPh$_2$)$_2$][PF$_6$] (E23)

To a solution of *cis*-[Ir(EtImCH$_2$CH$_2$PPh$_2$)$_2$][PF$_6$], (**E20)** (130 mg, 0.136 mmol) in 10 mL of CH_2Cl_2. Sulfur (8.0 mg, 0.273 mmol) was added at once. The color of the reaction mixture changed from orange red to yellow orange. The reaction mixture was stirred over night. Subsequently the solvent was removed under reduced pressure to yield a yellow orange residue which gives yellow crystals (yield = 110 mg, 0.112 mmol, 82%) by layering diethyl ether into a solution of **E23** in THF/acetonitrile (1/1).

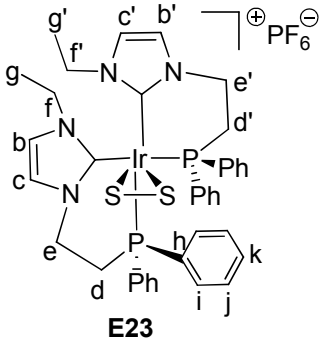

E23

^{1}H-NMR (500 MHz, CD_3CN): δ = 0.56 (t, 3H, $^3J_{HH}$ = 7 Hz, g); 1.25 (t, 3H, $^3J_{HH}$ = 7 Hz, g'), 2.54-2.64 (m, 2H, f), 2.83-3.68 (m, 2H, f'), 2.61-3.45 (m, 2H, e'), 3.10-3.43 (m, 2H, d), 4.37-4.91 (m, 2H, e), 4.66-5.21(m, 2H, d'), 7.03 (s, 1H, c'), 7.15 (s, 1H, b'), 7.27 (d, 1H, $^3J_{HH}$ = 2 Hz, b), 7.65 (d, 1H, $^3J_{HH}$ = 2 Hz, c), 6.80-7.43 (m, 20H, Ph).

^{13}C-NMR (125 MHz, CD_3CN): δ = 12.6 (s, CH_3, g), 14.8 (s, CH_3, g'), 27.3 (t, CH_2, $^2J_{PC}$ = 49 Hz, d), 29.7 (d, CH_2, $^2J_{PC}$ = 38 Hz, e'), 44.6 (CH_2, d), 46.1 (s, CH_2, f), 49.9 (s, CH_2, d'), 51.1 (s, CH_2, e), 119.3 (d, CH, $^3J_{HH}$ = 4 Hz, c'), 120.5 (s, CH, b), 123.1 (s, CH, b'), 124.5 (s, CH, c), 128.1, 133.2, 130.4 (m, CH, i, j, k), 138.5 (d, C_q, $^1J_{PC}$ = 39 Hz, h), 142.5 (d, C_q, $^1J_{PC}$ = 53 Hz, h'), 145.0 (dd, $C_{Carbene}$, $^2J_{PC}$ = 9 Hz, a'), 149.7 (d, $C_{Carbene}$, $^2J_{PC}$ = 12 Hz, a').

^{31}P-NMR (202 MHz, CD_3CN): δ = -12.7 (d, $^2J_{PP}$ = 18 Hz), -30.7 (d, $^2J_{PP}$ = 15 Hz).

IR (KBr disc): ν[cm^{-1}], 3445, 2963, 2360, 1435, 1261, 1097, 1022, 802, 697, 669, 557(ν_{SS}).

4.19 Synthesis of *cis*-[Ir(CO)(EtImCH$_2$CH$_2$PPh$_2$)$_2$][PF$_6$] (E24)

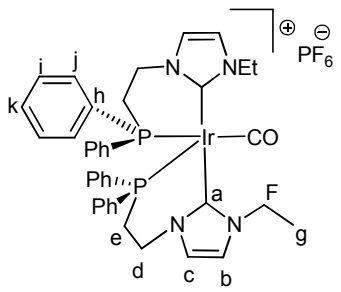

E24

CO gas was bubbled for 30 min. through a red orange THF solution (10 mL) of *cis*-[Ir(EtImCH$_2$CH$_2$PPh$_2$)$_2$][PF$_6$], **E20** (130 mg, 0.136 mmol). The color changed to pale yellow. Then the solvent was removed under reduced pressure to give a yellow precipitate of **E24** in high yield (130 mg, 0.132 mmol, 97 %).

^{1}H-NMR (500 MHz, CD_3CN): δ = 1.14 (t, 3H, $^3J_{HH}$ = 7 Hz, g), 1.64-2.11 (m, 2H, e), 3.06-3.56 (m, 2H, d), 3.90-4.4 (m, 2H, f), 6.8 (s, 1H, c), 7.06 (s, 1H, b), 6.50-7.64 (m, 20H, Ph).

^{13}C-NMR (125 MHz, CD_3CN): δ = 14.9 (s, CH_3, g), 27.4 (t, CH_2, $^2J_{PC}$ = 13 Hz, e), 45.6 (s, CH_2, f), 48.0 (s, CH_2, d), 119.8 (s, CH, b), 124.4 (s, CH, c), 129.2, 129.6, 133.2, 130.3, 128.6 (m, CH, Ph), 143.8 (t, $C_{Carbene}$, $^2J_{PC}$ = 13 Hz, a), 191.2 (t, CO, $^2J_{PC}$ = 45 Hz).

^{31}P-NMR (202 MHz, CD_3CN): δ = -12.0 (s), -144.4 (hept, $^1J_{PF}$ = 710 Hz).

IR (CaF_2): ν[cm^{-1}], 2018, 1900 (ν_{CO}).

4.20 Synthesis of *trans*-[Ir((CH$_3$)(I)(EtImCH$_2$CH$_2$PPh$_2$)$_2$)]I (E25)

Methyl iodide was added dropwise over 10 min at room temperature (1mL, 0.136 mmol) to a solution of *cis*-[Ir(EtImCH$_2$CH$_2$PPh$_2$)$_2$][PF$_6$] (130 mg, 0.136 mmol) in 10 mL of THF. The reaction mixture was stirred at room temperature for 1 h. The color changed from red orange to pale yellow. A pale yellow precipitate was observed which was collected by filtration. Subsequently the solvent was removed under vacuum to give the pale yellow product **E25**, which gave white crystals from concentrated THF solution (100 mg, 0.092 mmol, 68.4%).

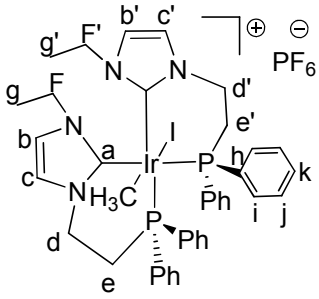

E 25A

^{1}H-NMR (500 MHz, CD_3CN): δ = 0.15 (s, 3H, $\underline{C}H_3Ir$), 0.9 (t, 3H, $^{3}J_{HH}$ = 7 Hz, g), 1.35 (t, 3H, $^{3}J_{HH}$ = 7 Hz, g'), 2.54-2.72 (m, 2H, e), 2.82-3.12 (m, 2H, e'), 2.9-3.13 (m, 2H, d), 3.25-3.44 (m, 2H, d'), 7.29 (m, 1H, b), 7.42 (m, 1H, c), 7.56 (m, 1H, b'), 7.56 (m, 1H, c'), 6.07 (t, 2H, $^{3}J_{HH}$ = 8 Hz, Ph), 7.14 (t, 2H, Ph), 7.23 (t, 4H, Ph), 7.42 (m, 4H, Ph), 7.30 (m, 4H, Ph), 7.42 (m, 4H, Ph).

^{13}C-NMR (125 MHz, CD_3CN): δ = 0.4 (s, CH_3, CH_3-Ir), 15.4 (s, CH_3, g), 15.9 (s, CH_3, g'), 29.4 (d, CH_2, $^{2}J_{PC}$ = 29 Hz, e), 30.2 (d, CH_2, $^{2}J_{PC}$ = 30 Hz, e'), 43.6 (s, CH_2, f'), 44.6 (s, CH_2, f''), 47.1 (s, CH_2, d), 47.8 (s, CH_2, d'), 120.8 (d, CH, $^{2}J_{CH}$ = 4 Hz, b), 122.1 (d, CH, $^{2}J_{CH}$ = 4 Hz, c), 124.4 (d, CH, $^{2}J_{CH}$ = 4 Hz, b'), 126.0 (d, CH, $^{2}J_{CH}$ = 4 Hz, c'), 126.4 (d, CH, $^{2}J_{PC}$ = 10 Hz, i), 127.4 (d, CH, $^{2}J_{PC}$ = 10 Hz, i or j), 128.5 (m, CH, i, k), 130.8 (s, CH, i, k, j), 132.3 (d, CH, $^{3}J_{PC}$ = 7 Hz, j), 133.4 (d, CH, $^{3}J_{PC}$ = 8 Hz, j), 134.1 (d, CH, $^{2}J_{PC}$ = 10 Hz, i), 135.6 (d, CH, $^{3}J_{PC}$ = 8 Hz, j), 144.1 (d, C_q, $^{1}J_{PC}$ = 14 Hz, h), 145.1 (d, C_q, $^{1}J_{PC}$ = 14 Hz, h), 146.6 (d, $C_{Carbene}$, $^{2}J_{PC}$ = 12 Hz, a), 147.6 (d, $C_{Carbene}$, $^{2}J_{PC}$ = 12 Hz, a').

^{31}P-NMR (202 MHz, CD_3CN): δ = -22.1 (d, $^{2}J_{PP}$ = 20 Hz), - 41.4 (d, $^{2}J_{PP}$ = 20 Hz), -144.0 (hept, $^{1}J_{PF}$ = 710 Hz).

4.21 Synthesis of *cis*-[Ir(I)$_2$(EtImCH$_2$CH$_2$PPh$_2$)$_2$][I$_3$] (E26)

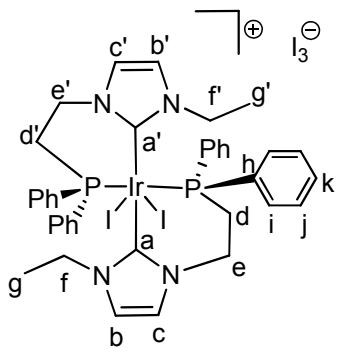

E26

I_2 (69 mg, 0.272 mmol) in THF (3 mL) was added dropewise through steel capilary needle over 10 min under argon atmosphere to a solution of *cis*-[Ir(EtImCH$_2$CH$_2$PPh$_2$)$_2$][PF_6] (130 mg, 0.136 mmol) in THF (10 mL) which was cooled to -50°C. After the reaction mixture was stirred at this temperature for 1 h, it was warmed to room temperature and stirred for another 1 h. The color of the reaction mixture changed from red orange to pale yellow. Now the solvent was removed under vacuum to give yellow **E26**, which gave single crystals from layering diisopropyl ether into concentrated acetonitrile solution of **E26** (200 mg, 0.100 mmol, 74.07 %).

^{1}H-NMR (500 MHz, CD_3CN): δ = 0.71 (t, 3H, $^{3}J_{HH}$ = 9 Hz, g), 1.23 (t, 3H, $^{3}J_{HH}$ = 7 Hz, g'), 2.69-2.95 (m, 2H, d), 2.82-3.16 (m, 2H, d'), 2.96-3.93 (m, 2H, f), 3.95-4.79 (m, 2H, f'), 4.52-5.75

(m, 2H, e), 4.52-5.74 (m, 2H, e'), 7.49 (s, 1H, c), 7.38 (d, 1H, b), 7.35 (s, 1H, b'), 7.43 (t, 1H, c'), 7.02-7.36 (m, 20 H, i, j, k).

^{13}C-NMR (125 MHz, CD_3CN): δ = 15.3 (s, CH_3, g), 15.6 (s, CH_3, g'), 31.7 (d, CH_2, $^2J_{PC}$ = 45 Hz, d), 31.9 (d, CH_2, $^2J_{PC}$ = 45 Hz, d'), 46.4 (s, CH, f), 47.4 (s, CH, f'), 48.5 (s, CH, e), 49.6 (s, CH, e'), 122.2 (s, CH, c), 122.6 (s, CH, b), 125.07 (s, CH, c'), 126.6 (s, CH, b'), 126.9 (s, CH, Ph), 127.7 (t, CH, $^3J_{PC}$ = 7 Hz, i, k, j), 128.8 (d, CH, $^2J_{PC}$ = 10 Hz, i), 130.05 (s, CH, i, k, j), 131.0 (t, CH, $^2J_{PC}$ = 7 Hz, i), 131.5 (t, CH, $^2J_{PC}$ = 7 Hz, i), 132.8 (d, CH, $^3J_{PC}$ = 3 Hz, j), 133.5 (d, CH, $^3J_{PC}$ = 4 Hz, j), 134.1 (CH, $^3J_{PC}$ = 5 Hz, j), 136.4 (d, C_q, $^1J_{PC}$ = 15 Hz, h).

^{31}P-NMR (202 MHz, CD_3CN): δ = 25.2 (d, $^2J_{PP}$ = 20 Hz), -54.7 (d, $^2J_{PP}$ = 20 Hz); -43.8 (s) (*trans*-Isomer, side product).

4.22 Synthesis of *trans*-[Ni(EtImCH$_2$CH$_2$PPh$_2$)$_2$][I]$_2$ (E27)

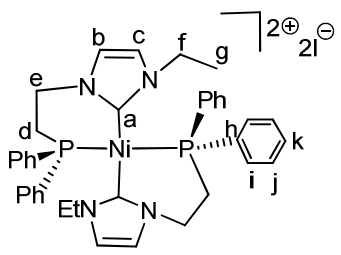

E27

$KN(SiMe_3)_2$ (100 mg, 460 µmol) was added to a solution of [$EtImCH_2CH_2PPh_2$]I, **E5** (200 mg, 460 µmol) in THF (20 mL). The suspension was stirred at room temperature for 60 min. After removal of KI by filtration [$Ni_7S(S^tBu)_8$][$BzEt_3N$] (166 mg, 153 µmol) was added to the filtrate. The color of the resulting suspension changed from pale yellow to black. After the reaction mixture was stirred at room temperature for another 1 h, it was concentrated giving a pale yellow precipitate which was collected by filtration and crystallised by slow evaporation of a concentrated acetonitrile solution to give **E27** yellow crystals.

^{1}H-NMR (500 MHz, $CDCl_3$): δ = 1.02 (t, 3H, $^3J_{HH}$ = 7 Hz, g), 2.38-2.89 (m, 2H, e), 3.44-4.64 (m, 2H, e), 4.98 (m, 2H, f), 5.32 (m, 2H, d), 7.01 (s, 2H, b), 7.23 (s, 2H, c), 6.95-7.66 (m, 20H, i, j, k).

^{13}C-NMR (125 MHz, $CDCl_3$): δ = 15.3 (s, CH_3, g), 25.0 (s, CH_2, e), 47.0 (s, CH_2, f), 50.0 (s, CH_2, d), 121.0 (s, CH, b), 124.0 (s, CH, c), 128.1, 129.2, 130.8, 132.6, 135.2 (CH, i, j, k), 164.2 (t, $C_{Carbene}$, $^2J_{PC}$ = 35 Hz, a).

^{31}P-NMR (202 MHz, $CDCl_3$): δ = 21.0 (s).

4.23 Synthesis of *trans*-[Pd(EtImCH$_2$CH$_2$PPh$_2$)$_2$][PF$_6$]$_2$ (E28)

To a solution of 3-[2-(diphenylphosphino)ethyl]-1-ethylimidazolium-hexafluorophosphate **E6** (195 mg, 0.46 mmol) in THF (10 mL) was added $KN(SiMe_3)_2$ (118 mg, 0.46 mmol + 30%) and the mixture was stirred at room temperature under inert atmosphere for 30 min. Then $[Pd(COD)Cl_2]$ (66 mg, 0.230 mmol) was added to the reaction mixture and the color changed from pale yellow to yellow orange. The reaction mixture was stirred another 2 h. A crude yellow product **E28** was obtained after the removel of the solvent under vacuum. Yellow crystals were obtained by layering diethyl ether onto a concentrated acetonitrile solution of **E28** (190 mg, 0.187 mmol, 75.0 %).

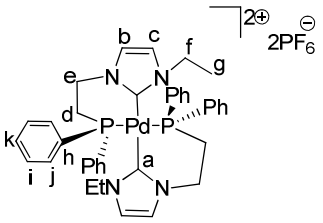

E28

^{1}H-NMR (500 MHz, CD_3CN): δ = 0.91 (t, 3H, $^{3}J_{HH}$ = 8 Hz, g), 2.81-2.89 (m, 2H, e), 2.91-3.05 (m, 2H, e), 3.32-3.75 (m, 2H, f), 3.86 (m, 2H, f), 4.79-4.99 (m, 2H, d), 6.72 (s, 2H, b), 7.20 (s, 2H, c), 6.79-7.53 (m, 20H, Ph).

^{13}C-NMR (125 MHz, CD_3CN): δ = 14.1 (s, CH_3, g), 28.5 (d, CH_2, $^{2}J_{PC}$ = 17 Hz, e), 45.8 (s, CH_2, f), 48.7 (s, CH_2, d), 121.0 (s, CH, b), 124.1 (s, CH, c), 129.9 (t, CH, $^{3}J_{PC}$ = 6 Hz, j or k), 129.6 (t, CH, $^{3}J_{PC}$ = 6 Hz, j or k), 130.7 (s, CH, i), 131.4 (s, CH, i), 132.9 (s, CH, i), 134.2 (t, CH, $^{2}J_{PC}$ = 8 Hz, j), 134.3 (t, CH, $^{2}J_{PC}$ = 8 Hz, j), 161.2 (d, C_q, $^{1}J_{PC}$ = 22 Hz, h), 162.3 (d, C_q, $^{1}J_{PC}$ = 22 Hz, h), 164.8 (t, $C_{Carbene}$, $^{2}J_{PC}$ = 12 Hz, a).

^{31}P-NMR (125 MHz, CD_3CN): δ = 17.9 (s), -144.0 (hept, $^{1}J_{PF}$ = 710 Hz).

4.24 Synthesis of *cis*-[Pd(EtImCH$_2$CH$_2$PPh$_2$)$_2$][PF$_6$]$_2$ (E28)

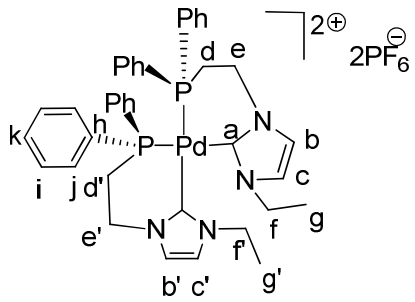

cis- **E28**

To a solution of 3-[2-(diphenylphosphino)ethyl]-1-ethylimidazolium-hexafluoro-phosphate **E6 (**195 mg, 0.46 mmol) in THF (10 mL) was added $KN(SiMe_3)_2$ (118 mg, 0.46 mmol [30% excess]) . The mixture was stirred at room temperature under inert atmosphere for 30 min. Now $[Pd(COD)Cl_2]$ (66 mg, 0.230 mmol) in 5mL of THF was added dropwise to the reaction mixture and the color changed from pale yellow to orange red. The reaction mixture was stirred for another 2 h. The yellow product was obtained after the removel of solvent under vacuum to give *cis*-**E28** (190 mg, 0.187 mmol, 75.0 %).

^{1}H-NMR (500 MHz, CD_3CN): δ = 0.91 (t, 3H, $^{3}J_{HH}$ = 7 Hz, g), 1.01 (t, 3H, $^{3}J_{HH}$ = 7 Hz, g'), 2.89-2.73 (m, 2H, d), 2.78-2.93 (m, 2H, d'), 3.31-3.75 (m, 2H, f), 3.24 (m, 2H, f'), 3.71-4.08 (m, 2H, e), 5.03-4.74 (m, 2H, e'), 6.72 (s, 1H, b), 6.37 (s, 1H, b'), 7.16 (s, 1H, c), 7.34 (s, 1H, c'), 6.79-7.53 (m, 20H, Ph).

^{13}C-NMR (125 MHz, CD_3CN): δ = 14.1 (s, CH_3, g), 14.5 (s, CH_3, g'), 27.6 (s, CH_2, f`), 28.5 (s,CH_2, f'), 30.1 (d, CH_2, $^{2}J_{PC}$ = 5 Hz, d), 30.4 (d, CH_2, $^{2}J_{PC}$ = 6 Hz), 45.9 (s, CH_2, e), 48.9 (s, CH_2, e'), 121.1 (s, CH, b), 122.2 (s, CH, c), 124.2 (s, CH, c'), 129.9 (t, CH, $^{3}J_{PC}$ = 6 Hz, j or i), 129.6 (t, CH, $^{3}J_{PC}$ = 6 Hz, j or k), 130.7 (t, CH, j or i), 131.4 (s, CH, j or k), 132.9 (s, CH, j or k), 134.2 (t, CH, $^{2}J_{PC}$ = 8 Hz, j), 134.3 (t, CH, $^{2}J_{PC}$ = 8 Hz, j), 161.2 (d, C_q, $^{1}J_{PC}$ = 21 Hz, h), 161.3 (d, C, $^{1}J_{PC}$ = 20 Hz, h), 164.8 (dd, $C_{Carbene}$, $^{2}J_{PC}$ = 23 Hz, $^{2}J_{PC}$ = 134 Hz, a).

^{31}P-NMR (125 MHz, CD_3CN): δ = 17.7 (s), -144.0 (hept, $^{1}J_{PF}$ = 710 Hz).

4.25 *Suzuki* coupling reaction.

A mixture of aryl halide (1 mmol), phenylboronic acid (1.5 mmol), cesium carbonate (2 mmol), Pd(II)-NHC **E28** (1 mol %, 0.009 g) and dioxane (3 mL) was stirred at 80°C for an appropriate period of time (8-48 h) under nitrogen. The solution was allowed to cool to ambient temperature. The reaction mixture was diluted with H_2O (10 mL) and Et_2O (10 mL) followed by twofold extraction with Et_2O. The combined organic layers were dried over Mg_2SO_4, filtered and evaporated under reduced pressure to a give crude product. The pure product was isolated by plate chromatography to give a biphenyl product as a colorless solid, which was characterized by ^{1}H-NMR spectroscopy.

.

5. Conclusion

The mixed bidentate phosphane imidazole donor ligands **E5** 3-[2-(diphenylphosphino)ethyl]-1-ethylimidazoliumiodide and **E6** 3-[2-(diphenylphosphino)ethyl]-1-ethylimidazolium-hexafluoro-phosphate were successfully synthesized and fully characterized (Figure 3.1). The counter ion was exchanged due to the difficulties encountered by us in the crystallization process. The formation of the carbene was investigated by addition of CS_2. Single crystals from this product **E8** were investigated by single crystal X-ray analysis (Figure 3.5) and by NMR-spectroscopic methods.

The novel *cis*-Rh(I) complexes $[Rh(EtImCH_2CH_2PPh_2)_2][X]$, (X = Cl, PF_6) **E10** and **E11**, respectively, were synthesized and characterized (Figure 3.8). These complexes were obtained in high yield. **E10** was obtained as yellow crystals from THF solution while **E11** is highly soluble in THF. Crystals of these complexes are suitable for single crystal X-ray analyses. They adopt a square planar geometry around the rhodium(I) atom (Figure 3.9, 3.10). In addition the novel *trans*-Rh(I) complex $[Rh(EtImCH_2CH_2PPh_2)_2]Cl$ **E12** was obtained by dropwise addition of the metal precursor $[Rh(\mu\text{-}Cl)(COD)]_2$ to an *in situ* generated carbene solution. **E13** $[Rh(EtImCH_2CH_2PPh_2)_2][PF_6]$ was obtained by a simple salt metathesis reaction. Both complexes were characterized by standard spectroscopic methods. Single crystal X-ray analyses of both complexes exhibit a square-planar environment around the Rh(I) atom (Figure 3.11, 3.12) as expected for Rh(I) complexes.

cis-**E10** can be converted to *trans*-**E12** by heating. The interconversion at elevated temperatures was discussed and fully elucitated by measuring ^{31}P-NMR spectra (Figures 3.14, 3.15). After prolonged heating, the ratio of *cis* to *trans* amounts to 1:2. Further heating gave no further change in ratio of both isomers indicating that the equilibrium is reached. A proposed mechanism of interconversion of **E10** *cis*-$[Rh(EtImCH_2CH_2PPh_2)_2]Cl$ to **E12** *trans*-$[Rh(EtImCH_2CH_2PPh_2)_2]Cl$ is showen (Figure 3.17).

Furthermore, the novel peroxo complexes **E14** and **E15**, *cis*-$[Rh(\eta^2\text{-}O_2)(EtImCH_2CH_2PPh_2)]^+$ and *trans*-$[Rh(\eta^2\text{-}O_2)(EtImCH_2CH_2PPh_2)]^+$, respectively, were synthesized (Figure 3.19). ^{31}P-NMR spectra of these peroxo complexes at different temperatures show the formation of two conformers of **E14** (Figure 3.21)**.** Also, ^{31}P-NMR spectra prove that the peroxo complex **E14** is capable of reversibl oxygen activation. These complexes were obtained in high yield and

characterized by NMR-spectroscopic methods. Single crystal X-ray analyses of **E14** and **E15** exihibt a trigonal-bipyramidal arrangement of the ligands around the Rh(III) atoms (Figure 3.23, 3.24). In the IR spectra of the complexes, absorption bands at 845 cm^{-1} can be attributed to the oxygen-oxygen stretching vibration typical for side-on coordinated peroxide ions.

The novel compound *cis*-$[Rh(\eta^2\text{-}S_2)(EtImCH_2CH_2PPh_2)]^+$ (**E16)** was synthesized as illustrated in Figure (3.25). It was obtained in high yield and characterised by NMR spectroscopic methods. Green single crystals of **E16** shows a distorted trigonal bipyramidal arrangement around the Rh(III) metal atom (Figure 3.27). The IR spectrum of **E16** exihibits a band at 557 cm^{-1} can be assigned to the S-S stretching vibration of the η^2-S_2-ligand.

The novel rhodium(III) complexes **E17** and **E18** are isomers of formula $[Rh(CH_3)(I)(EtIm\text{-}CH_2CH_2PPh_2)_2]I$. These complexes were obtained by the reaction of **E11** with MeI in high yield (86%). Unfortunately, all attempts to get crystals of these complexes failed.

The novel complex **E19**, *cis*-$[Rh(Cl)(I)(EtImCH_2CH_2PPh_2)_2][I_3]$ was synthesized by reaction of **E11** with iodine. **E19** was characterised by standard spectroscopic methodes. Interestingly, a single crystal X-ray analysis revealed the formation of this unexpected iodide-chloride adduct which most likely results from the exchange of iodide with chloride contained as small impurity in the starting material. The counter ion I_3^- is formed by the reaction of iodide with excess I_2. Yellow brown single crystals of **E19** reveal the formation of an octahedral Rh(III) complex (Figure 3.28).

With respect to **E10** the isoelectronic *cis*-iridium(I) complex, *cis*-$[Ir(EtImCH_2CH_2PPh_2)_2][PF_6]$ (**E20**) was synthesized (Figure 3.29) and characterised by NMR spectroscopy. The ^{31}P-NMR spectrum shows the signal of the phosphorous atoms at 16.8 ppm. A single crystal X-ray analysis of red single crystals of **E20** shows a square planar structure as expected for iridium(I) complexes (Figure 3.30).

The synthesis of a series of the novel iridium(III) complexes **E21**, **E22**, **E23**, **E25**, **E26,** *cis*-$[Ir(H)_2(EtImCH_2CH_2PPh_2)_2]^+$, *cis*-$[Ir(\eta^2\text{-}O_2)(EtImCH_2CH_2PPh_2)]^+$, *cis*-$[Ir(\eta^2\text{-}S_2)(EtIm\text{-}CH_2CH_2PPh_2)]^+$, *trans*-$[Ir(CH_3)(I)(ImCH_2CH_2PPh_2)_2]^+$, *cis*-$[Ir(I)_2(ImCH_2CH_2PPh_2)_2]^+$ also described (Figure 3.32). **E21** was obtained in high yield by reaction of **E20** with H_2 and characterised by NMR spectroscopy. The IR spectrum of **E21** shows sharp Ir-H stretching mode at 2013 and 2050 cm^{-1} which are in a good agreement with data of other iridium hydride

complexes. Also single crystal X-ray analysis of **E21** exhibits a distorted octahedral structure around the Ir(III) atom (Figure 3.33).

E22 *cis*-$[Ir(\eta^2\text{-}O_2)(EtImCH_2CH_2PPh_2)]^+$ was synthesized by reaction of **E20** with oxygen and fully characterized by standard spectroscopic methods. The reaction of iridium(I) with O_2 is irreversible as confirmed by ^{31}P-NMR spectra (Figure 3.33). The IR spectrum shows a sharp band which must be assigned to ν(O-O) at 854 cm^{-1}. An X-ray single crystal analysis of **E22** shows a trigonal-bipyramidal arrangement of the ligands around the iridium(III) atom (Figure 3.35).

E23 *cis*-$[Ir(\eta^2\text{-}S_2)(EtImCH_2CH_2PPh_2)]^+$ was synthesized by reaction of **E20** with sulfur and characterized by standard spectroscopic methods. A single crystal X-ray analysis of **E23** revealed a distorted octahedral ligand field. In the IR spectrum, the ν(S-S) band is located at 557 cm^{-1}. According to a single crystal X-ray analysis the ligands in **E23** adopt a trigonal-bipyramidal environment around the Ir(III) atom (Figure 3.36).

The five-coordinate Ir(I) carbonyl complex **E24** was synthesized by addition of CO to **E20** and identified by NMR-spectroscopic methods. The IR spectrum of **E24** shows an absorption band of CO at 2080 and 1900 cm^{-1}. Unfortunately, all attempts to crystallize this complex failed.

We observed remarkable differences in the reactivity of **E20,** Ir(I) toward CO and H_2 compared to the isoelectronic Rh(I) complex **E10**. The later shows no reactivity towards CO and H_2 at room temperature, while **E20** reacts with CO and H_2 even at room temperature.

In addition, the novel Ir(III) complexes **E25** and **E26,** *trans*-$[Ir(CH_3)(I)(ImCH_2CH_2PPh_2)_2]^+$, *cis*-$[Ir(I)_2(ImCH_2CH_2PPh_2)_2]^+$, were obtained by reaction of **E20** with MeI and I_2, respectively, in high yields and characterized by NMR spectroscopy. Both complexes contain in solution two isomers (A, B), which could not be seperated. Colorless single crystals of isomer B of both complexes contain according to X-ray diffraction measurements in both cases a distorted octahedral enviroment around the Ir(III) atoms (Figure 3.37, 3.39).

The new *trans*-Ni(II) and *trans*-Pd(II) complexes **E27**, **E28** $[Ni(EtImCH_2CH_2PPh_2)_2]^{2+}$ $[Pd(EtImCH_2CH_2PPh_2)_2]^{2+}$, respectively, were synthesized according to Figure 3.41 and 3.43 and fully characterized by spectroscopic methods. Both complexes adopt a distorted square-planar environment around the metal(II) atoms. The interconversion of *cis* to *trans* isomers in **E28** at high temperature was followed up by ^{31}P-NMR spectroscopy (Figure 3.45). The interconvertion of *cis* to *trans* at 70°C lead to an equilibrium between both isomers with a ratio of 1:2.

The *trans*-Pd(II) complex **E28** proved to be an effective catalyst for *Suzuki* coupling reactions. Table 3.19 shows its activity for the coupling of substituted aryl halides containing electron donating and withdrawing groups with phenyl boronic acids. Reaction times of about 24 h at 80°C are required for the production of unsymmetrical biaryl products in good yield.

6. Bibliography.

[1] a) E. Buchner, T. Curtius, *Ber. Dtsch. Chem. Ges*. **1885**, 8, 2377.
b) H. Staudinger, O. Kupfer, *Ber. Dtsch. Chem. Ges.* **1912**, 45, 501.
c) Ahistorical review, A. J. Arduengo III, R. Krafczyk, *Chem. Unsere Zeit*. **1998**, 32, 6.

[2] For general reviews on transient carbenes, see
a) Carbene chemistry, W. Kirmse, Ed, Academic press, NewYork. **1964** and **1971**.
b) Carbenes, M. Joness, R. A. Moss, Ed, Wiely: New York. **1973** and **1975**, Vols. I and II.
c) Carbene(cabonoide). In Methoden der organischen chemie(Houben-weyl), M. Ed . Regitz, George Thieme verlag: Stuttgarts, **1989**, E 19b (1-3).
d) Advances in Carbene chemistry, Ed U. H Brinker, Jai press:, Greenwich and Stamford, **1994** and **1998**, Vols.1 and 2.

[3] W. V. E. Doering, A. K. Hoffmann, *J. Am. Chem. Soc*. **1954**, 76, 6162.

[4] E. O. Fischer, A. Massboel, *Angew. Chem. Int. Ed*. 1**964**, 3, 580; *Angew. Chem*. **1964**, 76, 571.

[5] H. Tomika, *Acc. Chem. Res.* **1977**, 30, 315.

[6] A. Igau, H. Grutzmacher, A. Baceiredo, G. Bertrand, *J. Am. Chem. Soc*. **1988**, 110, 6463.

[7] A. J. Arduengo, III, R. L. Harlow, M. Kline, *J. Am. Chem. Soc*. **1991**, 113, 361.

[8] K. Oefele, *J. Organomet. Chem*. 1**968**, 12, P42.

[9] H. W. Wanzlick, H. J. Schonherr, *Angew. Chem. Int. Ed.* **1968**, 7, 141; *Angew. Chem*. 1**968**, 80, 154.

[10] H. W. Wanzlick, E. Schikora, *Angew. Chem*. **1960**, 72, 494.

[11] Y. Liu, P. E. Lindna, D. M. Lemal, *J. Am. Chem. Soc***. 1999**, 121, 10525.

[12] F. E. Hahn, L. Wittenbecher, D. Levan, R. Fröhlich, *Angew. Chem. Int. Ed.* **2000**, 39, 5410; *Angew. Chem*. **2000**, 112, 551.

[13] A. J. Arduengo, III, J. R. Görlich, W. J. Marshall, *J. Am. Chem. Soc*. **1995**, 117, 11027.

[14] R. W. Alder, P. R. Allen, M. Murray, A. G. Orpen, *Angew. Chem. Int. Ed*. **1996,** 35, 1121; *Angew. Chem.* **1996**, 108, 1190.

[15] E. Despagnet-Ayoub, R. H. Grubbs, *J. Am. Chem. Soc*. **2004,** 126, 10198

[16] V. Lavallo, J. Mafhouz, Y. Canac, B. Donnadieu, W. S. Wolfgang, G. Bertrand, *J. Am. Chem. Soc.* **2004**, 126, 8670.

[17] D. Bourissou, O. Guerret, F. Gabbai, G. Bertrand, *Chem. Rev.* **2000**, 100, 39.

[18] a) W. W. Schoeller, *J. Chem. Soc. Chem. Commun.* **1980**, 124.
b) L. Pauling, *J. Chem. Soc. Chem. Commun*. **1980**, 688.

[19] K. E. Irikura, W. A. Coddard, III, J. L. Beauchamp, *J. Am. Chem. Soc*. **1992**, 114, 48.

[20] H. Tomioka, T. watanabe, K. Hirai, K. Furukawa, T. Takui, K. Itoh, *J. Am. Chem. Soc*. **1995**, 117, 6374.

[21] a) J. L. Wang, J. P. Toscano, M. S. Platz, V. Nikolaev, V. Poplk, *J. Am. Chem. Soc.* **1995**,117, 5477.
b) P. Visser, R. Zuhse, M. W. Wong, C. Wentrup, *J. Am. Chem. Soc*. **1996**, 118, 12598.

[22] a) R. A. Moss, C. B. Mallon, C. T. Ho, *J. Am. Chem. Soc*. **1977**, 99, 4105.
b) S. Koda, *Chem. Phys. Lett.* **1978**, 55, 353.

[23] W. A. Herrmann, C. Köcher, *Angew. Chem. Int. Ed*. **1997**, 36, 2163; *Angew. Chem*. **1997**, 109, 2256.

[24] H. J. Schönherr, H. W. Wanzlick, *Liebigs, Ann. Chem*. **1970**, 731, 176.

[25] W. A. Herrmann, P. W. Roesky, M. Elison, G. Artus, K. Öfele, *Organometallics.* **1995**, 14, 1085.

[26] C. Heinemann, T. Müller, Y. Apeloig, H. Schwarz, *J. Am. Chem. Soc.* **1996**, 118, 2023.

[27] C. Böhme, G. Frenking, *J. Am. Chem. Soc*. **1996**, 118, 2039.

[28] V. Branchadell, R. M. Ortuno, A. Baceiredo, *J. Org. Chem*. **2005**, 70, 5671.

[29] a) H. W. Wanzlick, H. J. Kleiner, *Angew. Chem*. **1961**, 73, 493.
b) H. Wanzlick, *Angew. Chem. Int. Ed*. **1962**, 1, 75; *Angew. Chem.* **1962**, 74, 129.
c) H. Wanzlick, F. Esser, H. Kleiner, *J. Chem. Ber*. **1963**, 96, 1208.

[30] a) D. M. Lemal, R. A. Lovald, K. I. Kawano, *J. Am. Chem. Soc.* **1964**, 66, 2518.
b) H. E. Winberg, J. E. Camahan, D.D.Coffman, M. Brown, *J. Am. Chem. Soc*. **1965**, 8 2055.
c) N. Wiberg, *Angew. Chem. Int. Ed.* **1968**, 7, 766; *Angew. Chem*. **1968**, 80, 809.

[31] a) H. W. Wanzlick, H. Schoenher, *J. Liebiges. Ann. Chem*. **1977**, 731, 176.
b) Simlar results were obtained in the triazole series, R. Walentowski, H. W. Wanzlick, *Z. Naturforsch*. **1970**, 25b, 1421.

[32] H. J. Schoenherr, H. W. Wanzlick, *Chem. Ber*. **1970**, 103, 1037.

[33] a) W. A. Herrmann, M. Elison, J. Fischer, C. K. Köcher, G. R. J. Artus, *Chem. Eur. J*. **1996**, 2, 772.

b) W. A. Herrmann, C. Köcher, L. Gossen, G. R. J. Artus, *Chem. Eur. J* . **1996**, 2, 1627.

[34] N. Kuhn, T. Kratz, *Syntheses.* **1993**, 561.

[35] D. Enders, K. Breuer, G. Raabe, J. Runsink, J. H. Teles, J. P. Melder, K. Ebel, S. Brode, *Angew. Chem. Int. Ed.* **1995**, 34, 1021; *Angew*. *Chem*. 1995, 107, 1119.

[36] M. K. Denk, A. Thadane, K. Hatano, A. Lough, *Angew*. *Chem. Int. Ed.* **1997**, 36, 2607; *Angew*. *Chem*. **1997**, 109, 2719.

[37] R. W. Alder, M. E. Blake, Bortolotti, S. Bufali, Cp. Butts, E. Linehan, J. M. Oliva, A. G. Orepen, M. J. Quayle, *J. Chem. Soc*., *Chem. Commun*. **1994**, 241.

[38] A. J. Arduengo, III, J. R. Goerlich, R. Krafezyk, W. Marshall, *Angew. Chem. Int. Ed.* **1998**, 37, 1963; *Angew. Chem*. **1998**, 110, 2062.

[39] A. J. Arduengo, III, H. Bock, H. Chen, M. Denk, D. A. Dixon, J. C. Green, W. A. Herrmann, N. L. Jones, M. Wagner, R. West, *J. Am. Chem. Soc*. **1994**, 116, 6641.

[40] a) A. J. Arduengo, III, H. V. R. Dias, R. L. Halow, M. Kline. *J. Am. Chem. Soc.* **1992**, 114, 5530.

b) A. J. Arduengo , III, F. Davidson, H. V. R. Dias, J. R. Goerlich, D. Khasnis, W. J. Mashall, T. K. Prakasha, *J. Am. Chem. Soc*. **1997**, 119, 12742.

[41] F. F. Hahn, l. writtenbecher, R. Boese, D. B. Laeser, *Chem. Eur. J*. **1999**, 5, 1931.

[42] A. J. Arduengo, III, J. R. Goerlich, W. J. Marshall, *Liebigs Ann*. **1977**, 365.

[43] R. W. Alder, M. E. Blake, *J. Chem. Soc*., *Chem. Commun*. **1977**, 1513.

[44] R. W. Alder, C. P. Buts, A. G. Orepen, *J. Am. Chem. Soc*. **1998**, 120, 11526.

[45] Principles' and applications of organo transition metal chemistry, J. P. Collman, L. S. Hegedus, J. R. Norton, R. G. finke, Eda, university science Books, Millvalley **1987**.

[46] J. C. Garrison, W. J. Youngs, *Chem. Rev.* **2005**, 105, 3978.

[47] R. R. Schrock, J. S. Murdzek, G. C. Bazan, J. Robbins, M. Dimare, M. O'Regan, *J. Am. Chem. Soc*.**1990**, 112, 3875.

[48] J. C. Green, R. G. Scurr, P. L. Arnold, F. G. N. Clocke, *J. Chem. Soc., Chem. Commun***. 1997**, 1963.

[49] W. A. Herrmann, C. Köcher, L. J. Goossen, G. R. J. Artus, *J. Organomet. Chem*. **1997**, 530, 259.

[50] a) W. A. Herrman, K. Öfele, M. Elison, F. E. Kuehn, P. W. Roesky, *J. Organomet. Chem*. **1994**, 480, C7.

b) W. A. Herrman, G. M. Lobmaier, M. Elison, *J. Organomet. Chem*. **1996**, 520, 231.

[51] a) W. Baratta, W. A. Herrman, P. Rigo, J. Schwarz, *J. Organomet. Chem*. **2000**, 593-594, 489.

b) W. Baratta, E. Herdweck, W. A. Herrman, P. Rigo, J. Schwarz, *Organometallics* **2002**.

[52] W. A. Herrmann, G. Gerstberger, M. Spiegler, *Organometallics* **1997**, 16, 2209.

[53] C. Koecher, W. A. Herrman., *J. Organomet. Chem*. **1997**, 532, 261.

[54] W. A. Herrmann, L. J. Goossen, M. Spiegler, *J. Organomet. Chem*. **1997**, 547, 357.

[55] W. A. Herrmann, F. C. Munck, G. R. J. Artus, O. Runte, R. Anwander, *Organometallics* **1997**, 16, 682.

[56] W. A. Herrmann, L. J. Goossen, G. R. J. Artus, C. Köcher, *Organometallics* **1997**, 16, 2472.

[57] K. Öfele, W. A. Herrmann, D. Mihalios, M. E. Elison, E. Herdtweck, W. Schere, J. Mink, *J. Organomet. Chem*. **1993**, 459, 177.

[58] L. Huang, H. J. Schanz, E. D. Stevens, S. P. Nolan, *Organometallics* **1999**, 18, 2370.

[59] A. R. Chianese, LiX, M. C. Janzen, J. W. Faller, R. H. Crabtree, *Organometallic* **2003**, 22, 1663.

[60] A. C. Hillier, W. J. Sommer, B. S. Yong, J. L. Petersen, L. Cavallo, S. P. Nolan, *Organometallics* **2003**, 22, 4322.

[61] T. M. Lee, Hu C-H, *Organomet. Chem*. **2004**, 23, 976.

[62] R. H. Crabtree, *J. Organomet. Chem*. **2005,** 690, 5451.

[63] A. R. Chianese, A. Kovacevic, B. M. Zegles, J. W. Faller, R. H. Crabtree, *Organometallics* **2004**, 23, 2461.

[64] N. M. Scott, S. P. Nolan, *Eur. J. Inorg. Chem*. **2005**, 1819.

[65] R. Dorta, E. D. Stevens, N. M. Scott, C. Costabile, L. Cavallo, C. D. Hoff, S. P. Nolan, *J. Am. Chem. Soc*. **2005**, 127, 2485.

[66] B. K. M. Chan, N. H. Chan, M. R. Grimmett, *Aust. J. Chem*. **1977**, 30, 2005.

[67] M. R. Haque, M. Rasmussen, *Tetrahedron* **1944**, 50, 5535.

[68] M. R. Grimmett, Imidazole and Benzimidazole synthesis, Academie press, London, 1977.

[69] K. J. Harlow, A. F. Hiu, T. Welton, *Synthesis* **1996**, 697.

[70] A. J. Arduengo, *Us* 5077414, **1991**.

[71] A. A. Gridner, I. M. Mihaltseva, *Synth. Commun*. **1994**, 24, 1547.

[72] A. Kiyomri, J. F. Marcoux, S. L. Buchwald, *Tetrahedron Lett.* **1999**, 40, 2657.

[73] M. Scholl, S. D. Ding, C. W. Lee, R. H. Grubbs, *Org. Lett*. **1999**, L, 953.

[74] S. Saba, A. M. Brescia, M. K. Kaloustian, *Tetrahedron Lett*. **1991**, 32, 5031.

[75] K. Öfele, C. G. Kreiter, *Chem. Ber*. **1972**, 105, 529.

[76] K. Öfele, W. A. Herrmann, D. Mihalios, M. Elison, E. HerdtWeck, W. Schere, J. Mink, *J. Organomet. Chem*. **1993**, 459, 177.

[77] a) T. Weskamp, F. J. Kohl, W. Hieringer, D. Gleich, W. A. Herrmann, *Angew. Chem. Int. Ed.* **1999**, 38, 2416; *Angew. Chem*. **1999**, 111, 2573.

b) T. Weskamp, F. Kohl, W. A. Herrmann, *J. Organomet. Chem*. **1999**, 582, 362.

c) L. Ackerrmann, A. Fürstner, T. Weskamp, F. J. Kohl, W. A. Herrmann, *Tetrahedron. Lett.* **1999**, 40, 4787.

[78] P. B. HitchcocK, M. F. Lappert, P. L. Pye, *J. Chem. Soc., Dalton Trans*. **1978**, 826.

[79] A. A. Danopoulos, S. Winston, W. B. Motherwell, *Chem. Commun*. **2002**, 1376.

[80] W.A. Herrmann, J. Schütz, C. D. Frey, E. Herdtweck, *Organometallics* **2006**, 25, 2437.

[81] A. A. Danopouls, N. Tsoureas, J. A. Wright, M. E. Light, *Organometallics* **2004**, 23, 166.

[82] T. Weskamp, W. C. Schattenmann, M. Spiegler, W. A. Herrmann, *Angew. Chem. Int. Ed.* **1998**, 37, 2490; *Angew. Chem*. **1998**, 110, 2639.

[83] W. A. Herrmann, *Angew. Chem. Int. Ed.* **2002**, 41, 1290.

[84] C. Y. Liu, D. Y. Chen, G.H. Lee, S. M. Peng, S. T. Liu, *Organometallics* **1996**, 15, 1055.

[85] L. K. Johnson, R. J. Angelici, *Inorg. Chem*. **1987**, 26, 973.

[86] S. T. Liu, T. Y. Hsieh, G. H. Lee, S. M. Peng, *Organometallics* **1998**, 17, 993.

[87] H. M. J. Wang, I. J. B. Lin, *Organometallics* **1998**, 17, 972.

[88] W. A. Herrmann, D. Baskakov, E. Herdtweck, S. D. Hoffman, T. Bunksananusorn, F. R. Rampf, L. Rodefeld, *Organometallics* **2006**, 25, 2449.

[89] P. L. Arnold, F. G. N. Clocke, T. Geldbach, P. B.Hitchchcock, *Organometallics* **1999**, 18, 3228.

[90] P. L. Arnold, F. G. N. Clocke, T. Gldbach, P. B. Hitch Chcock, *Organometallics* **1999**, 18, 322

[91] D. S. Ms. Guiness, K. J. Cavell, B. F. Yates, *Chem. Commun*. **2001**, 355.

[92] A. Fürstner, G. seidel, D. Kremzow, C. W. Lehmann, *Organometallic*s **200**3, 22, 907.

[93] a) D. Bourisou, O. Guerret, F. P. Gabban, G. Bertrand, *Chem. Rev*. **2000**, 100, 39.

b) L. Jafarpour, S. P. Nolan, *J. Organomet. Chem*. **2001**, 617-718, 17.

. c) A. C. Hillier, G. A. Grasa, M. S. Viciu, H. M. Lee, C. Yang, S. P. Nolan, *J Organomet*. *Chem*. **2002**, 653, 69.

d) M. C. Perry, K. Burgess, *Tetrahedron, Asymmetry* **2003**, 14, 951.

[94] a) C. Yang, S. P. Nolan, *Organometallics* **2002**, 21, 1020.

b) N. Hadei, E. A. B. Kantchev, C. J. Brin, M. G. Organ, *Org. Lett*. **2005**, 7, 1991.

c) C. Yang, S. P. J. Nola, *J. Org. Chem.* **2002**, 67, 591.

[95] J. E. Hill, T. A. Nile, *J. Organomet. Chem.* **1977**, 137, 293.

[96] W. A. Herrman, C. P. Reisinger, M. Spiegler, *J. Organomet. Chem*. **1998**, 557, 93.

[97] a) T. Westcamp, V. P. W. Böhm, W. A. Herrmann, *J. Organomet. Chem*. **2000**, 600, 12.

. b) M. G. Gardiner, W. A. Herrmann, C. P. Reisinger, J. Schwarz, M. Spiegler, *J. Orgnomet.Chem*. **1999**, 572, 39.

c) M. G. Gardiner, W. A. Herrmann, C. –p. Reisinger, M. Spiegler, *J. Organomet. Chem*. **1999**, 572, 239.

d) M. T. Powell, D. R. Hou, M. C. Perry, X. Cui, K. Burgess, *J. Am. Chem. Soc***. 2001**, 123, 8878.

e) H. M. Lee, T. Jiang, E. D. Stevens, S. P. Nolan, *Organometallics* **2001**, 20, 1255.

f) M. Albrecht, J. R. Miecznikowski, A. Samuel, J. M. Faller, R. H. Crabtree, *Organometallics* **2002**, 21, 3596.

g) L. D. Vazquesz-Serrano, B. T. Owens, J. M. Buriak. *Chem. Comun*. **2002**, 2518.

h) J. R. Miecznikowski, R. H. Crabtree, *Organometallics* **2004,** 23, 692.

i) S. Kuhl, R. Schneider, Y. Fort, *Organometallics* **2003**, 22, 4184.

j) V. K. Dioumaev, D. J. Szalda, J. Hanson, J. A. Franz, R. M. Bullock, *Chem. Commun* **2003**, 1670.

k) E. Mass-Marza, M. Poyatos, M. Sanau, E. Peris, *Inorg. Chem***. 2004**, 43, 2213.

l) H. Kaur, F. K. Zinn, E. D. Stevens, S. P. Nolan, *Organometallics* **2004**, 23, 1157.

m) K. H. Park, S. Y. Kim, S. U. Son, Y. K. Chung, *Eur. J. Org. Chem*. **2003**, 4341.

n) W. L. Duan, M. She, G. B. Rong, *Chem. Commun*. **2003**, 2916.

o) J. W. Sprengers, M. J. Mars, M. A. Duin, K. J. Cavell, C. J. Elsevier, *J. Organomet. Chem*. **2003**, 679, 149.

p) I. E. Marko, S. Sebastien, O. Buisine, G. Mignani, P. Branlard, B. Tinant, J. P. Declereq, *Science* **2002**, 298, 204.

q) E. Mas-Marza, M. Poyatos, M. Sanau, E. Peris, *Organometallics* **2004**, 23, 1857.

r) G. A. Grasa, A. Moore, K. L. Martin, E. D. Stevenes, S. P. Nolan, V. Paquet, H. Lebel, *J. Organomet. Chem*. **2002**, 658, 126.

s) H. Vanrensburg, R. P. Tooze, D. F. Foster, A. M. Z. Slawin, *Inorganic Chem*. **2004**, 43, 2468.

t) A. C. Chen, L. Ren, A. Decken, C. M. Crudden, *Organometallics* **2000**, 19, 3459.

u) Y. Sato. T. Yoshino, M. Mori, *Org. Lett*. **2003**, 5, 31.

[98] a) L. Ackermann, A. Fürstner, T. Weskamp, F. J. Kohl, W. A. Herrmann, *Tetrahedron Lett*. **1999**, 40, 4787.

b) W. A. Herrmann, K. Öfele, D. V. Preysing, S. K. Schneider, *J. Organomet. Chem.* **2003**, 687, 229, and refrence edited therein.

c) W. A. Herrmann, C. A. Reisinger, M. Spiegler, *J. Organomet. Chem*. **1998**, 557, 93.

d) C. W. K. Gstöttmayr, V. P. W. Böhm, E. H. Herdtweck, M. Grosche, W. A. Herrmann, *Angew. Chem. Int. Ed*. **2002**, 41, 1363.

[99] W. A. Herrmann, L. J. Goossen, C. Köcher, G. R. J. Artus, *Angew. Chem. Int. Ed.* **1996,** 35, 2805; *Angew. Chem*. **1996**, 108, 2978.

[100] B. A. Messerle, M. J. Page, P. Tuener, *Dalton Transaction* **2006**, 3927.

[101] a) S. P. Stanforth, *Tetrahedron* **1998**, 54, 263.

b) A. R. Martin, Y. H. Yang, *Acta. Chem. Scand.* **1993**, 47, 221.

c) A. Suzuki, *Pure. Appl. Chem*. **1991**, 63, 419.

[102] Hand book of organopalladium chemistry for organic syntheses. E. Negishi; John Wiley & Sons: Newyork, **2002**.

[103] a) J. Roneuli, *Chem. Rev*. **1992**, 92, 711.

b) K. Yamamurasono, H. Ogoshi, H. Masuda, Y. Kuroda, *Syn. Lett*. **1989**, 18.

[104] S. Caddick, F. G. N. Clocke, G. K. B. Clentsmith, P. B. Hitchcock, D. Mckeirecher, L. R.

Titcomb, M. R. V. Williams, *J. Organomet. Chem*. **2001**, 617-618, 635.

[105] C. Yang, S. P. Nolan, *Syn. Lett*. **2002**.

[106] V. P. W. Böhm, T. Weskamp, C. W. K. Gstöttmayr, W. A. Herrmann, *Angew. Chem. Int. Ed*. **2000**, 39, 1602; *Angew. Chem*. **2000**, 112, 1672.

[107] J. Huang, S. P. Nolan, *J. Am. Chem. Soc*. **1999**, 121, 9889.

[108] a) N. Miyaura, A. Suzuki, *Chem. Commun*. 1**979**, 866.

b) N. Miyaura, T. Yanage, A. Suzuki, *Synth. Commun*. **1981**, 11, 513.

c) T. N. mitchelln, *Synthesis* **1992**, 803.

d) A. Suzuki, *J. Organomet. Chem*. **1999**, 576, 147.

e) N. Miyaura, A. Suzuki, *Chem. Rev*. 1**995**, 95, L and Stannanes inStille reactions.

F) D. Milsteins, J. K. Stille, *J. Am. Chem. Soc*. **1979**, 101, 4992.

g) V. Farina, Pur. *Appl. Chem*. **1996**, 68,73.

[109] G. A. Grasa, S. P. Nolan, *Org. Lett*. **2000**, 3, 119.

[110] W. A. Herrmann, M. Elison, J. Fischer, C. Köcher, G. R. J. Artus, *Angew. Chem. Int. Ed*. **1995**, 34, 2371; *Angew. Chem*.1995, 107, 2602.

[111] A. D. Littke, C. Dai, C. G. Fu. *J. Am. Chem. Soc.* **2000**, 122, 4020, J. P. Wolfe, R. A Singer, B. H. Yang, S. L. Buchwald, *J. Am. Chem. Soc*. **1999**, 121, 9550.

[112] W. A. Herrmann, C. P. Reiinger, M. Spiegler, *J. Organomet. Chem*. **1998**, 557, 39.

[113] K. Arentsen, S. Caddick, F. G. N. Cloke, A. P. Herring, P. B. Hitchcock, *Tetrahedron Lett*. **2004**, 45, 3511.

[114] O. Navarro, H. Kaur, P. Mahjoor, S. P. Nolan, *J. Org. Chem***. 2004**, 69, 3171.

[115] H. Lebel, M. K. Janes, A. B. Charette, S. P. Nolan, *J. Am. Chem. Soc*. **2004**, 126, 5046.

[116] T. Mizoroki, K. Mori, A. Ozaki, Bull. *Chem. Soc. Jpn*. **1972**, 44, 581.

[117] a) G. Altenhoff, R. Goddard, C. W. Lehmann, F. Glorius, *Angew. Chem. Int. Ed*. **2003**, 42, 3690; *Angew. Chem*. **2003**, 115, 3818.

b) G. Altenhoff, R. Goddard, C. Lehmann, F. Glorius. *J. Am. Chem. Soc*. 2**004**, 126, 15196.

c) M. C. Guinness, D. S. Cavell, *Organometallics* **2000**, 19, 741.

[118] O. Navarro, R. A. Kelly, S. P. Nolan, *J. Am. Chem. Soc*. **2003**, 125, 16194.

[119] C. Amatore, A. Jutand, *Acc. Chem. Res*. **2000**, 33, 314.

[120] N. Tsoureas, A. A. Danpoulos, A. A. D. Tulloch, M. E. Light, *Organometallics* **2003**, 22, 4750.

[121] H. M. Lee, J. Y. Zeng, C. -H. Hu, M. -T. Lee, *Inorg. Chem*. **2004**, 43, 6822.

[122] C. L. Yang, H. M. Lee, S. P. Nolan, *Org. Lett*. **2001**, 3, 1511.

[123] S. -T. Lin, M.-F. Ding, C. -W. Chang, S. -S. Lue, *Tetrahedron* **2004**, 60, 9441.

[124] J. A. Davies, J. G. Mierzwiak, R. J. Syed, *J. Coordination. Chem*. **1988**, 17, 25.

[125] N. Kuhn, H. Bohnen, J. Kreutzberg, D. Bläser, R. Boese, *J. Chem. Soc., Chem. Commun* . **1993**, 1136.

[126] V. Langer, K. Huml, G. Reck, *Acta Crystallogr*. Sec. B. **1982**, 38, 298.

[127] A. K. Abdul-Sada, A. M. Greenway, P. B. Hitchcock, T. J. Mohammed, K. R. Seddon, K. R. Zora, *J. Chem. Soc., Chem. Commun*. **1986**, 1753.

[128] N. Kuhn, G. Henkel, J. Kreutzberg, *Z. Naturforsch, TeillB* **1991**, 46, 1706.

[129] N. Kuhn, G. Henkel, T. Kratz, *Chem. Ber*. **1993**, 126, 2047.

[130] N. Kuhn, G. Weyers, G. Henkel, *Chem. Commun*. **1997**, 627.

[131] J. M. Praetorius, M. W. Kotyk, J. D. Webb, C. M. Crudden, *Organometallics* **2007**, 26, 1057.

[132] a) M. V. Baker, S. K. Brayshaw, B. W. Skelton, A. H. White, *Inorg. Chim. Acta***. 2004**, 357, 2841.

[133] M. T. Zarka, M. Bortenschlager, K. Wurst, O. Nuyken, R. Weberskirch, *Organometallics* **2004**, 23, 4817.

[134] R. S. Simono, P. Custer, C. A. Tessier, W. J. Youngs, *Organometallic* **2003**, 22, 1979.

[135] L. D. Field, B. A. Messerle, K. Q. Vuong, P. Turner, *Organometallics* **2005**, 24, 4241.

[136] M. C. Perry, X. Cui, M. T. Powell, D. R. Hou, J. H. Reibenspies, K. Burgess, *J. Am. Chem. Soc*. **2003**, 125, 113.

[137] W. A. Herrmann, J. Schütz, G. D. Frey, E. Herdtweck, *Organometallics* **2006**, 25, 2437.

[138] M. Poyatos, P. Uriz, J. A. Mata, C. Claver, E. Fernandez, E. Peris, *Organometallics* **2003**, 22, 440.

[139] X. -Y. Yu, B. B. O. Patrick, B. R. James, *Organometallics* **2006**, 25, 4870.

[140] M. Ahijado, T. Braun, D. Noveski, N. Kocher, B. Neumann, D. Stalke, H Georgstammler, *Angew. Chem. Int. Ed*. **2005**, 44, 6947; *Angew. Chem.* **2005**, 117, 7107.

[141] a) L. Vaska, *Acc. Chem. Res*. **1976,** 9, 175.

b) V. Circu, M. A. Fernandes, L. Carlton, *Polyhedron* **2002**, 21, 1775-1778.

[142] a) D. P. Allen, C. M. Crudden, L. A. Calhoun, R. Wang, A. Decken, *J. Organomet. Chem.* **2005**, 690, 5736.

b) G. A. Grasa, Z. Moore, K. L. Martin, E. D. Stevens, S. P. Nolan, V. Praquet, H. J. Lebel, *Organomet. Chem*. **2002**, 658, 126.

[143] a) N. M. Scott, R. Dorta, E. D. Stevens, A. Correa, L. Cavallo, S. P. Nolan, *J. Am. Chem. Soc*. **2005**, 127, 3516.

b) R. Dorta, E. D. Stevens, S. P. Nolan, *J. Am. Chem. Soc.* **2004**, 126, 5054.

[144] a) P. Bazinet, G. P. A. Yap, D. S. Richeson, *J. Am. Chem. Soc*. **2003**, 125, 13314.

b) A. A. Danopoulos, S. Winston, M. B. Hursthouse, *J. Chem. Soc., Dalton Trans*. **2002**, 3090.

[145] A.P. Ginsberg, W. E. Lindsell, C. R. Sprinkle, K. W. West, *Inorg. Chem*. **1982**, 21, 3666.

[146] N. Kuhn, H. Bohnen, G. Henkel, *Z. Naturforsch*. **1994**, 49b, 1473.

[147] A. C. Chen, L. Ren, A. Dechen, C. M. Crudden, *Organometallics.* **2000**, 19, 3459.

[148] S. Burling, L. D. Field, H. L. Li, B. A. Messerle, P. Turner, Eur. *J. Inorg. Chem*. **2003**, 3179.

[149] G. Esquius, J. Pons, R. Yáñez, J. Ros, R. Mathieu, B. Donnadieu, N. Lugan, *Eur. J. Inorg. Chem*. **2002**, 2999.

[150] M. P. Anderson, A. L. Casalnuovo, B. J. Johnson, B. M. Mattson, A. M. Mueting, L. H. Pignolet, *Inorg. Chem*. **1988**, 27, 1649.

[151] M. Viciano, E. M. Marzá, M. Poyatos, M. Sanau, R. H. Crabtree, E. Peris, *Angew. Chem. Int. Ed*. **2005**, 44, 444; *Angew. Chem*. **2005**, 117, 448.

[152] D. E. Chebi, P. E. Fanwick, I. P. Rothwell, *Organometallics* **1990**, 9, 2948.

[153] J. F. Frazier, J. S. Merola, *Polyhedron*. **1992**, 11, 2917.

[154] M. D. Fryzuk, K. Joshi, S. J. Rettig, *Polyhedron*. **1989**, 8, 2291.

[155] P. P. Deutsch, R. Eisenberg, *J. Am. Chem. Soc*. **1990**, 112, 714.

[156] B. E. Mann, B. F. Taylor, 13C NMR Data for Organometallic Compounds, *Academic* : *New York*. **1981**.

[157] C. J. Jameson, In Phosphorus-31 NMR Spectroscopy in Stereo Chemical Analxsis, J. G. Verkade, L. D. Quin, VCH Publishers: *Deerfield, FL*, **1987**, Chapter 6.

[158] I. –G. Schatmann, P. S. White, M. Brookhart, *Organometallics* **2004**, 23, 1766-1776.

[159] M. Janka, A. Ç. Atesin, D. j. Fox, Ch. Flaschenriem, W. W. Brennessel, R. Eisenberg, *Inorg. Chem*. **2006**, 45, 6559.

[160] J. A. McGinnerty, R. Doedens, J. A. Ibers, *Science*, **1967**, 155, 709; *Inorg. Chem*. **1967**, 6, 2243.

[161] a) H. Allen, O. Hill, Dioxgen, Superoxide and Peroxide. In Comprehensive. Coordination. Chemistry; G. Wilkinson, R. D. Gillard, J. A. McCleverty, J. A. Eds, *Pergamon Press*: *Oxford, England* **1987**, Vol. 2, P315.

b) Oxygen Complexes and Oxygen Activation by Transition Metals, A. E. Martell, D. T. Sawyer, Eds., *Plenum Press: New York*, **1988**.

[162] M. Kretschmer, P. S. Pregosin, A. Albinati, A. Togni, *J. Organomet. Chem*. **1985**, 281, 365. and refs. Therein.

[163] A. P. Ginsberg, J. H. Osborne, C. R. Sprinkle, *Inorg. Chem.* **1983**, 22, 254.

[164] A. C. Hillier, H. M. Lee, E. D. Stevens, S. P, Nolan, *Organometallics* **2001**, 20, 4246.

[165] M. Poyatos, E. Mas-Marzá, M. Sanaú, E. Peris, *Inorg. Chem*. **2004**, 43, 1793.

[166] A. Kovacevic, S. Gründemann, J. R. Miecznikowski, E. Clot, O. Eisenstein, R. H. *Crabtree*, *Chem. Commun*. **2002**, 21, 3596.

[167] F. Hanasaka, K. -I.. Fujita, R. Yamaguchi, *Organometallics* **2004**, 23, 1490.

[168] S. Gründemann, A. Kovacevic, M. Albrecht, J. W. Faller, R. H. J. Crabtree, *Am. Chem. Soc*. **2002**, 124, 10473.

[169] B. Rybtchinski, Y. Ben-David, D. Milstein, *Organometallics* **1997**, 16, 3786.

[170] A. Haynes, A. J. H. M. Meijer, J. R. Lyons, H. Adams, *Inorg. Chem*. **2009**, 48, 28.

[171] M. V. Baker, B. W. Skelton, A. H. White, C. C. Williams, *Organometallics* **2002**, 21, 2674.

[172] M. V. Baker, B. W. Skelton, A. H. White, C. C. Williams, *J. Chem. Soc. Dalton Trans*. **2001**, 111.

[173] C. C. Lee, W. C. Ke, K. TingChan, C. -L. Lai, C. H. Hu, H. M. Lee, *Chem. Eur. J*. **2007**, 13, 582.

[174] R. Jothibasu, H. Vinh Huynh, *Organometallics* **2009**, 28, 2505.

[175] W. -H. Yang, Ch. Shiang Lee, S. Pal, Y. Nian Chen, *J. Organomet. Chem*. **2008**, 693, 3729.

[176] K. Matsubara, K. Ueno, Y. Shibata, *Organometallics* **2006**, 25, 3422.

[177] P. L. Chiu, C. L. Lai, C. F. Chang, C. H. Hu, H. M. Lee, *Organometallics* **2005**, 24, 6169.

[178] H. M. Lee, P. L. Chiu, J. Y. Zeng, *Inorg. Chim. Acta* **2004**, 357, 4313.

[179] D. D. Perrin, W. L. F. Armarego, Purification of Laboratory chemicals. 3rd ed, Pergamon Press, Oxford, **1993**.

[180] L. J. Herde, J. C. Lambert, C. V. Senoff, *Inorg. Synth*. **1974**, 14, 18.

[181] G. C. Giordano, R. H. Crabtree, *Inorg. Synth*. **1990**, 28, 88.

[182] D. Drew, J. R. Doyle, *Inorg. Synth*. **1972**, 13, 53.

[183] M. Özer, Ph. D.Thesis, Paderborn 2009.

7. Appendix

Table 7.1: Crystal data and structure refinement for **E6**

	E6
Identification code	a1951
Empirical formula	C_{19} H_{22} F_6 N_2 P_2
Formula weight	454.33
Temperature	120(2) K
Wavelength	0.71073 Å
Crystal system	Monoclinic
Space group	P2(1)/n
Unit cell dimensions	a = 8.4391(8) Å
	b = 13.6878(13) Å
	c = 18.1986(17) Å
	α = 90°
	β = 97.623(2)°
	γ = 90°
Volume	2083.6(3) $Å^3$
Z	4
Density (calculated)	1.448 Mg/m^3
Absorption coefficient	0.269 mm^{-1}
F(000)	936
Crystal size	0.37 x 0.31 x 0.19 mm^3
Theta range for data collection	1.87 to 27.88°
Index ranges	$-11 \leq h \leq 11$, $-18 \leq k \leq 18$, $-23 \leq l \leq 23$
Reflections collected	16418
Independent reflections	4923 [R(int) = 0.0874]
Completeness to theta = 27.88	99.5 %
Absorption correction	Semi-empirical from equivalents
Max. and min. transmission	0.9507 and 0.9071
Refinement method	Full-matrix least-squares on F^2
Data / restraints / parameters	4923 / 0 / 262
Goodness-of-fit on F^2	0.998
Final R indices [$I>2\sigma$ (I)]	R1 = 0.0643, wR2 = 0.1544
R indices (all data)	R1 = 0.1278, wR2 = 0.1942
Largest diff. peak and hole	0.521 and -0.373 $e.Å^{-3}$

Table 7.2: Crystal data and structure refinement for **E8** and **E9**

	E8	**E9**
Identification code	S1616	e1214
Empirical formula	C_{20} H_{21} N_2 P S_2	C_{12} H_{20} N_2 S_2
Formula weight	384.48	256.42
Temperature	120(2) K	120(2) K
Wavelength	0.71073 Å	0.71073 Å
Crystal system	Monoclinic	Monoclinic
Space group	C2/c	C2/c
Unit cell dimensions	a = 20.125(3) Å	a = 13.9880(15) Å
	b = 13.832(2) Å	b = 9.0697(10) Å
	c = 13.920(2) Å	c = 11.5600(12) Å
	α = 90°	α = 90°
	β = 90.884(3)°	β = 110.895(2)°
	γ = 90°	γ = 90°
Volume	3874.7(10) $Å^3$	1370.1(3) $Å^3$
Z	8	4
Density (calculated)	1.318 Mg/m^3	1.243 Mg/m^3
Absorption coefficient	0.363 mm^{-1}	0.366 mm^{-1}
F(000)	1616	552
Crystal size	0.43 x 0.40 x 0.38 mm^3	0.48 x 0.40 x 0.40 mm^3
Theta range for data collection	1.79 to 27.88°	2.73 to 27.88°
Index ranges	$-26 \leq h \leq 24$, $-16 \leq k \leq 18$, $-15 \leq l \leq 18$	$-18 \leq h \leq 18$, $-11 \leq k \leq 11$, $-15 \leq l \leq 15$
Reflections collected	11269	6678
Independent reflections	4450 [R(int) = 0.0295	1631 [R(int) = 0.0538
Completeness to theta = 27.88	96.3 %	100.0 %
Absorption correction	Semi-empirical from equivalents	Semi-empirical from equivalents
Max. and min. transmission	0.8745 and 0.8597	0.979 and 0.829
Refinement method	Full-matrix least-squares on F^2	Full-matrix least-squares on F^2
Data / restraints / parameters	4450 / 0 / 226	1631 / 0 / 77
Goodness-of-fit on F^2	1.037	1.076
Final R indices [$I>2\sigma$ (I)]	R1 = 0.0387, wR2 = 0.1058	R1 = 0.0396, wR2 = 0.0947
R indices (all data)	R1 = 0.0450, wR2 = 0.1100	R1 = 0.0504, wR2 = 0.0982
Largest diff. peak and hole	0.447 and -0.209 e.$Å^{-3}$	0.281 and -0.289 e.$Å^{-3}$

Table 7.3: Crystal data and structure refinement for **E10** and **E11**

	E10	**E11**
Identification code	s1615	a1772
Empirical formula	C_{38} H_{42} Cl N_4 P_2 Rh	C_{42} H_{50} F_6 N_4 O P_3 Rh
Formula weight	755.06	936.68
Temperature	120(2) K	120(2) K
Wavelength	0.71073 Å	0.71073 Å
Crystal system	Triclinic	Triclinic
Space group	P-1	P-1
Unit cell dimensions	a = 13.279(2) Å	a = 11.032(2) Å
	b = 16.172(2) Å	b = 19.481(4) Å
	c = 18.636(3) Å	c = 20.305(4) Å
	α = 103.457(4)°	α = 81.115(4)°
	β = 100.846(4)°	β = 76.855(4)°
	γ = 99.490(4)°	γ = 87.308(4)°
Volume	3730.5(9) $Å^3$	4198.4(14) $Å^3$
Z	4	4
Density (calculated)	1.344 Mg/m^3	1.482 Mg/m^3
Absorption coefficient	0.647 mm^{-1}	0.586 mm^{-1}
F(000)	1560	1928
Crystal size	0.48 x 0.11 x 0.05 mm^3	0.39 x 0.33 x 0.05 mm^3
Theta range for data collection	1.33 to 27.88°	1.37 to 27.88°
Index ranges	$-17 \le h \le 17$, $-18 \le k \le 21$, $-24 \le l \le 24$	$-14 \le h \le 14$, $-25 \le k \le 25$, $-26 \le l \le 25$
Reflections collected	32822	36802
Independent reflections	17669 [R(int) = 0.1163]	19836 [R(int) = 0.0567
Completeness to theta = 27.88°	99.2 %	99.0 %
Absorption correction	Semi-empirical from equivalents	Semi-empirical from equivalents
Max. and min. transmission	0.9684 and 0.7466	0.9713 and 0.8036
Refinement method	Full-matrix least-squares on F^2	Full-matrix least-squares on F^2
Data / restraints / parameters	17669 / 0 / 833	19836 / 10 / 1048
Goodness-of-fit on F^2	0.836	0.971
Final R indices [$I>2\sigma$ (I)]	R1 = 0.0642, wR2 = 0.1158	R1 = 0.0557, wR2 = 0.1153
R indices (all data)	R1 = 0.1376, wR2 = 0.1340	R1 = 0.1045, wR2 = 0.1342
Largest diff. peak and hole	0.930 and -0.925 $e.Å^{-3}$	0.925 and -0.579 $e.Å^{-3}$

Table 7.4: Crystal data and structure refinement for **E12** and **E13**

	E12	**E13**
Identification code	s1614	a1779
Empirical formula	C_{38} H_{42} Cl N_4 P_2 Rh	C_{46} H_{62} F_6 N_4 O_2 P_3 Rh
Formula weight	755.06	1012.82
Temperature	120(2) K	120(2) K
Wavelength	0.71073 Å	0.71073 Å
Crystal system	Monoclinic	Monoclinic
Space group	Cc	C2/c
Unit cell dimensions	a = 11.8053(17) Å	a = 20.601(3) Å
	b = 16.513(2) Å	b = 11.6546(18) Å
	c = 18.900(3) Å	c = 21.108(3) Å
	α = 90°	α = 90°
	β = 98.510(3)°	β = 108.900(3)°
	γ = 90°	γ = 90°.
Volume	3643.8(9) $Å^3$	4794.7(12) $Å^3$
Z	4	4
Density (calculated)	1.376 Mg/m^3	1.403 Mg/m^3
Absorption coefficient	0.662 mm^{-1}	0.521 mm^{-1}
F(000)	1560	2104
Crystal size	0.37 x 0.25 x 0.14 mm^3	0.46 x 0.24 x 0.05 mm^3
Theta range for data collection	2.14 to 27.88°	2.04 to 27.87
Index ranges	$-15 \leq h \leq 15$, $-21 \leq k \leq 21$, $-24 \leq l \leq 24$	$-27 \leq h \leq 27$, $-15 \leq k \leq 15$, $-27 \leq l \leq 27$
Reflections collected	15598	20594
Independent reflections	4351 [R(int) = 0.0715]	5734 [R(int) = 0.0485
Completeness to theta = 27.88°	100.0 %	99.9 %
Absorption correction	Semi-empirical from equivalents	Semi-empirical from equivalents
Max. and min. transmission	0.9130 and 0.7918	0.9744 and 0.7957
Refinement method	Full-matrix least-squares on F^2	Full-matrix least-squares on F^2
Data / restraints / parameters	4351 / 0 / 209	5734 / 0 / 281
Goodness-of-fit on F2	1.021	1.042
Final R indices [I>2σ (I)]	R1 = 0.0373, wR2 = 0.0726	R1 = 0.0358, wR2 = 0.0817
R indices (all data)	R1 = 0.0472, wR2 = 0.0755	R1 = 0.0461, wR2 = 0.0863
Largest diff. peak and hole	0.692 and -0.788 $e.Å^{-3}$	0.946 and -0.281 $e.Å^{-3}$

Table 7.5: Crystal data and structure refinement for **E14A**

	E14A, counter ion [Cl]	**E14A,** counter ion [PF_6]
Identification code	a1751	a1968
Empirical formula	C_{46} H_{61} Cl_5 N_4 O_3.50 P_2 Rh	C_{40} H_{45} F_6 N_5 O_2 P_3 Rh
Formula weight	1068.09	937.63
Temperature	120(2) K	120(2) K
Wavelength	0.71073 Å	0.71073 Å
Crystal system	Triclinic	Orthorhombic
Space group	P-1	$P2_12_12_1$
Unit cell dimensions	a = 11.1357(17) Å	a = 10.8163(4) Å
	b = 12.1567(18) Å	b = 10.8672(4) Å
	c = 18.395(3) Å	c = 34.6160(12) Å
	α = 88.808(3)°	α = 90°
	β = 81.782(3)°	β = 90°
	γ = 69.035(3)°	γ = 90°
Volume	2300.2(6) $Å^3$	4068.9(3) $Å^3$
Z	2	4
Density (calculated)	1.542 Mg/m^3	1.531 Mg/m^3
Absorption coefficient	0.779 mm^{-1}	0.608 mm^{-1}
F(000)	1106	1920
Crystal size	0.37 x 0.21 x 0.18 mm^3	0.44 x 0.27 x 0.19 mm^3
Theta range for data collection	1.79 to 27.88°	1.96 to 27.87°
Index ranges	$-14 \le h \le 14$, $-15 \le k \le 15$, $-24 \le l \le 24$	$-13 \le h \le 14$, $-14 \le k \le 14$, $-45 \le l \le 45$
Reflections collected	20292	38882
Independent reflections	10876 [R(int) = 0.0254	9698[R(int) = 0.0679]
Completeness to theta = 27.88	99.1 %	99.9 %
Absorption correction	Semi-empirical from equivalents	Semi-empirical from equivalents
Max. and min. transmission	0.8725 and 0.7615	0.8933 and 0.7759
Refinement method	Full-matrix least-squares on F^2	Full-matrix least-squares on F^2
Data / restraints / parameters	10876 / 0 / 487	9698/ 0 / 515
Goodness-of-fit on F^2	1.059	1.011
Final R indices [$I>2\sigma(I)$]	R1 = 0.0562, wR2 = 0.1607	R1 = 0.0436, wR2 = 0.0985
R indices (all data)	R1 = 0.0686, wR2 = 0.1700	R1 = 0.0505, wR2 = 0.1023
Largest diff. peak and hole	0.971 and -0.765 $e.Å^{-3}$	1.195 and -0.596 $e.Å^{-3}$

Table 7.6: Crystal data and structure refinement for **E15**

	E15
Identification code	a1732
Empirical formula	C_{39} H_{44} Cl_2 F_6 N_4 O_2 P_3 Rh
Formula weight	981.50
Temperature	120(2) K
Wavelength	0.71073 Å
Crystal system	Orthorhombic
Space group	Pna2(1)
Unit cell dimensions	a = 23.394(4) Å
	b = 14.722(2) Å
	c = 12.2306(19) Å
	α = 90°
	β = 90°
	γ = 90°
Volume	4212.4(11) $Å^3$
Z	4
Density (calculated)	1.548 Mg/m^3
Absorption coefficient	0.713 mm^{-1}
F(000)	2000
Crystal size	0.48 x 0.17 x 0.15 mm^3
Theta range for data collection	1.63 to 27.88°
Index ranges	$-30 \leq h \leq 30$, $-18 \leq k \leq 19$, $-16 \leq l \leq 15$
Reflections collected	35987
Independent reflections	9726 [R(int) = 0.0684]
Completeness to theta = 27.88	100.0 %
Absorption correction	Semi-empirical from equivalents
Max. and min. transmission	0.9006 and 0.7260
Refinement method	Full-matrix least-squares on F^2
Data / restraints / parameters	9726 / 121 / 514
Goodness-of-fit on F^2	1.051
Final R indices [I>2σ (I)]	R1 = 0.0480, wR2 = 0.0872
R indices (all data)	R1 = 0.0670, wR2 = 0.0932
Largest diff. peak and hole	0.692 and -0.699 $e.Å^{-3}$

Table 7.7: Crystal data and structure refinement for **E16**

	E16
Identification code	a1744
Empirical formula	$C_{40}\ H_{46}\ Cl_4\ F_6\ N_4\ P_3\ Rh\ S_2$
Formula weight	1098.55
Temperature	120(2) K
Wavelength	0.71073 Å
Crystal system	Monoclinic
Space group	P2(1)/c
Unit cell dimensions	a = 18.487(3) Å
	b = 14.982(3) Å
	c = 18.296(3) Å
	$\alpha = 90°$
	$\beta = 117.209(4)°$
	$\gamma = 90°$
Volume	4506.9(13) $Å^3$
Z	4
Density (calculated)	1.619 Mg/m^3
Absorption coefficient	0.876 mm^{-1}
F(000)	2232
Crystal size	0.33 x 0.22 x 0.19 mm^3
Theta range for data collection	1.24 to 27.88°
Index ranges	$-24 \le h \le 23, -19 \le k \le 19, -19 \le l \le 24$
Reflections collected	39010
Independent reflections	10736 [R(int) = 0.0799]
Completeness to theta = 27.88	100.0 %
Absorption correction	Semi-empirical from equivalents
Max. and min. transmission	0.8512 and 0.7608
Refinement method	Full-matrix least-squares on F^2
Data / restraints / parameters	10736 / 45 / 538
Goodness-of-fit on F^2	0.976
Final R indices [$I>2\sigma$ (I)]	R1 = 0.0588, wR2 = 0.1461
R indices (all data)	R1 = 0.0951, wR2 = 0.1595
Largest diff. peak and hole	0.994 and -0.983 $e.Å^{-3}$

Table 7.8: Crystal data and structure refinement for **E19**

Identification code	a1832
Empirical formula	C_{40} H_{45} Cl I_4 N_5 P_2 Rh
Formula weight	1303.71
Temperature	120(2) K
Wavelength	0.71073 Å
Crystal system	Monoclinic
Space group	P2(1)/c
Unit cell dimensions	a = 12.085(3) Å
	b = 30.141(8) Å
	c = 13.032(4) Å
	α = 90°
	β = 108.894(7)°
	γ = 90°
Volume	4
Z	1.928 Mg/m^3
Density (calculated)	3.295 mm^{-1}
Absorption coefficient	3.295 mm^{-1}
F(000)	2496
Crystal size	0.18 x 0.10 x 0.04 mm^3
Theta range for data collection	1.78 to 27.88
Index ranges	$-15 \leq h \leq 15$, $-39 \leq k \leq 36$, $-16 \leq l \leq 17$
Reflections collected	39508
Independent reflections	10699 [R(int) = 0.2268]
Completeness to theta = 27.88	99.9 %
Absorption correction	Semi-empirical from equivalents
Max. and min. transmission	0.8795 and 0.5885
Refinement method	Full-matrix least-squares on F^2
Data / restraints / parameters	699 / 0 / 479
Goodness-of-fit on F^2	0.854
Final R indices [I>2σ (I)]	R1 = 0.0589, wR2 = 0.0738
R indices (all data)	R1 = 0.2000, wR2 = 0.1035
Largest diff. peak and hole	0.981 and -0.930 e.$Å^{-3}$

Table 7.9: Crystal data and structure refinement for **E20**

Identification code	a1702
Empirical formula	$(C_{38}\ H_{42}\ Ir\ N_4\ P_2)(P\ F_6)$
Formula weight	953.87
Temperature	120(2) K
Wavelength	0.71073 Å
Crystal system	Monoclinic
Space group	P2(1)/n
Unit cell dimensions	a = 15.659(2) Å
	b = 16.405(2) Å
	c = 16.608(2) Å
	α = 90°
	β = 114.886(3)°
	γ = 90°
Volume	3870.0(9) $Å^3$
Z	4
Density (calculated)	1.637 Mg/m^3
Absorption coefficient	3.636 mm^{-1}
F(000)	1896
Crystal size	0.40 x 0.32 x 0.30 mm^3
Theta range for data collection	1.50 to 27.88°
Index ranges	$-20 \le h \le 20$, $-21 \le k \le 19$, $-21 \le l \le 21$
Reflections collected	33920
Independent reflections	9221 [R(int) = 0.0829]
Completeness to theta = 27.88	99.8 %
Absorption correction	Semi-empirical from equivalents
Max. and min. transmission	0.4084 and 0.3241
Refinement method	Full-matrix least-squares on F^2
Data / restraints / parameters	9221 / 120 / 469
Goodness-of-fit on F^2	0.844
Final R indices [I>2σ (I)]	R1 = 0.0372, wR2 = 0.0556
R indices (all data)	R1 = 0.0731, wR2 = 0.0612
Largest diff. peak and hole	0.967 and -0.944 $e.Å^{-3}$

Table 7.10: Crystal data and structure refinement for **E21**

Identification code	a1709
Empirical formula	C_{38} H_{44} Cl Ir N_4 P_2
Formula weight	846.36
Temperature	120(2) K
Wavelength	0.71073 Å
Crystal system	Monoclinic
Space group	P2(1)/c
Unit cell dimensions	a = 11.235(3) Å
	b = 19.771(5) Å
	c = 19.027(4) Å
	α = 90°
	β = 102.568(4)°
	γ = 90°
Volume	4125.2(16) $Å^3$
Z	4
Density (calculated)	1.363 Mg/m^3
Absorption coefficient	3.407 mm^{-1}
F(000)	1696
Crystal size	0.38 x 0.35 x 0.23 mm^3
Theta range for data collection	1.50 to 27.88°
Index ranges	$-13 \leq h \leq 14$, $-26 \leq k \leq 25$, $-25 \leq l \leq 25$
Reflections collected	35712
Independent reflections	9831 [R(int) = 0.0602]]
Completeness to theta = 27.88	100.0 %
Absorption correction	Semi-empirical from equivalents
Max. and min. transmission	0.5079 and 0.3575
Refinement method	Full-matrix least-squares on F^2
Data / restraints / parameters	9831 / 3 / 424
Goodness-of-fit on F^2	0.980
Final R indices [I>2σ (I)]	R1 = 0.0397, wR2 = 0.0941
R indices (all data)	R1 = 0.0543, wR2 = 0.0989
Largest diff. peak and hole	1.035 and -0.937 $e.Å^{-3}$

Table 7.11: Crystal data and structure refinement for **E22**

Identification code	a1871
Empirical formula	$C_{42}\ H_{50}\ F_6\ Ir\ N_4\ O_3\ P_3$
Formula weight	1057.97
Temperature	120(2) K
Wavelength	0.71073 Å
Crystal system	Orthorhombic
Space group	$P2_12_12_1$
Unit cell dimensions	a = 13.817(4) Å
	b = 16.678(5) Å
	c = 18.534(5) Å
	α = 90°
	β = 90°
	γ = 90°
Volume	4271(2) $Å^3$
Z	4
Density (calculated)	1.645 Mg/m^3
Absorption coefficient	3.309 mm^{-1}
F(000)	2120
Crystal size	0.47 x 0.12 x 0.11 mm^3
Theta range for data collection	1.64 to 27.88°
Index ranges	$-18 \le h \le 18, -21 \le k \le 21, -24 \le l \le 24$
Reflections collected	37415
Independent reflections	10187 [R(int) = 0.0996]
Completeness to theta = 27.88	99.9 %
Absorption correction	Semi-empirical from equivalents
Max. and min. transmission	0.7123 and 0.3054
Refinement method	Full-matrix least-squares on F^2
Data / restraints / parameters	10187 / 45 / 528
Goodness-of-fit on F^2	0.977
Final R indices [I>2σ (I)]	R1 = 0.0394, wR2 = 0.0738
R indices (all data)	R1 = 0.0523, wR2 = 0.0774
Largest diff. peak and hole	1.637 and -0.636 $e.Å^{-3}$

Table 7.12: Crystal data and structure refinement for **E23**

Identification code	a1866
Empirical formula	$C_{44}\ H_{53}\ F_6\ Ir\ N_5\ O\ P_3\ S_2$
Formula weight	1131.14
Temperature	120(2) K
Wavelength	0.71073 Å
Crystal system	Monoclinic
Space group	P2(1)/c
Unit cell dimensions	a = 18.382(2) Å
	b = 15.050(2) Å
	c = 18.237(2) Å
	α = 90°
	β = 116.563(3)°
	γ = 90°
Volume	4512.7(10) $Å^3$
Z	4
Density (calculated)	1.665 Mg/m^3
Absorption coefficient	3.224 mm^{-1}
F(000)	2272
Crystal size	0.43 x 0.38 x 0.29 mm^3
Theta range for data collection	1.83 to 27.88°
Index ranges	$-24 \le h \le 24$, $-19 \le k \le 17$, $-22 \le l \le 23$
Reflections collected	39199
Independent reflections	10754 [R(int) = 0.0433]
Completeness to theta = 27.88	100.0 %
Absorption correction	Semi-empirical from equivalents
Max. and min. transmission	0.4549 and 0.3378
Refinement method	Full-matrix least-squares on F^2
Data / restraints / parameters	10754 / 45 / 483
Goodness-of-fit on F^2	1.001
Final R indices [I>2σ (I)]	R1 = 0.0342, wR2 = 0.0855
R indices (all data)	R1 = 0.0468, wR2 = 0.0898
Largest diff. peak and hole	1.805 and -0.691 $e.Å^{-3}$

Table 7.13: Crystal data and structure refinement for **E25**

Identification code	a1825
Empirical formula	C_{43} H_{53} I_2 Ir N_4 O P_2
Formula weight	1149.83
Temperature	120(2) K
Wavelength	0.71073 Å
Crystal system	Monoclinic
Space group	P2(1)/c
Unit cell dimensions	a = 14.259(2) Å
	b = 13.699(2) Å
	c = 22.408(4) Å
	α = 90°
	β = 96.028(4)°
	γ = 90°
Volume	4353.1(13) $Å^3$
Z	4
Density (calculated)	1.754 Mg/m^3
Absorption coefficient	4.596 mm^{-1}
F(000)	2240
Crystal size	0.25 x 0.20 x 0.17 mm^3
Theta range for data collection	1.44 to 27.88°
Index ranges	$-18 \leq h \leq 18$, $-17 \leq k \leq 18$, $-29 \leq l \leq 27$
Reflections collected	38039
Independent reflections	10368 [R(int) = 0.1097]
Completeness to theta = 27.88	99.9 %
Absorption correction	Semi-empirical from equivalents
Max. and min. transmission	0.5088 and 0.3929
Refinement method	Full-matrix least-squares on F^2
Data / restraints / parameters	10368 / 0 / 475
Goodness-of-fit on F^2	0.919
Final R indices [I>2σ (I)]	R1 = 0.0485, wR2 = 0.1015
R indices (all data)	R1 = 0.0802, wR2 = 0.1106
Largest diff. peak and hole	1.165 and -0.947 $e.Å^{-3}$

Table 7.14: Crystal data and structure refinement for **E27**

Identification code	a1666
Empirical formula	C_{42} H_{48} I_2 N_6 Ni P_2
Formula weight	1011.31
Temperature	153(2) K
Wavelength	0.71073 Å
Crystal system	Monoclinic
Space group	P2(1)/n
Unit cell dimensions	a = 11.4419(14) Å
	b = 18.767(2) Å
	c = 20.573(3) Å
	α = 90°
	β = 95.940(3)°
	γ = 90°
Volume	4394.0(9) $Å^3$
Z	4
Density (calculated)	1.529 Mg/m^3
Absorption coefficient	1.955 mm^{-1}
F(000)	2024
Crystal size	0.38 x 0.25 x 0.20 mm^3
Theta range for data collection	1.47 to 27.88°
Index ranges	$-14 \leq h \leq 15$, $-24 \leq k \leq 24$, $-27 \leq l \leq 26$
Reflections collected	38434
Independent reflections	10465 [R(int) = 0.0361]
Completeness to theta = 27.88	100.0 %
Absorption correction	Semi-empirical from equivalents
Max. and min. transmission	0.6958 and 0.5237
Refinement method	Full-matrix least-squares on F^2
Data / restraints / parameters	10465 / 0 / 482
Goodness-of-fit on F^2	1.045
Final R indices [I>2σ (I)]	R1 = 0.0328, wR2 = 0.0716
R indices (all data)	R1 = 0.0436, wR2 = 0.0753
Largest diff. peak and hole	0.769 and -0.288 e.$Å^{-3}$

Table 7.15: Crystal data and structure refinement for **E28**

Identification code	a1807
Empirical formula	$C_{44}\ H_{51}\ F_{12}\ N_7\ P_4\ Pd$
Formula weight	1136.20
Temperature	120(2) K
Wavelength	0.71073 Å
Crystal system	Triclinic
Space group	P-1
Unit cell dimensions	a = 11.114(2) Å
	b = 11.343(2) Å
	c = 20.243(4) Å
	α = 77.490(4)°
	β = 83.580(5)°
	γ = 85.301(4)°
Volume	2471.4(8) $Å^3$
Z	2
Density (calculated)	1.527 Mg/m^3
Absorption coefficient	0.590 mm^{-1}
F(000)	1156
Crystal size	0.42 x 0.20 x 0.20 mm^3
Theta range for data collection	1.04 to 27.10°
Index ranges	$-14 \le h \le 14$, $-14 \le k \le 14$, $-24 \le l \le 25$
Reflections collected	20506
Independent reflections	10803 [R(int) = 0.0318]
Completeness to theta = 27.88	99.0 %
Absorption correction	Semi-empirical from equivalents
Max. and min. transmission	0.8911 and 0.7896
Refinement method	Full-matrix least-squares on F^2
Data / restraints / parameters	10803 / 30 / 560
Goodness-of-fit on F^2	1.179
Final R indices [I>2σ (I)]	R1 = 0.0494, wR2 = 0.1339
R indices (all data)	R1 = 0.0600, wR2 = 0.1402
Largest diff. peak and hole	0.947 and -0.960 $e.Å^{-3}$

Conference contributions:

3/09 GDCh-Jahrestagung 2009 Essen (poster: “Rhodium complexes with NHC-phosphine hybride ligands and their reactivity towards oxygen”).